VISUAL FIELD AND STRUCTURAL ALTERATIONS IN AGE-RELATED MACULAR DEGENERATION

JENNIFER HELOISE ACTON
Doctor of Philosophy

ASTON UNIVERSITY
February 2010

Aston University

Visual Field and Structural Alterations in Age-Related Macular Degeneration

Jennifer Heloise Acton

Doctor of Philosophy

2010

The thesis investigated progression of the central 10° visual field with structural changes at the macula in a cross-section of patients with varying degrees of age-related macular degeneration (AMD). The relationships between structure and function were investigated for both standard and short-wavelength automated perimetry (SWAP).

Factors known to influence the measure of visual field progression were considered, including the accuracy of the refractive correction on SWAP thresholds and the learning effect. Techniques of assessing the structure to function relationships between fundus images and the visual field were developed with computer programming and evaluated for repeatability. Drusen quantification of fundus photographs and retro-mode scanning laser ophthalmoscopic images was performed. Visual field progression was related to structural changes derived from both manual and automated methods.

Principal Findings:

- Visual field sensitivity declined with advancing stage of AMD. SWAP showed greater sensitivity to progressive changes than standard perimetry.
- Defects were confined to the central 5°. SWAP defects occurred at similar locations but were deeper and wider than corresponding standard perimetry defects.
- The central field became less uniform as severity of AMD increased. SWAP visual field indices of focal loss were of more importance when detecting early change in AMD, than indices of diffuse loss.
- The decline in visual field sensitivity over stage of severity of AMD was not uniform, whereas a linear relationship was found between the automated measure of drusen area and visual field parameters.
- Perimetry exhibited a stronger relationship with drusen area than other measures of visual function.
- Overcorrection of the refraction for the working distance in SWAP should be avoided in subjects with insufficient accommodative facility.
- The perimetric learning effect in the 10° field did not differ significantly between normal subjects and AMD patients.
- Subretinal deposits appeared more numerous in retro-mode imaging than in fundus photography.

Perimetry; Short-wavelength automated perimetry; Drusen; Scanning laser ophthalmoscope

For Smilex

Acknowledgements

I wish to thank my supervisor Robert Cubbidge and my associate supervisor Jonathan Gibson for their support and advice.

Thanks to my fellow postgraduate students and staff at Aston University, in particular, Mark Dunne for his guidance on computer programming, Richard Armstrong for his statistical advice and Hannah Bartlett for help in recruiting patients.

I would like to thank Helen King and Paul Galsworthy (Ophthalmology, Heart of England NHS Foundation Trust, Solihull, UK) for acquiring grading data, used in Chapter 6.

I am also grateful to R. Theodore Smith and Noah Lee (Columbia University, New York City, USA) for supplying the software for automated drusen segmentation used in Chapter 8; and Birmingham Optical Group for permitting the use of Nidek instrumentation.

Finally, I am indebted to all participants who took part in each of the studies.

List of Contents

List of Figures

List of Tables

1. Introduction

1.1 Interpretation of the Visual Field

1.1.1 Standard Perimetric Indices and Probability Analysis

Global indices are summary measures which describe the visual field as a single value. Normal databases have been established from large populations, so that indices could be calculated, using the STATPAC software incorporated into the perimeter for the Humphrey Field Analyser (HFA; Carl Zeiss Ltd., Welwyn Garden City, Hertfordshire, UK) (Heijl et al. 1987b) and Program J0 on the Octopus (Jenni et al. 1983). Analysis of visual fields without a normal database is vulnerable erroneous confusion of subtle abnormalities with normal physiological variations. Table 1-1 shows a description of indices of the HFA and Octopus perimeters.

Visual field loss may be characterised by diffuse and focal components. Diffuse loss is a generalised depression of the hill of vision, and may be caused by media opacities, miosis or defocus. Diffuse loss is represented by the global index, MD. Focal loss is sensitivity loss in a localised area of the visual field, and is represented by the PSD. Focal loss in glaucoma is caused by loss in the nerve fibre layer.

STATPAC software allows for probability analysis and displays this on the standard HFA printout (Figure 1-1). Probability analyses indicate the statistical likelihood of a measured threshold value occurring, based on a normal database of age-corrected values (Heijl et al. 1987b). The Total Deviation analysis represents the threshold differences between the measured field and the age appropriate normal value, for each point in the field. Pattern Deviation indicates the sensitivity differences from normal and is adjusted for overall differences in height of the hill of vision. The probability plots are presented both as a numeric map and as a probability plot on the HFA printout. The values which have a probability of occurring in 5%, 2%, 1% or 0.5% of the age-matched population are mapped (Figure 1-1). Pattern deviation represents focal loss

which may be hidden by a general depression of the hill of vision. The total and pattern probability plots separate the diffuse from the focal loss.

A measure of fixation is made by the gaze tracking system of the HFA (HFA II – *i* series: user's manual). Infrared lights situated in the perimeter bowl allow a measure of the distance between the first corneal reflex (Purkinje 1) and the pupil centre. Real-time image analysis is performed and displayed at the bottom of the HFA printout in the form of a gaze graph (Figure 1-1). The graph denotes eye movements as upward markings, whereby the magnitude up to 10° is illustrated by the size of the mark but directional information is not given. Downward markings indicate the system was unable to detect the gaze direction, which occurs during blinks.

Clinical screening procedures frequently test the visual field out to 30° or 24° from fixation, with a stimulus separation of 6°. However, stimulus configurations with a spatial resolution of 1.4° and 0.7° were shown to be advantageous in the detection of macular disease since the high resolution allows detection of small scotomata (Kaiser et al. 1994).

Any automated visual field examination is exacerbated by several factors including patient performance factors, response errors, pupil size, correction of refractive error and age effects such as cataract. The principal problems with measuring the progression of visual field loss are physiological variability (short-term fluctuation and long-term fluctuation), effects of learning and fatigue, ageing effects and threshold estimating errors. It is necessary to identify changes due to these confounding factors for an individual, before actual field changes can be discovered. True visual field loss should be repeatable on retesting.

Indices		Equation	Definition
Mean Sensitivity (MS)		$\frac{1}{n}\cdot\sum_{i=1}^{n}\bar{x}_i$	The average sensitivity value across the field.
Mean Deviation (MD)	HFA	$\left\{\frac{1}{n}\cdot\sum_{i=1}^{n}\frac{(\bar{x}_i - z_i)}{s1i^2}\right\}/\left\{\frac{1}{n}\cdot\sum_{i=1}^{n}\frac{1}{s1i^2}\right\}$	The average sensitivity difference between the measured and the age corrected normal value at each location. This is weighted at each point for the variation in threshold with increased eccentricity for the HFA. The Octopus index is unweighted.
Mean Defect	Octopus	$\frac{1}{n}\cdot\sum_{i=1}^{n}(z_i - \bar{x}_i)$	
Pattern Standard Deviation (PSD)	HFA	$\sqrt{\left\{\frac{1}{n}\cdot\sum_{i=1}^{n}s1i^2\right\}\cdot\left\{\frac{1}{n-1}\cdot\sum_{i=1}^{n}\frac{(\bar{x}_i - z_i - MD)^2}{s1i^2}\right\}}$	Measures which are sensitive to focal loss. LV is the variance around the MD, whereas PSD is the standard deviation around the mean that constitutes the MD. As with MD, PSD incorporates a weighting function which corrects for eccentricity.
Loss Variance (LV)	Octopus	$\frac{1}{(n-1)}\cdot\sum_{i=1}^{n}(z_i - MD - \bar{x}_i)^2$	
Short-term Fluctuation (SF)	HFA	$\sqrt{\left\{\frac{1}{10}\cdot\sum_{j=1}^{10}s_{2j^2}\right\}\cdot\left\{\frac{1}{10}\cdot\sum_{j=1}^{10}\frac{(x_{j1} - x_{j2})^2}{2\left(s_{2j^2}\right)}\right\}}$	The intra-test variability or measurement error. The root mean square of the difference between double determinations of threshold. The HFA value is weighted for differences between intra-individual sensitivity and makes ten double determinations. The Octopus performs a two phase test and measures SF on the basis of double determinations at every location.
	Octopus	$\sqrt{\frac{1}{n}\cdot\sum_{i=1}^{n}(SD_i)^2}$	

Corrected Pattern Standard Deviation (CPSD)	HFA	$\sqrt{PSD^2 - (k \cdot SF^2)}$	CPSD is the PSD corrected for the SF value in order to remove the normal variability. A weighting function is applied, which corrects for the difference in spatial distribution of the 10 repeated threshold determinations of the SF calculation. CLV is the LV corrected for the SF. Unlike CPSD, this unweighted value is squared. A considerably larger SF than PSD results in a negative value of $CPSD^2$, thus CPSD is set to 0, since the shape deviation is entirely due to measurement error.
Corrected Loss Variance (CLV)	Octopus	$LV - \left\{\frac{1}{n} SF^2\right\}$	

Table 1-1. Visual field indices

Where:

n = the total number of stimulus locations

x = the measured sensitivity

$\bar{x}_i$ = the mean of repeated thresholds at location *i*

z = the expected sensitivity (normal value)

1/s1i = a weighting function which allows for the variation in the shape of the hill of vision with increasing age.

xj_1 = the first determination of sensitivity at a stimulus location *j*

xj_2 = the second determination of sensitivity at a stimulus location *j*

sj_2 = the normal intra-test variance at location *j* and is only known by the perimeter manufacturer.

$1/sj_2^2$ = the weighting function which minimises the SF in normal subjects.

SD_i = the standard deviation at location *i*

k = a constant greater than 1, which corrects for the difference in spatial distributions of the 10 stimulus locations used in the calculation of SF

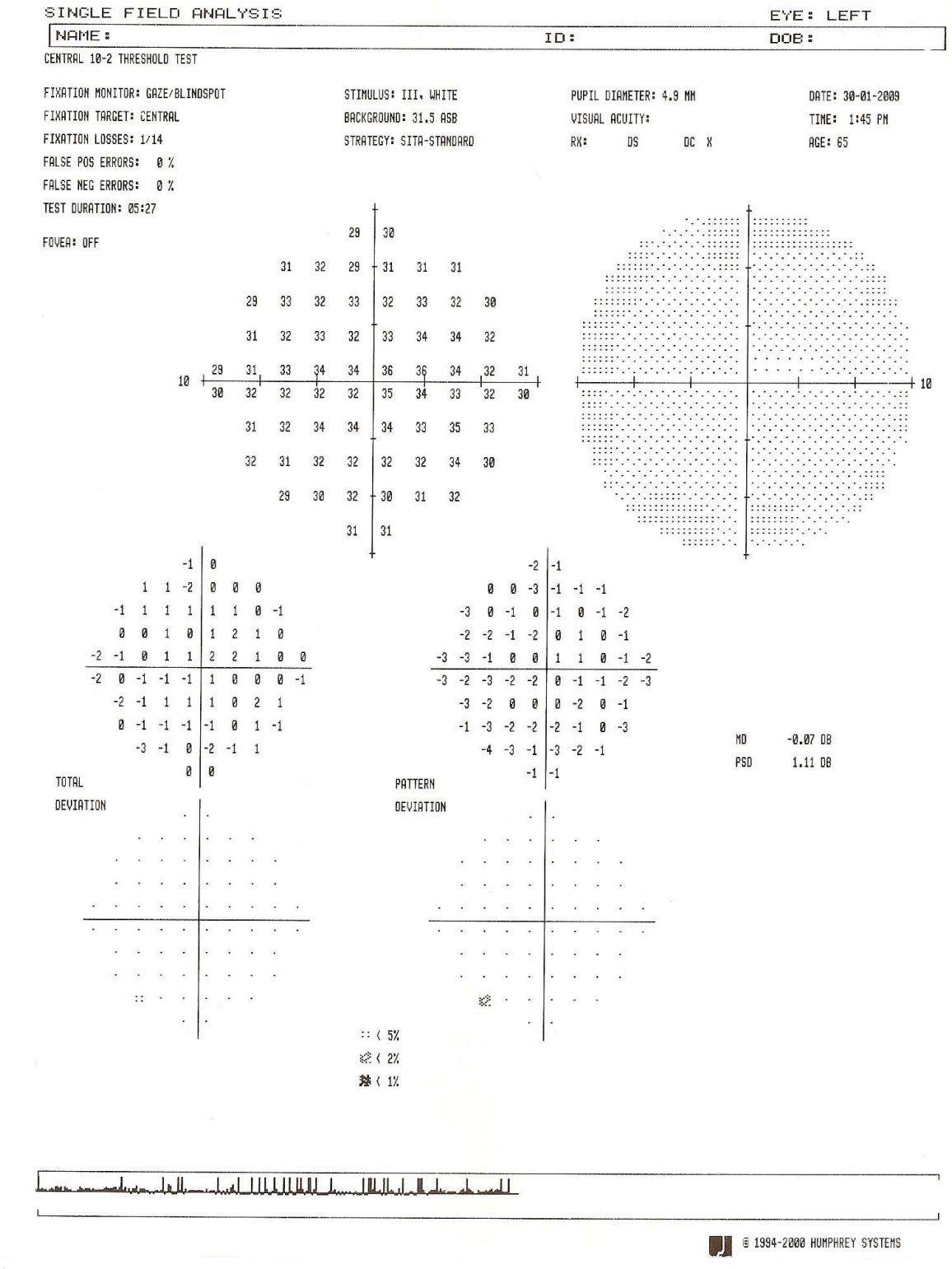

Figure 1-1. HFA printout using the 10-2 program

10 degree visual field, with a stimulus separation of 2°, in a normal subject

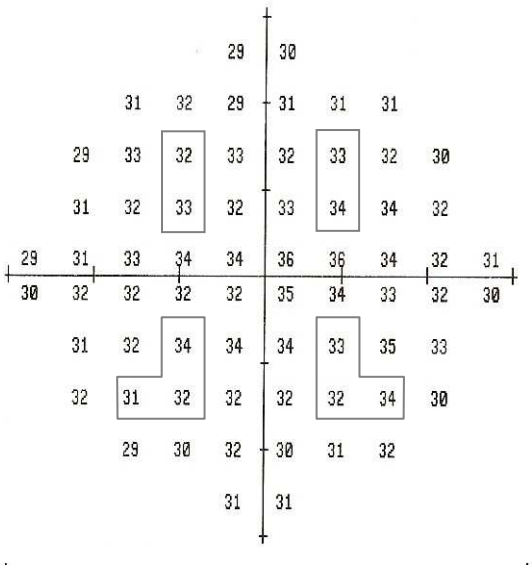

Figure 1-2. Location of the ten points of double determination used to calculate the short-term fluctuation in the ten degree field, on the HFA

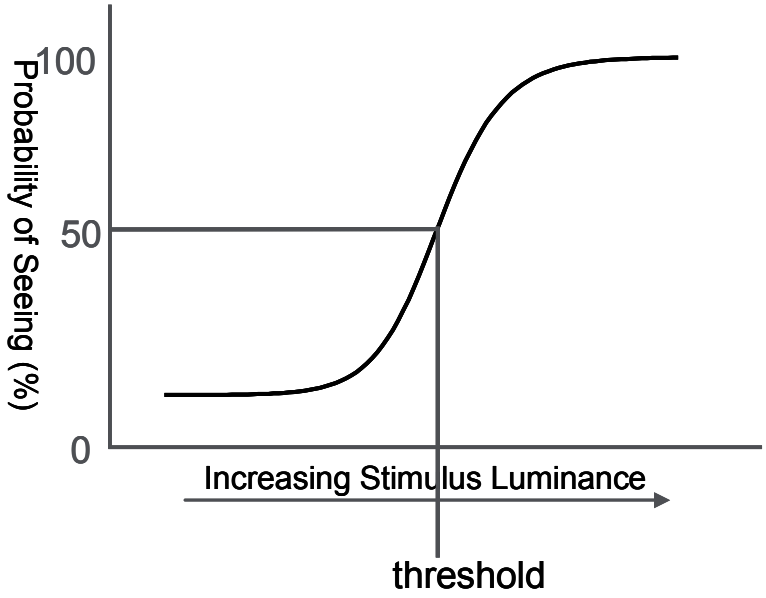

Figure 1-3. Frequency of seeing curve.
Threshold sensitivity is the luminance at which stimuli are detected with a probability of 50%.

1.1.2 Short-term Fluctuation and Long-term Fluctuation

Variability is the difference in threshold which occurs on repeated testing due to random fluctuations, and reflects reproducibility, or confidence in detection of change. Short-term fluctuation (SF) and long-term fluctuation (LF) are the components of variability in automated static perimetry (Bebie et al. 1976). The psychophysical measurement of the differential light threshold is the ratio of the light stimulus from its background that has a probability of being seen 50% of the time (Flammer et al. 1984b; Figure 1-3). Due to the abbreviated staircases used in perimetry inevitably, there is always scatter around this measurement. SF defines that scatter which occurs during a single examination. It is necessary to know the magnitude of the SF in order to detect localised defects (Flammer et al. 1984b). LF is defined as the measure of variability between two or more visual field examinations, after the effect of SF has been removed (Flammer et al. 1984a). In order to quantitatively compare visual fields the value of LF should be known (Flammer et al. 1984a). Calculation of the LF is not included in routine clinical practice.

The HFA determines the threshold twice at ten fixed stimulus locations (Figure 1-2), which are used in the calculation of the SF. Double determinations may be performed at more points where values fall outside of expected values compared to adjacent points (Heijl et al. 1987b), but these are not used in the calculation of the SF. The SF defines the within-test variability and is calculated by taking the root mean square of the difference between the double determinations of threshold. The main factor which influences the SF is the value of the global mean sensitivity (Flammer et al. 1984c). SF is also affected by the threshold estimating algorithm. SF was noted to be greater in the mid-periphery than centrally (Heijl et al. 1987a), while another study found no variation in SF with eccentricity in normal subjects, and a greater value in the superior field in glaucomatous patients (Flammer et al. 1984c). Global SF is not influenced by the number of threshold determinations at a given stimulus location (Chauhan et al. 1991). Variability indices depend on the perimeter, as SF and heterogenous LF were

found to be greater when using the Octopus perimeter than the HFA (Brenton & Argus 1987). The Octopus perimeter assesses the SF from double determinations at all stimulus locations rather than the ten locations used in the HFA.

SF and LF have a significantly greater magnitude in glaucoma patients than in normal subjects (Flammer et al. 1984a). Increased SF is thought to be a sign of future glaucomatous visual field loss (Rabineau et al. 1985; Werner & Drance 1977). LF varies between individuals and therefore affects interpretation of progression by different amounts. In order for detection of progression, field loss must to be greater than LF, which unfortunately tends to be greater in patients with advanced field defects. Despite helping to overcome some problems of interpretation due to variability, repeated testing is demanding for the patient and resource consuming.

There are two components of LF; the homogeneous component, LF(Ho) which influences all locations equally, and the heterogeneous component LF(He), which is the variation between locations (Flammer et al. 1984b). A two-factor analysis of variance (ANOVA) with replications has been used to calculate LF(Ho) and LF(He) (Flammer et al. 1983). This technique of calculating LF between two examinations has been applied to the ten points of double determination for calculation of SF using the HFA (Hutchings et al. 2000). LF(Ho) was calculated as the difference in average overall sensitivity between two examinations; and LF(He) as the variation in sensitivity between locations (Flammer et al. 1983). LF(Ho) was found to be larger than LF(He) in normal subjects and glaucoma patients (Flammer et al. 1983, 1984a). Using a HFA, in normal patients LF(He) and LF(Ho) were reported to be 0.2dB and 0.5dB, respectively; and in glaucoma patients, 0.5dB and 1.2dB (Hutchings et al. 2000). LF(Ho) is significantly correlated with SF, however the relationship is not strong enough to allow the prediction of the LF from the SF (Flammer et al. 1984b).

A multitude of other calculations have been used to describe LF, including other types of AVOVA, standard deviation of the variance at each point in the field indicating the

total between-examination variability at all locations (Katz & Sommer 1987; Werner et al. 1989) and measures of between-examination variability for individual locations in the field (Heijl et al. 1987a; Rutishauser et al. 1989; Werner et al. 1989).

1.1.3 The Learning Effect in Standard Perimetry

In perimetry, the learning effect occurs whereby performance improves as patient experience increases. The learning effect manifests as an increase in sensitivity and reduction in variability. SF decreases with experience (Heijl et al. 1989; Wood et al. 1987). The learning effect occurs during the first examination and is transferred between eyes (Searle et al. 1991; Wild et al. 1989). With respect to visual field progression, the learning effect diminishes the reliability of assessment of a series of fields and when selecting a baseline field.

In normal subjects, the greatest sensitivity increase occurs over the first few tests, where on average, a sensitivity increase of 1-2dB is seen (Autzen & Work 1990; Heijl et al. 1989). In most patients, the learning effect is rapid and plateaus after the first exam of the first eye (Wild et al. 1989). The learning effect was also shown to persist over successive examinations. Eight out of ten young normal subjects displayed an increase in sensitivity over five sessions on the Octopus perimeter, each spaced one day apart (Wood et al. 1987). Three different patterns of learning were noted. The first was a large increase in sensitivity at the 2nd session, and then a plateau until the last session; secondly, a gradual increase in sensitivity over 5 sessions; and lastly no evident sensitivity increase (Wood et al. 1987). It was deemed appropriate to discard only the first perimetric exam when inspecting a series of fields, in patients who show a large increase in sensitivity at the second examination (Wood et al. 1987).

The learning effect in suspected glaucoma patients was found to be similar to normals using the HFA (Wild et al. 1989). Learning effects largely occur between the first two exams in glaucoma patients (Heijl & Bengtsson 1996; Marchini et al. 1991), and in glaucoma suspect patients (Werner et al. 1990). At the second examination, the mean

deviation was significantly lower than the first in glaucoma patients (Kulze et al. 1990). In the longer term, learning effects in glaucoma patients were observed to be insignificant after follow-up visits of 5-15 months (Hudson et al. 1994; Wild et al. 1991), however the learning effect may last for several years in patients who are infrequently tested, once a year (Gardiner et al. 2008).

The learning effect tends to be greater in the periphery compared to the central field (Heijl et al. 1989; Searle et al. 1991; Werner et al. 1990). When examining the Octopus Program 21 field, which tests 76 points with a separation of 15°, a greater learning effect was demonstrated in the superior field, which was thought to be due to the patient learning to keep the upper lid raised (Wood et al. 1987). Conversely, a significant learning effect was demonstrated in all but the superior temporal quadrant, which also exhibited the greatest variablility, in 33 normal subjects tested on the Octopus perimeter (Autzen & Work 1990). A decline in MD was found in all areas of glaucomatous fields, except for the superior periphery, between two visits with a separation of 4 months (Kulze et al. 1990). In glaucoma patients the learning effect manifests especially in areas of moderate field loss rather than areas of mild or severe loss (Heijl & Bengtsson 1996).

Large amounts of variability attributed to learning effects were found between normal individuals of all ages, using the HFA in a study which comprised 74 subjects (Heijl et al. 1989). It was concluded that most normal patients give a reliable perimetric result at their first examination, but a minority of patients are profoundly affected by the learning effect (Heijl et al. 1989; Werner et al. 1990). Variability between individuals was however noted to decline with experience (Heijl et al. 1989). In patients who are significantly affected by the learning effect, the characteristics seen are concentric narrowing of the field and the successive tests then become normal (Heijl et al. 1989). Indeed, a learner's index was calculated in order to identify those who require greater perimetric experience to produce reliable fields (Olsson et al. 1997). This is a linear

discriminant function devised from the variability across concentric zones from fields typical of “learners”. However the complex statistical methodology is not explicitly stated and the technique has not gained widespread use.

There is an inverse relationship between the learning effect and the magnitude of sensitivity at the initial examination (Heijl et al. 1989; Wild et al. 1989). Due to the learning effect, factors which affect automated perimetry are the order in which eyes are examined and the interval between sessions (Wild et al. 1989). In normal subjects, the dependence of learning on age has been noted to exist (Autzen & Work 1990) and also not to be present (Heijl et al. 1989). Neither age, race nor gender were demonstrated to vary with the learning effect in a study where examinations were separated by months in glaucoma patients (Kulze et al. 1990). In addition, the threshold estimating algorithm and perimeter used may cause variability in the learning effect (Capris et al. 2008; Yenice & Temel 2005). Full Threshold strategy on the HFA may produce a greater learning effect than SITA standard (Yenice & Temel 2005).

1.1.4 The Fatigue Effect

The fatigue effect interacts in opposition to the learning effect and can also be detrimental to patient performance in perimetry, causing a progressive decline in light sensitivity as the examination proceeds, particularly at peripheral stimulus locations (Heijl & Drance 1983; Hudson et al. 1994). It can occur during a single examination or transfer to the second eye tested (Hudson et al. 1994; Searle et al. 1991). Investigation of the fatigue effect is normally carried out in experienced patients in order to control for the learning effect.

Various studies have investigated the fatigue effect in normal subjects (Johnson et al. 1988b; Searle et al. 1991), ocular hypertensives (Hudson et al. 1994; Wild et al. 1991), glaucoma patients (Fujimoto & Adachiusami 1993; Heijl & Drance 1983; Johnson et al. 1988b; Wild et al. 1991) and in neuro-ophthalmic disorders (Keltner & Johnson 1995; Reitner et al. 1996). Fatigue effects caused around 1-1.5dB sensitivity loss in normal

subjects (Heijl 1977; Heijl & Drance 1983). In contrast, an earlier study reported no fatigue effect during 1 hour of field testing on an Octopus perimeter using Program 31 in a group of 8 patients (Rabineau et al. 1985).

The fatigue effect has a greater magnitude in glaucoma and suspected glaucoma patients than in normal subjects (Heijl 1977). Fatigue effects in the central 10° were demonstrated in glaucoma patients, who had reduced mean sensitivity (MS) at the third determination of stimulus locations in the field, but not in normal and optic neuritis patients (Fujimoto & Adachiusami 1993). Hudson et al. (1994) reported almost no difference in performance between normals and ocular hypertensives, who exhibited fatigue over examinations lasting approximately 15 minutes. After a long-term follow-up of 5-15 months, inter-eye fatigue was still present in the second eye tested in glaucoma and ocular hypertension patients (Hudson et al. 1994; Wild et al. 1991).

Using the Octopus perimeter, the fatigue effect was seen to cause a progressive generalised depression of the hill of vision and focal loss, greater in the peripheral field between 17° and 30° (Hudson et al. 1994). The effect increases at greater eccentricities away from fixation (Cubbidge 1997; Hudson et al. 1994; Johnson et al. 1988b; Wild et al. 1991). Areas of glaucomatous defect and areas close to the defects, showed greater deterioration than normal areas (Heijl 1977; Heijl & Drance 1983). Furthermore, the presence of field defects due to glaucoma and optic neuritis, was reported to be weakly associated with the fatigue effect (Johnson et al. 1988b).

The design of studies involving automated perimetry may allow for some compensation of the fatigue effect by introducing rest periods between tests or by randomising the order of eyes tested (Artes et al. 2002). Rest periods within examinations lessen the impact of the fatigue effect, especially at greater eccentricities (Johnson et al. 1988b). Hudson et al. (1994) concluded that a rest period of 3 minutes between eyes was not long enough to be rid of the effects of fatigue from the previous eye. It was recommended that the optimum examination duration should be less than 8-10

minutes, since maximum sensitivity loss due to fatigue occurs after this time interval (Johnson et al. 1988b). The effect of the order of eyes tested was investigated using the SITA standard 24-2 test in glaucoma and suspect glaucoma patients experienced in perimetry (Barkana et al. 2006). It was reported that neither the MD nor the test reliability were affected by the order of eyes tested and inter-eye fatigue was suggested not to be clinically significant when using the SITA algorithm (Barkana et al. 2006). Diminished fatigue with shortened test duration has been reported in patients with neuro-ophthalmic disorders (Reitner et al. 1996).

It has been suggested that the cause of fatigue may be associated with reduced concentration and lack of attention during the monotonous task of perimetry (Barkana et al. 2006). Furthermore the Ganzfeld blankout or Troxler phenomenon, whereby the patient perceives a transient darkening of the field during perimetry is thought to contribute to the fatigue effect (Fuhr et al. 1990; Hudson et al. 1994; Searle et al. 1991). The use of a translucent occluder was found to prevent Ganzfeld blankout and increase threshold sensitivity during standard perimetry (Fuhr et al. 1990).

Patient vigilance may be another source contributing to fatigue. Pupil diameters of 12 glaucoma patients were monitored using an eye tracker, whilst performing a similar task to perimetry, displayed at the monitor of the eye tracker (Henson & Emuh 2009). Signs of sleepiness were observed as pupillary constriction, as well as “pupillary fatigue”, observed as oscillations in pupil size. A Pupillary Fatigue Index (PFI) was derived to describe changes in pupil size and unrest. Reduced sensitivity was found to be associated with loss of vigilance which in turn influences visual field variability (Henson & Emuh 2009).

1.1.5 Threshold Estimating Algorithms

Threshold sensitivity is determined by a staircase algorithm, which is a psychophysical technique. A compromise between the test duration, accuracy and reproducibility is made when estimating the threshold sensitivity. Variability occurs depending on the

accuracy of the threshold estimation algorithm used. Scatter in the data is present, due to the measurement of differential light threshold (Flammer et al. 1984b).

Supra-threshold and threshold are the two static examination strategies which may be used in perimetry. The supra-threshold strategy presents stimuli at an intensity above threshold and is used for rapid screening purposes in the determination of normality, to give an approximation of the visual field. Threshold strategies determine the threshold for each point in the visual field and are used for more accurately determining visual field loss. The most common threshold estimating algorithms for threshold strategies are described here.

The Full Threshold strategy on the HFA employs a 4-2 double reversal staircase procedure to determine the threshold sensitivity at each test location. The initial step size is 4dB, which is reduced to 2dB after initially crossing the threshold (reversal). The threshold is recorded as the last seen stimulus after the 2dB step size has crossed the threshold again. Such an algorithm is sometimes referred to as a double reversal algorithm. The Full Threshold strategy measures the central 30° field in around 12 minutes in normal subjects and may take as long as 20 minutes in glaucoma patients (Anderson & Patella 1992). This older algorithm employs a greater number of reversals, which produces longer testing staircase sequences. Consequently the examinations are longer, leading to fatigue to the detriment of the test reliability.

The FASTPAC program was developed with the aim of decreasing test duration. This strategy of threshold estimation uses 3dB steps and crosses the threshold only once (Flanagan et al. 1993a). FASTPAC was demonstrated to reduce test duration by 36-40% compared to the Full Threshold strategy (Flanagan et al. 1993b; Mills et al. 1994) but yielded an increased SF (Flanagan et al. 1993a,b; Mills et al. 1994). Contradictory findings have been reported regarding the ability of FASTPAC to detect visual field defects. Erroneous underestimation (Flanagan et al. 1993b) and overestimation (O'Brien et al. 1994) of defect severity by the FASTPAC algorithm have been

observed. No significant difference of FASTPAC from Full Threshold strategy, in criteria based defect detection has also been noted (Mills et al. 1994). Nevertheless, the FASTPAC algorithm increases the number of patients capable of performing reliable threshold perimetry (O'Brien et al. 1994).

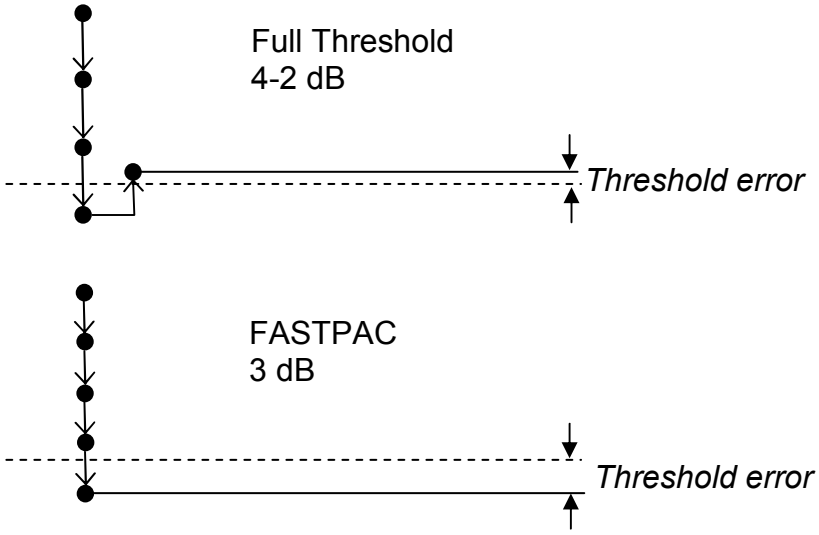

Figure 1-4. Full Threshold and FASTPAC algorithms

The next generation of algorithms, Swedish Interactive Threshold Algorithms (SITA), were created with the intent of minimising test duration whilst maintaining the quality of data comparable to the Full Threshold strategy (Bengtsson et al. 1997b). SITA operates using a probability model of the threshold value constructed from databases of known normal and glaucomatous visual fields. Prior to the start of visual field testing, models of normal and glaucomatous visual fields are constructed. These include information about the age-corrected normal values at each stimulus location (Heijl et al. 1987a), the frequency-of-seeing curves and the correlations between threshold values at different stimulus locations (Bengtsson et al. 1997b). A higher correlation exists between adjacent test points than stimuli situated further apart and points depressed due to glaucomatous field loss mostly occur in clusters corresponding

to the shape of the retinal nerve fibre layer (Bengtsson et al. 1997b). Initially, thresholds are determined at four seed locations by the standard 4-2dB staircase sequence with two reversals. The seed locations are then used to calculate the starting threshold estimates at adjacent points. Patient responses to stimuli and the known distribution models are used to calculate posterior probability distributions, an approach used in Bayesian statistics (Bengtsson et al. 1997b). The posterior probability of a threshold occurring is the conditional probability that is assigned after previous responses and information from the models are taken into account. Posterior probability functions are recalculated following each stimulus presentation and continuously change shape with more responses, facilitating new threshold estimates and continuation of the staircase. The values from the known models gradually exert less influence on the threshold estimates with more response data added to the models. Testing is stopped once the measurement error estimates reach a predetermined limit of accuracy, the error related factor (ERF). ERF values were established based on computer simulation of visual field assessment (Bengtsson et al. 1997b). If the estimated value is greater than 12dB from the initial predicted value, SITA repeats the staircase, as opposed to the Full Threshold strategy, which repeats the staircase if the estimated value is greater than 4dB from the initial value (Bengtsson & Heijl 1998a; Turpin et al. 2003). As well as the advent of a new threshold estimating algorithm, SITA incorporated novel processes for timing and the estimation of false answers. The timing algorithm is repeatedly adjusted based on each response throughout testing. Like older threshold estimating algorithms, false negatives are measured using catch trials, however false positive answers are detected during periods when no responses are expected, rather than performing separate catch trials. A post processing step is implemented in SITA, which recalculates all threshold values taking into account the influence of the patient reaction times and the frequencies of false answers on the probability curves used in threshold estimation (Bengtsson et al. 1997b). As a result of the more efficient threshold estimating algorithm, the elimination

of catch trials for false positives and the more effective timing algorithm, SITA reduced the examination duration of older algorithms, whilst maintaining reproducibility comparable to Full Threshold strategy (Bengtsson et al. 1998; Bengtsson & Heijl 1998b). SITA Standard was reported to take approximately half the time of the Full Threshold strategy and 84-85% of the time of FASTPAC, in normal subjects (Bengtsson et al. 1998) and glaucoma patients (Bengtsson & Heijl 1998b). Furthermore, the number of stimuli presented was decreased by 29% in normals and 26% in glaucoma patients (Bengtsson et al. 1997b).

SITA Standard and SITA Fast are the two algorithms available on the HFA, which correspond to Full Threshold and FASTPAC algorithms, respectively. The threshold estimation in SITA Fast interrupts the stimulus sequence earlier than in SITA Standard, by increasing the limit of the ERF, such that a diminished accuracy of test results is accepted and thus fewer stimuli are presented (Bengtsson & Heijl 1998a). SITA Fast was reported to present 30-34% fewer stimuli than FASTPAC in normal and glaucomatous visual field tests (Bengtsson & Heijl 1998a). SITA algorithms have reduced between-subject variability, compared to Full Threshold and FASTPAC algorithms, therefore narrowing confidence limits for definition of normality (Bengtsson & Heijl 1999a; Wild et al. 1999). In normal subjects, SITA MS values have been reported to be around 1dB higher when compared to Full Threshold values (Artes et al. 2002; Shirato et al. 1999; Wild et al. 1999). Moreover, the normal hill of vision was noted to be slightly higher and flatter than the Full Threshold algorithm (Bengtsson & Heijl 1999a). This bias between algorithms has been hypothesised to be caused by a reduced fatigue effect when using the briefer SITA examinations (Bengtsson & Heijl 1999b), however it has been argued that factors other than fatigue are responsible for the difference (Artes et al. 2002; Shirato et al. 1999; Turpin et al. 2003). It has been suggested that the magnitude of the bias is related to the size of the ERF (Artes et al. 2002). The difference in threshold values between the Full Threshold and SITA

strategies were found to vary in a nonlinear pattern with sensitivity in glaucoma patients (Artes et al. 2002). In glaucomatous visual fields, the SITA algorithms detected a greater number of pattern deviation defects than the Full Threshold algorithm despite producing similar MD values (Bengtsson & Heijl 1999b). Normal individuals naïve to perimetry were also observed to have more significantly depressed pattern deviation points when tested with SITA standard compared to Full Threshold strategies (Schimiti et al. 2002). A limitation in the performance of SITA was recognised in a study using computer simulations of visual field testing (Turpin et al. 2003). When response errors were made by simulated patients, the accuracy and precision of sensitivity estimates were poor when the initial estimate of threshold was not close to the true threshold (Turpin et al. 2003).

1.1.6 Age

Advancing age causes changes which confound the interpretation of visual field progression. In the standard visual field, sensitivity in the normal eye declines with increase in age such that a depression and steepening of the hill of vision occurs (Heijl et al. 1987a; Jaffe et al. 1986). Mean sensitivity has been reported to decline at rate between 0.07 to 0.10dB per year for standard perimetry (Heijl et al. 1987a; Johnson et al. 1989; Jaffe et al. 1986; Wild et al. 1998) and at more rapid rates of 0.15 to 0.20dB in short-wavelength automated perimetry (SWAP) (Johnson et al. 1988a; Wild et al. 1998). The age-related decline in visual field sensitivity is thought to correspond to an age-related decline in the photoreceptor population, cells in the ganglion cell layer and retinal pigment epithelium (Curcio et al. 1993; Gao & Hollyfield 1992; Panda-Jonas et al. 1995). Cataract and senile miosis also contribute to the generalised depression of the hill of vision with age.

The age-corrected normal threshold values employed by commercially available perimeters follow the models for decline in the visual field sensitivity with age. The Octopus perimeter uses a linear decline of 0.1dB per year, across the entire visual field

(Cubbidge 1997). The model applied by the HFA is based on empirical data, in which the threshold variability between normal individuals, between tests and within a single test was observed to increase with eccentricity (Heijl et al. 1987a). Subsequently, the model allows the hill of vision to change in height and shape with age.

1.1.7 Visual Field Progression in Standard Perimetry

Visual field progression describes the perimetric changes over time, as they chart the course of disease. Progression may occur as deepening or enlargement of a defect, an appearance of a new defect, or a combination of these. In automated static perimetry, methods for defining visual field progression have largely been developed to investigate glaucomatous visual field loss. A variety of techniques exist including subjective assessment of serial field plots, statistical methods, statistical analysis by software and clinical trial criteria, however there is no standardised method for defining progression.

A change analysis printout is available on the HFA, which presents change represented as boxplot summaries of visual field data over time (Figure 1-5). The boxplot is a modified histogram and represents a five number summary of a sample distribution. In change analysis, the sample indicates the pointwise differences between the measured field and normal field. The box limits represent the 15^{th} and 85^{th} percentiles, the centre line represents the median and the tails represent the 0 and 100^{th} percentiles (Heijl et al. 1987b).

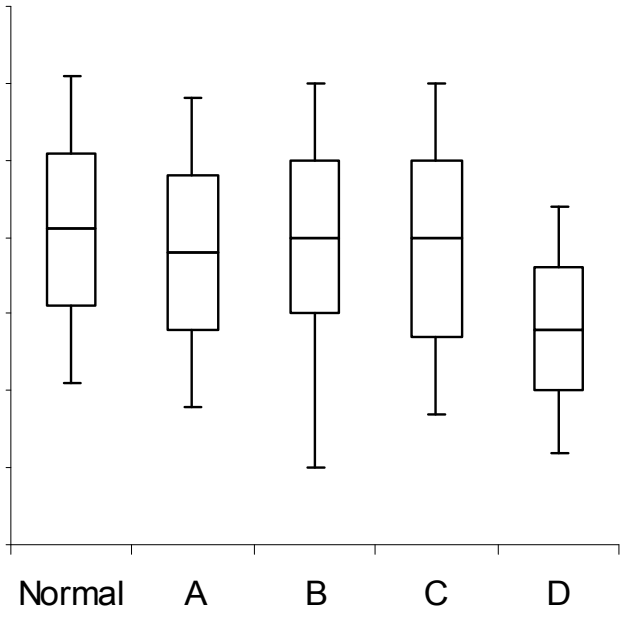

A. Depressed sensitivity without any localised loss (normal shape but overall depressed height)

B. Deepened scotoma (elongated tail)

C. Enlarged scotoma (elongated box)

D. Enlarged scotoma and/or newly formed scotoma (box depressed, median worsened, top shrunk)

Figure 1-5. Boxplot representation of visual field change

Mikelberg et al. (1986) calculated regression of “scotoma mass” with time in glaucomatous defects. Course of change over time was defined as linear, curvilinear, or step-wise in pattern. It was found that eyes with a greater scotoma mass showed a more rapid rate of visual loss. A visual field defect scoring system was devised and analysed over time in progression measurement (Gaasterland et al. 1994). Several large clinical trials have created criteria for glaucomatous progression, such as the Early Manifest Glaucoma Treatment Study (EMGT) (Heijl et al. 2003), the AGIS (Gaasterland et al. 1994), and the Ocular Hypertension Treatment Study (OHTS) (Gordon & Kass 1999). Progression was defined in terms of minimum number of clusters of abnormal points to signify change due to disease. Cluster analyses over time have been criticised as being insensitive to glaucomatous change (Chauhan et al. 1990).

Event-based analysis identifies where visual field change exceeds test-retest variability, as quantified by repeated measurement of stable glaucomatous fields over a short period of time. Software programs such as Glaucoma Change Probability (GCP) and Delta were created to analyse progression based on the probability that threshold sensitivity at a specific point in the visual field has changed, greater than predicted. GCP assesses field change in the total deviation plot over time and compares depths and patterns of loss, to baseline measurements and a database of stable glaucomatous fields. Changes which are greater than the stable fields are more likely to represent true change. GCP can sufficiently distinguish between stable and deteriorating fields (Morgan et al. 1991). Using pattern deviation rather than total deviation analysis on GCP maps has been advocated as a highly sensitive method of early glaucomatous progression detection (Heijl et al. 2002). Pattern deviation values compensate for changes in the general height of the visual field, thought to be principally caused by cataract (Bengtsson et al. 1997a). More recently, Glaucoma Progression Analysis (GPA) software was introduced to the Humphrey Field Analyser.

This software performs event-based analyses using pattern deviation values and was found to detect progression with a sensitivity and specificity of 93% and 95%, respectively (Arnalich-Montiel et al. 2008). However, a lower incidence of progression with GPA was found when compared with GCP (Katz 2000). Correspondingly, pattern deviation analysis was found to classify progression in approximately 15% fewer eyes than total deviation analyses (Artes et al. 2005). This was explained by the presence of both focal and diffuse components in glaucomatous visual field progression (Artes et al. 2005).

Trend analysis refers to the model of the pattern of change in sequential visual fields over time. Pointwise linear regression (PLR) considers the sensitivity of each point in the field against time, which gives the rate of loss in decibels per year. The statistical significance of change over the entire series of examinations is established. PLR has been demonstrated as a sensitive method to detect glaucomatous progression (Katz et al. 1997; Smith et al. 1996; Viswanathan et al. 1997). PROGRESSOR is a software program which implements PLR and identifies change with respect to LF (Fitzke et al. 1996). Clinical agreement of progression detection was superior when using PROGRESSOR compared to inspection of a series of Humphrey printouts (Viswanathan et al. 2003). It has been demonstrated that PLR gives a similar performance to GCP (McNaught et al. 1996) and has detected progression sooner than GCP analysis (Viswanathan et al. 1997). Although, PLR was shown to be less effective in progression detection in early follow-up of glaucoma patients, when compared with GCP and the Advanced Glaucoma Intervention Study (AGIS) algorithm (Nouri-Mahdavi et al. 2007). Univariate linear regression analysis has also been used to detect change for individual test points, in hemifields, and applied to clusters of points defined by the Glaucoma Hemifield Test (GHT) (Katz et al. 1997; Smith et al.1996). Pointwise analysis of stimulus locations showed the greatest declines in sensitivity and offered the advantage of highlighting the exact locations of change (Katz

et al. 1997; Smith et al. 1996). Yet the higher variability of individual locations relative to clusters or global indices meant greater loss was necessitated before it was detected statistically (Katz et al. 1997; Smith et al. 1996). Supplementary to this, it is known that adjacent locations are not statistically independent of each other (de la Rosa et al. 2002). Regression of clusters was surmised as a sufficient compromise between variability and spatial information (Katz et al. 1997; Smith et al. 1996). Other programs using regression analysis include graphical analysis of topographical trends (GATT) and Threshold Noiseless Trend (TNT). GATT is included in Peridata and displays serial topographic changes in sensitivity, derived by superimposing greyscales (Weber & Krieglstein 1989). Horizontal stripes are used to represent visual field deteriorations and vertical stripes indicate improvement and chequerboard pattern illustrates highly variable regions. TNT employs spatial filtering procedures (see Chapter 1.2.4) to reduce threshold fluctuation. The filter is based on the relations of interdependence of stimulus locations analysed in glaucomatous visual fields (de la Rosa et al. 2002). TNT also provides regression analysis in relation to the Cumulative Defect Curve (de la Rosa 2008). The Cumulative Defect Curve is constructed by ranking the thresholds at each location from best to worst. TNT showed better agreement with expert observers and higher sensitivity but lower specificity in comparison to GPA (Diaz-Aleman et al. 2009). Mathematically, there are a number of different methods of PLR which include criteria such as the slope significance level and addition of confirmation points (Gardiner & Crabb 2002). Unfortunately, there is no universally agreed value for regression slope or significance value for progression. Wilkins et al. (2006) found that optimum detection of glaucomatous progression was achieved where criterion required change in two points in a nerve fibre bundle sector using a slope of 1dB/year and the choice of significance value depended on the data characteristics. Linear trends were reported to best fit the glaucomatous visual field changes (Katz et al. 1997; Nouri-Mahdavi et al. 2007) and linear regression had been observed to best predict future risk of progression (Heijl et al. 2003).

An index of the rate of glaucoma progression, the glaucoma progression index (GPI), was derived for the HFA 30-2 and 24-2 stimulus patterns (Bengtsson & Heijl 2008). The calculation of the GPI involved the pattern deviation probability maps, whereby defects were scored according to a weighted function which emphasised the central points. When examining glaucoma progression rates by linear regression of indices over five years, the GPI was reported to be less affected by cataract than the MD (Bengtsson & Heijl 2008). Unlike the MD, the centre weighting of the GPI is based on cortical magnification and consequently more closely reflects retinal ganglion cell loss and visual function (Bengtsson & Heijl 2008). However, since the GPI primarily depicts focal loss, the diffuse loss due to glaucoma progression may be underestimated by this index. The pattern deviation values are influenced by the general height index, or the 85th percentile of the distribution of TD values, which represents diffuse loss. It was noted that overestimation of the general height index could occur in the presence of localised glaucomatous loss (Åsman et al. 2004). This would lead to an underestimation in the significance displayed by the pattern deviation values, giving an underestimation of focal loss. It was concluded that a better method of examining the diffuse component of loss was required and this was thought to apply to the 10-2 field and to SWAP (Åsman et al. 2004). PLR of the total deviation plot was found to be a better predictor of true visual field progression than PLR of the pattern deviation plot, especially in moderately advanced glaucoma (Manassakorn et al. 2006). It was suggested that pattern deviation analyses of progression underestimates the full extent of progression in glaucoma (Artes et al. 2005).

1.1.8 Summary

An ideal visual field progression algorithm should be reproducible and sensitive to change, such that it is able to detect small amounts of progression. It is necessary to consider potential confounding effects, by calculation, for example measurement of the learning effect. Separating true field deterioration from the *noise* arising from

physiological and psychological factors which influence visual field measurement is of paramount importance when determining progression. The number of confirmatory tests needed should be minimal. Pointwise or sector analysis may be preferable as it is essential to measure location of visual field progression, particularly in relation to the fovea and threat to fixation. Determination of the rate of field loss allows visual field change to be conveyed in terms of severity of disease, such that prediction of loss can be made. Subsequently this may assist treatment decisions and anticipate visual disability and quality of life.

1.2 The Interpretation of SWAP

SWAP presents Goldmann size V (1.72°) blue stimuli, with a peak transmission of 440nm, similar to the maximum response of the short-wavelength sensitive (blue) cones in the retina. The narrow band blue light therefore stimulates the short-wavelength sensitive pathway and is presented with the standard stimulus duration of 200ms. The high luminance yellow background, with intensity 100cd/m^2, transmits wavelengths greater than approximately 530nm. This saturates the long- and medium-wavelength sensitive (red and green) cones and suppresses rod activity, which gives isolation of the short-wavelength sensitive pathway (Cubbidge & Wild 2001; Sample et al. 1996). SWAP is mediated by the small bistratified ganglion cells, which contribute approximately 9% of the total population of retinal ganglion cells (Dacey & Lee 1994).

SWAP can be performed on the HFA and the Octopus, amongst other perimeters. The dynamic range is the measurement range of possible stimulus luminances of the perimeter. The HFA permits a maximum stimulus brightness (assigned as 0dB) of 65 apostilbs for SWAP, and 10,000 apostilbs for standard perimetry. The maximum stimulus brightness of the Octopus perimeter is 16 apostilbs and 1000 apostilbs for SWAP and standard perimetry, respectively. The dynamic range is narrower in SWAP due to the brighter yellow background luminance. As a result, the decibel scales are

not directly comparable between the two types of perimetry and SWAP is implicated as less capable in the detection of very advanced defects.

The magnitude of isolation for the HFA was measured to be 15dB and to decrease linearly with greater eccentricity away from fixation (Cubbidge & Wild 2001). Another group found the approximate short-wavelength-sensitive pathway isolation to be 13dB at the fovea and 9dB at an eccentricity of 20°, on the HFA (Sample et al. 1996). This amount of isolation was thought to be appropriate for the investigation of patients with paracentral defect depths up to 12-14dB in standard perimetry (Demirel & Johnson 2000). Greater defect depths which exceed the amount of isolation alter detection of the blue stimulus such that it is no longer be mediated purely by the short-wavelength sensitive pathway (Demirel & Johnson 2000; Felius et al. 1995). In such circumstances, stimulus detection is mediated by the medium- and long-wavelength sensitive mechanisms, which are the mechanisms underlying detection in standard perimetry (Demirel & Johnson 2000; Felius et al. 1995; Lewis et al. 1993). Thus there is no benefit in examination by SWAP over standard perimetry in the presence of a large defect (Hart et al. 1990, Wild 2001). Use of a 450nm narrowband stimulus has been advocated in SWAP, since this would improve the dynamic range and diminish between-subject variability (Cubbidge & Wild 2001).

The optimal conditions for SWAP depend on the background and stimulus parameters providing the maximum isolation of the short-wavelength sensitive pathway, the dynamic range, pupil size, optical defocus and pre-retinal absorption. Adequate saturation of the rod pathway was thought to be achieved by yellow backgrounds with intensities of 300cd/m^2 (Yeh et al. 1989) and 330cd/m^2 (Hudson et al. 1993). The bright backgrounds generated more light scatter and backgrounds greater than 80.9cd/m^2 were deemed only to increase thresholds rather than increase the magnitude of isolation (Sample & Weinreb 1990). Two types of stimuli were used in the modified versions; a narrowband with a peak at 440nm or a broadband with a peak

at 460nm. The broadband stimulus achieved a greater dynamic range (Moss et al. 1995) but stimulated the medium-wavelength sensitive pathway in the presence of a large defect (Sample & Weinreb 1990). The narrowband stimulus was less influenced by ocular media absorption (Sample et al. 1996).

SWAP exhibits a larger between-subject and within test variability than standard perimetry (Blumenthal et al. 2000; Hutchings et al. 2001; Kwon et al. 1998; Wild et al. 1995; Wild 2001). Indeed, the frequency-of-seeing curve was significantly flatter in SWAP than in standard perimetry, which explains the greater measurement variability (Gilmore et al. 2005). The sensitivity decline with increased age is greater in SWAP than in standard perimetry, especially at eccentricities of greater than 10°, after correction for ocular media absorption (Johnson et al. 1988a; Wild et al. 1998). Within-subject variability of short-wavelength sensitivity becomes greater with advancing age (Remky et al. 2001a).

The principal confounding factors in the interpretation of SWAP are pre-receptoral absorption of the stimulus, due to lenticular and macular pigment absorption; and additionally learning and fatigue effects are greater for SWAP than for standard perimetry. SWAP data can be manipulated statistically to enhance interpretation. Additionally knowledge of the LF in SWAP will improve understanding of progression of sensitivity loss.

1.2.1 Pre-receptoral Absorption

1.2.1.1 Macular Pigment

Macular pigment is composed of two xanthophyll carotenoids, lutein and zeaxanthin (Bone et al. 1985). It has a peak density at the centre of the fovea, which reduces to an eccentricity of 5°, where it is optically undetectable (Snodderly et al. 1984). There are several psychophysical and optical techniques of measuring macular pigment optical density including heterochromic flicker frequency, minimum motion photometry, raman spectrometry, imaging reflectometry, autofluorescence spectrophotometry and

imaging (Wolf 2006). There is a large between-subject (Hammond et al. 1997; Pease et al. 1987) and within-subject (Hammond & Fuld 1992; Wild & Hudson 1995) variation in macular pigment measures in normal observers.

Macular pigment is thought to be protective against age-related macular degeneration (AMD) (Beatty et al. 1999) and has been measured in relation to known risk factors of AMD. In a large sample study (n = 800), of healthy subjects aged 20-60 years, macular pigment optical density was significantly reduced with advancing age, current or past smoking, and family history of AMD, but not female gender (Nolan et al. 2007). In the same study, no significant interocular difference was found. Other groups have measured an age-related decline in macular pigment (Beatty et al. 2001; Neelam et al. 2005). Fellow eyes of neovascular AMD were also found to have significantly reduced macular pigment (Beatty et al. 2001). In a small sample, smokers were found to have less macular pigment than non-smokers (Hammond et al. 1996c). Males were found to have more macular pigment than females (Hammond et al. 1996a). Eyes with lighter iris colour were reported to have a significantly lower macular pigment density (Hammond et al. 1996b). Studies have shown that lutein and zeaxanthin in the diet have a protective effect against exudative AMD (Seddon et al. 1994). Examples of food sources rich in these carotenoids are spinach and sweetcorn.

Macular pigment absorbs short-wavelength light. The absorption spectrum of macular pigment has a peak at 460nm, thereby decreasing macular sensitivity to short-wavelength light (Pease et al. 1987) and it does not absorb wavelengths greater than 560nm (Bone et al. 1985). The influence of macular pigment on SWAP is limited to the fovea, where it may cause a depression in the hill of vision and an increase in the SF in the foveal region (Wild & Hudson 1995). Macular pigment absorption, measured using a HFA with modifications, was found to be negligible at 5.5° (Wild & Hudson 1995). The combined effects of absorption due to ocular media and macular pigment on

SWAP were measured to be 0.8 log units at the fovea and around 0.4 log units at other eccentricities (Wild & Hudson 1995).

1.2.1.2 Ocular Media

The interpretation of SWAP is also confounded by the ocular media, which absorbs short-wavelength light (Sample et al. 1988, 1989). Short-wavelength light is also scattered by the ocular media (Moss et al. 1995). There are two components of scatter, forward scatter and back scatter. Forward scatter or veiling glare, is that which is directed towards the retina. It is increased by cataract, particularly posterior subcapsular cataract and preferentially affects the short-wavelength sensitive cone pathway, by reducing the height of the hill of vision in SWAP (Moss et al. 1995). Back scatter is that which is directed in the opposite direction, away from the lens. Only a limited correlation between forward and backward scatter exists (de Waard et al. 1992). Scatter is considered to have less impact than absorption, since it is less dependent upon wavelength.

Ocular media absorption increases with age (Sample et al. 1988; Wild et al. 1998). This was discovered to be a linear relationship (Wild et al. 1998). With the exception of the lens, the ocular media absorption is independent of wavelength and exhibits little variation in transmittance with age (Wyszecki & Stiles 1982). Lens density increases gradually with age, the greatest increase being between the ages of 60 and 70 yrs (Sample et al. 1988). Older patients gave rise to larger between-individual variations. As expected, pseudophakic eyes had lower lens density index values compared to eyes with cataract, when controlled for age (Sample et al. 1988).

A method of measuring the lens density index was derived, using modifications to a perimeter in which scotopic thresholds were determined for 560nm & 410nm stimuli presented at an eccentricity of 15°, following 30 mins of dark adaptation (Sample et al. 1989). The selected wavelengths have equal sensitivity to rhodopsin, therefore the differences in threshold are due to wavelength dependent absorption by the ocular

media, and can be used as an index of lens density (Sample et al. 1989). Another group used a fluorometer to measure lens autofluorescence and found significant correlation of the lens transmission index with SWAP sensitivities (Teesalu et al. 1997).

Cataracts, which are related to increased lens density, profoundly affect perimetry, such that a general reduction in sensitivity occurs (Moss et al. 1995). Increase in lens density was found to cause diffuse reduction in the short-wavelength visual field (Sample et al. 1994). The relationship between lens density and short-wavelength threshold was linear (Sample et al. 1994). Posterior subcapsular cataract had a greater effect than other types of cataract on SWAP mean deviation (Moss et al. 1995). The increase in ocular media absorption for short wavelengths with age, was measured to be 0.03-0.06 log units per decade and the ocular media was asserted to account for 30-40% of the SWAP sensitivity decline with age (Johnson et al. 1988a).

The influence of applying a correction to SWAP thresholds for the influence for lenticular absorption is ambiguous. Methods implementing the correction of SWAP sensitivity involved the addition of the ocular media absorption value to each point in the visual field (Moss et al. 1995). The age decline in SWAP sensitivity was noted to increase with greater eccentricities, especially in the superior field at eccentricities greater than 9°, after correction for ocular media absorption (Wild et al. 1998). Correction for ocular media in SWAP had the effect of increasing the MS at each point, however the standard deviation remained unchanged (Wild et al. 1995). The reduction in the general height of the hill of vision due to ocular media absorption, increases with a decrease of stimulus wavelength. Before correction for ocular media, the distribution of sensitivities for SWAP on the HFA was found to have an overall Gaussian distribution. However after correction for ocular media, it was entirely Gaussian (Wild et al. 1998).

Some investigators noted that correcting for ocular media decreased the between-individual variability found in SWAP, and also improved the confidence limits predictive

of change (Wild et al. 1998). Ocular media correction was also found not to have any significant effect on between subject variability of SWAP sensitivities (Wild et al. 1995). Conversely, other investigators have shown that correcting for absorption increases between-subject variability, thereby hindering interpretation (Johnson et al. 1988a). It was suggested that this increase may be due to the correction factor for ocular media absorption having a relationship to the SWAP sensitivities. Eyes with greater ocular media correction factors were found to have the highest SWAP sensitivities. Thus increased lens yellowing was suggested to have a protective effect against damage from light, on SWAP sensitivities (Johnson et al. 1988a). Another reason for the finding of increased variability after correction for absorption could be due to the assumptions made about the retinal threshold, when making the correction measurements. In many cases the retina is abnormal and has altered threshold properties, when the correction measurements are made. Prior to the commercial availability of perimeter hardware to implement SWAP, instrumentation for early research involving SWAP was a modified HFA. This employed differing parameters to the currently commercially available SWAP, which may also explain some differences in the results regarding variability.

It has previously been advocated that correction for lenticular absorption is unnecessary in SWAP, due to the diffuse nature of the change in the visual field with increasing lens density (Sample et al. 1994). Glaucoma diagnosis in SWAP was similar from fields with and without lens density testing, based on results of the Glaucoma Hemifield Test (Sample et al. 1994). Despite the difficulty in differentiating lens effects from glaucomatous diffuse loss, diffuse loss due to glaucoma alone is uncommon, occurring in 4.4% of subjects (n=113) (Chauhan et al. 1997). There is no significant difference between the lens density index of normal and glaucoma patients (Sample et al. 1988). The duration of lens density testing at the perimeter is 40 minutes, which is clinically impractical due to the effects of fatigue.

Although macular pigment absorption may attenuate central threshold values of the 10° SWAP visual field, any correction for pre-receptoral absorption would artificially increase the perimetric sensitivity. There are several other factors which confound the correction of SWAP thresholds for macular pigment absorption. The large between-subject (Pease et al. 1987; Hammond et al. 1997) and within-subject (Hammond & Fuld 1992; Wild & Hudson 1995) variability in the measurement of macular pigment absorption would introduce a further source of fluctuation to the data. How the correction of SWAP for macular pigment absorption affects the normal prediction limits is currently unknown. Correction for pre-receptoral absorption does not take into account the difficulty in stimulus detection caused by reduced stimulus contrast nor the effects of light scatter. Additionally, commercially available measures of macular pigment absorption generate a single figure, rather than a range of measures for each eccentricity. The measurement of the complete distribution of the profile of macular pigment optical density, which peaks at the fovea and declines with increasing eccentricity, is very time consuming and is difficult for some subjects, especially those with impaired vision (Bone & Landrum 2004). Thus any potential correction for macular pigment absorption cannot easily take this distribution into account. Furthermore, methods that employ retinal adaptation to measure macular pigment and ocular media absorption assume normal retinal function (Sample et al. 1988; Wild et al. 1995; Wild et al. 1998; Wild & Hudson 1995) which is incorrect in the presence of retinal disease.

The effects of pre-retinal absorption on the SWAP visual field are symmetrical and characterised by diffuse loss, therefore the use of a statistical approach has been recommended to separate focal loss by analysis of change to the shape of the hill of vision and hemifield comparisons (Wild & Hudson 1995; Sample et al. 1994). Furthermore, the psychophysical measures of ocular media and macula pigment absorption are time consuming and arduous for the patient and thus are not clinically viable.

1.2.1.3 The Lens Opacities Classification System

The Lens Opacities Classification System (LOCS) is a classification system, in which cataract severity is graded, in terms of nuclear colour (NC), nuclear opalescence (NO), cortical cataract (C) and posterior subcapsular cataract (P) (Chylack et al. 1993). LOCS is a measure of back scatter (Moss et al. 1995). LOCS III, which was updated from a more basic version, LOCS II (Chylack et al. 1989), has a six step scale for NO and NC, and five grades of C and P. More precise grading may be made by decimalising ten intervals between steps, although this reduces agreement between graders (Chylack et al. 1993).

Grading is carried out by comparison to standardised photographs, originally with slit-lamp photographs of cataract. When carried out at the slit-lamp, grading was found to be only slightly less accurate than photographic grading (Karbassi et al. 1993). The classification, NO, is assessed by the average opalescence of the entire nucleus. To grade NC, the nucleus is viewed in cross-section to evaluate nuclear brunescence quality of brunescent colour from the posterior reflex. The combined area of C opacities, graded by retro-illumination, is measured in comparison to the standard photographs. Posteriorly focused retro-illumination images are used to grade P opacities, which should be located centrally, rather than peripherally (Chylack et al. 1993).

The influence of ocular media on SWAP is to limit the dynamic range and increase between-subject variability. Consequently several studies involving SWAP, have excluded patients with lens changes greater than NCIII (nuclear colour III), NOIII (nuclear opalescence III), CI (cortical I), or PI (posterior subcapsular I), according to LOCS III (Cubbidge et al. 2002; Remky et al. 2001b; Wild et al. 1998).

1.2.2 The Learning Effect in SWAP

SWAP is a more physically difficult task than standard perimetry, as the examination duration is longer and the resolution of the short-wavelength sensitive pathway is poor

(Green 1968; Kelly 1973; Rabin & Adams 1990; Swanson 1989). The between- and within-examination variability and the between-subject variability is greater in SWAP than in standard perimetry (Wild et al. 1998). The greater between-subject variability in SWAP increases with greater eccentricity away from fixation (Kwon et al. 1998; Wild et al. 1998). Therefore, confidence intervals for normality in SWAP are larger than in standard perimetry (Wild et al. 1998) and it would be expected that learning effects have a greater magnitude in SWAP compared to standard perimetry (Gardiner et al. 2008).

Previous experience of standard perimetry does not influence the learning effect in SWAP (Wild & Moss 1996; Zhong et al. 2008). In explanation, standard perimetry involves the detection of a difference in luminance, whereas SWAP requires detection of the chromatic difference of the blue stimulus on the yellow background (Wild et al. 2006). The learning effect involving the luminance detection mechanism cannot transfer directly to the mechanism governing detection of chromatic difference.

Unlike in standard perimetry where the greatest learning effect takes place between the first two examinations (Heijl & Bengtsson 1996), the learning effect in SWAP was noted to remain present until the 4th examination in normal subjects (Wild & Moss 1996) and in ocular hypertensives (Rossetti et al. 2006). Additionally, the learning effect in SWAP was found to be present over 5 examinations in patients with ocular hypertension and open-angle glaucoma, with the greatest improvements in performance seen in the first 3 visits (Wild et al. 2006). In contrast, the learning effect was reported to have no significant effect on global indices by the third visit, leading to a recommendation of one training session for SWAP examinations (Zhong et al. 2008). The learning effect in SWAP was measured to be an 8.2% improvement in global MS, in the first eye examined, at the fourth examination (Wild & Moss 1996). In a study spanning 8 years the learning effect in SWAP was seen to be in effect until the 6th year in early and suspect glaucoma patients, who were tested infrequently as experienced in a clinical

situation (Gardiner et al. 2008). Mean deviation was the visual field parameter which was most sensitive to change, in the detection of a learning effect in glaucoma patients (Rossetti et al. 2006). The learning effect in SWAP in the 24-2 field varied greatly between individuals, using a HFA 750 (Wild et al. 2006).

Learning and fatigue effects work in opposition to each other (Hudson et al. 1994). In the second eye tested, the fatigue effect would appear to diminish the learning effect (Wild et al. 2006). In order for the learning effect to be detected, it must have a greater magnitude than the fatigue effect (Wild & Moss 1996). The effect of fatigue has not been widely investigated in SWAP. When investigating standard fields and SWAP fields in patients with neuro-ophthalmic disorders, fatigue effects were discovered (Keltner & Johnson 1995). Performance was seen to be worsened in the field carried out last in the order of examinations, for both SWAP and standard fields. The use of a translucent occluder was found to reduce the sensitivity decline due to fatigue in SWAP and fatigue effects in normal subjects were found to be greater for SWAP than standard perimetry (Cubbidge 1997).

1.2.3 Statistical Interpretation of SWAP

Interpretation in SWAP has more variability than in standard perimetry when detecting progression and detecting abnormality. Optimisation of the parameters of SWAP and improvement of threshold estimating algorithms increases accuracy for interpretation.

Glaucomatous visual field loss was found to be significantly larger in SWAP than in standard perimetry (Hart et al. 1990; Sample & Weinreb 1990) and progression was noted to be detected earlier (Johnson et al. 1993b,c; Sample & Weinreb 1992). Despite this, SWAP did not gain widespread clinical use due to the increased variability in the 30° visual field. In order for a defect to achieve statistical significance, it must be deeper, due to the greater between-subject variability. The increased between-subject variability of SWAP reduces confidence limits when interpreting loss (Wild et al. 1995). SWAP also exhibits a greater short-term fluctuation (SF) than standard perimetry

(Kwon et al. 1998; Wild et al. 1995; Wild et al. 1998). In normal subjects the SF was 1.89dB and 1.61dB in SWAP and standard perimetry, respectively, using the FASTPAC strategy (Wild et al. 1998). Furthermore, the sensitivity decline with advancing age in the normal eye is greater for SWAP than standard perimetry. After correction for ocular media absorption, 1.43dB of loss per decade was found for SWAP, compared to 0.72dB loss per decade in standard perimetry, in the 30-2 field (Wild et al. 1998). In the 10° field, the average loss per decade was 0.89dB and 0.45dB for SWAP and standard perimetry, respectively (Conway 2003).

Adapting the threshold estimating algorithm can improve on the intrinsic variability in SWAP. Previously the FASTPAC strategy has been recommended in SWAP, over the Full Threshold strategy as it offered a reduced examination duration with no deterioration in staircase efficiency (Wild et al. 1998). FASTPAC was also quoted to be appropriate for long-term follow-up in SWAP (Cubbidge et al. 2002). More recently, SITA has been applied to SWAP and reduced the examination duration by 70% compared to the Full Threshold strategy (Bengtsson & Heijl 2003). In normal subjects, SITA SWAP yielded higher sensitivities and diminished between-subject variability (Bengtsson & Heijl 2003). SITA SWAP and the Full Threshold algorithm were found to identify glaucomatous visual field loss comparably (Bengtsson & Heijl 2006). However, SITA SWAP has only been applied to the 30-2 and 24-2 visual field patterns and is not yet available for the 10-2 pattern.

Focal loss in glaucoma was demonstrated to be wider and deeper in SWAP, than in standard perimetry (Wild et al. 1995). Statistically raising or lowering the height of the hill of vision can greatly influence the depth of focal loss seen in the pattern deviation plot. Despite the potentially obscured interpretation of diffuse loss by pre-receptoral absorption, in central retinal conditions such as AMD, focal rather than diffuse loss is of more importance.

1.2.4 Spatial Filtering

Spatial filtering is an image processing technique for the enhancement of digital information. In standard perimetry, a Gaussian filter has been applied to threshold sensitivity values (Crabb et al. 1995; Fitzke et al. 1995). The filter is calculated using a 3 x 3 grid. The central point is replaced by a weighted average of the points in the grid, according to their proximity to the centre. The filter is passed over each location in the field, with the exception of the most peripheral locations. This "smoothing" process decreased between examination variability and noise (Crabb et al. 1997) and improved repeatability (Fitzke et al. 1995). Using an alternative approach to spatial filtering, a median filter was applied to perimetric thresholds (Crabb et al. 1995; Fitzke et al. 1995). Similar to the 3 x 3 grid in the Gaussian filter, the new filtered value simply becomes the median or middle value of the nine points in the grid (Figure 1-6).

A global index was derived from the median filter, the local spatial variability (LSV), in which the level of variability removed by the process was quantified (Crabb et al. 1995). The pointwise sensitivity difference, between the raw field and the filtered field, gives the *residuals*. The root mean square of the residuals is a summary measure which describes the LSV. If the LSV is large, this indicates an irregular field. LSV was shown to be significantly correlated with global indices, SF and pattern standard deviation (PSD) (Crabb et al. 1995). LSV is a relatively unmanipulated index since it is determined without reference data from normal subjects or replicate threshold measurements. It is a measure of focal loss which does not incorporate the measurement of the height of the hill of vision.

The spatial processing technique was used in the determination of glaucomatous progression (Crabb et al. 1997). Hemifields were processed separately due to their physiologic independence, which excluded further points from the filter at edges, corners and along the horizontal meridian. Pointwise linear regression was used to model change in sensitivity over time. Analysis of the difference between predicted

change and actual change at 1- and 2-year follow up fields was determined for comparison with and without spatial filtering. Spatial filtering improved the predictive performance, to a greater extent at the 2-year follow up (Crabb et al. 1997).

The reduced variability achieved by spatial processing acts to reduce the LF. This decreases the necessity for repeat testing to detect change and thus lessens the burden on resources. In contrast, the Gaussian filter may be less efficient at detecting small amounts of loss, whereby diminished sensitivity in a minimal number of locations may be averaged out in the filter. This disadvantage has more impact in the 30° field than the 10° field, which is the principal area of interest in AMD.

The Gaussian filter does not take into account the anatomical structure of the retinal nerve fibre layer. Gardiner et al. (2004) designed a new spatial filter to take into account the structure of the nerve fibre layer, using a database of the visual fields of 14,675 suspected glaucomatous patients. The correlations and covariances between sensitivities of glaucomatous visual field points were analysed to develop the filter (Gardiner et al. 2004; Strouthidis et al. 2006). Computer simulated visual fields tested the novel filter which was found to diminish noise in glaucoma (Gardiner et al. 2004). Detection of glaucomatous progression using the novel filter resulted in similar specificity to the use of PLR with confirmatory testing, but had a greater rate of progression detection, in ocular hypertensive patients (Strouthidis et al. 2007).

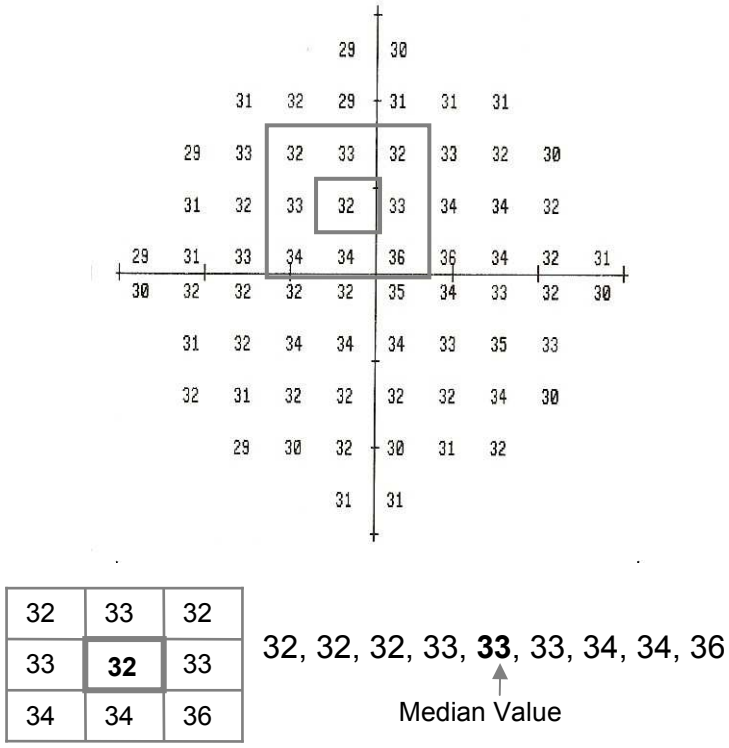

32	33	32
33	**32**	33
34	34	36

32, 32, 32, 33, **33**, 33, 34, 34, 36

Median Value

Figure 1-6. Spatial filtering: a median filter

1.2.5 Long-term Fluctuation in SWAP

Long-term fluctuation (LF) is the measure of variability, aside from the SF, between two or more visual field examinations, in the absence of pathologic changes. Identification of the LF and SF facilitates detection of significant change due to disease progression. The global index of LF has not been calculated for previous visual field studies with AMD patients.

LF has been reported to be correlated with eccentricity, differential light sensitivity, mean visual field defect, age, IOP and SF (Kwon et al. 1998). Both SF and LF have a greater magnitude in SWAP than in standard perimetry, in normal patients (Kwon et al. 1998). In glaucoma patients LF was also illustrated as being greater for SWAP than standard perimetry (Blumenthal et al. 2000; Hutchings et al. 2001).

Various different statistical methods have been adopted to measure LF in SWAP, not all of which have measured LF(He) and LF(Ho) components separately. Kwon et al (1998) determined the LF for normal subjects, by calculating the statistical variance (in dB^2) of threshold sensitivities from four sequential SWAP exams. LF was found to increase with eccentricity. Other investigators defined an index of long-term variability, which incorporates LF as well as SF. Long-term variability was calculated as the average SD of three fields for each point in the field (Blumenthal et al. 2000). For stable primary open-angle glaucoma patients, long-term variability was 0.55dB greater in SWAP than in standard perimetry (Blumenthal et al. 2000). The explanation given for favouring the calculation of long-term variability over LF in this study, was due to the relatively few locations used to determine SF in the HFA Program 24-2. It was suggested that since SF is location dependent, it was not appropriate to use the global SF, calculated from only 10 locations, for each point in the entire field (Blumenthal et al. 2000). A method which did determine separately the LF(He), LF(Ho) and error components of LF, in glaucoma suspects and stable primary open-angle glaucoma patients, in SWAP, incorporated a two-factor ANOVA with replications (Hutchings et al.

2001). As part of a progression study, long-term variability was calculated using the 99th percentile of the standard deviations of thresholds over three examinations, in patients with stable glaucoma (Kono et al. 2000). Two types of variability were defined. The variability of fixed location analysed pointwise change over time and the variability of ranked location examined the variability of the Cumulative Defect or Bebié Curve. The variability was found to increase with decreasing sensitivity (Kono et al. 2000).

1.2.6 Visual Field Progression in SWAP

Various investigators have identified glaucomatous visual field progression in SWAP which precedes the progression in standard perimetry (Johnson 1993b,c; Sample & Weinreb 1992, Sample et al. 1993, Demirel & Johnson 2001). These studies have employed differing analytical methods in order to define visual field abnormalities and detect progression.

In a pair of longitudinal studies which examined patients annually over 5 years, SWAP defects were found to occur three to four years earlier than defects in standard perimetry in 38 patients with ocular hypertension (Johnson et al. 1993b) and 16 patients with early glaucoma (Johnson et al. 1993c). Progression was defined in terms of abnormal stimulus locations, which were considered abnormal if they fell outside of the confidence intervals of a normal database. The normal database was collected during the same study and consisted of SWAP data derived from 62 subjects (Johnson et al. 1993b,c).

Another longitudinal study in which progressive loss in SWAP was noted sooner than loss in standard perimetry, assessed 21 patients with primary open-angle glaucoma over two visits separated by 6 to 26 months (Sample & Weinreb 1992). Thresholds were considered abnormal if they deviated by predefined absolute values from thresholds of 21 age-matched normal subjects. Progression was determined by the number of abnormal thresholds increasing globally, pointwise and in quadrants (Sample & Weinreb 1992).

The prevalence and incidence of SWAP abnormalities was inspected in a prospective study of 250 ocular hypertensive patients, who were examined annually over a period of 5 years (Demirel & Johnson 2001). In the patient group, there was a greater prevalence of SWAP field defects occurring; 9.4% in SWAP and 1.2% in standard perimetry. However the incidence of new defects occurred at a similar rate of approx 1.2% per year for both perimetry types (Demirel & Johnson 2001). Visual field deficits were defined according to whether the average sensitivity values in ten zones of the Glaucoma Hemifield Test (Åsman & Heijl 1992) fell within the calculated confidence intervals from 60 normal subjects tested in the same study. It was discovered that newly developed SWAP defects were more prominent and more persistent than new defects in standard perimetry (Demirel & Johnson 2001).

Sample et al. (1993) demonstrated the predictive ability of SWAP in 25 ocular hypertensive patients followed over 12 to 37 months (Sample et al. 1993). The risk of developing glaucoma was assessed and the subsequent development of glaucoma occurred in five eyes. These five eyes had previously been classified as high or medium risk, due to significantly higher MD and number of defects than the other eyes. Other researchers have investigated the predictive power of SWAP in 152 patients with primary open-angle glaucoma over 30 months (Bayer & Erb 2002). Progression was defined when the appearance of a new defect occurred, which had to be a cluster of three or more points depressed by a specified decline of absolute values in dB, from a previously normal region of the visual field. SWAP was found to predict future progression of standard visual field defects in nearly 80% of glaucomatous eyes, within 6 to 24 months (Bayer & Erb 2002). In another study, which examined 160 eyes of 83 subjects, good predictive ability of SWAP and structural assessment of the retinal nerve fibre layer were found, in detecting perimetric loss in suspect glaucoma patients (Polo et al. 2002). Initial SWAP abnormalities and nerve fibre layer losses predicted

standard perimetry loss after three years with a sensitivity of 93% and 73%, respectively (Polo et al. 2002).

Other methods of quantifying progressive visual field loss in SWAP have been described. Progressive loss was presented based on the Cumulative Defect Curve and pointwise analysis in a study of 85 glaucoma patients followed over 52 months (Kono et al. 2000). The long-term variability was subtracted from the baseline curve, which was compared to a follow-up curve, in order to detect progression. Pointwise deterioration was identified if the decline between follow-up and baseline exceeded the long-term variability at each stimulus location. A significant correlation was noted between the curve and pointwise progression for the number of locations exhibiting progression. It was argued that the ranking of Cumulative Defect Curves is insensitive to spatial information and does not account for the regional dependent physiological threshold variation, thus has limited ability in separating diffuse and focal loss (Åsman & Olsson 1995).

Several study designs incorporated both SWAP and frequency doubling technology (FDT; see Chapter 1.4.3.6.) to investigate glaucomatous progression (Bayer & Erb 2002; Horn et al. 2007; Landers et al. 2003b; Leeprechanon et al. 2007). It was determined that FDT could predict glaucomatous change in standard perimetry in the same way as SWAP (Bayer & Erb; Landers et al. 2003b). SWAP and FDT showed similar abilities in the detection of glaucomatous loss (Bayer & Erb 2002; Leeprechanon et al. 2007) and the combination of both types of perimetry yielded better diagnostic results than each test performed separately (Horn et al. 2007).

1.2.7 SWAP and Diabetes

The comparison between SWAP and standard perimetry in diabetic patients has been made in numerous studies (Afrashi et al. 2003; Agardh et al. 2006; Bengtsson et al. 2005; Bengtsson et al. 2008; Hudson et al. 1998; Remky et al. 2000; Remky et al. 2003). The 10° SWAP visual field was implicated as a useful measure in defining

functional loss in patients with early ischaemic damage to the macula (Agardh et al. 2006; Remky et al. 2000). The relationship between perimetry and damage of the perifoveal capillary network due to diabetes was evaluated and a stronger relationship was discerned in SWAP than in standard perimetry (Remky et al. 2000). In SWAP, eyes with macular oedema displayed a greater number of depressed points compared to eyes without macular oedema, whereas no difference between groups was observed in standard perimetry (Agardh et al. 2006). Clinically significant macular oedema was detected using an analysis of asymmetry between the hemifields of the 10° field, which was designed to negate pre-receptoral absorption effects (Hudson et al. 1998). SWAP detected macular oedema with greater sensitivity than standard perimetry (Hudson et al. 1998). In the 30° field, more severe SWAP MD values were reported in diabetic patients with no retinopathy when compared to control subjects, however the indices of focal loss were not different between groups (Afrashi et al. 2003). In contrast, focal loss was better detected by SWAP than by standard perimetry in diabetic retinopathy (Bengtsson et al. 2005). This was observed in the correlation of structural retinal measures on fundus photographs to the number of depressed points within a 6° radius of the visual field (Bengtsson et al. 2005). Standard perimetry and SWAP performed similarly when monitoring visual function in the 24-2 visual field in patients with various degrees of diabetic retinopathy (Bengtsson et al. 2008)

1.2.8 Summary

The greater variability of the SWAP visual field in comparison to standard perimetry requires greater change to occur before progression can be reliably discerned (Wild 2001). However, other factors should be considered when evaluating the effectiveness of SWAP. SWAP has demonstrated an increased sensitivity in progression detection. Newer threshold estimating algorithms such as SITA SWAP have reduced threshold variability in SWAP but they have not been applied to the 10-2 spatial grid. Additionally, the application of statistical procedures such as spatial filtering and the

separation of focal from diffuse loss act to improve the usefulness of SWAP in the measurement of visual field loss.

1.3 Structural Changes in Age-Related Macular Degeneration (AMD)

1.3.1 Introduction

AMD is a disease affecting the central vision of individuals over the age of 45. Late stage AMD causes severe visual loss and is one of the most common reasons for visual impairment leading to blindness in western industrialised countries. In the UK, 3.7% of the population aged 75 years or older and 14.4% aged over 90 years have visual impairment due to AMD (Evans et al. 2004). Pooled data from several population based studies indicates that in the US, the prevalence of late stage AMD is 1.47% of the population over the age of 40, or 1.75 million individuals; and in Western Europe, there are 3.35 million cases of AMD (Friedman et al. 2004). In the future, it is expected that these figures will increase due to the expanding elderly population.

Initial signs of AMD seen in the fundus are drusen. Derived from the German word *druse*, meaning a crust of crystals lining a rock cavity, the plural, drusen refer to small yellow-white deposits of extracellular material between the basement membrane of the retinal pigment epithelium (RPE) and the inner collagenous zone of Bruch's membrane. Many types of drusen have been identified including hard and soft drusen. Drusen change in number, size, colour & distribution gradually (Gass et al. 1973). Hard drusen are yellow, punctuate deposits smaller than 63μm and if seen in large numbers, may predispose to soft indistinct drusen and pigmentary changes (Klein et al. 2007). As drusen increase in size, their borders merge to become confluent. Histologically, drusen larger than 63μm have a lobulated appearance on light microscopy which suggests they are formed by confluence of a group of drusen (Sarks et al. 1999). Soft drusen are subcategorised into distinct and indistinct. Distinct drusen have uniform density, sharp edges and a solid appearance and indistinct drusen have decreasing density from centre to periphery and fuzzy borders (Klein et al. 1991). Incidence data

collected in the Rotterdam study confirmed the natural course of AMD as the progression of hard drusen to soft distinct drusen to soft indistinct drusen (van Leeuwen et al. 2003b). Reticular pseudodrusen refer to a yellowish indistinct interlacing network, 125μm to 250μm in diameter (Arnold et al. 1995). They are typically distributed along the arcades, especially the superior arcade. Pigmentary changes may occur as hyperpigmentation or hypopigmentation of the RPE. The presence of pigmentary changes poses a greater risk to the development of atrophic or neovascular AMD (van Leeuwen et al. 2003b). Geographic atrophy (GA) is later seen as areas of circumscribed atrophy of the RPE, beneath which choroidal vessels are more visible, and may occur with regression of soft drusen (Fine et al. 1999). GA progresses slowly and often spares the foveal avascular zone until later in the course of the disease (Sunness 1999). Late stage exudative disease occurs when the RPE separates from Bruch's membrane and a pigment epithelial detachment (PED) occurs. The confluence of several soft drusen may result in a drusenoid pigmentary epithelial detachment (Fine et al. 1999; Hartnett et al. 1992). The PED may be further complicated by choroidal neovascularisation, whereby abnormal new vessels from the choriocapillaris breach Bruch's membrane and invade in the direction of the RPE (Fine et al. 1999). The new vessels are compromised and leak serous fluid and blood. Finally, a disciform scar is left, in which the structure of the retina is disrupted and lacks perfusion. The amount of scar tissue formed depends on the duration and extent of haemorrhage and exudation.

The pathogenesis of AMD is unknown. Several theories have been proposed, including oxidative stress, Bruch's membrane abnormalities, ocular blood flow changes and inflammatory processes (Ambati et al. 2003; Holz et al. 2004; Zarbin 2004). The retina is particularly susceptible to oxidative damage caused by reactive oxygen intermediates (ROI). Examples of ROI include free radicals, hydrogen peroxide and singlet oxygen. The RPE phagocytosis of photoreceptor outer segments generates

ROI. Lipofuscin is a group of autofluorescent lipid and protein aggregates. The formation of lipofuscin has been linked to oxidatively damaged photoreceptor outer segments. Lipofuscin accumulates in RPE cells, causing a mechanical disruption to RPE function. The role of macular pigment in absorbing blue light and quenching ROI is thought to limit retinal oxidative damage (Beatty et al. 2000). One of the mechanisms which generates ROI in the retina is light exposure (Beatty et al. 2000). Blue light, which carries more energy than longer wavelength light, has been found to cause photoreceptor cell death by apoptosis in the rat retina (Wu et al. 1999) and has been linked to neovascular AMD in patients with low plasma antioxidant levels in the European Eye study (Fletcher et al. 2008). Bruch's membrane lies between the choriocapillaris and the RPE, and maintains photoreceptor homeostasis. Extracellular material containing lipid accumulates in Bruch's membrane, which may disturb its integrity and thus may affect the development of AMD (Ambati et al. 2003). The abnormal material manifests as drusen, and is likely to originate in the RPE. Impaired choroidal blood flow has been suggested to be related to the pathogenesis of AMD, in which lack of perfusion could lead to loss or dysfunction of RPE cells, however the evidence does not directly indicate that vascular abnormalities precede the development of AMD (Erlich et al. 2008). Evidence for the role of inflammation in the pathogenesis of AMD has been determined in the molecular composition of drusen and neovascular complexes (Zarbin et al. 2004). The involvement of growth factors in the mechanism of neovascularisation in AMD, have been postulated, including vascular endothelial growth factor (VEGF) (Das & McGuire 2003; Holtz et al. 2004). VEGF inhibitors are routinely used in the treatment of exudative AMD.

1.3.2 Risk Factors of AMD

The known risks factors of AMD include age, smoking, hypertension, female gender, social background, diet and genetic factors. Other risk factors involving signs of disease in the eye have been considered.

Age has been identified as a principal risk factor of AMD. Analysis of pooled data from several population studies illustrates a strong age-related increase in the prevalence of large drusen, GA, neovascular AMD, and any AMD (Friedman et al. 2004). In the UK, smokers aged over 75 were twice as likely to have AMD as non-smokers (Evans et al. 2005). Increased chance of development of neovascular AMD was discovered in smokers (Yanuzzi et al. 1992). Indeed, smoking was found to be a major risk factor in thirteen studies (Thornton et al. 2005). Men who were current smokers of more than 20 cigarettes a day were found to have an increased risk compared to those who smoked less (Christen et al. 1996). In women the risk of AMD increased with an increasing number of pack-years (Seddon et al. 1996). Association of atherosclerosis with AMD has been reported (Friedman 2000). Inconsistency exists regarding hypertension as a risk factor, since it has been found to be associated with neovascular AMD (Hyman et al. 2000) and was also found to have no association with early AMD (Klein et al. 2003). Diabetes is not thought to be related to increased risk of AMD (Klein et al. 2003). Women were found to be at a greater risk of developing neovascular disease than men (Mitchell et al. 2002). Despite the consistent agreement between population based studies that women have a slightly increased risk, it has been speculated that age effects may not have been completely excluded from this estimate (Evans 2001). The use of hormone replacement therapy has been shown to reduce the likelihood of large drusen and women who have had a greater number of births were found to have more large drusen (Freeman et al. 2005). The prevalence of AMD was less widespread in black than in white patients for neovascular AMD in the AREDS study (Milton et al. 2005) and for any AMD in another study (Klein et al. 2003). Social class and years of education have also been suggested to have an impact on AMD, although these factors are difficult to control for. In a study of South-East Asian patients, a lower level of education was significantly associated with early AMD (Cackett et al. 2008). Dietary fat intake, especially in processed baked goods was associated with increased risk of AMD progression and fish intake due to omega-3 fatty

acids was observed to have a protective effect (Seddon et al. 2003b). Antioxidant micronutrient intake has been shown to reduce risk of disease (AREDS 2001a). A greater body mass index, above 25, was demonstrated to increase the risk of progression of the disease (Seddon et al. 2003a). A weak association between hyperopia and AMD has been suggested (Wang et al. 2004), and the risk of AMD has been reported to be lower in highly myopic eyes in a Chinese population (Xu et al. 2007). Genetic factors have been investigated, as family history is an established risk factor of AMD (Klein et al. 1994) and several genetic variants have been strongly associated with AMD (Haddad et al. 2006). Variation in geographic location has different incidences of AMD, although this could be attributed to differences in environment or genetic factors (Klein et al. 2004b). There have been inconsistencies in findings of association of iris colour and sunlight exposure with AMD. In Australian populations, light coloured irides (Mitchell et al. 1998; Nicolas et al. 2003), light exposure (Darzins et al. 1997) and abnormal skin sensitivity to sunlight (Mitchell et al. 1998) were associated with increased disease progression rates, whereas no such associations were reported in a British study (Khan et al. 2006).

Small numbers of hard drusen, less than 63μm in diameter are not considered to be a risk factor of AMD, however large numbers of hard drusen are likely to indicate pathological accumulations (Sarks et al. 1999). In the Beaver Dam Eye Study, after 15 years, the presence of 8 to 144 hard drusen was shown to predict the incidence of large, soft drusen and pigmentary changes, when compared to the presence of smaller numbers of hard drusen (Klein et al. 2007). Large drusen and focal hyperpigmentation are considered risk factors for the development of neovascular AMD (Bressler et al. 1990). A stronger risk factor for the progression to advanced AMD was present when there were large drusen in both eyes than in one eye alone (AREDS 2001a). Drusen larger than 50μm were highly associated with confluence of drusen and greater number of drusen in fellow eyes of neovascular AMD (Bressler et al. 1990). Although, in some

cases large soft drusen are seen to fade and disappear, which was found to be accompanied by degenerative changes of the RPE (Sarks et al. 1999). In a large epidemiologic study over 6.5 years, van Leeuwen et al. (2003b) discovered that the risk of progression of disease from hard or soft drusen, in the presence of pigmentary abnormalities, was three times greater than drusen without pigmentary abnormalities. Reticular pseudodrusen have been indicated as a strong risk factor for the development of GA and CNV (Klein et al. 2008a). In the Beaver Dam Eye Study, the enlargement of GA was 6.4mm^2, over a five year period in 95 patients, where computerised-assisted tracing of the area of GA on digitised colour fundus slides was performed (Klein et al. 2008b). Eyes with multiple areas of GA were more likely to have the GA lesions increase in size and extend to foveal involvement than eyes with single GA areas (Klein et al. 2008b).

It is known that there is a greater chance of developing exudative AMD if the fellow eye has an existing exudative lesion. A yearly rate of developing a neovascular membrane in the fellow eye of patients with neovascular AMD in one eye was 8.8% in a prospective study over 4.5 years (Sandberg et al. 1998). Investigation has been carried out to discover whether decreased visual function occurs in an eye, whose fellow eye has exudative disease. Some researchers have not demonstrated a decrease in functional vision in eyes with this risk factor, when measuring central visual field sensitivity, contrast sensitivity, macular recovery function (Midena et al. 1997) and short-wavelength sensitive acuity (Beirne et al. 2006). However, others have found reduced sensitivity in fellow eyes of exudative AMD, for SWAP thresholds in the 10° visual field (Remky et al. 2001b). Similarly in a small sample (n = 3), decreased short-wavelength sensitivity, was detected in the fellow eye of disciform scars and GA, measured under conditions similar to SWAP (Sunness et al. 1989). The relationships between short wavelength sensitivity and AMD are discussed in more detail in sections 1.4.2.2 and 1.4.2.3.

1.3.3 Classification of AMD

1.3.3.1 Grading & Staging systems

A number of grading systems exist in order to define and classify the signs of AMD from fundus photographs. The most widely used systems are the Wisconsin Age-related Maculopathy Grading System (Klein et al. 1991), the International Classification and Grading System (Bird et al. 1995) and the Age-Related Eye Disease (AREDS) classification system (AREDS 2001b). Some grading systems use the term age-related maculopathy (ARM) to indicate the presence of drusen and pigmentary changes and AMD, to refer to later changes such as GA and CNV (Bird et al. 1995; Klein et al. 1991). Other systems refer to all forms of the condition as AMD (AREDS 2001b) and is the convention followed throughout this thesis.

The Wisconsin ARM Grading System standardised a circular grid (Figure 1-7), to be centred on the fovea of stereoscopic fundus photographs (Klein et al. 1991). The grid is divided into subfields, consisting of three concentric circles of diameters 500, 1500, and 3000μm, also centred at the macula. Standard circle sizes are used for estimation of lesion area. The grid and photographs are mounted in clear plastic sheets and graded upon a light box with a colour temperature of 6200K, such that the wavelength has a less yellow hue to facilitate identification of subtle drusen. Three main divisions of the grading system are drusen, other AMD lesions and other abnormalities. Both extent and location of lesions are quantified. Assessment of the Wisconsin ARM Grading System revealed good inter-observer agreement, from independent grading of 857 eyes. Weighted kappa values ranged from 0.48 to 0.87 for characteristics of AMD (Klein et al. 1991). The kappa statistic ranges from -1 indicating exact disagreement to +1, representing exact agreement (Landis & Koch, 1977). The following interpretation of kappa values was proposed as 0.41 to 0.60 indicating moderate agreement, 0.61 to 0.80 substantial agreement, and 0.81 to 0.99 almost perfect agreement (Landis & Koch, 1977).

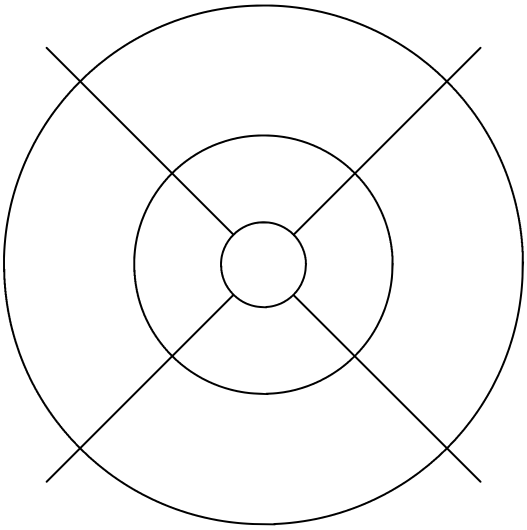

Figure 1-7. Standard grading grid

The International Classification and Grading System defines lesions according to features, predominant type, number, size, and estimation of area occupied within the standard grid (Bird et al. 1995). The subfield circle diameters of the grid are 1000, 3000 and 6000μm. Predominant drusen type is graded by the categories, hard, soft intermediate, soft distinct and soft indistinct; most common within the outer circle. Only drusen larger than 63μm are counted separately. Estimation of area within the subfields, predominant size of drusen and estimation of the percentage of confluence of drusen is noted. Hyperpigmentation or hypopigmentation are classified by presence and main location. GA and neovascular AMD are recorded by presence, most central location and area covered. Percentage agreement of assessment of fundus photographs of 50 eyes ranged from 59 to 99% between three observers and from 62 to 100% within observers (Scholl et al. 2003).

AREDS was a major clinical trial designed to investigate the natural history and risk factors of AMD and cataract; and to evaluate the effect of nutrition on the progression of AMD. A grading system, in extension of the Wisconsin ARM Grading System, was developed to define AMD abnormalities in fundus photographs. The same grading grid

and light box method was used (AREDS 2001b). Weighted kappa values ranged from 0.51 to 0.88 for the grading of abnormalities (AREDS 2001b).

No universal agreed classification exists as to the exact progression of disease in early AMD. In order to measure progression of the disease, some groups have developed staging systems based on risk factors as measured in epidemiologic studies.

The Rotterdam Study defined progression stages of disease, after grading signs according to the International Classification System (Klaver et al. 2001). Subsequently, van Leeuwen et al. (2003b) found that the risk of developing late-stage disease was three times greater, when both hard and soft drusen were present with RPE abnormalities, compared to the presence of drusen alone. The staging used in this study, based on definitions from a longitudinal epidemiologic study, categorises by drusen type and pigmentary abnormalities, and accounts for the increased risk of drusen with pigment abnormalities (Table 1-2). This system of staging has been used in other studies (Augood et al. 2006; Beirne et al. 2006; Hamada et al. 2006). Beirne et al (2006) studied the relationship between short-wavelength sensitive acuity and stages of early AMD. Fundus photographs were graded using the Wisconsin ARM Grading System and staging was defined by the system used by van Leeuwen et al. (2003b).

Stage	Clinical Features
0a	No signs of ARM at all
0b	Hard drusen (<63μm) only
1a	Soft distinct drusen (≥ 63μm) only
1b	Pigmentary abnormalities only, no soft drusen (≥ 63μm)
2a	Soft indistinct drusen (≥ 125μm) or reticular drusen only
2b	Soft distinct drusen (≥ 63μm) with pigmentary abnormalities
3	Soft indistinct drusen (≥ 125μm) or reticular drusen with pigmentary abnormalities
4	Atrophic or neovascular AMD

Table 1-2. Classification of Mutually Exclusive Stages of ARM (van Leeuwen et al. 2003b)

Yet some controversy exists regarding the correlation of this staging system with functional changes. Only weak relationships were observed between short-wavelength sensitive resolution acuity and the stages 1a to 2b (Beirne et al. 2006) and between scotopic interferometric acuity (SIA) and the stages 0 to 3 (Hogg et al. 2007). Revised staging systems were suggested: to stage 0, stages 1a to 2b combined and stage 3 (Beirne et al. 2006); and to the four stages, no ARM features or drusen smaller than 63μm, drusen only but >63μm, hyperpigmentation only, and drusen plus hyperpigmentation (Hogg et al. 2007). The revised systems produced significant relationships between functional measures and increasing severity of disease (Beirne et al. 2006; Hogg et al. 2007).

The AREDS severity scale summarised AMD features into a four point severity scale. The stages involved a large range of features and in the late disease stages, included visual acuity in the criteria (AREDS 2001a,b).

Other investigators graded macula photographs according to the International Classification and Grading System for AMD to describe six stages (Tikellis et al. 2006). Increased level of stage was associated with increased risk of developing late AMD. This system of staging differentiated between hyperpigmentation and hypopigmentation, as it is suggested that hyperpigmentation is more easily detected and thus noticed earlier. Importantly, photographs in this study were re-graded and re-staged according to systems proposed by the Rotterdam Study and AREDS. It was discovered when comparing the different re-evaluated progression rates, that they only differed by a few percent.

Stage	Clinical Features
1	No drusen or <10 small drusen without pigment abnormalities
2	Approximately ≥10 small drusen or <15 intermediate drusen, or pigment abnormalities associated with ARM a. Drusen b. RPE changes (hyperpigmentation and hypopigmentation) c. Both drusen and RPE changes
3	Approximately ≥15 intermediate drusen or any large drusen a. No drusenoid RPED b. Drusenoid RPED
4	Geographic atrophy with involvement of the macular centre, or noncentral geographic atrophy at least 350 μm in size
5	Exudative AMD, including nondrusenoid pigment epithelial detachments, serous or hemorrhagic retinal detachments, CNVM with subretinal or sub-RPE haemorrhages or fibrosis, or scars consistent with treatment of AMD a. Serous RPED, without CNVM b. CNVM or disciform scar

Table 1-3. The Clinical Age-Related Maculopathy Staging System (CARMS) (Seddon et al. 2006)

Modified from the AREDS system, the Clinical Age-Related Maculopathy Staging System (CARMS) was developed for simplicity and greater ease of use by an inexperienced grader (Seddon et al. 2006). The classes are estimated according to presence, size and approximate number of drusen; presence of RPE abnormalities, GA or CNV (Table 1-3). The system shows good levels of reliability for inter-observer agreement (Seddon et al. 2006), however drusen in association with pigmentary changes are grouped together in an early stage.

1.3.3.2 Computerised Drusen Measurement

Methods have been developed to accurately measure the area of drusen by semi-automated or automated computerised techniques (Smith et al. 2005a,b). A normal fundus background has very variable reflectance. The least reflectance is found at the macula, due to luteal pigment. Background levelling is carried out using a mathematical model of quadratic polynomials. In the fully automated method, this is followed by automated threshold selection and segmentation, to quantify the area of

drusen. The automated technique was found to be comparable to the manual method of estimation of drusen area (Smith et al. 2005b) and drusen quantification is more precise than the traditional methods (Smith et al. 2005a). Computerised drusen measurement is reviewed in more detail in Chapter 5.

1.3.4 Non-invasive Imaging in AMD

Traditional imaging methods such as fluorescein angiography, which is considered clinically necessary in the diagnosis of exudative AMD and allows for classification of neovascular lesions, involves intravenous injection of fluorescein dye and the associated risks to the patient. Therefore this review will concentrate on non-invasive techniques of imaging in AMD, which pose minimal risk to the patient and infer greater ease for clinical use.

1.3.4.1 Fundus Photography

Sequential stereo fundus photography is a widely used technique in ophthalmology and involves one image taken after the other or two images taken simultaneously. Once the area of interest is selected, the first image is taken near the left edge of the pupil. A lateral shift with the joystick or camera base is made to take the second image, near the right edge of the pupil. Greater horizontal separation of the images increases the stereo base of the photographs, but is limited by pupil size and lens opacity.

The main advantage of stereophotography in grading AMD is for differentiation of edges of large drusen and RPE depigmentation. The additional depth perception is more likely to distinguish pigment epithelial detachments from large areas of hypopigmentation, and aid viewing of other raised lesions. The limitations of this technique involve the separation between the images, which may differ between subjects, giving rise to an inconsistent 3D effect between patients. Therefore, no measures of absolute depth can be taken (Saine & Tyler 1997).

The original standard for grading involved stereoscopic photographic 35mm film slides, mounted in clear plastic sheets, graded at a fluorescent light box with a colour

temperature of 6200K, through a stereoscopic viewer. Following the widespread use of digital photograph, several studies have graded AMD from digital images (Beirne et al. 2006; Bjornsson et al. 2006; Scholl et al. 2004). When compared to film images, digital images have been shown to yield no significant difference in grading AMD (Klein et al. 2004a; van Leeuwen et al. 2003a). Good agreement in AMD grading between fundus photography and slit-lamp biomicroscopy has been found for digital images graded according to the Wisconsin ARM Grading System (Neelam et al. 2009a) and for colour slides graded using the International Classification System (Tikellis et al. 2000). In fundus photography for grading of AMD, the variables affecting visualisation of the image need to be specified. These include the distance and angle of viewing, monitor resolution, magnification and also methods of image manipulation.

Digital stereo photography is limited by the number of pixels of the system. The amount of light falling on a specific pixel is number between 0 and 255 for an 8-bit camera (since 2^8=256). To indicate colour each pixel location has a red (R), green (G) or blue (B) value. The pixel count shows the resolution of the system e.g. 1035 x 1370 pixels, or for higher resolution 2036 x 3060. If the pixel is smaller, the resolution is finer. Although the monitor resolution in pixels is a limitation, zooming the image can help to overcome this. The recommended standards for grading diabetic retinopathy are a monitor of at least 19", with a pixel resolution of 1600 x 1200 (UK National Screening Committee, 2009), which fulfils the image resolution requirement of at least 20 pixels per degree.

The traditional stereoscopic viewer employed prisms to view stereoscopic pairs of images. The LCD (liquid crystal display) technique is a computer display of images making up the stereo pair. The images are alternately viewed through computer controlled LCD shutter glasses. The PC controls an infrared signal to the glasses, which controls the opacity of the lenses, flickering at a rate of more than 30 images per second, between the two stereo images (Saine & Tyler 1997).

1.3.4.2 Fundus Autofluorescence

Fundus autofluorescence (FAF) non-invasively images the retina using a confocal scanning laser ophthalmoscopy to topographically map lipofuscin distribution at the level of the RPE. Lipofuscin accumulates in the RPE with age, which is believed to be a by-product of the constant phagocytosis of shed photoreceptor outer segment discs.

A more detailed description of confocal scanning laser ophthalmoscopy can be found in Chapter 6.1. Briefly, the confocal optics collect reflectance and fluorescence from the same plane, avoiding autofluorescence from the lens and cornea. A blue excitation laser of wavelength 488nm is used in FAF imaging in commercially available instruments. One such instrument, the Heidelberg Retinal Angiograph 2 (HRA 2; Heidelberg Engineering, Germany) detects emitted light above 500nm. The image quality degrades in the presence of lenticular opacities.

The monochromatic FAF image of a normal fundus shows a diffuse grey area at the posterior pole with gradual decrease or darkening towards the macula, due to macular pigment. Retinal vessels appear dark due to absorption and the optic disc appears dark due to lack of autofluorescent material. In AMD patients areas of increased or decreased FAF are seen on the fundus in comparison to the homogenous surrounding areas, due to areas of increased or decreased lipofuscin accumulation. The eight phenotypic patterns of FAF in early AMD were classified as normal, minimal change, focal increased, patchy, linear, lacelike, reticular, and speckled (Bindewald et al. 2005a). Hyperpigmentation may appear as dark or light areas. It was found that FAF intensities over hard and soft drusen were not different from the normal background and the age-matched controls (von Rückmann et al. 1997). Localised areas of high FAF were seen which did not correspond to drusen and in some cases matched pigmentary changes (von Rückmann et al. 1997). Large soft drusen and hyperpigmentation were significantly associated with focally increased autofluorescence in a study which examined automated drusen segmentation with

computerised FAF image analysis (Smith et al. 2006). GA has the appearance of a marked dark patch on FAF images, which corresponds to RPE cell death and accompanying absence of lipofuscin. Increased FAF is seen adjacent to GA (Smith et al. 2006). A classification system has been derived of FAF patterns in the junctional zone of atrophy in GA, involving four main phenotypic patterns; focal, banded, patchy and diffuse (Bindewald et al. 2005b). CNV presents irregular FAF patterns, which may be increased or decreased.

1.3.4.3 Infrared Imaging

Infrared imaging of the fundus using a scanning laser ophthalmoscope (SLO) provides better visibility of sub-retinal features such as drusen than visible light (Elsner et al. 1996). Scanning laser ophthalmoscopy and infrared imaging is reviewed in more detail in Chapter 6.

1.3.4.4 Optical Coherence Tomography

Optical coherence tomography (OCT) is a non-invasive retinal imaging technique which produces cross-sectional images of the retinal structures. It was first described in 1991 (Huang et al. 1991) and the most recent commercially available instrumentation is the spectral or Fourier domain OCT.

OCT is analogous to B-scan ultrasonography, where light rather than sound measurements are made from tissue boundaries. OCT imaging is based on the principle of Michelson interferometry, whereby light passing through the eye creates different reflections by the different cell layers. The echo delay and intensity of the reflected light is measured to produce cross-sectional tomographic images. Fourier domain OCT allows for high speed acquisition of higher resolution images, in which further distinction between the retinal layers is possible. One such instrument is the Cirrus HD-OCT (Carl Zeiss Meditec, CA, USA) which has an axial and transverse resolution of 5μm and 25μm, respectively. The combination of OCT with a SLO has allowed for three-dimensional fundus mapping and further improved resolution, for

example the Spectal OCT SLO (OPKO Instruments, FL, USA), whose axial and transverse resolution is 5-6μm and 15 μm, respectively, and incorporates microperimetry.

The use of OCT in AMD is evident in the detection of drusen and RPE atrophy (Pieroni et al. 2006), intraretinal fluid, pigment epithelial detachment and neovascular membranes (Ahlers et al. 2006), in which quantitative measures may be made. OCT has been used in the monitoring of retinal thickness in patients following treatment with the anti-VEGF drug, Avastin (Avery et al. 2006). A spectral OCT SLO (Spectralis HRA + OCT, Heidelberg Engineering, Heidelberg, Germany) was used to assess simultaneous fundus autofluorescence and high-resolution OCT images in patients with GA (Wolf-Schnurrbusch et al. 2008). The principal outcome was structural alterations to retinal layers, seen as partial loss of defined boundaries between layers. Alterations were observed in junctional zones surrounding the GA as well as in the GA areas (Wolf-Schnurrbusch et al. 2008). Outer retinal layers were altered where inner retinal layers were not, especially at the external limiting membrane in junctional zones. It was speculated this may be due to swelling of damaged RPE cells resulting from increased accumulation of lipofuscin at junctional zones (Wolf-Schnurrbusch et al. 2008). Six different commercially available OCT instruments, including one conventional time-domain OCT and five Fourier domain instruments were found to produce significantly differing measures of retinal thickness, due to different retinal segmentation algorithms. Consequently, the instruments cannot be used interchangeably (Wolf-Schnurrbusch et al. 2009).

1.3.5 Topographical Changes at the Macula in AMD

AMD affects the photoreceptors secondarily to the RPE, Bruch's membrane and the choriocapillaris, which results in the impairment of visual function (Jackson et al. 2005). The anatomy of the macula at the fovea contains a peak population of cones with a sharp decline to an eccentricity of 3.5° (Curcio et al. 1990). Surrounding this, the rods

dominate the photoreceptor population of the parafovea (Figure 1-8). The total rod to cone ratio is 20:1 (Curcio et al. 1990). The eccentricity decline in cone density immediately surrounding the fovea is slightly faster along the vertical than the horizontal meridian, such that half the maximum cone density is achieved at 120μm (inferior) and 150μm (temporal) from the fovea. This generates an elliptical pattern of cone isodensity contour maps. The rods are absent from the centre of the fovea and first appear at 100-200μm (0.4-0.7°) from the foveal centre and increase rapidly to form a horizontal elliptical rod ring of maximum density at approximately the same eccentricity as the optic disc centre. The most rapid increase in rod density occurs along the superior vertical meridian and least rapidly along the nasal horizontal meridian. From the rod ring crest, rod density falls gradually into the far periphery (Curcio et al. 1990). Foveal cone density does not show age-related changes, whereas a progressive loss of 30% of rods occurs over an adult lifetime (Curcio et al. 1993). The greatest rod loss with age occurs at 1 to 3 mm (3.5-10°) from the fovea (Jackson et al. 2002).

Short-wavelength sensitive cones represent 6.8% of the total cone population within 4mm of the foveal centre (Curcio et al. 1991). Their distribution in the retina shows an absence at the foveal centre and a peak density at a distance of 100-300μm from the fovea, which is consistent with psychophysical findings of foveal tritanopia (Curcio et al. 1991). The profile of blue cone density resembles that of the rods, rather than the overall distribution of cones. It is unknown whether the radial asymmetry of the rods is mirrored by the blue cone topography, due the sparse nature of the data for short-wavelength sensitive cones (Curcio et al. 1991).

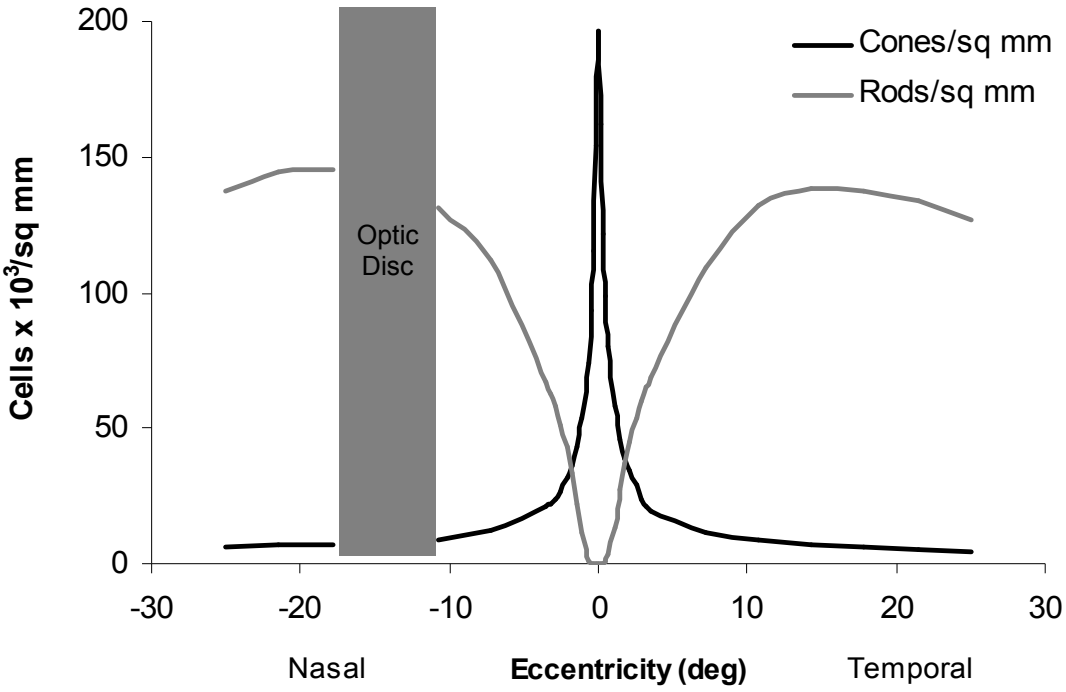

Figure 1-8. Photoreceptor distribution across the horizontal meridian.

Displayed as a left eye, replotted from Curcio et al. 1990, data downloaded from http://cvision.ucsd.edu/index.htm.

The selective vulnerability of rod loss over cone loss in AMD has been suggested in histopathologic studies. Photoreceptor loss was determined in a study of donor eyes, divided into three groups; normal, non-exudative and exudative AMD (Curcio et al. 1996). The non-exudative AMD group consisted of five eyes with drusen, pigmentary changes with and without GA. The exudative AMD group included eight eyes with extensive GA, pigment clumping with and without neovascular changes. There were two eyes in the normal control group. In non-exudative eyes, foveal cones were spared and loss of parafoveal rods and cones occurred (Curcio et al. 1996). The mosaic of inner segments was irregular at 2mm in the parafovea in non-exudative AMD, unlike the regular arrangement seen in the control eyes (Curcio et al. 1996). In eyes with exudative AMD, the presence of mostly cones remained along the margins of and overlying disciform scars (Curcio et al. 1996).

Changes to the ganglion cell layer were examined in six donor eyes with non-exudative AMD, five eyes with exudative AMD and 15 control eyes of patient ages over 60 years (Medeiros & Curcio 2001). Contour maps showed the greatest density of ganglion cell layer neurons occurred in a horizontal ellipse 0.5 to 2mm from the foveal centre in all eyes. It was found that even where large photoreceptor loss was present in exudative AMD eyes, proportionally large amounts of ganglion cell layer neurons survived (Medeiros & Curcio 2001). Exudative AMD eyes had 47% less ganglion cell layer neurons than control eyes, however ganglion cell layer neurons in non-exudative eyes were not significantly different from the number in control eyes (Medeiros & Curcio 2001).

1.4 Functional Changes in AMD

Changes in visual function in AMD have been investigated by various means. This review includes standard clinical measures and also non-standard research methods, which have been studied in AMD, and which are relevant to the studies included in this thesis.

1.4.1 Standard Clinical Measures

1.4.1.1 Visual Acuity and Contrast Sensitivity

Visual acuity (VA) is the standard measure of visual function in clinical practice, where it is normally expressed as a Snellen fraction. For research purposes, a LogMAR chart is favoured due to the geometric progression in size of optotypes between lines. Unlike VA which is a measurement at 100% contrast, contrast sensitivity (CS) is a clinical measure of the contrast threshold required to visualise a target, which may be an optotype or a sinusoidal grating. Letter target measures of CS are often used in clinical studies supplementary to VA, and are briefly reviewed here.

In a population based study as part of the Beaver Dam Eye Study, early AMD features were associated with loss of two or less letters on the ETDRS LogMAR chart and late stage features were associated with a loss of seven lines (Klein et al. 1995). Although the loss in early AMD was significant, this finding was disputed as a loss of two letters is less than the measurement variability of the LogMAR chart (Neelam et al. 2009b). Other studies have found large variations in VA results in patients with GA and CNV, due to extent of foveal involvement and tissue composition of the macular lesion (Hogg et al. 2003; Sunness et al. 1999). In a longitudinal study, it was found that forty eyes with GA lost three to six lines of LogMAR acuity over two years, whereas nine eyes with drusen and pigmentary changes did not exhibit any significant loss (Sunness et al. 1997). The strongest risk factors for prediction of VA loss from developing GA were found to be reduced low luminance VA, measured with a neutral density filter before the eye on an ETDRS chart, and reduced reading speed (Sunness et al. 2008).

CS was found to be significantly impaired in patients at various stages of AMD (Abadi & Pantazidou 1996; Feigl et al. 2005; Kleiner et al. 1988; Stangos et al. 1995; Sunness et al. 1997), although these studies did not appear to have excluded subjects with lenticular opacities. Significant CS loss at high and middle spatial frequencies was found in eyes with drusen and normal visual acuity, compared to control eyes, however

it was concluded that CS loss was not predictive of CNV (Stangos et al. 1995). A longitudinal study determined moderate correlation between ETDRS VA and Pelli-Robson CS in eyes with neovascular disease, at baseline and after 2 years (Bellmann et al. 2003). Contradictory findings were made in a study using low contrast letter Regan acuity measurement in early AMD and normal subjects. Regan letter charts are similar to LogMAR charts, except that the letters vary in contrast levels. Better performance in the normal group was found at all contrast levels, suggesting that the low contrast letter measurement provided no further useful information (Abadi & Pantazidou 1996). However, there was a relatively limited number of patients (n = 6) and normal subjects (n = 12) in this study. Poorer performance using Regan charts was found in patients with drusen and Snellen VA of 6/6 when compared with age-matched normal subjects (Kleiner et al. 1988). The difference between the two groups increased with decrease in letter contrast and categories of drusen severity correlated with CS loss (Kleiner et al. 1988). VA and CS are limited to foveal measures of visual function and therefore are relatively insensitive to changes due to AMD.

1.4.1.2 Reading Speed

Another measure of visual function is reading speed. This is a more complex task, as it involves visual resolution as well as eye movement control and cortical processes. Several studies have demonstrated diminished performance in reading speed in AMD (Bullimore & Bailey 1995; Elliott et al. 2001; Legge et al. 1985; Legge et al. 1992; Sunness et al. 1997). There are many reasons for this, including the use of eccentric viewing (Timberlake et al. 1986), the size of scotoma and associated impaired eye movement control (McMahon et al. 1991; White & Bedell 1990; Whittaker et al. 1991), reduced perceptual span (Bullimore & Bailey 1995; Crossland & Rubin 2006) and impaired fixation stability (Crossland et al. 2004).

Lack of fixation stability has been associated with slow reading speed by a linear relationship, however fixation stability was not related to VA, scotoma size or CS

(Crossland et al. 2004). Fixation patterns were examined in patients with macular scotomata using a SLO, where three patients fixated with a single preferred retinal locus adjacent to the scotoma and fixation stability was also not related to VA in this study (Timberlake et al. 1986).

Using an eye tracker and the MNREAD acuity charts, binocular viewing was not significantly advantageous over monocular reading speed (Kabanarou & Rubin 2006). The reading speed of patients with AMD, who underwent training exercises to practise control of eye positions and movements, significantly increased after training (Seiple et al. 2005). As an everyday task, the measure of reading speed is of value and loss of reading performance is highly correlated with vision-related quality of life score (Hazel et al. 2000).

1.4.1.3 Colour Vision

Colour vision function in AMD has been assessed in many studies, where abnormalities tended to be tritan defects (Applegate et al. 1987; Arden & Wolf 2004; Cheng & Vingrys 1993; Collins 1986; Eisner et al. 1991; Eisner et al. 1992; Feigl et al. 2005; Frennesson et al. 1995). There exists relatively fewer studies which did not find defective colour vision in AMD patients (Atchison et al. 1990, Midena et al. 1997). Various colour vision tests were used to reach these findings.

D-15 and desaturated D-15 testing was significantly worse in patients with drusen with or without pigmentary changes compared to control subjects, but no significant change in colour vision was seen after a year (Feigl et al. 2005). D-15 and Rayleigh colour matching tests were administered in fellow eyes of eyes with exudative AMD in 41 patients (Eisner et al. 1991). High risk eyes, which had large confluent drusen with or without hyperpigmentation, failed the D-15 test and exhibited abnormal colour matching (Eisner et al. 1991). The same tests were measured longitudinally over 18 months in fellow eyes of exudative AMD in 47 patients and it was found that colour matching in combination with dark adaptation was the most effective method in determining the

development of CNV (Eisner et al. 1992). Farnsworth-Munsell 100-hue and D-15 tests were administered in four eyes of three AMD patients and demonstrated development of a prominent tritan defect following a small pigment epithelial detachment in one patient and after diagnosis of a subretinal neovascular membrane in another patient (Applegate et al. 1987). Conversely, the Farnsworth-Munsell 100-hue detected no abnormalities in patients with drusen with or without pigmentary changes (Midena et al. 1997). Contrasting findings are present in two studies of patients with drusen and pigmentary abnormalities, tested using the desaturated D-15 test; no difference was exhibited between patients and control subjects in one study (Atchison et al. 1990), and tritan defects significantly different from the control group, were found in patients in an earlier study (Collins et al. 1986)

Detection of colour contrast sensitivity using optotypes displayed by means of a computer graphics system has been implemented (Arden & Wolf 2004, Frennesson et al. 1995). Colour contrast sensitivity was significantly lower in patients with drusen, with and without pigment changes for the protan and deutan and especially the tritan axes (Frennesson et al. 1995). Greater tritan defects were related to increasing severity of fundus changes (Arden & Wolf 2004).

1.4.1.4 Dark Adaptation Function

Dark adaptation tests measure the slow recovery of visual sensitivity in the dark, after brief exposure to a field of high luminance which bleaches the visual pigment in the photoreceptors. The typical dark adaptation function consists of two portions. The early portion is a rapid reduction in threshold to a plateau and is exclusively mediated by the cones. A transition to rod function occurs at around 10 minutes, where there is a sudden change in the slope of the curve, known as the rod-cone break. Following this, a slow reduction in threshold occurs over approximately 35 minutes, exclusively mediated by the rods (Schwartz 2004). The rod-mediated portion of dark adaptation was noted to be significantly slower in older adults than younger adults (Jackson et al.

1999). This has been linked to symptoms of difficulty in seeing under low illumination and at night experienced by healthy older adults. In patients with early AMD, who had normal visual acuity, the rod-mediated dark adaptation was approximately 13 minutes slower than control subjects (Owsley et al. 2001). The delay in rod-mediated dark adaptation is greater than that for cone-mediated dark adaptation in early AMD (Jackson et al. 2002).

Scotopic retinal sensitivity is mediated by the rods. It is measured away from the fovea using a short-wavelength stimulus (450-550nm) after 30 to 45 minutes of dark adaptation. Several psychophysical studies have observed reduced scotopic sensitivity in AMD patients using a HFA modified for scotopic conditions (Owsley et al. 2000, 2001; Scholl et al. 2004; Steinmetz et al. 1993) and a dark adaptometer (Brown et al. 1986). This corresponds to the histopathological findings of selective vulnerability for rod loss in AMD. Another study using an adapted HFA did not find reduced scotopic sensitivities, although the suggestion was made that less advanced age-related changes were present in the patient group compared to previous studies (Haimovici et al. 2002). A commercial instrument, the Scotopic Sensitivity Tester-1 did not find any significant dark adaptation abnormalities in patients with early AMD when compared with normal subjects (Jackson et al. 2006). No correlation between the scotopic sensitivity and structural measures of drusen on fundus photography was observed (Owsley et al. 2000; Steinmetz et al. 1993), although functional loss did correlate with areas of increased fundus autofluorescence (Scholl et al. 2004).

1.4.2 Perimetry and AMD

1.4.2.1 Standard Perimetry and AMD

Several studies have examined the central visual field in AMD using a Humphrey Field Analyser (Atchison et al. 1990; Cheng & Vingrys 1993; Feigl et al. 2005; Frennesson et al. 1995; Midena et al. 1994,1997; Tolentino et al. 1994). All of these studies analysed as the main outcome, global mean sensitivity (MS) and in some cases, its standard

deviation. Other global indices, such as the mean deviation (MD) and probability analyses were not calculated, even when a large range of ages among the sample was present. One exception to this was a study which used number of defects from normal in a 16 point 6° by 4° stimulus grid (Tolentino et al. 1994).

Midena et al. (1994, 1997) found reduced sensitivity in the HFA 10-2 field in patients with early AMD, when fundi were graded using the International Classification System, in groups comprising approximately 30 patients. In eyes with drusen, MS was significantly lower in eyes with soft drusen compared to eyes without soft drusen, and in eyes with drusen larger than 63μm compared to eyes with drusen smaller than 63μm (Midena et al. 1994). A later study by the same group found significantly lower MS in patients, compared to age-matched controls (Midena et al. 1997). MS showed no significant differences with number of drusen (Midena et al. 1994, 1997). A progressive decrease in sensitivity was noticed with increased confluence of drusen, however, MS was unaffected by neither the presence of focal hyperpigmentation, nor RPE atrophy (Midena et al. 1997). The findings of these two studies has less impact when it is considered that where significant differences in MS were found, they were of very small magnitudes, of 1 to 2dB.

Cheng & Vingrys (1993) also discovered that patients with early AMD exhibited reduced mean sensitivities on the HFA 10-2 test compared to age-matched normal subjects, although this was not statistically significant. Most of the defects detected were in the parafovea, at 5° to 10°. In contrast to this, Atchison et al. (1990) compared HFA 10-2 and 24-2 fields in 15 subjects with drusen and pigmentary changes to 15 age-matched normals and reported no significant difference between the two groups. Similarly, Frenesson et al. (1995) discovered normal 10-2 central visual fields in 27 subjects with pigmentary changes and soft drusen, some of which were confluent. Feigl et al. (2005) reported that 10-2 MS was within normal limits in thirteen patients with early AMD, graded using the AREDS grading system. This was not significantly

different from thirteen age-matched normal subjects, at baseline and one year after baseline (Feigl et al. 2005). Tolentino et al. (1994) detected that reduced sensitivity and drusen area were not significantly correlated, but sensitivity was reduced significantly with increased RPE atrophy.

Earlier studies involving a Friedmann Visual Field Analyser, an autoplot tangent screen (Swann & Lovie-Kitchin 1991) and a Goldmann perimeter using the static mode in the central 10° (Hart et al. 1983) have shown paracentral scotomata and preservation of central vision. Scanning laser ophthalmoscope (SLO) perimetry has been utilised to measure visual fields in AMD. The accuracy of fixation monitoring is improved over standard perimetry as correction can be made for loss of fixation. This advantage is evident as central visual field loss due to AMD is known to be associated with poorer fixation (Fujii et al. 2003). SLO perimetry is reviewed in section 1.4.3.1.

1.4.2.2 SWAP and AMD

Short-wavelength automated perimetry (SWAP) has been well documented in the early detection of glaucoma (Johnson et al. 1993b,c; Sample & Weinreb 1992). Glaucomatous progression was detected three to four years earlier in SWAP than in standard perimetry (Johnson et al. 1993b,c). SWAP also offered improved detection of focal defects in diabetic macular oedema, than standard perimetry (Hudson et al. 1998, Remky et al. 2000). Clinically, the use of SWAP did not become widespread following these findings, due to its greater variability in the 30° field, compared to standard perimetry (Wild et al. 1998). However in the central 10°, SWAP has a flatter hill of vision and the between-subject variability of SWAP is significantly less than in the 30° field (Kwon et al. 1998; Wild et al. 1998). This allows for a more accurate statistical interpretation using standard perimetric methodology and greater capability in the detection of focal loss (Cubbidge et al. 2002). It is known that patients with AMD have a diminished short-wavelength sensitive cone mechanism sensitivity (Chapter 1.4.2.3).

The number of studies documenting the measurement of SWAP in AMD is scarce (Remky et al. 2001b; Remky & Elsner 2005).

In 126 patients with early AMD, 75 of which had late AMD in the fellow eye, central 10° field SWAP was performed, using a HFA (Remky et al. 2001b). A decline in MS with age was found. In eyes of equal age and LogMAR acuity, those with soft drusen had significantly decreased MS compared to eyes without. Fellow eyes of eyes with exudative AMD had lower sensitivities compared to patients without exudative disease. Focal pigmentation was found to be related to an eccentricity effect. Eyes with hyperpigmentation had reduced sensitivity centrally compared to peripherally and the opposite was true for eyes without hyperpigmentation. The authors quoted SWAP sensitivity loss as a risk factor of AMD, although standard visual field data was not collected in their study (Remky et al. 2001b).

Another blue-on-yellow perimetry technique, using a scanning laser ophthalmoscope, has been employed to study early AMD (Remky & Elsner 2005). Reduced sensitivity in a 10° rectangular stimulus configuration consisting of 16 stimuli was recorded in 24 early AMD patients and age-matched controls. Patients with soft drusen were found to have lower MS values and higher between-subject variation than those with hard drusen. Areas of drusen, atrophic patches, and hyperpigmentation had lower sensitivity than areas without, thus showing focal loss in addition to the diffuse loss (Remky & Elsner 2005).

1.4.2.3 Short-Wavelength Sensitive Cone Pathway Sensitivity

The decline in sensitivity with age in SWAP is approximately 15dB per decade (Johnson et al. 1988a). Other psychophysical tests have determined an age-related loss of the short-wavelength sensitive cone pathway sensitivity at the fovea (Eisner et al. 1987a; Werner & Steele 1988).

Investigators have observed diminished short-wavelength sensitive cone pathway sensitivity in patients with AMD (Eisner et al. 1987b; Haegerstrom-Portnoy et al. 1989).

Eisner et al. (1987a,b, 1991, 1992) employed a two-channel Maxwellian view testing device, where isolation of the short-wavelength sensitive pathway was achieved using small stimuli, 3° and 1° in diameter of wavelength 440nm upon a 6° chromatic background of wavelength 580nm. A 20Hz square wave flickering stimulus was used to determine threshold sensitivity (Eisner et al. 1987a,b, 1991, 1992). A significantly lower sensitivity was ascertained in fellow eyes of patients with CNV, which had drusen, with and without hyperpigmentation, compared to an age-matched normal group (Eisner et al. 1987b). Using similar instrumentation, but differing stimulus conditions (440nm and 480nm, 2° stimulus on a 20° field, which flickered at 25Hz), patients with drusen and pigmentary changes had significant sensitivity loss and greater variability around the measure compared to control subjects (Haegerstrom-Portnoy et al. 1989). By contrast, within the same study, sensitivity in another patient group, who had less extensive retinal changes and good visual acuities, did not significantly differ from control subjects.

Low foveal short-wavelength sensitive cone pathway sensitivities were found to predict the development of exudative changes in fellow eyes of exudative disease followed over 18 months (Eisner et al. 1992). In fellow eyes of exudative disease with good acuity, eyes with any of the high risk features, focal hyperpigmentation, more than minimal confluence of drusen and large drusen; had significantly lower short-wavelength sensitive cone pathway sensitivity than low risk eyes without these features (Eisner et al. 1991). A modified Tübinger perimeter was employed to measure foveal short-wavelength sensitive cone pathway sensitivity using a flickering 2° blue stimulus, 450nm on a yellow chromatic background of 578nm, and a correction for lens density and macular pigment was included (Sunness et al. 1989). A weak correlation between high risk drusen, defined as soft drusen, confluence of drusen or hyperpigmentation and decreased sensitivity was illustrated (Sunness et al. 1989). In this study, Sunness et al. (1989) highlighted a predictive ability of reduced short-wavelength sensitive cone

pathway sensitivity based on its appearance in advance of clinical detection. Another two-channel Maxwellian view system using a 1° flickering stimulus on 9° circular chromatic background isolated short, medium and long wavelength sensitive cones using various filters, revealed loss of sensitivity in the short-wavelength cones alone, in both exudative and non-exudative disease, in a small sample of three subjects (Applegate et al. 1987).

Beirne et al. (2006) investigated the relationship between short-wavelength sensitive grating acuity and severity of stage of early AMD. Fundus photographs were graded by the Wisconsin grading system and staged according to the definitions used in the Rotterdam Eye Study. Resolution acuity was found to be reduced in eyes with AMD, however there was no direct relationship with increased disease stage.

It has been reported that normal elderly subjects who had high macular pigment density also had higher short-wavelength cone sensitivity than subjects with lower macular pigment density (Hammond et al. 1998). The study implied a protective role of macular pigment over visual sensitivity.

1.4.3 Other Non-standard Perimetric Techniques and AMD

1.4.3.1 Microperimetry

Microperimetry allows for simultaneous real-time fundus imaging and computerised threshold perimetry, which gives exact correlation between retinal lesions and corresponding functional defects. Previously, the SLO was adapted to perform microperimetry, whereby the fundus was illuminated with an infrared laser. The SLO 101 (Rodenstock, Germany), which is no longer available, projected a stimulus Helium-Neon laser beam (632.8nm) and an infrared laser (780nm) through a slightly confocal aperture onto the fundus (Rohrschneider et al. 2008). The exact location of individual fixation locus and the increment threshold could be quantified, however the SLO did not incorporate real-time fundus tracking, had a limited field of view of 33° by 21°, and was not fully automatic.

A commercially available microperimeter, the MP1 (Nidek Instruments Inc, Padova, Italy), has a 45° field of view and allows for automated full threshold perimetry. This instrument is not a SLO, it uses an infrared fundus camera to view the fundus and a liquid crystal display background to perform perimetry. Initial selection of retinal landmarks serves the automated tracking system which enables automatic compensation for eye movements during perimetric examination. Fixation characteristics, location and stability are also quantified. Perimetry is implemented by means of infrared projection onto the retina and a range of stimulus sizes are available from Goldmann size I to V. Background luminance is 1.27cd/m^2 and can be white or red. Central field testing can extend to 10° and pre-defined stimulus configurations are arranged in concentric rings (Figure 1-9), however custom configurations may also be defined. The perimetric results are displayed as numeric, symbolic or interpolated thresholds overlaid onto the fundus image.

Normal values of threshold sensitivity have been collected from 349 eyes of 176 normal subjects aged between 20 and 75 years (Midena et al. 2006) and this database has been incorporated into the instrument software (Rohrschneider et al. 2008). Although the statistical information essential in the interpretation of standard perimetry, such as the global indices of repeatability, use of visual field modelling, and the newer generation of threshold estimating algorithms does not yet appear to have been employed. It has been ascertained that there is an age-related linear decline in MP1 mean sensitivities (Midena et al. 2006; Shah & Chalan 2009). The normal MS of the MP1 at age 20 years was found to be 19.7dB (Midena et al. 2006), which divulges the limitation of the narrow dynamic range of the MP1 of 20dB and implies underestimation of high MS values. Test-retest variability in fifty patients with a variety of macular diseases was 2.56dB for the central 10°, using the 10-2 stimulus configuration, which was the coefficient of repeatability for the mean defect (Chen et al. 2009).

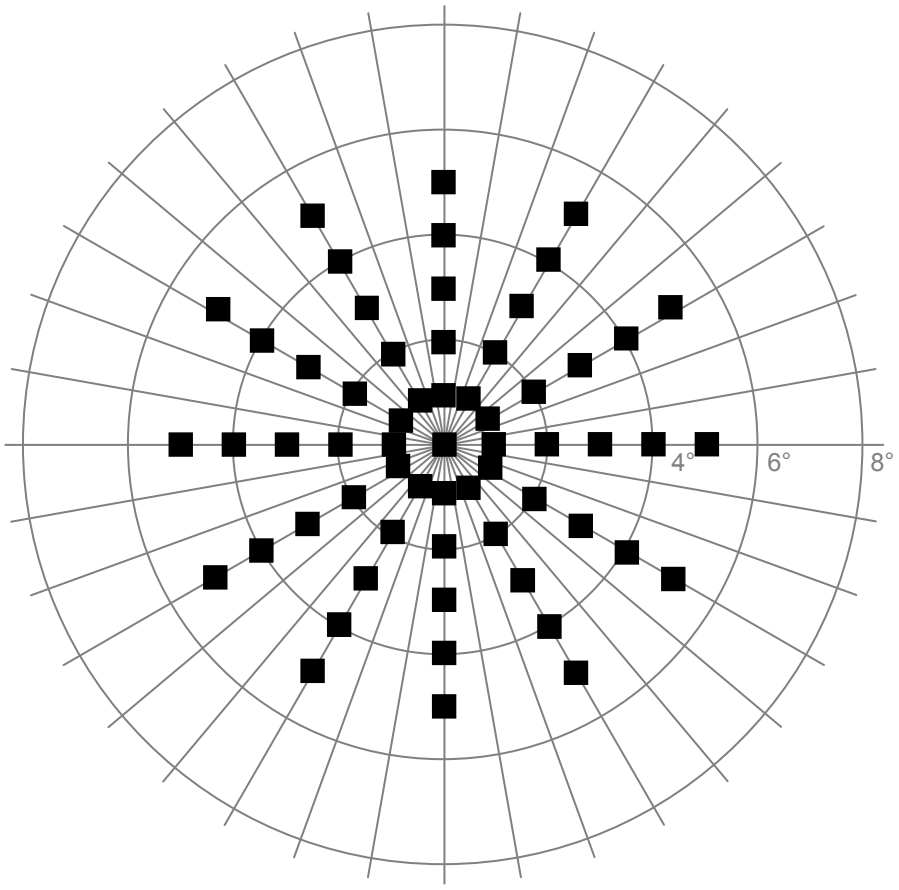

Figure 1-9. MP1: 5° stimulus configuration for central screening, 61 stimuli, Goldman size III, with a 1° cross fixation target.

Other functions of the MP1 include kinetic perimetry and other functional tasks such as contrast sensitivity, reading and fixation tasks. The Spectral OCT SLO (OPKO Instruments, FL, USA) is an instrument which combines microperimetry with spectral domain OCT imaging, allowing for retinal thickness and volumetric analysis in direct relation to functional sensitivity.

Due to differing instrumentation, setups and software, comparison of results between SLO and MP1 microperimetry, and also to standard perimetry cannot be made directly. In patients with macular disease, it was found that the MP1 tended find deeper defects than the SLO 101, which had superior quality fundus images, especially useful in early pathology (Rohrschneider et al. 2005). Sensitivity values on the MP1 were comparable to Octopus values, with greater differences in the inferior field (Springer et al. 2005).

Microperimetry has been used to detect functional loss over large drusen (Midena et al. 2007; Takamine et al. 1998). Reduced retinal sensitivity of greater than 5dB in areas of large drusen with a distinct border, compared to non-drusen areas was found in 9 out of 23 eyes, using SLO microperimetry, although no relationship between sensitivity loss and size of drusen was noticed (Takamine et al. 1998). Soft drusen with indistinct borders did not have reduced overlying sensitivities (Takamine et al. 1998). In a study involving thirteen patients with drusen, pigmentary changes and RPE atrophy less than 125μm, fundus autofluorescence and MP1 microperimetry was carried out (Midena et al. 2007). Sensitivity loss was noted over drusen larger than 125μm, but no significant loss was noted over drusen smaller than 125μm in diameter. Pigmentary changes were also significantly associated with loss of sensitivity, and the sensitivity loss was even greater when there were pigmentary changes in the presence of large drusen (Midena et al. 2007). The magnitude of difference in sensitivity between large drusen with and without pigment was approximately 2dB. However the ANOVA analysis in this study appears to have employed absolute sensitivity values overlying each feature,

summed together across all patients. This method did not appear to take into account the between-subject variability or the age difference between patients.

A wide variety in number of scotoma points was found in patients with GA, using SLO microperimetry (Sunness et al. 1997). In patients with CNV, SLO microperimetry was performed using a single staircase threshold estimating algorithm, to find areas of absolute and relative scotoma (Ergun et al. 2003). A significant correlation was found between reading speed and size of absolute scotoma, but not with size of relative scotoma (Ergun et al. 2003). Comparison between SLO perimetry and indocyanine green angiography was made in the detection of CNV (Schneider et al. 1996). Agreement was found such that well-defined CNV produced significantly deeper scotomata than eyes with occult CNV (Schneider et al. 1996).

175 patients with subfoveal CNV were examined with SLO microperimetry and it was found that 75% of eyes had predominantly central fixation and 28% of eyes had a dense central scotoma which was associated with longer time since onset of symptoms (Fujii et al. 2003). A subset 15 untreated eyes of this patient group was then followed over 18 months to investigate the sequence of visual loss (Fujii et al. 2003). An initial a mild decrease in central retinal sensitivity and VA was followed by a gradual decrease in fixation stability. Finally, visual function progressed to absolute central scotoma and eccentric fixation. Increased duration of disease was associated with sensitivity deterioration (Fujii et al. 2003). It was stated that some eyes with subfoveal CNV had parafoveal scotoma with a preserved central island and conversely, other eyes had absolute foveal scotoma with good parafoveal sensitivity (Fujii et al. 2003). However, the differences between lesion characteristics were not precisely quantified with regard to sensitivity loss or prevalence in this study.

SWAP has been applied to SLO microperimetry in AMD patients (Remky & Elsner 2005). These findings are discussed in section 1.4.2.2.

Microperimetry represents a useful and accurate tool in the measurement of the visual field in AMD and other macular diseases. The main advantage compared to standard perimetry is enhanced fixation monitoring, however most patients with early AMD and even with late stage disease have central fixation. The MP1 makes assumptions of retinal distance based on vessel width, by measuring the diameter of the superior temporal vein as it leaves the optic disc, rather than the standard assumptions such as optic disc diameter or papillomacular distance. Moreover, microperimetry currently does not incorporate statistical software for visual field interpretation, has a limited dynamic range and a restricted capability of threshold estimating algorithms.

1.4.3.2 Flicker Perimetry

Flicker perimetry has been reported to correlate well with SWAP in glaucoma patients (Landers et al. 2003a). There are two types of flicker used in flicker perimetry; mean-modulated flicker and pedestal flicker. Mean-modulated flicker varies luminance about a background level. Pedestal flicker modulates a luminance increment over time, resulting in both a flickering component and a change in the time-averaged luminance (Anderson & Vingrys 2000).

Flicker perimetry, using pedestal flicker, was investigated in 25 patients with early AMD and 34 age-matched normals (Phipps et al. 2004). Larger and deeper field defects were discovered for flickering targets compared to static targets in the diseased group and flicker thresholds were more affected in the AMD group compared to the normal group. In explanation, it was suggested that the increased metabolic demand and retinal blood flow required to detect flicker was less available from the AMD fundus.

Foveal flicker sensitivity was suggested to be predictive of exudative AMD (Mayer et al. 1994). In 16 fellow eyes of patients with exudative AMD in their other eye, signs of AMD were graded from nonstereoscopic photographs using the Wisconsin ARM Grading System. Mean-modulated flicker sensitivities for low and mid-temporal

frequencies were significantly lower in 7 patients, who subsequently developed exudative disease.

1.4.3.3 Amsler Grid

The Amsler grid is a clinical test for the rapid detection of metamorphopsia and scotoma in the central field. It consists of a 10° grid of lines spaced at intervals of 1°. A computerised adaptation of the Amsler grid was developed, using a touch sensitive monitor (Fink & Sadun 2004). This presents the grid at different contrasts, to produce a three-dimensional model of the hill of vision. The computerised version of the Amsler grid allows for more precise definition of a central field defect, however it is not widely used.

1.4.3.4 Preferential Hyperacuity Perimetry

The disadvantages of the Amsler grid are unreliable fixation, cortical image completion or filling in of scotoma, and the visual "crowding" effect (Loewenstein et al. 2003). The preferential hyperacuity perimeter (PHP) was created to overcome these disadvantages. It is based on the visual phenomenon of hyperacuity or Vernier acuity, which is the ability to perceive a very small difference in the relative spatial localisation of stimuli (Loewenstein et al. 2003). The PHP tests 500 points within the central 14° of the visual field with a resolution of 0.75°. The stimulus is a line of white dots on a black background. The subject responds to distortion by a touch-sensitive screen. Artificial distortions of different magnitudes are then generated to quantify the depth of the defect, determined by preferential looking analysis (Alster et al. 2005). The PHP has improved sensitivity compared to the Amsler grid in detecting defects, however it has a higher rate of false-positives (Goldstein et al. 2005). The PHP can detect most cases of CNV of recent onset with few false-positive results (Alster et al. 2005).

1.4.3.5 Multifocal ERG

The multifocal electroretinogram (mfERG) is an electrophysiological technique, which measures simultaneously the electrical responses to hexagonal stimuli, from multiple

areas of the retina. The waveform response from the mfERG typically has a positive and negative kernel. The latency and amplitudes of the waveforms are used in analysis.

A VERIS-System (visual evoked response imaging system) was used to record mfERG in patients with early AMD and an age matched normal group (Li et al. 2001). Significant abnormality was discovered in the foveal amplitude and the foveal latency of mfERG in the AMD group, in both the diseased eyes and in the asymptomatic contralateral eyes. mfERG in a small number of patients with CNV (n = 4) was noted to be well correlated with visual acuity measures, although not with lesion size (Jurklies et al. 2002). In fact, when compared to stereoscopic fundus photographs and fluorescein angiograms, mfERG did not display a significant relationship to retinal appearance (Gerth et al. 2003).

Rod-mediated mfERG was measured, by adapting the parameters of the mfERG, using dark adaptation and a blue filter in front of the stimulus array (Chen et al. 2004). Evidence of decreased rod function greater than that for cone function, was found in early AMD. Other investigators have found that rod-mediated responses were delayed in early AMD patients, whereas cone-mediated responses were not (Feigl et al. 2005).

1.4.3.6 Other Techniques

Frequency doubling technology (FDT) presents a grating of low spatial frequency that is flickered in counterphase at a high frequency. This causes a frequency doubling illusion, whereby the grating appears to have double the number of bars actually present (White et al. 2002). The frequency doubling illusion is thought to be caused by reduced cortical sensitivity to the temporal phase of achromatic counterphased gratings (White et al. 2002). FDT perimetry has demonstrated good sensitivity and specificity in the detection of glaucomatous field loss (Cello et al. 2000). However in early AMD, it was determined that the instrument was not sensitive enough to identify small macular lesions within the central 3° and modifications were necessary to detect small lesions

(Sheu et al. 2002). More recently, the Humphrey Matrix FDT perimeter has incorporated test patterns containing 2° wide stimuli, for assessing the central 10° visual field (Anderson et al. 2005), which has not yet been measured in patients with AMD.

Scanning laser entoptic perimetry is a technique whereby a patient views a monochromatic field of random particle motion. If field loss is present, the particle motion appears qualitatively different or even disappears to be replaced with grey if there is a dense scotoma. The patient traces the outline of the area of disturbance with a digital pen in a 30° field. The results from entoptic perimetry in AMD patients were compared with ophthalmologically graded fundus photographs. Good specificity and sensitivity was found for detecting all stages of AMD (Freeman et al. 2004).

2. Rationale and Logistics

2.1 Rationale

Late stage age-related macular degeneration (AMD) causes severe visual loss and is one of the most common reasons for visual impairment leading to blindness in western industrialised countries. In the future, it is expected that the morbidity of AMD will increase due to the expanding elderly population. Knowledge of the rate of functional loss is fundamental to the comprehension of the natural progression of disease in terms of visual function and the development of macular lesions. Detailed information about the progression of early AMD in relation to visual function may help to identify earlier, those who may benefit from treatment and facilitate clinical decisions regarding treatment. With the development of new treatment options for the earlier non-exudative form of AMD, which accounts for the majority of cases, it is increasingly more important to detect early changes due to AMD. The earlier identification of patients where treatment is necessary may help to improve visual prognosis and therefore diminish the social and financial burden of partial sight and blind registration. The identification of both structural and functional change at all stages of AMD aids the detection of the early disease changes.

The quantification of structural changes in AMD have previously been standardised by grading and staging systems relating to fundus photographs (Bird et al. 1995; Klein et al. 1991; van Leeuwen et al. 2003b; AREDS 2001; Seddon et al. 2006). The value of digital image analysis is in providing objective measures to help reduce the variability between graders in manual grading. The increasingly aged population will amplify the strain on medical resources and thus will benefit from widespread screening of individuals for diseases such as AMD and telemedicine. The development of digital image analysis will facilitate such clinical strategies.

Numerous tests of functional change have been examined in AMD, however psychophysical testing relates more to visual experience than any other test of visual

function (McClure et al. 2000). Perimetry is a psychophysical test which measures the functional vision of the eye across the visual field by measuring the differential light sensitivity. It has long been considered essential in the diagnosis and management of eye diseases such as glaucoma. The visual field is traditionally represented as the "hill of vision" in which sensitivity peaks at fixation and gradually declines towards the periphery. A perimeter familiar to most clinicians is the Humphrey Field Analyser (HFA) and is considered to be the gold standard in glaucoma diagnosis and monitoring. The findings in this thesis, using the HFA are therefore representative of an instrument which is already widely used and is immediately available. Despite poor fixation being associated with AMD, it has been reported that 75% of eyes with choroidal neovascularisation had predominantly central fixation (Fujii et al. 2003). Visual field progression has been widely investigated in glaucoma, but the progression of severity of AMD has received little attention. No attempt has yet been made to quantify the rate of visual field loss across stage of severity of AMD, using perimetry.

Previous research has suggested the suitability of measuring short-wavelength automated perimetry (SWAP) in AMD (Remky et al. 2001b; Remky & Elsner 2005). Despite the failure of SWAP to gain wide spread clinical use due to greater threshold measurement variability, the central 10 degrees of the visual field is known to present less variability (Cubbidge et al. 2002), and is primarily the area of interest in AMD. Using a previously collected normal empirical SWAP 10-2 database (Conway 2003), it was possible to calculate visual field indices and generate probability analyses in order to quantify the status of the visual field. No previous study has yet compared SWAP and standard perimetry using empirically derived visual field parameters for the SWAP 10° visual field in patients with AMD.

2.2 Aims

The aims of this research were to measure the visual field in patients with AMD, examine the structure to function relationships in AMD and quantify the progression of

visual field loss. In order to implement these aims, it was necessary to evaluate several factors influencing the methodology and any errors which might occur in the assessment of visual field progression. These included the accuracy of the refractive correction on SWAP, the learning effect in the 10° field, techniques of assessing the structure to function relationships between fundus imaging types and the visual field and the variability of structural measures between imaging types. The detailed aims were to:

- Investigate the effect of spherical defocus on SWAP. The blue stimulus and yellow background in SWAP cause a chromatic difference of refraction at the eye and an attempt was made to correct this using spherical defocus. The aims were to determine the effect of defocus on threshold sensitivity, with a view to finding the optimum refractive correction to be used in SWAP.

- Evaluate the learning effect in subjects with and without AMD in standard perimetry and SWAP, in the 10° visual field. It is known that in a series of standard visual field examinations using a white stimulus presented against a white background, the largest learning effect occurs between the first two visits (Heijl et al. 1989; Heijl & Bengtsson 1996). Knowledge of the greatest magnitude of any learning effect present is useful in determining the amount of progression of true visual field loss.

- Write computer programs to perform imaging analyses, in order to facilitate the grading of features of AMD from fundus photographs and to map the visual field onto the fundus image. It was necessary to develop techniques to relate structural and functional changes and to determine the accuracy with which this could be performed. Additionally, the variation in clinical judgement between graders when grading images using the custom written program, was of importance since the determination of progression of visual field loss in Chapter 7 was based on the assigned stage of AMD.

- Compare the appearance of drusen in colour fundus photography and retro-mode scanning laser imaging by quantifying drusen in both imaging types. The difference in appearance between the two imaging types bears differing structural measures, thus influencing the determination of severity of disease and the relationships to functional measures.
- Measure the visual field progression in AMD in a cross-section of patients at various stages of disease, using standard perimetry and SWAP. The aims were to compare the relationship between the stage of disease to the functional loss in standard perimetry and in SWAP. Supplementary to this, the purpose was to assess the position of visual field defects and the ability of visual field parameters to detect visual field loss.
- Examine the relationships between functional change in the visual field and structural changes at the macula, as measured by automated drusen segmentation software. The structural measures were evaluated on a continuous scale of severity as opposed to the ordinal scale of stage of disease, which offered further statistical manipulation.

2.3 Logistics

The research was conducted at the Aston University Day Hospital within the Ophthalmic Research Group at Aston University, Birmingham. The study investigating defocus in SWAP (Chapter 3) gained ethical approval from Aston University Human Science Ethical Committee and undergraduate optometry students were recruited. Approval from the Aston University Human Science Ethical Committee and the NHS West Midlands Research Ethics Committee was obtained for the investigation of structural and functional measures on patients with and without AMD. Patients with AMD were recruited from the Birmingham and Midland Eye Centre, City Hospital, Birmingham and the Aston University Eye Clinic. Normal subjects were recruited as spouses of the patient group, from the Aston University Eye Clinic and from the general

public. The patients were diagnosed with AMD in the hospital clinic, where access to the hospital notes was available, or they had previously been diagnosed in another hospital clinic or were diagnosed from fundus imaging by an ophthalmologist, Professor Jonathan Gibson, who also confirmed diagnoses of all patients.

The main reasons for exclusion of subjects from the study either during recruitment or afterwards were diabetes, treatment of AMD, large refractive error, other retinal disease, family history of glaucoma and high number of fixation errors. Pseudophakic subjects were included in the recruitment, however they comprised a small minority of three subjects and ultimately their data was removed from the analyses. Data collected from each participant was included according to the study criteria and the inclusion details for each participant is shown in Table 2-1.

Detailed written and verbal explanations of the study were given to each subject before partaking in any of the studies. Before being formally enrolled, written informed consent was obtained and the opportunity to ask questions was given. Subjects were informed that they were free to withdraw from the studies at any time.

Imaging instrumentation was borrowed with permission from Birmingham Optical Group, who permitted use of the F-10 scanning laser ophthalmoscope and the RS-3000 OCT (Nidek, Japan). Limited time in which to use these instruments narrowed the time in which to collect data and limited the number of patients.

Expert graders from Heart of England NHS Foundation Trust, Solihull, UK performed drusen quantification on anonymised images using the custom written software, for the study in Chapter 6. The programs developed in Chapter 5 were written in Liberty BASIC (Shoptalk Systems, Massachusetts, USA) under the guidance of Dr Mark Dunne. Permission to use the drusen segmentation software, RIALAB, was given by Dr R. Theodore Smith and Noah Lee from the University of Columbia, USA, who sent a version of the software.

Data management was carried out by entry of all data into a database. Statistical analysis was performed using SPSS (version 15.0).

AMD Patients	Stage of AMD RE / LE	Ch. 4	Ch. 5	Ch. 6	Ch. 7	Ch. 8	Normal Subjects	Ch. 4	Ch. 7
1	0 / -		x		x	x	1	x	x
2	1 / 1	x	x	x	x	x	2	x	x
3	- / 1	x	x	x	x	x	3	x	x
4	1 / 1	x	x	x	x	x	4	x	x
5	2 / 1	x	x	x	x	x	5	x	x
6	- / 0	x	x	x	x	x	6	x	x
7	2 / 2	x	x	x	x	x	7	x	x
8	- / 2	x	x		x	x	8	x	x
9	1 / 1	x	x				9	x	x
10	4 / 4	x	x	x	x	x	10	x	x
11	4 / 4	x	x		x	x	11	x	x
12	1 / -	x	x	x	x	x	12	x	x
13	- / 4	x	x		x	x	13	x	x
14	2 / 4		x				14	x	x
15	1 / -	x	x	x	x	x	15	x	x
16	3 / 3	x	x	x	x	x	16	x	x
17	4 / 4		x		x	x	17	x	x
18	4 / 4	x	x	x	x	x	18	x	x
19	4 / 2	x	x		x	x	19	x	x
20	0 / 0	x	x	x	x	x	20	x	x
21	0 / 0	x	x		x	x	21	x	x
22	0 / 0	x	x	x	x	x	22	x	x
23	2 / -	x	x	x	x	x			
24	1 / 3	x	x	x	x	x			
25	- / -		x						
26	0 / 0	x	x	x	x	x			
27	1 / -		x	x	x	x			
28	4 / 1	x	x		x	x			
29	0 / 0	x	x	x	x	x			
30	0 / 4	x	x	x	x	x			
31	0 / 0		x	x					

Table 2-1. Participants included in each study throughout the thesis.
x indicates subjects who took part in each study, stage of each eye is shown in the format right eye AMD stage/left eye AMD stage, - indicates an excluded eye or an eye for which it was not possible to assign a stage.

3. Investigation of Longitudinal Chromatic Aberration on Short-Wavelength Automated Perimetry (SWAP) Using Spherical Defocus

Summary

In short-wavelength automated perimetry (SWAP) a 440nm blue stimulus is presented against a high luminance broadband yellow background. Since the eye focuses on the yellow background, longitudinal chromatic aberration will cause the blue stimulus to be defocused by approximately -1.00D. The aim of the study was to examine the influence of the chromatic interval on short-wavelength sensitivity as a function of positive and negative defocus and of visual field eccentricity. Twenty-eight emmetropes (mean age 21.8; SD 2.81) were examined under cycloplegia. Short-wavelength visual field sensitivity was obtained at six locations for eleven levels of spherical defocus ranging from +2.00D to -2.00D. The overall effect of spherical defocus on mean sensitivity (MS) was significant ($p < 0.001$). Positive defocus caused a significant decline in MS (Spearman's correlation coefficient: rho = -0.114, $p < 0.001$). Negative defocus had no significant effect on MS (rho = 0.014, $p = 0.661$), due to a slope of 0.066dB per dioptre. Eccentricity had a significant effect on MS ($p < 0.001$), exhibiting a peak at 7.2°, and a decline towards the periphery, due to the normal physiological profile of the hill of vision. These results suggest that SWAP is robust to defocus, when using low powered negative spherical lenses.

3.1 Introduction

SWAP presents a narrowband 440nm blue Goldmann size V (1.72°) stimulus against a high luminance broadband yellow background, of intensity 100cd/m^2. These parameters provide approximately 1.5 log units of short-wavelength sensitive pathway isolation, by suppressing neural activity in the rod, medium- and long- wavelength sensitive pathways (Cubbidge & Wild 2001; Sample et al. 1996).

Chromatic aberration is the dispersion of white light into component colours, by an optical system. Like other optical systems, the eye exhibits chromatic aberration, which leads to different wavelengths of light focusing at different lateral and axial points of the retina (Howarth & Bradley 1986). Longitudinal chromatic aberration (LCA) represents an axial difference in focus between wavelengths and transverse chromatic aberration (TCA), is a lateral shift of focus between wavelengths. Although TCA has much greater variation between individuals than LCA, the mean foveal TCA is zero (Rynders et al. 1995), and therefore TCA can be considered to have a negligible impact on measured thresholds in SWAP. Similarly, there is a negligible effect of the chromatic difference in magnification (CDM) between different wavelengths, which has a very small effect of less than 1 % between 400 and 700 nm (Zhang et al. 1993). For the human eye, the peak spectral sensitivities of the medium- and long-wavelength sensitive cones are 530 and 560 nm respectively (Schnapf et al. 1987).

Under the adapting conditions of SWAP, the eye is focused on the yellow background. When the blue stimulus is presented in the field for 200 ms, it will be defocused due to the LCA of the eye. Thus the difference in wavelength between the background and stimulus luminance, yields a chromatic difference of refraction at the eye. LCA can be expressed as the magnitude of the chromatic difference of refraction of the human eye, which has been determined experimentally in vivo, by numerous investigators (Howarth & Bradley 1986; Rabbetts 1998; Thibos et al. 1992; Williams et al. 1983). When the human eye is in focus for medium wavelengths, the point of focus for the short

wavelengths to which the blue cones are most sensitive, falls in front of the retina, creating a chromatic aberration of about -1.00 D (Williams et al. 1991).

The spectral distribution of the yellow background in SWAP on the Humphrey Field Analyser (HFA) 750, as measured by a spectroradiometer, shows a peak at 624nm (Figure 3-1; Cubbidge 1997). A four-term Cauchy equation of chromatic dispersion, shows the variation in refractive index of optical materials with wavelength (Cauchy 1895). Empirical data obtained by Atchison & Smith (2005) was reported to accurately conform to the Cauchy equation for the chromatic difference of refraction at a given wavelength, $R_x(\lambda)$. Where,

$$R_x(\lambda) = 1.60911 - \frac{6.70941 \times 10^5}{\lambda^2} + \frac{5.55334 \times 10^{10}}{\lambda^4} - \frac{5.59998 \times 10^{15}}{\lambda^6}$$

gives the chromatic difference of refraction between a wavelength, λ, and the reference wavelength of 590nm. This equation takes into account the refractive indices of the ocular media of the human eye, from the Gullstrand number 1 schematic eye with a gradient refractive index lens. The chromatic difference of refraction between the wavelengths of the stimulus and background parameters used in SWAP (440nm and 624nm, respectively), is given by the difference between $R_x(624)$ and $R_x(440)$.

$$R_x(440) = -1.147 \text{ D}$$

$$R_x(624) = 0.157 \text{ D}$$

$$\text{Therefore, } R_x(624\text{-}440) = 1.30 \text{ D}$$

Thus the difference between the two values gives the chromatic difference of refraction in SWAP to be -1.30D (Figure 3-2).

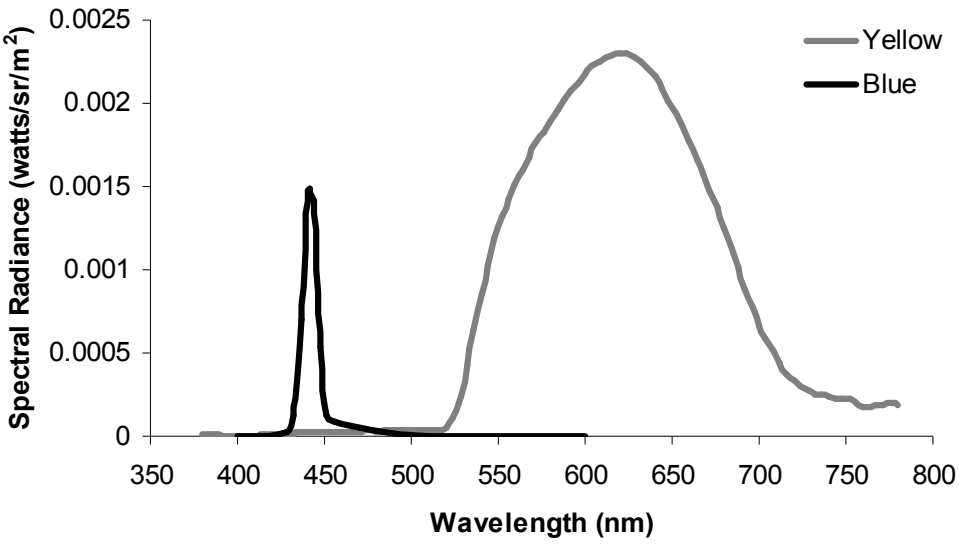

Figure 3-1. The spectral distribution of SWAP. The yellow background exhibits a peak at 624nm and the blue stimulus shows a peak at 440nm (Cubbidge 1997).

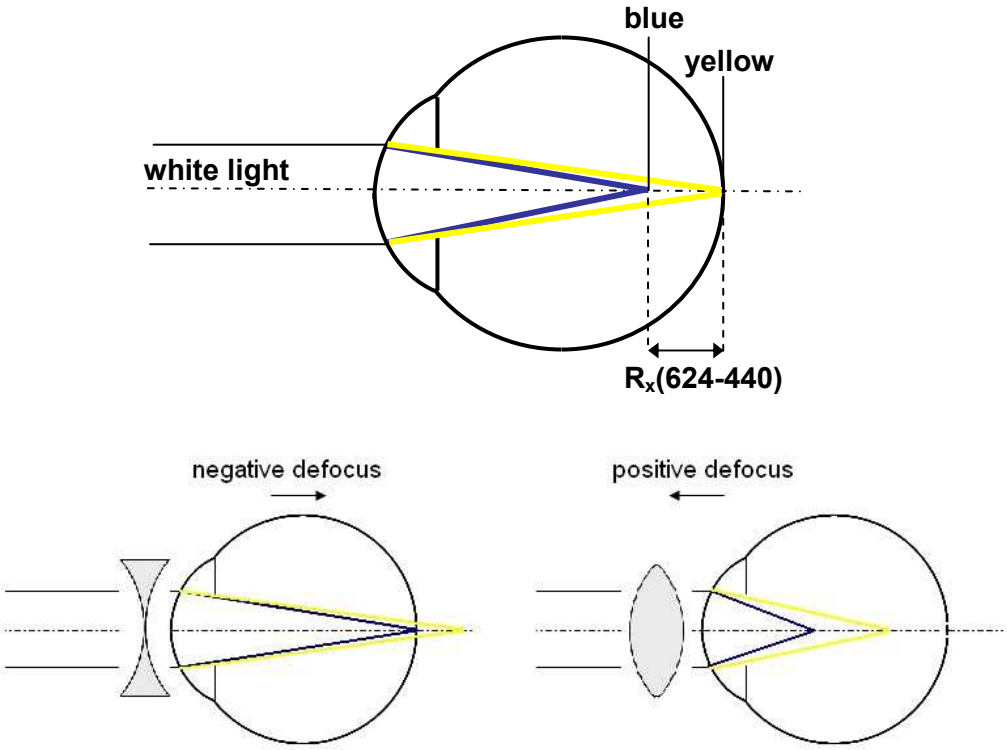

Figure 3-2. Longitudinal Chromatic Aberration
The emmetropic eye focuses on the yellow background, which dominates the visual field. Consequently, the blue stimulus is focused in front of the retina. When defocus is applied, there is a shift of focus in opposing directions for positive and negative defocus.

In standard perimetry, defocus causes a reduction in threshold sensitivity especially for small sized stimuli (Anderson et al. 2001; Atchison 1987; Sloan 1961). The effect of defocus declines at greater eccentricities away from fixation (Anderson et al. 2001; Benedetto & Cyrlin 1985; Fankhauser & Enoch 1962; Maguire 1971; Sloan 1961). This function has less impact on larger stimulus sizes (Atchison 1987; Sloan 1961). The effect of optical defocus on SWAP has not previously been investigated using lenses of negative dioptric power. Positive spherical lenses have been used to simulate uncorrected refractive error in SWAP (Adams et al. 1987; Johnson et al. 1993a). Defocus up to +5.00D was found to have minimal effect on SWAP sensitivity (Adams et al. 1987; Johnson et al. 1993a). Little difference between foveal and peripheral sensitivities in SWAP has been documented (Johnson et al. 1993a).

The aim of this study was to examine the influence of LCA, expressed as the chromatic dioptric difference, on short-wavelength sensitivity as a function of both positive and negative defocus and visual field eccentricity.

3.2 Methods

The sample consisted of twenty-eight normal observers (mean age 21.8, SD 2.81, range 19-31 years), including 12 males and 16 females. Inclusion criteria were Snellen visual acuity in the dominant eye of 6/6 or better, no colour vision abnormalities, clear ocular media, intra-ocular pressure less than 21mmHg (Pulsair EasyEye, Keeler Ltd., Windsor, UK), normal optic nerve appearance, open angles, no systemic medication known to affect the visual field, no previous ocular surgery or trauma, no history of diabetes mellitus and no family history of glaucoma or diabetes mellitus. Only emmetropic subjects, with refractive errors within ± 0.50 dioptres, were included in the study. Ethical approval was obtained for all procedures from the Aston University Human Sciences Ethical Committee and written informed consent was acquired for each patient.

Subjects underwent three visits consisting of SWAP examinations, on the HFA 750,

using their dominant eye. The first visit was a central 24-2 examination using the FASTPAC algorithm, which was discarded to reduce the learning effect (Autzen & Work 1990; Heijl et al. 1989; Searle et al. 1991; Wild et al. 1989; Wild & Moss 1996; Wood et al. 1987). At the second examination each subject underwent cycloplegia using 1 drop of tropicamide 1% (*Minims*, Bausch & Lomb). At full cycloplegia the pupil was fixed and dilated with a mean diameter of 8.3mm (SD 0.99). Pupil size remained constant throughout perimetric testing, as observed by the video monitor of the HFA. The custom stimulus configuration consisted of an array of six stimulus locations situated in the inferior temporal quadrant, at eccentricities between 2 and 20° from fixation. The inferior field in SWAP yields greater sensitivity than the superior field (Sample et al. 1997). Indeed, the inferior temporal quadrant of the visual field is the most sensitive to short-wavelength stimuli (Cubbidge 1997), therefore giving rise to the lowest between-subject variability in this area, since greater sensitivity generates smaller confidence intervals. The 4-2dB double reversal Full Threshold staircase strategy was used to estimate the threshold for the selected stimulus locations. Although FASTPAC strategy is recommended in SWAP (Wild et al. 1998), using the 4-2dB strategy did not give rise to a significantly different test duration, due to the minimal number of stimulus locations in the custom test pattern.

A +3.00D lens was placed in front of the eye during perimetry to correct for the distance of the perimeter cupola in the absence of accommodation. The desired level of defocus was added to the correcting lens. In addition to the zero defocus measurement, thresholds were measured at the six stimulus locations for five levels of negative defocus; -0.50D, -0.75D, -1.00D, -1.50D and -2.00D. The third visit employed five levels of positive defocus; +0.50D, +0.75D, +1.00D, +1.50D and +2.00D. All lenses were presented in a random order for each subject in order to avoid order effects. Prior to perimetry, each subject underwent three minutes of adaptation to the yellow background, to enable saturation of the rods and the medium- and long-

wavelength sensitive cone pathways. Each individual visual field test lasted approximately 90 seconds. Five minute rest breaks were given between each test. Identical instructions were given to each subject. Throughout visual field testing, fixation was monitored continuously via the video monitor of the HFA, the gaze tracker and the Heijl-Krakau blind spot monitor. Visual fields were repeated where it was noted that fixation was lost. The accommodative state of each subject was measured between examinations to ensure that cycloplegia was maintained throughout the duration of examination. The back vertex distance of the trial lens was maintained at 12 mm.

All subjects had experience of standard perimetry, but were naïve to the procedure of SWAP. Previous experience of standard perimetry does not influence the learning effect in SWAP (Wild & Moss 1996).

3.3 Analysis

Whenever double determinations of threshold were made during a visual field testing session, the average of the two thresholds was used in the analysis. Mean sensitivity (MS) values were not normally distributed (Kolmogorov-Smirnov: $p < 0.001$). Friedman's two-way non-parametric analysis of variance was used to find the effects of defocus and eccentricity on MS. For defocus, the global index MS was calculated from the six stimuli. For eccentricity, the group threshold sensitivity values without defocus conditions were used. Post-hoc comparisons were made using the Wilcoxon signed-rank test. Correlations between MS and defocus level were examined using Spearman's correlation coefficient, and at each level of eccentricity.

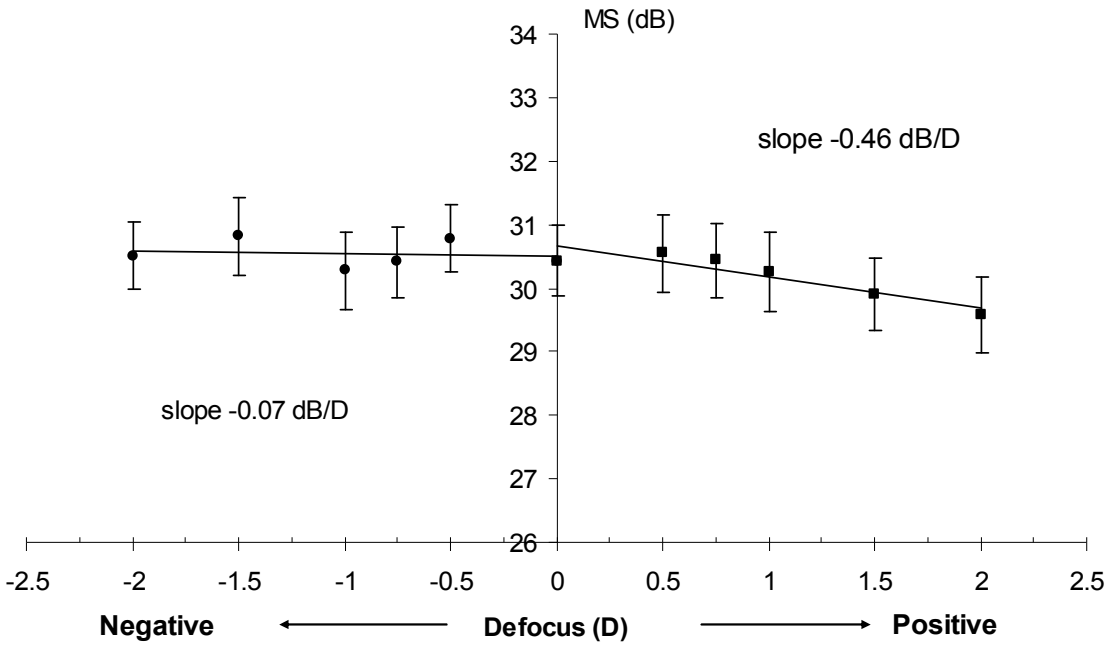

Figure 3-3. The effect of spherical defocus on short-wavelength sensitivity
Graph showing the correlation for short-wavelength sensitivity with positive and negative defocus, error bars indicate one standard error of the group mean.

3.4 Results

3.4.1 The Influence of Defocus on Short-Wavelength Sensitivity

The overall influence of defocus on MS was significant (Friedman test: Chi-square = 34.058, $p < 0.001$). The group MS for optical defocus between +2.00D and -2.00D, is shown in Figure 3-3. The correlation between defocus and short-wavelength sensitivity was investigated for positive defocus and negative defocus. There was a weak but significant decline in MS with positive defocus (Spearman's correlation coefficient: rho = -0.114, $p < 0.001$). Conversely, there was no significant correlation between short-wavelength sensitivity and negative defocus (rho = 0.014, $p = 0.661$) indicating that SWAP is resistant to negative defocus. This finding was further supported by analysis of positive and negative defocus as separate groups, using the Friedman test. The effect of positive defocus had a significant effect on MS (Chi-square = 23.180, $p < 0.001$), whereas the effect of negative defocus did not reach significance (Chi-square = 9.950, $p = 0.077$). Post hoc comparisons between defocus levels indicated significant

differences between MS, between the pairs plano and +2.00 (Wilcoxon signed-rank test: Z = -2.602, p = 0.009), +0.50 and +1.00 (Z = -2.041, p = 0.041), +0.50 and +2.00 (Z = -3.631, p < 0.001), +0.75 and +1.50 (Z = -2.199, p = 0.028), +0.75 and +2.00 (Z = -2.907, p = 0.004), +1.00 and +2.00 (Z = -2.132, p = 0.033).

3.4.2 The Influence of Eccentricity on Short-Wavelength Sensitivity

When the effect of defocus was removed, the main influence of stimulus eccentricity on the group MS was significant (Friedman test: Chi-Square = 57.118, p < 0.001). The graph in Figure 3-5 exhibits peak short-wavelength sensitivity at 7.2° with a decline towards the fovea and towards the periphery. A similar trend was seen for each level of defocus. Post hoc comparisons using the Wilcoxon signed-rank test indicated significant differences between MS at all eccentricities, except for 2 and 5° (Z = -0.924, p = 0.355), 2 and 10° (Z = -0.082, 0.935), 2 and 15° (-1.570, p = 0.061), 5 and 10° (Z = -1.072, p = 0.284) and 15 and 20° (Z = -1.820, p = 0.069).

The effect of defocus on MS for each level of eccentricity is shown in Figure 3-4 and the correlation between positive defocus and MS for each level of eccentricity is shown in Table 3-1. For positive defocus, the correlation with MS at each eccentricity, showed the steepest slope at 15°, with a decline in MS by 0.72dB per dioptre of defocus (Figure 3-4). Of all eccentricities measured, the correlation coefficients at 2.2, 5 and 15° achieved statistical significance for a weak negative correlation with sensitivity (Table 3-1). For negative defocus, there were no significant correlations at any level of eccentricity.

Eccentricity (°)	Slope (dB/D)	Spearman's correlation coefficient, rho	p-value
2.2	-0.496	-0.153	**0.048***
5	-0.580	-0.169	**0.028***
7.2	-0.488	-0.108	0.163
10	-0.391	-0.084	0.276
15	-0.720	-0.188	**0.015***
20	-0.108	-0.064	0.412

* significant

Table 3-1. Correlation coefficients for positive spherical defocus, for each level of eccentricity

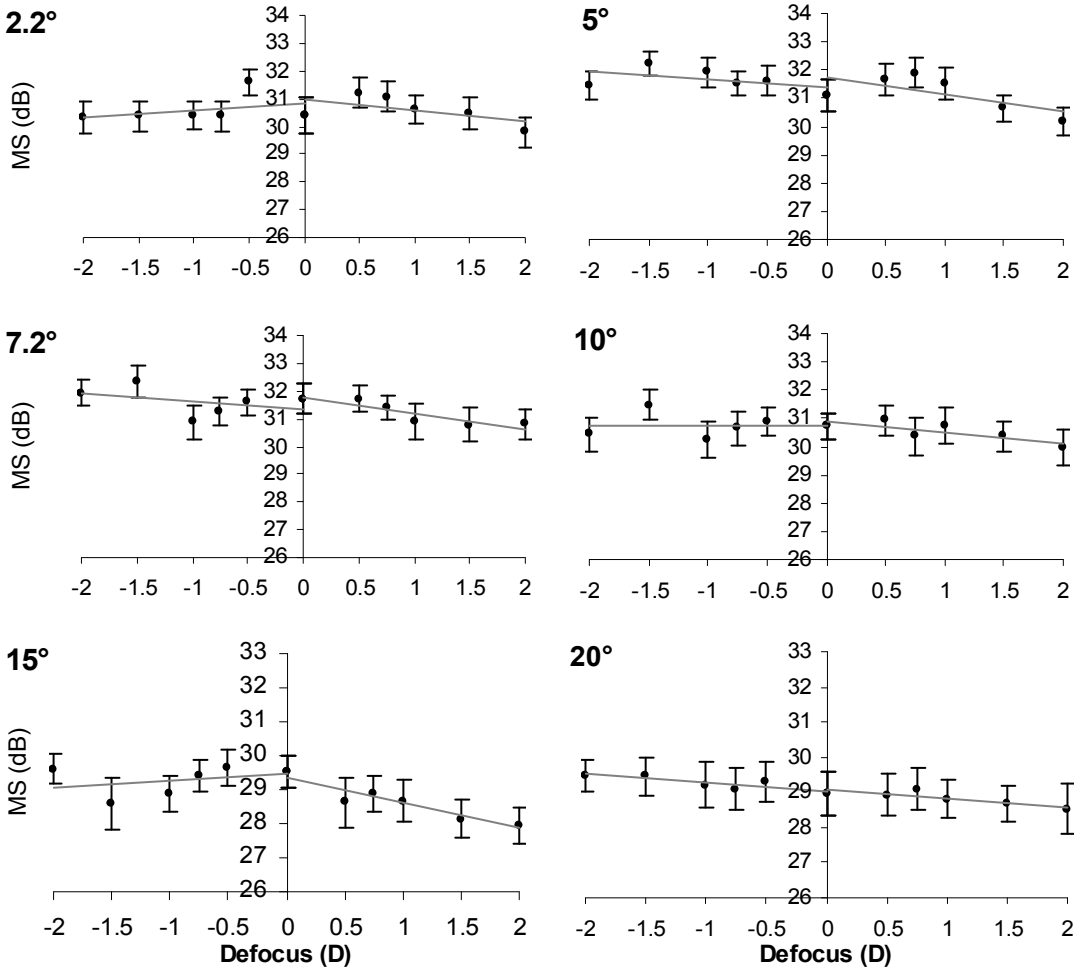

Figure 3-4. The effect of spherical defocus on MS for each level of eccentricity. Error bars indicate one standard error of the group mean.

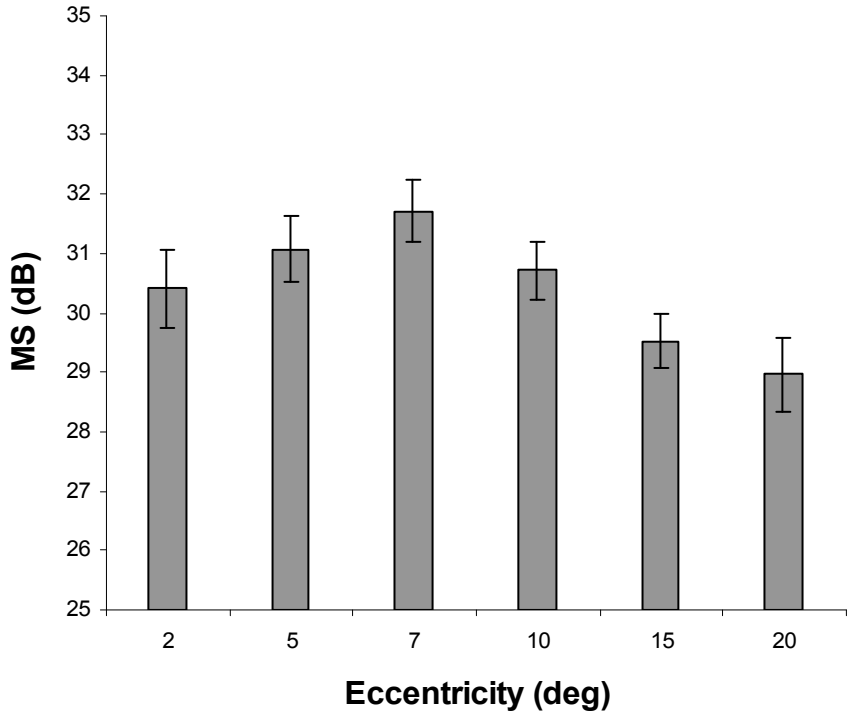

Figure 3-5. The effect of eccentricity on short-wavelength sensitivity, with no induced defocus
Error bars indicate one standard error of the group mean.

3.5 Discussion

The accommodation response is slower for short-wavelength sensitive cones alone compared to long- and medium-wavelength sensitive cones (Rucker & Kruger 2004) and varies greatly between individuals (Rucker & Kruger 2001). In SWAP, under normal accommodation, when short-wavelength sensitive cones are isolated, the eye focuses the yellow component of the retinal image on the retina. This leaves the blue component in front of the retina due to the longitudinal chromatic aberration of the eye (Figure 3-2), despite the resulting blur from defocus (Seidemann & Schaeffel 2002). Isolating the short-wavelength sensitive cone pathway causes the eye to over-accommodate to deliberately allow the blue image to be myopic. Due to longitudinal chromatic aberration, the habitual focus condition for the blue component of an image, when viewed in white light also lies in front of the retina. In explanation, this occurs due to the relative paucity of short-wavelength sensitive cones in the retina, which

make up 5-10% of the entire cone population (Curcio et al. 1991). LCA does not allow the high spatial frequencies of the blue component to reach the smaller number of short-wavelength sensitive cones in the retinal mosaic, in order to prevent aliasing (Williams et al. 1983). Aliasing is a distortion or misperception, which occurs due to undersampling, where detail in the retinal image is too fine to be resolved.

These results present evidence that SWAP is more robust to negative defocus than positive defocus between ±2.00D. In SWAP, the chromatic difference of refraction which occurs between the blue and yellow wavelengths, causes the chromatic focus for blue to lie in front of the retina. The addition of negative defocus, which brings the blue stimuli into sharper focus, neither caused sensitivities to increase nor decrease, for a target of low spatial frequency. However, the addition of positive defocus acts to shift the focus in the opposite direction, making the stimuli more blurred, which causes greater decline in sensitivity, than for negative defocus (Figure 3-2). These results have an impact on subjects who lack in accommodative facility for the working distance of the perimeter. The longitudinal chromatic aberration of the eye increases with accommodation (Rabbetts 1998). Under conditions of short-wavelength pathway isolation, defocus of less than 1.50D had no significant effect on letter acuity in pre-presbyopic subjects with normal accommodative facility (Rabin & Adams 1990). However, in a minority of subjects with large accommodative errors, significantly reduced acuity of the short-wavelength sensitive pathway was achieved. Swanson (1989) measured the resolution acuity of the short-wavelength sensitive pathway using square wave grating stimuli, through negative corrective lenses (Swanson 1989). The acuity was highly dependent upon accommodative state, and the younger subjects used a wide range of accommodative states, which was suggested to be caused by the weak accommodative cues of the blue-on-yellow stimuli. Under cycloplegia, acuity decreased with increasing power of negative lens.

Although the results for positive defocus appear to conflict with previous studies of defocus and SWAP (Adams et al. 1987; Johnson et al. 1993a), direct comparisons cannot be made. These earlier studies generated SWAP with a modified HFA (Johnson et al. 1993a) and a Berkeley Colour Threshold Test (Adams et al. 1987). The instrumentation parameters had higher luminance yellow backgrounds of 200cd/m^2 (Johnson et al. 1993a) and 500cd/m^2 (Adams et al. 1987) and broadband blue stimuli and did not employ cycloplegia to control for pupil diameter. The higher luminance yellow background caused pupillary miosis and therefore greater resistance to defocus. The broadband blue stimulus allowed for less isolation of the short-wavelength sensitive cones and different adaptation levels. The effect of negative defocus has not previously been investigated in SWAP and thus the comparison between positive and negative defocus has not been made. In a study which simulated conditions similar to standard perimetry, foveal threshold sensitivity declined with both positive and negative defocus (Anderson et al. 2001), whereas the decline in short-wavelength sensitivity only occurred with positive defocus in the present study. The rate of sensitivity decline with positive defocus in standard perimetry within a 5° field was reported to be -1.84dB/D (Herse 1992). The corresponding results in the present study were -0.50dB/D and -0.58dB/D, at 2.2 and 5°, respectively. A diminished effect of defocus on SWAP compared to standard perimetry is to be expected as a result of the differing stimulus sizes employed. The high spatial frequencies contained within the small achromatic stimulus (0.43°) are more degraded by defocus than the low spatial frequency components of the SWAP stimulus (1.72°). Indeed, the decline in foveal threshold sensitivity with defocus has been found to occur at a greater rate for smaller stimuli (Anderson et al. 2001). SWAP is therefore relatively unaffected by defocus in comparison to standard perimetry. The greatest group mean difference in MS between defocus levels was 1.26dB, which occurred between +2.00D and -1.50D. Previous measurement of the magnitude of the average short-term fluctuation (SF) in SWAP ranges between 0.46 and 2.02dB (Kwon et al. 1998; Takahashi et al. 1999; Wild et al.

1998). Thus the effect of defocus on SWAP in the present study could be regarded as insignificant, as it is within the magnitude of the SF. The relative insensitivity of SWAP to defocus may be somewhat accounted for by the poor resolution of the short-wavelength sensitive pathway (Green 1968; Kelly 1973; Rabin & Adams 1990; Swanson 1989), since lower acuity yields a greater tolerance to defocus (Legge et al. 1987).

An additional explanation for the robustness of SWAP threshold to defocus may have a neurological basis. At the fovea, acuity for achromatic stimuli is optically limited, whereby the optics of the eye do not pass spatial frequencies greater than the spatial sampling limit of the neural array. Foveal acuity for short-wavelength sensitive stimuli however, was found to be sampling limited as evidenced psychophysically by aliasing (Anderson et al. 2002). The resolution limit of the short-wavelength sensitive pathway is therefore much lower than the limit defined by the optics of the eye and is relatively less affected by lower optical quality due to defocus than other pathways.

The variation in MS with eccentricity is steeper in SWAP than in standard perimetry (Landers et al. 2006). The results show that MS varied with eccentricity, whereby a peak was noted at 7°, and a decline towards the fovea and towards more peripheral eccentricities. The decline from 7° to 20° can be attributed to the profile of the normal hill of vision. This was confirmed by the normal database for SWAP on the HFA, for a 22 year old, using the 24-2 program and the full threshold algorithm, which showed the decline of 2dB between 4 and 21° (31dB to 29dB). A similar magnitude and decline in sensitivity was observed in this study (Figure 3-5). The decline in MS at eccentricities of 5° and less may accounted for by the presence of macular pigment, which is known to cause a depression at the fovea and parafovea in the SWAP hill of vision (Wild 2001). Indeed, the peak density of macular pigment occurs at the centre of the fovea and declines to an eccentricity of 5° (Snodderly et al. 1984). Furthermore, the foveal threshold exhibits larger between-subject variability than immediately surrounding

stimulus locations in SWAP, due to physiological foveal tritanopia and peak density of macular pigment (Wild et al. 1998). For this reason, the foveal threshold was not assessed in this study.

Positive defocus caused a decline on MS at all eccentricities, although this failed to achieve statistical significance for correlations at 7, 10 and 20°. The mean density profile of blue cones in the inferior and temporal retina peaks at around 2000 cones/mm^2 at an eccentricity of less than 1°, before tapering off to an asymptote of 500–600 cones/mm^2 beyond 12–15° (Curcio et al. 1991). If beyond 15° there is not a large short-wavelength sensitive response, due to the relatively small number of short-wavelength sensitive cones, different mechanisms may influence the defocus effect, thereby lending less credence to the data at 20° and relatively greater importance to the data at 2 and 5°.

In conclusion, when compared to the effects of defocus on standard perimetry in previous studies, SWAP appears to be more resistant to defocus than standard perimetry. SWAP is more robust to negative defocus than positive defocus. The clinical implications relate to the correcting lens used in SWAP, for presbyopic patients and subjects with insufficient accommodative facility for the working distance of the perimeter. The near vision addition used to correct for working distance must not be overcorrected, but a slight undercorrection is of less clinical importance.

4. The Learning Effect in the Central Standard and Short-Wavelength Visual Fields

Purpose: To document the magnitude of any learning effect for standard perimetry and short-wavelength automated perimetry (SWAP) in the ten degree visual field in patients with age-related macular degeneration (AMD) and normal control subjects.

Methods: Twenty-five patients with AMD and 22 normal subjects underwent standard and SWAP field examinations with the Humphrey Field Analyser (HFA) on two occasions, separated by one week. At each visit, both eyes were tested using Program 10-2 of the HFA. Between visit and inter-eye changes in global indices and pointwise evaluation of probability analyses were documented.

Results: Significant improvements were observed between visits in the mean sensitivity (MS) ($p = 0.042$), mean deviation (MD) ($p = 0.036$) and examination duration ($p = 0.047$) for standard perimetry; and the MS ($p = 0.012$) and MD ($p = 0.005$) in SWAP, in the patient group. In the normal control group, the standard MS ($p = 0.001$), standard MD ($p = 0.001$), SWAP MS ($p = 0.004$), SWAP MD ($p = 0.004$) and number of total deviation defects for SWAP ($p = 0.044$) significantly improved. The mean improvement in the MD at the second visit was 0.38dB in standard perimetry and 0.90dB in SWAP, in the patient group. The mean improvement in the MD at the second visit was 0.55dB in standard perimetry and 0.72dB in SWAP, in the normal group. The second eye examined exhibited a more severe MD than the first eye in all groups. A reduced learning effect in the second eye examined compared to the first eye was evident for all groups except for the patient group performing SWAP, where there was no significant difference. The magnitude of the difference in MD between visits was not significantly different between patients and normal subjects. Stage of AMD did not have a significant effect on the magnitude of change in MD between visits.

Conclusions: A learning effect was demonstrated between the first two visits for the standard and SWAP central visual field, for the global indices MS and MD. The magnitude of learning was not significantly different between the patient group and the normal group and was not influenced by stage of AMD. Deterioration between eyes during visits could be attributed to the fatigue effect.

4.1 Introduction

The learning effect in standard perimetry and SWAP has been described by several researchers (see review in Chapter 1.1.3 and 1.2.2). Aspects of learning have been widely examined in healthy and glaucomatous subjects, but the learning effect in patients with age-related macular degeneration (AMD) is unknown. The learning effect is greater in the peripheral regions of the 24° and 30° field, in standard perimetry (Heijl et al. 1989; Heijl & Bengtsson 1996) and in SWAP (Rossetti et al. 2006; Wild et al. 2006). However the learning effect has not been examined for the ten degree visual field in either standard perimetry or in SWAP.

It has been noted that the greatest learning effect occurs between the first two examinations in standard perimetry (Heijl et al. 1989; Heijl & Bengtsson 1996). Knowledge of the greatest magnitude of any learning effect present enables insight into possible errors involved in assessment of visual field progression from serial and cross-sectional analysis. Therefore, the aim of this study was to evaluate the presence of a learning effect on visual field parameters in the 10° field in standard perimetry and SWAP in normal subjects and AMD patients.

4.2 Methods

4.2.1 Sample

Based on the SF and an estimation of the standard deviation of the MD in SWAP using the FASTPAC threshold estimating algorithm (1.89dB and 5dB, respectively), a sample of 19 would give a 90% confidence level and a sample of 27 would give 95% confidence of detecting change.

Patients and their spouses were recruited from Birmingham and Midland Eye Centre and the Aston University Eye Clinic. The sample comprised 25 patients (mean age 70.0 years, SD 8.6, range 46-88 years, 6 males, 19 females) at various stages of AMD and 22 normal subjects (mean age 67.5 years, SD 7.5, range 49-78 years, 13 males, 9 females). The normal subjects were age-matched to the AMD patients as closely as

possible. All patients had experience of at least one visual field screening examination, as part of routine optometric care, however all patients were naïve to SWAP and to the 10° field examination. Participating subjects conformed to the inclusion criteria of distance refractive error of less than ±5.00D sphere and ±2.00D cylinder in each eye, clear ocular media as defined by Lens Opacity Classification System LOCS III (Chylack et al. 1993) graded at a slit lamp, no greater than NC3, NO3, C1, P1, no pseudophakia, intraocular pressures less than 21mmHg using non-contact tonometry (Pulsair), normal optic nerve head appearance, no family history of glaucoma, no history of ocular disease other than untreated AMD, no ocular trauma, no neurological history or systemic disease, no systemic medication known to influence the visual field and no congenital colour vision defect using the Farnsworth-Munsell 100 Hue test. The distribution of visual acuities is shown in Figure 4-1. Corrected visual acuity was at least 0.1 logMAR in each eye, in the normal group. Informed consent was obtained from each subject and the study had approval from the Aston University Human Sciences Ethical Committee and the NHS West Midlands Research Ethics Committee. Characteristics of the sample are given in Appendix 1.

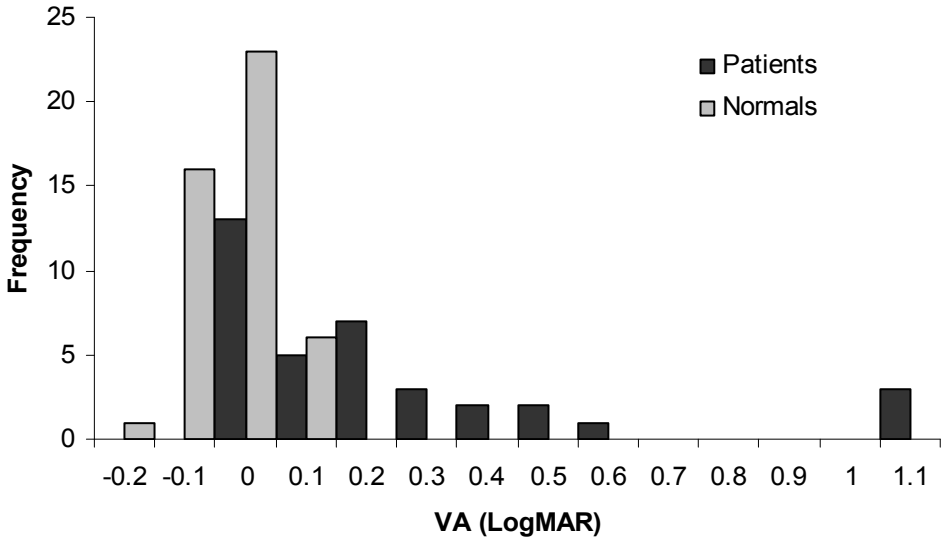

Figure 4-1. Frequency histogram showing the distribution of visual acuity (VA) in the patient and normal groups

4.2.2 AMD Grading

Fundus photography was performed on patients with dilated pupils, in order to optimise image quality. A non-mydriatic camera (Canon EOS 10D camera, 6.3 megapixels) was used to acquire stereoscopic pairs of 30° field digital images centred at the macula. Images were stored as high quality JPEG files (large/fine, ~2.4MB, 3072 x 2048) and graded in a random order for the retinal features according to the International Classification and Grading System (Bird et al. 1995). Stage of disease was determined according to the stages of severity defined by an epidemiologic study, based on progression rates of features over a 6.5-year period (van Leeuwen et al. 2003b). Grading and stage determination was carried out by two independent, masked graders (JMG & JHA). For the purposes of this thesis, the subjects who had gradable features using this classification were defined as belonging to the AMD patient group.

4.2.3 Perimetry

Each subject underwent standard perimetry and SWAP using the HFA 750 on two separate occasions using Program 10-2. The 10-2 program is a 10° field, with a stimulus separation of 2°. For standard perimetry, the stimulus size was Goldmann size III (0.43°) and background illumination was 31.5 apostilbs. The projected stimuli may be varied in intensity over a range of more than 51 decibels (between 0.08 and 10,000 apostilbs) and were presented with a duration of 200ms. Background and stimulus conditions for SWAP are described in Chapter 1.2. SITA Standard and FASTPAC algorithms were employed for the standard and SWAP fields, respectively, in order to mimic clinical practice as closely as possible. Each visit was separated by eleven days (range 7-15 days). A short interval such as this to study learning effects in perimetry has been advocated due to the shorter time period emphasising the visual field improvement and its ability to estimate learning over longer periods (Wild & Moss 1992). Furthermore, two baseline fields performed within a short period are recommended in the detection of visual field change (Hoskins et al. 1988).

Both eyes were examined at each visit and the data was discarded from 8 patients. Six patients had one treated eye (PDT or laser), one patient had a macular hole and one patient was pseudophakic in one eye. In the normal group visual field data was discarded from 3 patients due to poor fixation. The age-matched normal database from which the global indices are calculated in SWAP was collected on subjects with normal lens yellowing in older adults. The normal sinking of the hill of vision due to lens changes is not present in subjects with pseudophakia, who achieve abnormally high indices. Thus, it was necessary to exclude pseudophakic eyes. Consequently, 42 eyes and 41 eyes were included in the analysis for the patient and normal groups, respectively. The right eye was always examined first with the exception of subjects in the patient group where there was a large difference in visual acuity between the two eyes, in which case the better eye was examined first. One researcher (JHA) conducted all testing and issued identical instructions to each patient. The non-examined eye was occluded with an opaque patch and the refractive correction appropriate to the bowl distance was placed before the test eye with full aperture trial lenses. The order in which the visual fields were examined was standard perimetry first and then SWAP. Fatigue effects are known to be greater in SWAP than in standard perimetry (Cubbidge 1997). As a result a greater recovery period would have been necessary had the SWAP fields been performed first, in a randomised order design.

Before each examination, subjects underwent three minutes of adaptation to the bowl luminance and its chromatic properties. Fixation losses were less than 20% in 256 field examinations. In the remaining 76 fields, 10 were discarded due to high fixation losses and 60 fields had less than 33% fixation losses. Although 20% fixation losses were previously advocated (Katz & Sommer 1988) evidence from reliability trials has increased the recommended value to 33% (Johnson & Nelson-Quigg 1993). 6 fields had less than 47% fixation losses and the decision to include these fields in the

analysis was made based on all the parameters of fixation monitoring. The gaze tracker continually monitors fixation and the perimetrist constantly observed fixation via the video monitor of the HFA in order to judge the quality of fixation, whereas the catch trials sample the fixation at an inconsistent frequency. Fixation is inherently more difficult for patients with central scotomata, which was the case for the fields with fixation losses. False negative and false positive responses were less than 33%, which is the standard recommendation (Sanabria et al. 1991). Rest periods were enforced, each lasting one minute and introduced at four minute intervals during the examination. A five minute rest period was given between eyes, and ten minutes between standard perimetry and SWAP examinations.

4.2.4 Analysis

The weighted global indices mean deviation (MD) and pattern standard deviation (PSD) were obtained from the HFA printout. For SWAP the indices, MD, PSD, short-term fluctuation (SF) and corrected pattern standard deviation (CPSD) were unweighted and calculated from a previously collected normal database (Conway 2003). The weighting of indices has been evaluated in past studies. It was reported that the weighted mean deviation index was not significantly advantageous over the unweighted mean defect in the evaluation of the 30° glaucomatous field (Funkhauser & Fankhauser 1991). This was disputed with the argument that perimetric threshold variability is eccentricity dependent and weighted indices represent the visual field with greater accuracy (Heijl et al. 1992). Nevertheless, the weighting of the indices between stimulus locations allows for the increasing variation found at the more peripheral locations of the 24-2 and 30-2 fields (Hejl et al. 1987), and therefore is unlikely to affect validity of the global indices and probability analyses of the central 10° field (Cubbidge et al. 2002). The SITA algorithms do not perform double determinations because variability in the threshold is incorporated into the threshold modelling procedure. Hence the indices SF and CPSD are not calculated for standard perimetry.

Additionally for both perimetry types the examination duration and number of defects on pattern deviation and total deviation analyses were determined. It was not possible to make direct comparisons of thresholds between the differing decibel scales of standard perimetry and SWAP, since the scales are referenced to the maximum stimulus luminance of the perimeter. The dynamic range in standard perimetry is 0 to 10,000 apostilbs (5 log units) whereas in SWAP it is 0 to 65 apostilbs (1.5 log units).

Between visit changes were identified for all eyes examined using the global indices and other visual field parameters. Consideration of the effect of the order in which eyes were tested and the analysis for between-eye differences in visual field parameters included only subjects where data was available for both eyes, and in the patient group, only eyes which were at the same stage of AMD. This included 17 patients and 19 normal subjects.

The magnitude of the learning effect was assessed by examining the change in the MD between visits, since the MD was the principal global index which exhibited a learning effect with the greatest significance. Analysis of the effect of order of eye tested included only patients where data was available for both eyes. The effects of stage of disease and age were considered. Pointwise analysis of the change in probability level at each stimulus location on pattern deviation probability maps was performed.

4.3 Results

In the patient group, the field parameters examined mostly did not exhibit a normal distribution (Kolmogorov-Smirnov test), with the exception of the parameters: number of SWAP TD defects ($p = 0.200$) and change in standard ($p = 0.200$) and SWAP ($p = 0.200$) MD between visits ($p = 0.200$) in the patient group. In the normal group, the visual field parameters with a normal distribution were the standard ($p = 0.200$) and SWAP ($p = 0.200$) MS, the standard ($p = 0.200$) and SWAP MD ($p = 0.092$), the standard PSD ($p = 0.200$), SF ($p = 0.200$) and change in SWAP MD between visits ($p = 0.200$). Consequently, parametric and non-parametric tests were used where

appropriate. The use of boxplot representations of the data in this chapter is discussed in Appendix 3. The group mean (SD) and median (IQR) of the global indices and examination duration are shown in Table 4-1.

Patients		Visit 1		Visit 2	
		Mean (S.D)	Median (IQR)	Mean (S.D)	Median (IQR)
SAP	MS	28.55 (6.62)	31.11 (4.53)	28.95 (6.63)	31.90 (6.28)
	MD	-3.35 (6.52)	-0.99 (4.66)	-2.97 (6.54)	-0.32 (5.75)
	PSD	2.98 (3.03)	1.59 (2.20)	3.03 (3.34)	1.39 (1.32)
	Duration	06:36 (01:30)	06:11 (01:49)	06:20 (01:13)	06:08 (02:07)
SWAP	MS	17.19 (7.19)	19.86 (9.75)	17.93 (7.32)	20.02 (10.25)
	MD	-8.66 (6.79)	-6.00 (9.57)	-7.75 (6.85)	-5.54 (10.59)
	PSD	3.76 (2.10)	2.99 (1.61)	3.64 (2.25)	2.69 (1.63)
	SF	2.68 (0.88)	2.42 (1.16)	2.58 (0.97)	2.55 (1.20)
	CPSD	2.03 (2.73)	1.00 (3.02)	2.31 (2.77)	1.42 (3.24)
	Duration	08:54 (01:16)	08:45 (01:44)	08:56 (01:33)	08:32 (01:49)
Normals		Visit 1		Visit 2	
		Mean (S.D)	Median (IQR)	Mean (S.D)	Median (IQR)
SAP	MS	31.91 (1.25)	32.04 (1.44)	32.43 (1.16)	32.44 (1.54)
	MD	-0.19 (1.23)	-0.15 (1.37)	0.37 (1.04)	0.38 (1.55)
	PSD	1.29 (0.27)	1.25 (0.34)	1.19 (0.21)	1.18 (0.26)
	Duration	05:27 (00:35)	05:17 (00:32)	05:17 (00:36)	05:10 (00:45)
SWAP	MS	23.13 (3.28)	23.75 (3.88)	23.85 (3.15)	24.31 (3.91)
	MD	-2.92 (3.03)	-2.33 (3.14)	-2.20 (2.86)	-1.79 (3.87)
	PSD	2.43 (0.79)	2.27 (0.58)	2.28 (0.43)	2.20 (0.64)
	SF	2.41 (0.66)	2.32 (1.03)	2.23 (0.69)	2.22 (0.88)
	CPSD	0.58 (1.08)	0 (0.94)	0.69 (0.77)	0.36 (1.23)
	Duration	08:05 (01:13)	07:54 (00:52)	07:44 (00:52)	07:33 (00:43)

Table 4-1. Summary table of visual field parameters for all eyes in the patient group

4.3.1 Mean Sensitivity (MS)

4.3.1.1 Between Visit Change in MS: Overall Differences between All Eyes Examined

The group MS values at both visits in both patient groups for standard perimetry and SWAP are shown in Figure 4-2. In the AMD patient group, statistically significant improvements at visit 2 were found for the standard MS (Wilcoxon signed-rank test, $Z = -2.032$, $p = 0.042$) and the SWAP MS ($Z = -2.527$, $p = 0.012$). Similarly, in the normal group, significant improvements at visit 2 were found for the standard MS (paired t test:

t = -3.543, p = 0.001) and SWAP MS (t = -3.019, p = 0.004). The patient group exhibited a greater spread of MS values in comparison to the normal group, as shown by the longer boxplots in Figure 4-2.

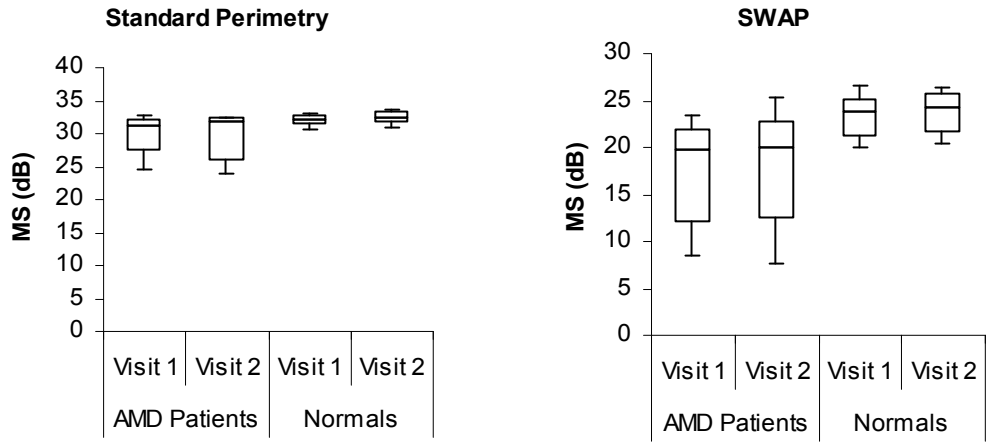

Figure 4-2. Mean sensitivity (MS) values at each visit for all eyes examined for standard perimetry and SWAP
Boxplots limits indicate the 15th, 25th, 50th, 75th and 85th percentiles along the abscissa.

4.3.2 Mean Deviation (MD)

4.3.2.1 Between visit change in MD: Overall Differences between All Eyes Examined

The group MD for each subject group for standard perimetry and SWAP is shown in Figure 4-3. In the AMD patient group, statistically significant improvements at visit 2 were found for the standard MD (Wilcoxon signed-rank test: Z = -2.097, p = 0.036) and SWAP MD (p = 0.005). Similarly, in the normal group, significant improvements at visit 2 were found for the standard MD (paired t test: t = -3.556, p = 0.001) and SWAP MD (t = -3.027, p = 0.004). The patient group exhibited a greater spread of values.

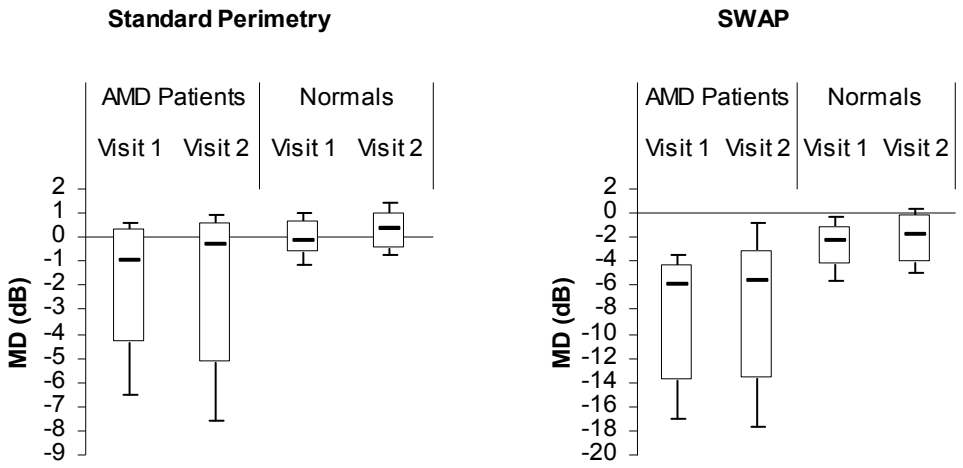

Figure 4-3. Mean deviation (MD) values at each visit for all eyes examined for standard perimetry and SWAP
Boxplots limits indicate the 15th, 25th, 50th, 75th and 85th percentiles along the abscissa.

4.3.2.2 Between Visit Change in MD: Effect of Order of Eyes Examined

For all first and second eyes examined, the group MD for each subject group for standard perimetry and SWAP are shown in Figure 4-4 and the statistical significance of between visit changes for each eye tested is shown in Table 4-2. For standard perimetry, statistically significant improvements at visit 2 were found for the MD in the first eye of the patient group ($p = 0.041$) and in both eyes in normal patients (1st eye: $p = 0.021$, 2nd eye: $p = .0027$). For SWAP, a significant improvement in the MD was found for the second eye of the patient group ($p = 0.008$) and the first eye of the normal group ($p = 0.007$).

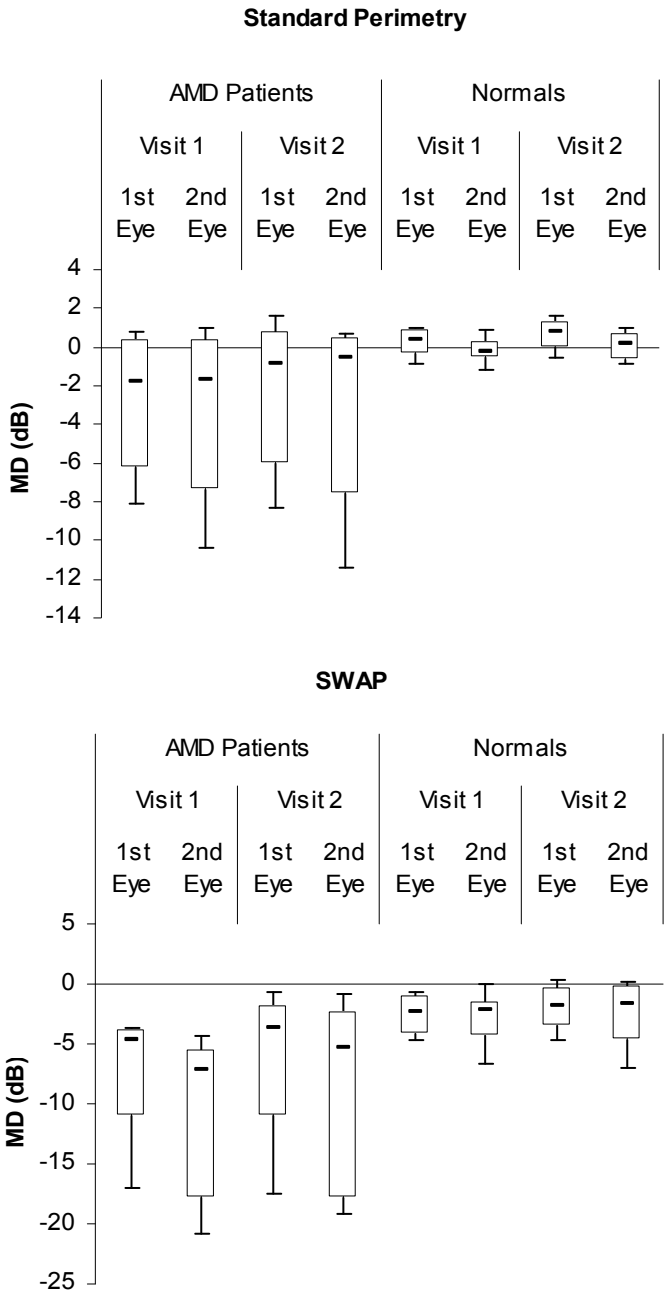

Figure 4-4. MD values as a function of visit and order of eye examined.
Boxplots limits indicate the 15th, 25th, 50th, 75th and 85th percentiles.

4.3.2.3 Inter-Eye Changes in MD

In the patient group, comparisons between eyes were made only where both eyes were graded at an equal stage of AMD. Unlike the between visit changes, the MD was more severe in the second eye compared to the first, which achieved significance only for the SWAP MD (Wilcoxon signed-rank test: Z = -2.667, p = 0.008) at the first visit in

the patient group. In the normal group, the deterioration between eyes was significant for the standard MD at the second visit (paired t test: t = 4.409, p < 0.001).

Between visit differences			Standard MD	SWAP MD
AMD Patients	1st Eye	Z	-2.040	-1.511
		p	**0.041***	0.131
	2nd Eye	Z	-0.471	-2.667
		p	0.638	**0.008***
Normals	1st Eye	t	-2.528	-3.044
		p	**0.021***	**0.007***
	2nd Eye	t	-2.403	-0.933
		p	**0.027***	0.364

* significant difference

Table 4-2. Difference in MD between visits (Wilcoxon signed-rank test and paired t test), for order of eye examined

4.3.2.4 Magnitude of Learning Between Visits

The amount of learning between visits is shown in Figure 4-5 for all eyes examined, and Figure 4-6 for first and second eyes tested. There was no significant difference in the magnitude of learning between AMD patients and normal subjects for standard perimetry (Mann-Whitney U test: Z = -0.578, p = 0.563) and SWAP (unpaired t test: t = 0.517, p = 0.607).

For standard perimetry and SWAP the mean change in MD between visits was 0.38 and 0.90dB in the patient group; and 0.56 and 0.72dB in the normal group, respectively. The corresponding change in MS between visits was 0.49 and 0.77dB in the patient group and 0.53 and 0.72dB in the normal group. The magnitude of learning differed slightly between MD and MS since the unmanipulated raw thresholds used to calculate the MS were whole numbers in dB, whereas the corresponding subtraction for MD involved decimalised values. Furthermore, the MD calculation in standard perimetry MD incorporated an unknown weighting function.

Significant differences were revealed for the change in MD between visits for standard perimetry for AMD patients between the first and second eyes examined (paired t test: t = 2.286, p = 0.043), where learning was exhibited for the first eyes examined but not for the second eyes. In SWAP, learning in the second eye was significantly greater than that in the first eye (paired t test: t = -3.668, p = 0.004). In the normal group the magnitude of learning between first and second eyes was not significantly different for standard perimetry (Wilcoxon signed-rank test: Z = -0.101, p = 0.920) and was significantly different for SWAP (paired t test: t = 2.155, p = 0.046).

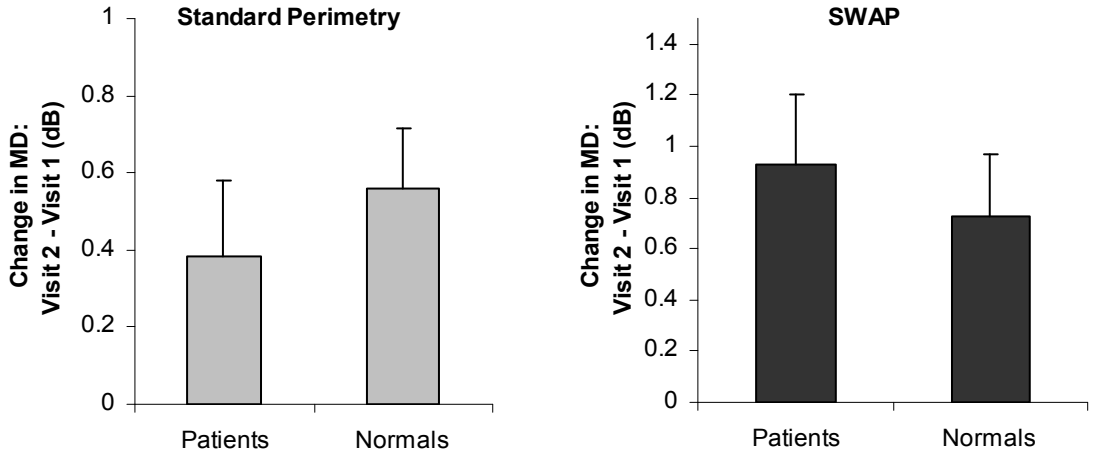

Figure 4-5. Change in MD (Visit 2 – Visit 1) indicating the magnitude of learning in the patient group and normal group for standard perimetry and SWAP.
Error bars represent 1 standard error

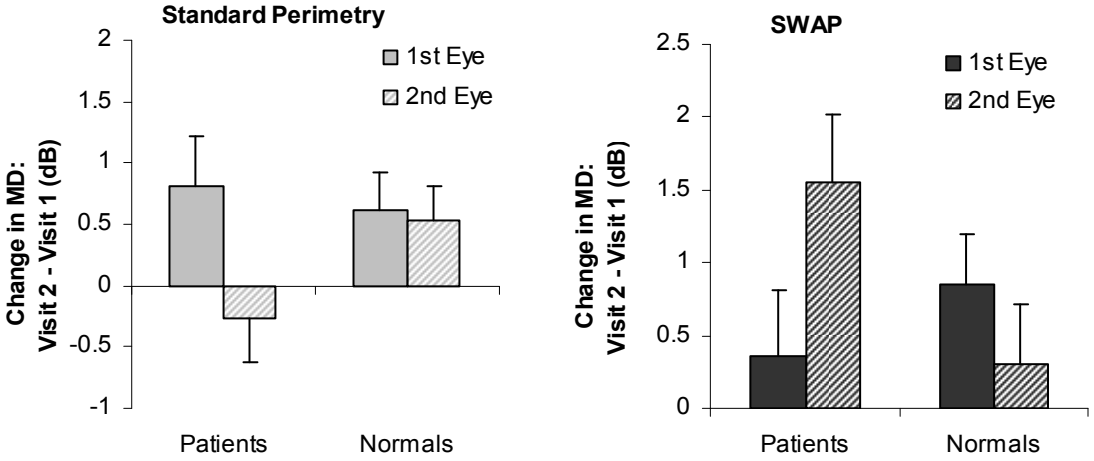

Figure 4-6. Change in MD (Visit 2 – Visit 1) indicating the magnitude of learning in the patient group and normal group for standard perimetry and SWAP for first and second eyes examined. Error bars represent 1 standard error

4.3.2.5 The Effect of Stage of AMD and Age on the Magnitude of Learning

The effect of stage of AMD on change in MD was investigated using the Kruskal-Wallis test for standard perimetry data and a one-way analysis of variance (ANOVA) for SWAP data. No statistically significant effect of stage of disease was found for standard perimetry (Chi-square = 9.193, p = 0.102) or SWAP (One-way ANOVA: F = 0.198, p = 0.962). Post hoc analysis (Tukey HSD) revealed no differences between SWAP learning at individual stages. No significant correlation (Pearson's correlation for parametric data and Spearman's rho for non-parametric data) existed between age and change in MD between visits (p > 0.300 for all groups).

4.3.3 Pattern Standard Deviation (PSD)

4.3.3.1 Between Visit Change in PSD: Overall Differences between All Eyes Examined

The group PSD for each subject group for standard perimetry and SWAP is shown in Figure 4-7 and the PSD mean and median values for each visit are shown in Table 4-1. No significant differences were found between visits for the standard perimetry PSD the AMD patient group (Wilcoxon signed-rank test: Z = -0.965, p = 0.335). However, in the normal group there was a significant improvement at the second visit (paired t test: t = 2.205, p = 0.033). Between visits, no significant difference between the SWAP PSD was found for both the patient group (Wilcoxon signed-rank test: Z = -1.035, p = 0.301) and the normal group (Wilcoxon signed-rank test: Z = -1.048, p = 0.294). The patient group exhibited a greater spread of values.

4.3.3.2 Between Visit Change in PSD: Effect of Order of Eyes Examined

For all first and second eyes examined, the group PSD for each subject group for standard perimetry and SWAP are shown in Figure 4-8. No statistically significant between visit changes in PSD were found for either of the subject groups for either perimetry type (Table 4-3).

4.3.3.3 Inter-Eye Changes in PSD

No significant changes between eyes were found for the PSD for either subject group.

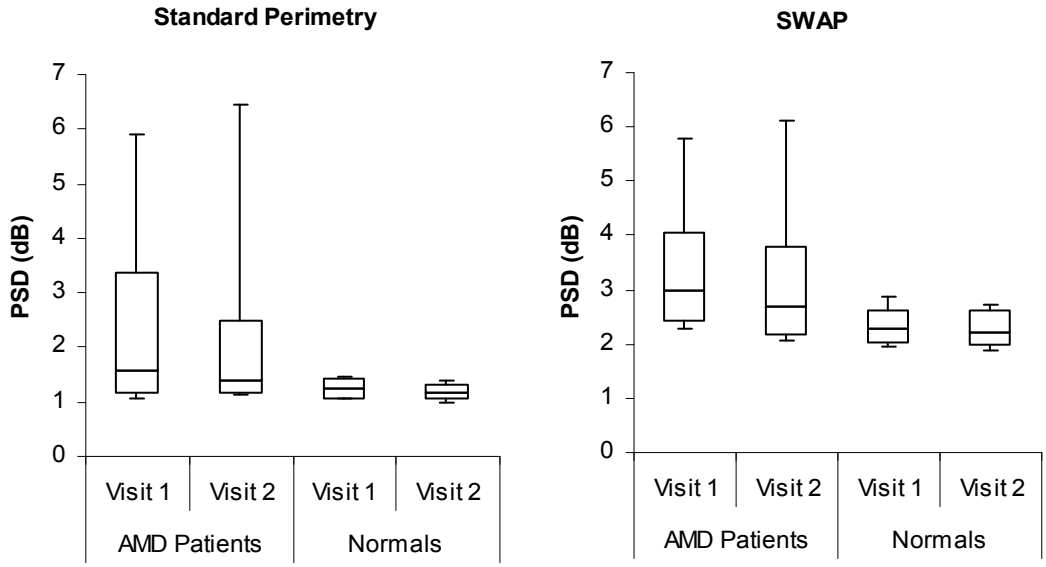

Figure 4-7. PSD values at each visit for all eyes examined for standard perimetry and SWAP
Boxplots represent the 15th, 25th, 50th, 75th and 85th percentiles

4.3.4 Other Visual Field Parameters: SF, CPSD, Examination Duration and Number of Defects

4.3.4.1 Between Visit Change Visual Field Parameters: Overall Differences between All Eyes Examined

The group examination duration for each subject group for standard perimetry and SWAP is shown in Figure 4-9 and the corresponding changes for the number of pattern deviation (PD) and total deviation (TD) defects are shown in Figure 4-10. The statistical significance of the between visit changes were tested for using the Wilcoxon signed-rank test and are shown in Table 4-4. A significant improvement at visit 2 was found for the standard examination duration ($p = 0.047$) in the patient group and the number of TD defects in both the patient group ($p = 0.034$) and the normal group ($p = 0.038$).

4.3.4.2 Between Visit Change in Visual Field Parameters: Effect of Order of Eyes Examined

For each eye tested, the only statistically significant between visit changes were in the normal group for the SWAP examination duration in the first eye examined (Wilcoxon

signed-rank test: Z = -2.296, p = 0.022) and the number of SWAP TD defects (Z = -2.238, p = 0.025).

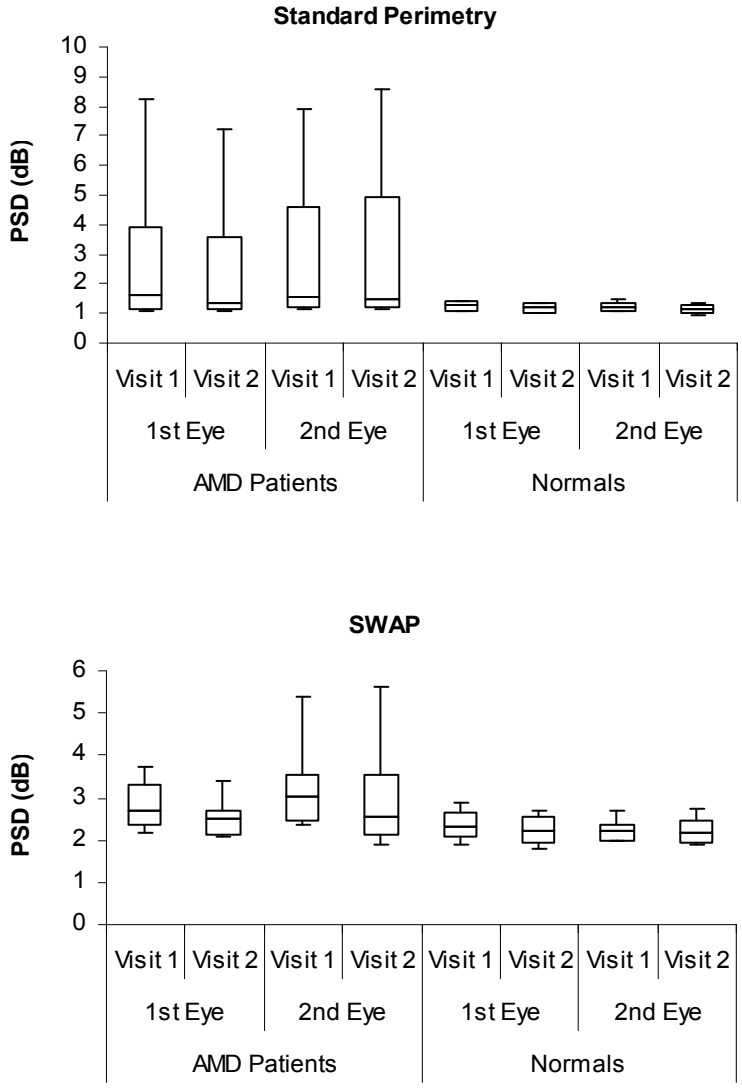

Figure 4-8. PSD values as a function of visit and order of eye examined.
Boxplot limits show the 15th, 25th, 50th, 75th and 85th percentiles

Between visit differences			Standard PSD		SWAP PSD
AMD Patients	1st Eye	Z	-1.023		-1.689
		p	0.306		0.091
	2nd Eye	Z	-1.216		-0.711
		p	0.224		0.477
Normals	1st Eye	t	1.465	Z	-1.154
		p	0.160	p	0.248
	2nd Eye	t	1.664	Z	-0.065
		p	0.113	p	0.948

Table 4-3. Difference between PSD between visits (Wilcoxon signed-rank test and paired t test), for order of eye examined

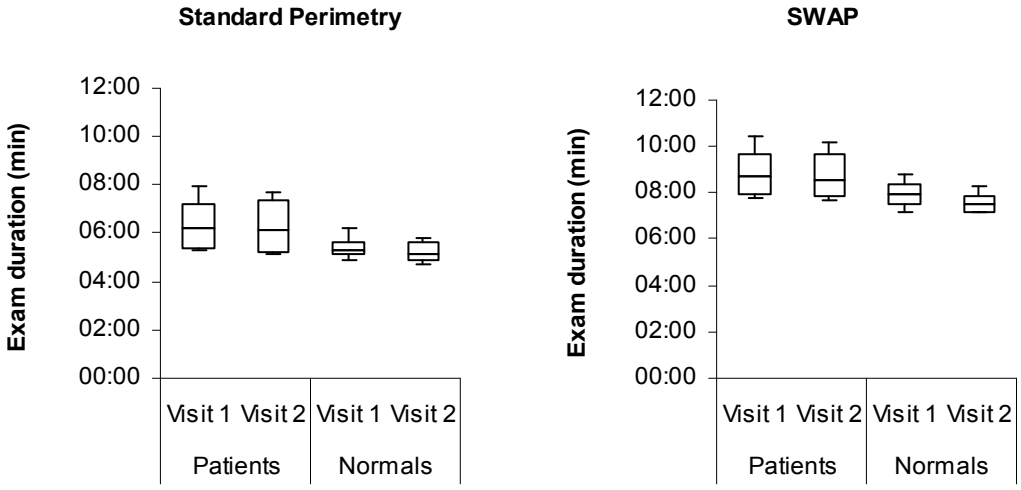

Figure 4-9. Examination duration values for all eyes examined
Boxplot limits show the 15th, 25th, 50th, 75th and 85th percentiles

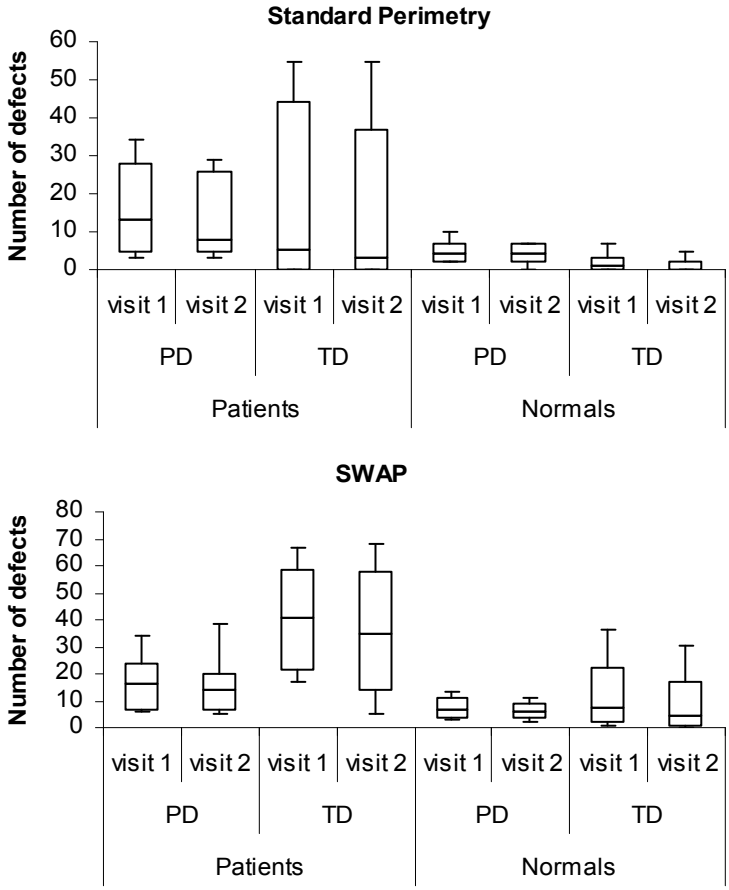

Figure 4-10. Number of defects identified by pattern deviation (PD) and total deviation (TD) as a function of visit number, for all eyes examined
Boxplots limits indicate the 15th, 25th, 50th, 75th and 85th percentiles along the abscissa.

Standard Perimetry				
Between visit differences		Exam Duration	No. PD Defects	No. TD Defects
AMD Patients	Z	-1.990	-1.344	-1.498
	p	**0.047***	0.179	0.134
Normals	Z	-1.445	-1.186	-1.780
	p	0.148	0.236	0.075

SWAP						
Between visit differences		SF	CPSD	Exam Duration	No. PD Defects	No. TD Defects
AMD Patients	Z	-0.674	-0.823	-0.255	-1.015	-1.395
	p	0.500	0.411	0.798	0.310	0.163
Normals	Z	-1.022	-1.438	-1.943	-1.053	-2.018
	p	0.307	0.150	0.052	0.292	**0.044***

* significant difference

Table 4-4. Differences between visual field parameters between visits (Wilcoxon signed-rank test)

4.3.5 Pointwise Pattern Deviation Probability Analysis

Pointwise analysis of the pattern deviation probability maps was considered in preference to the total deviation because it is less affected by possible lens yellowing in SWAP. The change in the number of probability levels between visits at each stimulus location was calculated. The change in the number of levels of probability between visits was defined as negative if deteriorating, such that the probability level changed so that it had a smaller chance of occurring in the normal database; and positive if improving. For example a probability level of $p<5\%$ at visit 1 and $p<1\%$ at visit 2, was interpreted as a change of -2 levels of probability. The mean change in number of probability levels of the pattern deviation probability analysis between visits 1 & 2, at each stimulus location, for AMD patients and normal subjects is shown in Figure 4-11 for standard perimetry and Figure 4-12 for SWAP. The maps are displayed as a right eye. Lighter shading in Figure 4-11 and Figure 4-12 represent improvement in the field at visit 2 and deterioration is indicated by darker shading. In standard perimetry, the improvement in the visual field at visit 2 occurred in the central field within an approximate eccentricity of 6 degrees and deterioration tended to occur at the more peripheral regions of the field in both subject groups (Figure 4-11). In SWAP, areas of improvement were interspersed with areas of deterioration and the areas of greatest improvement occurred most frequently in the paracentral regions of the 10-2 field. There were slightly fewer stimulus locations exhibiting improvement in the SWAP field compared to the standard field for both subject groups.

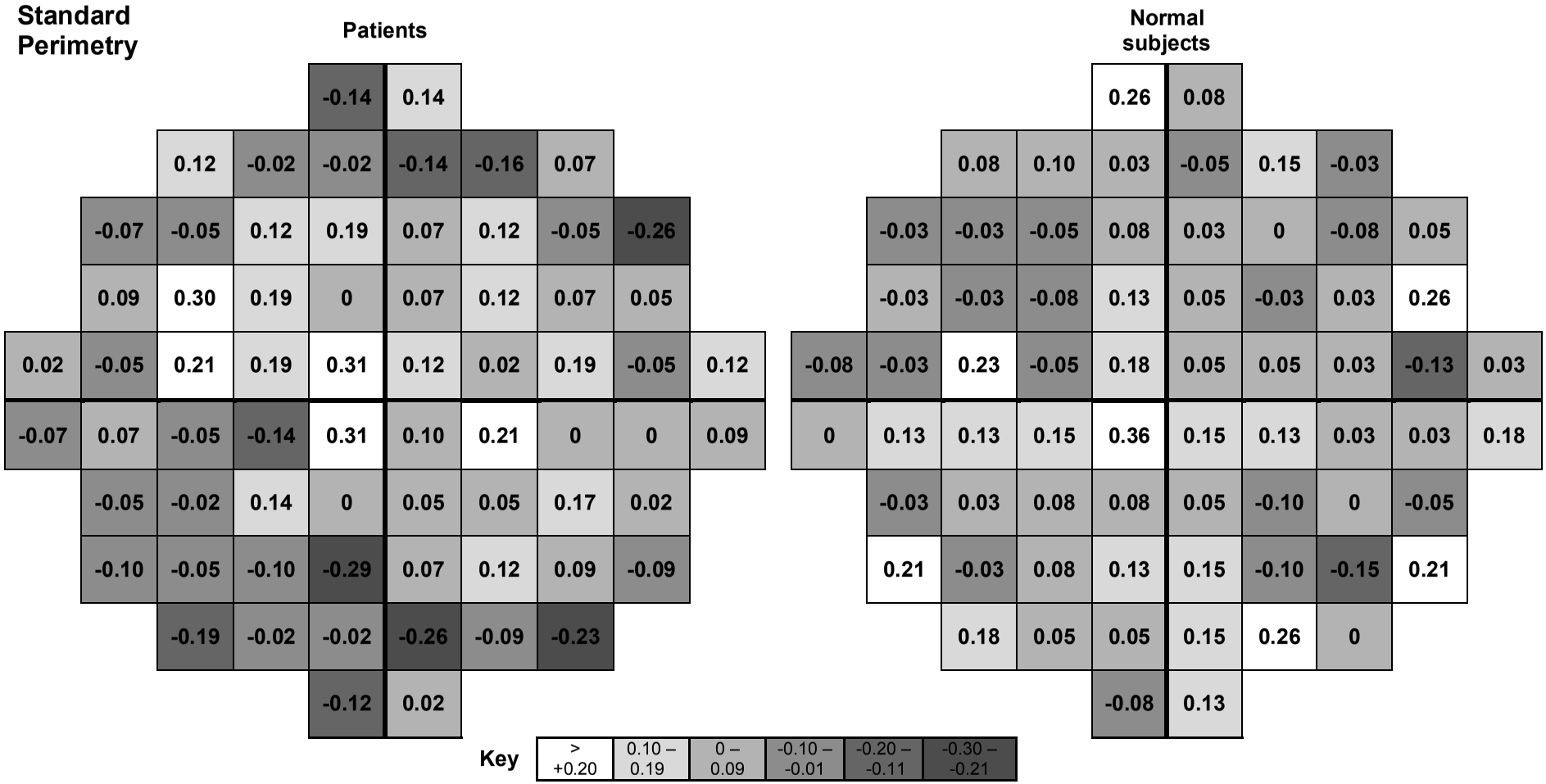

Figure 4-11. Mean number of probability levels of the pattern deviation probability analysis which changed between visits, at each stimulus location, for AMD patients and normal subjects for standard perimetry. Positive values indicate an improvement in the field, negative values indicate deterioration and zero indicates no change in probability level.

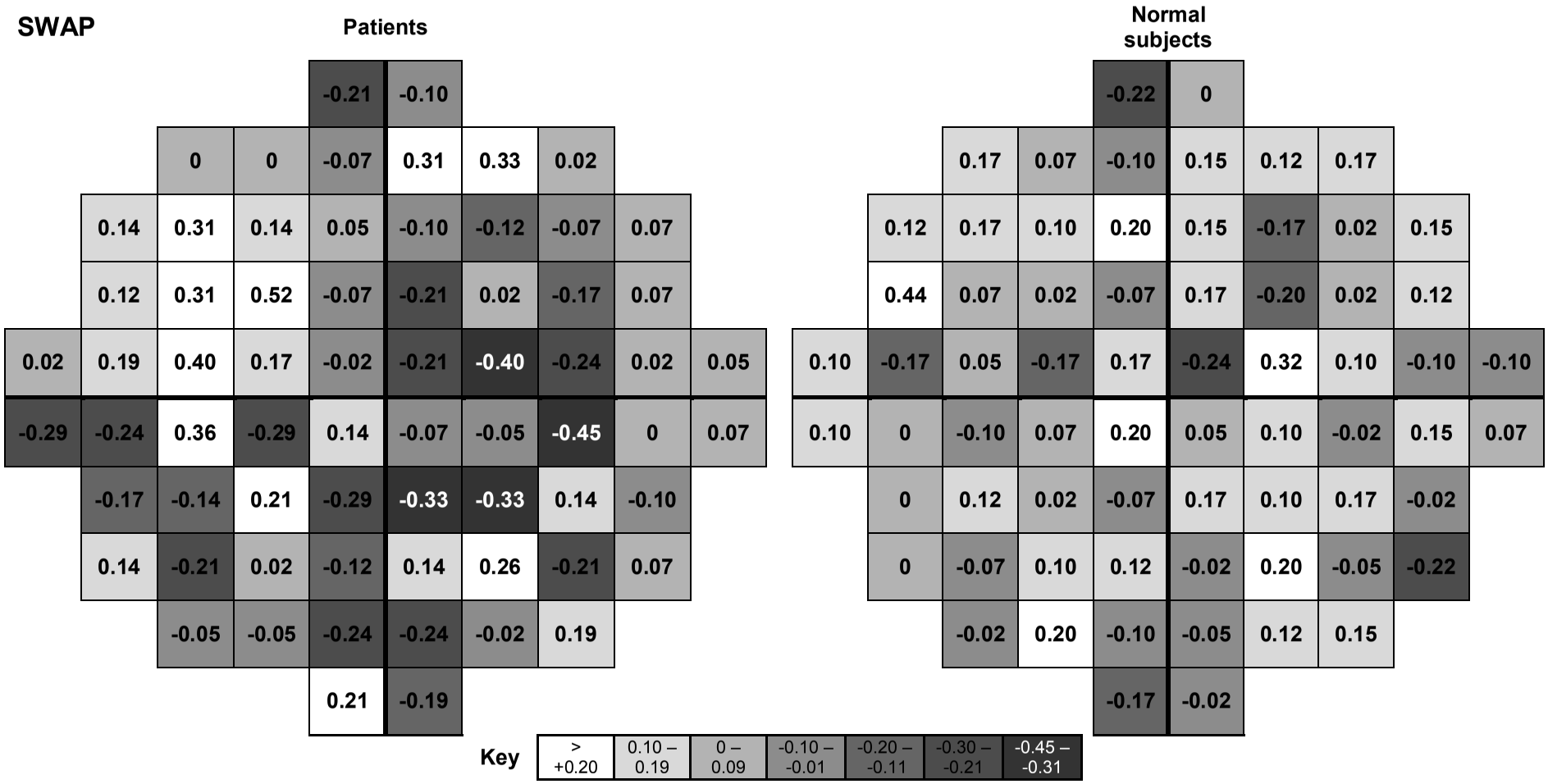

Figure 4-12. Mean number of probability levels of the pattern deviation probability analysis which changed between visits, at each stimulus location, for AMD patients and normal subjects for SWAP. Positive values indicate an improvement in the field, negative values indicate deterioration and zero indicates no change in probability level.

4.4 Discussion

In summary, the results demonstrated a significant learning effect between two visits separated by eleven days in patients with AMD and in normal subjects for standard and SWAP 10° visual fields, for the global indices, mean sensitivity and mean deviation. The overall magnitude of learning was not significantly different between the patient group and the normal group, and was not influenced by stage of AMD. Evidence of fatigue was observed where the MD showed deterioration between eyes.

The average change in MS between visits was 0.4-0.5dB for standard perimetry for both subject groups. By comparison to existing research in standard perimetry applied to the 30° field, this magnitude is rather less than the average learning effect of 1-2dB (Autzen & Work 1990; Heijl et al. 1989), which suggests a diminished magnitude of learning in the 10° field relative to the 30° field. In SWAP the average change in MS was 0.7dB for both subject groups, which is similar to the learning effect calculated in the 10° region of the 30-2 field, where the MS was found to increase by 0.6dB in SWAP, in a group of ocular hypertensives (Rossetti et al. 2006). The SWAP MD in the 24-2 field in patients with ocular hypertension and open-angle glaucoma was found to improve by 0.6-1.2dB between the first two visits (Wild et al. 2006), which is consistent with these results, where the SWAP MD improved by 0.7-0.9dB. Current evidence suggests that a learning effect in the 10° field would be smaller than that for a 30 or 24° field, since greater learning effects were seen in peripheral concentric rings of a 30-2 field, where learning was found to increase linearly with eccentricity (Heijl & Bengtsson 1996). For SWAP, the learning effect was noted to be greater in the peripheral 20 to 30° as opposed to the central 10° (Rossetti et al. 2006). Moreover, the between subject variability is reduced in the central visual field (Bengtsson et al. 2008; Cubbidge et al. 2002), leading to greater accuracy of the threshold measurement in the central 10° explains the smaller learning effect in this area.

The overall magnitude of learning was not different between the patient and normal groups. The magnitude of the learning effect was independent of stage of AMD in this study. In standard perimetry, the pointwise change in probability level of PD defects indicated a similar pattern in both patient and normal groups. The greatest improvements at the second visit occurred in the central field within an approximate eccentricity of 6 degrees in standard perimetry (Figure 4-11). This apparent improvement in the central region of visual field was not consistent across all subjects in the AMD patient group and may be attributed to normal variability. In SWAP, the areas of greatest improvement occurred most frequently in the paracentral regions of the 10° field. These areas in Figure 4-12 correspond to the areas of highest threshold sensitivity illustrated in Figure 7.6 which indicates a consistency with previous findings that locations of high sensitivity exhibit a greater learning effect than more depressed points (Heijl & Bengtsson 1996).

In SWAP, the mean deviation index was quoted as being the most sensitive parameter to learning (Rossetti et al. 2006), which is concordant with these results where the mean deviation was also the principally affected parameter by learning. This indicates a diffuse component to the learning effect, which is further supported by the results indicating no significant changes in the PSD, which represents focal loss. Pointwise differences between stimulus locations were however observed in the pattern deviation analyses. In standard perimetry, deteriorations tended to occur in the periphery of the field. The peripheral stimuli are the last thresholds determined in the visual field examination where stimuli are presented in a pseudo-random manner. It would be expected that the observed deterioration in peripheral sensitivity is likely to have been caused by fatigue.

In standard perimetry, no significant inter-eye difference in MD was noted in the patient group, which is consistent with the findings of Barkana et al. (2006), who did not find any effect of the order of eyes tested on the MD using the SITA standard algorithm and

the 24-2 test pattern in glaucomatous patients. Paradoxically, in the normal group, there was a significant decline in the MD between eyes at the second visit, in standard perimetry, in which the magnitude of decline was 0.6dB. The corresponding decline at the first visit was 0.5dB, which did not achieve statistical significance. It is possible these findings were adversely affected by a type 1 error and a more stringent alpha level could have protected against this. Wild et al. (2006) attributed worsened MD values in the second eye examined to the fatigue effect in SWAP. This reasoning is applicable to the present study where more severe MD values were also found in the second eye for all patients and for both standard perimetry and SWAP, despite frequent rest periods. Indeed the extreme values of the SWAP MD for the second eye tested in the normal group were marginally more severe than the least severe MD values in the patient group (Figure 4-4). In addition to the effect of fatigue, this can also be explained by the wider confidence intervals in SWAP and the normal appearance of fields of the patients at stage 0 AMD, who were acute observers. The magnitude of learning in the second eye of the patient group for SWAP was significantly greater than the learning exhibited by the first eye (Figure 4-6). Parallel findings are evident in the learning study in SWAP (Wild et al. 2006), in which the second eyes of the subgroup of glaucoma patients showed a larger improvement in MD at the second visit compared to the first eyes, as well as markedly more severe MD values with larger standard deviations in the second eyes.

Whilst learning in standard perimetry is not thought to affect learning in SWAP due to the different mechanisms involved in detection (Wild & Moss 1996), there is the likelihood that fatigue due to the standard fields was transferred to the SWAP fields, which were performed second in this study. However, it is not possible to separate the magnitude of any transferred fatigue effect between perimetry types, due to the inherently increased confidence limits of normality in SWAP compared to standard perimetry (Wild et al. 1998; Wild 2001) and difference in dynamic range, such that

absolute value decibel comparisons cannot be made. Had the study design randomised the order of perimetry type, or separated the sessions by perimetry type, a transferred fatigue effect may have been negated. The magnitude of the fatigue effect is greater in SWAP (Cubbidge 1997), so it is likely that the transferred fatigue effect would be greater if SWAP had been performed first. Alternatively, had the study been designed such that standard perimetry and SWAP were carried out on different days, this would have less reflected clinical practice and would have introduced greater variation in the time between visits.

The experimental designs employed in comparative studies adopted a greater number of visits, such as examination at weekly intervals over five consecutive weeks (Heijl & Bengtsson 1996; Rossetti et al. 2006; Wild et al. 2006). This study design could not be implemented in the present study for logistical reasons and clinical viability. In standard perimetry, the greatest learning effect was observed between the first two visits (Heijl et al. 1989; Heijl & Bengtsson 1996). In SWAP, the greatest learning effect has been found to occur over the first three visits in the 24° field, where in fact the largest increase in MD occurred at the second visit (Wild et al. 2006); and over the first two visits in the 30° field (Zhong et al. 2008). Consequently, the design of the present study was optimised to detect the greatest learning effect present. This is of value in the estimation of any further learning effects which may occur at subsequent visits in a longitudinal study, since they are likely to have a smaller magnitude. When examining visual field data cross-sectionally, across stages of disease, ideally data analysed would be from the 5th visit of five consecutive weekly fields. In the present study, the magnitude of the learning effect detected between the first two visits is minimal relative to measures of variability such as the SF. Although the cross-sectional analysis of data from visit two may incur greater error than analysis of potential data from visit five, the difference is not likely to exceed the other variability measures. Additionally in a clinical situation it is not viable to assess a patient five times at weekly intervals. There are

often long periods of time in between clinical visits, the interpretation of visual fields in this circumstance would also benefit from information about the learning effect.

The results in this study present a small magnitude of learning in the 10° field which improves confidence in the accurate detection of change attributable to disease from errors due to opposing effects of learning and fatigue. MD is the index most sensitive to learning, which is of importance when examining AMD patients, where change in focal loss and variability is of more interest, rather than diffuse changes. Thus, the suitability and reliability of 10° visual field assessment of functional change in AMD is reinforced. The magnitude of learning was not significantly different between the patient group and the normal group, and was not influenced by stage of AMD.

5. Programming in Ophthalmic Imaging Analyses: Mapping the visual field and the standard grading grid onto fundus photographs

Summary

Computer programming was used to map spatial information onto digital fundus images, with the purpose of reducing the error of performing such tasks manually. The first program mapped perimetric data to the fundus image and the second positioned the standard age-related macular degeneration (AMD) grading grid onto the fundus image. Description and evaluation of the programs are given. The application of the program to the grading of AMD features was implemented.

The spatial repeatability associated with the mapping processes was investigated using the coefficient of repeatability, and was approximately 80μm and 65μm for the perimetric fundus map and fundus grading grid programs, respectively. The greatest contribution to this error was the position of the user-defined macula. Accuracy of the Perimetric Fundus Map program in terms of drusen size indicates that isolated drusen, larger than 80μm can be associated with coinciding visual field defects at individual stimulus locations, but it is not possible to make the same interpretations with smaller drusen

Application of the program for the grading of features of AMD was carried out by two independent observers. The inter-observer agreement ranged from weighted kappa values of 0.42 to 1, indicating moderate and perfect agreement, respectively. When grading AMD using the custom program, graders should consider the spatial variability which might occur in grading hard drusen or other small features at the edge of subfields of the grading grid.

The advantages of the semi-automated programs over the corresponding manual methods are that of speed, convenience and known accuracy levels. The programs provide useful tools for the analysis of digital fundus photographs.

5.1 Introduction

In order to examine the structure to function relationships in AMD, the central visual loss must be related to the retinal manifestations of the disease. Measures of visual function are not easily transposed to their structural correlates on the retina because of the optical properties of the eye and magnification factors. The projection of the retinal image is not linear due to the multiple aspheric surfaces of the eye, which have differing refractive indices. The assumptions made are based on models involving a schematic eye, which represents a simplification of true optics. Although sophisticated models may account for a gradient-index lens and optical aberrations (Navarro et al. 2006), the commonly used model for retinal projection does not allow for such features. In optics, the linear magnification of an image is the image height divided by the object height. The amount of magnification in fundus photography depends several factors including the degree of eccentricity of the measured object from the optical axis (Bennet et al. 1994), the distance of the camera from the eye examined (Bengtsson & Krakau 1977, 1992), the magnification due to the camera (camera factor) and the magnification due to the eye (ocular factor) (Garway-Heath et al. 1998). In fundus photography, the magnification of an image is defined by the equation

$$t = pqs$$

where, t is the true retinal size, p is a camera factor, q is an ocular factor and s is the image size (Bennet et al. 1994; Patton et al. 2006). The magnification due to the camera is constant for a given camera (Garway-Heath et al. 1998). Ocular magnification can be calculated by obtaining biometric data for the eye, or it may be estimated from other measures such as the refraction of the eye, corneal curvature or axial length (Bengtsson & Krakau 1992; Bennet et al. 1994). Calculating the true size of retinal features from fundus photographs may be avoided by the use of ratio measures.

The original manual grading of AMD was performed with slides at a light box and clear plastic overlays (Bird et al. 1995; Klein et al. 1991). Ratio measures were employed to measure features, which made reference to the optic disc diameter. However, the positioning of the standard grading grid onto the fundus photograph may lead to spatial errors especially when performed by multiple graders. With the increasingly ubiquitous use of digital fundus photography, methods which avoid the use of plastic overlays have been developed. The grading grid has been digitally reproduced and resized in Adobe Photoshop (Adobe Systems Inc, San Jose, USA) to match the fundus image (Scholl et al. 2004). Other methods of digital grading in AMD have involved the use of a graphics tablet to manually mark digital fundus images (Smith et al. 2005b).

The aim was to use computer programming to map spatial information onto digital fundus images in order to reduce the error associated with incorrect manual grid positioning. Secondary aims were to evaluate the programs using the repeatability of positional measures. Thirdly, subsequent to evaluation of the programs, application of the program to the grading of AMD features was described as well as the associated inter-observer agreement.

Two programs were proposed. Firstly, a program was written to map visual field data onto digital fundus images, thus facilitating the analysis of structure to function relationships in perimetry. The second program was designed to place the standard AMD grading grid onto the fundus image, for ease and improved accuracy of digital image grading. Both programs were written using Liberty BASIC (Shoptalk Systems, Massachusetts, USA), a form of BASIC language capable of Windows programming. Digital fundus images and perimetric data from patients with AMD were acquired in a previous study (see Chapter 4). The fundus photography was performed on dilated pupils, using a non-mydriatic camera (Canon EOS 10D camera, 6.3 megapixels). Stereoscopic pairs of images were captured whereby the first image was taken near the left edge of the pupil and following a lateral shift of the camera base, the second

image was taken near the right pupil edge. Images were stored as high quality jpeg files (large/fine, ~2.4MB, 3072 x 2048) and converted to bitmap files in order for compatibility with Liberty BASIC.

The standard assumption of the projection of the visual field on to the retina is based on research using trigonometrical ray tracing in a schematic eye with an aspheric cornea, where the retinal distance within an eccentricity of 10° from the fovea was found to be 1° = 270-275μm (Drasdo & Fowler 1974). This assumption of distance declines with eccentricity, such that at approximately 30°, 1° is equivalent to 260μm.

The longstanding clinical assumption of the average vertical optic disc diameter is 1500μm. This figure was applied to the AMD grading systems (AREDS 2001b; Bird et al. 1995; Klein et al. 1991) in the development of the standard grading grid, such that the circular dimensions could be expressed in terms of ratios of disc diameters. These grading systems (AREDS 2001b; Klein et al. 1991) quoted a preference for the longstanding assumption, even in the knowledge that a more accurate in vivo measure of disc diameter indicated a value of 1800-1900 μm (Jonas et al. 1988; Mansour et al. 1990). Therefore the assumption used for the grading program follows this convention.

The following description relates to the programs stored on the disc accompanying Appendix 2. Instructions for running the programs are given in Appendix 2.

5.2 PROGRAM 1: Perimetric Fundus Map

A series of windows were programmed to map the visual field upon the digital fundus photograph. The program runs as follows:

1. The first dialogue box allows the user to open a bitmap fundus image.
2. The initial user input is the macula to disc distance. The visual angle between the macula and the centre of the optic disc eye is 15° (Rabbetts 1998), or it is possible to determine this distance perimetrically using a custom stimulus configuration. In this case, the known distance may be entered at this point.

3. The user is then instructed to mark the optic disc margins and macula with mouse clicks, which allows the distance between the centre of the optic disc and the macula to be calculated in pixels.

4. A pixel to degree conversion factor is calculated by the program and the points corresponding to the 10-2 stimulus configuration are generated onto the fundus (Figure 5-1).

5. The following windows allow the perimetric data to be entered in two ways (Figure 5-2). Threshold sensitivities, probability deviation values or any numerals may be entered directly as numeric values (Figure 5-3A). Defects can be entered by their probability values for example where p<1%, "**1" should be entered for a probability symbol to be displayed (Figure 5-3B). The data may be copied and pasted from a spreadsheet directly into the textbox in Figure 5-2A. Alternatively, the value can be entered once into the textbox in Figure 5-2B and placed in numerous places on the map using the positional buttons, which may be more convenient where defects occur in a minimal number of locations. Threshold sensitivity values can be exported from the perimeter using software such as PeriData Software (GmbH, Huerth, Germany), which allows a Microsoft Office feature, to export the data to an Excel file.

6. The threshold values displayed on the map are colour coded according to a scale to represent severity. The colour contrast may be adjusted depending on the visibility over the background colour of the fundus.

7. Further display options are available including right or left eye indicator and the vertical downward displacement of the macula from the centre of the disc in degrees.

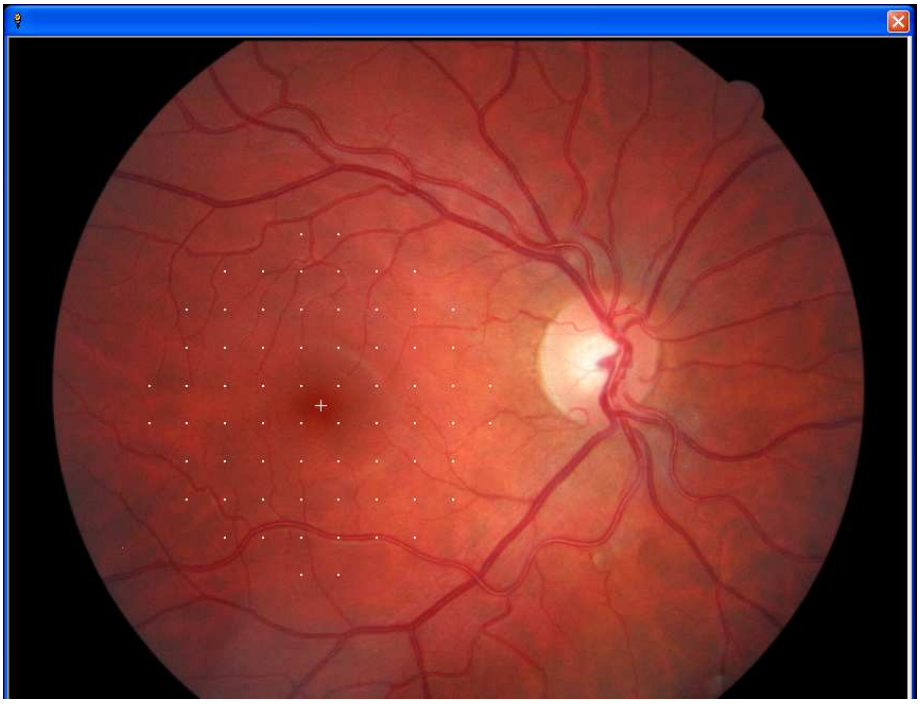

Figure 5-1. Fundus image with visual field stimulus locations superimposed

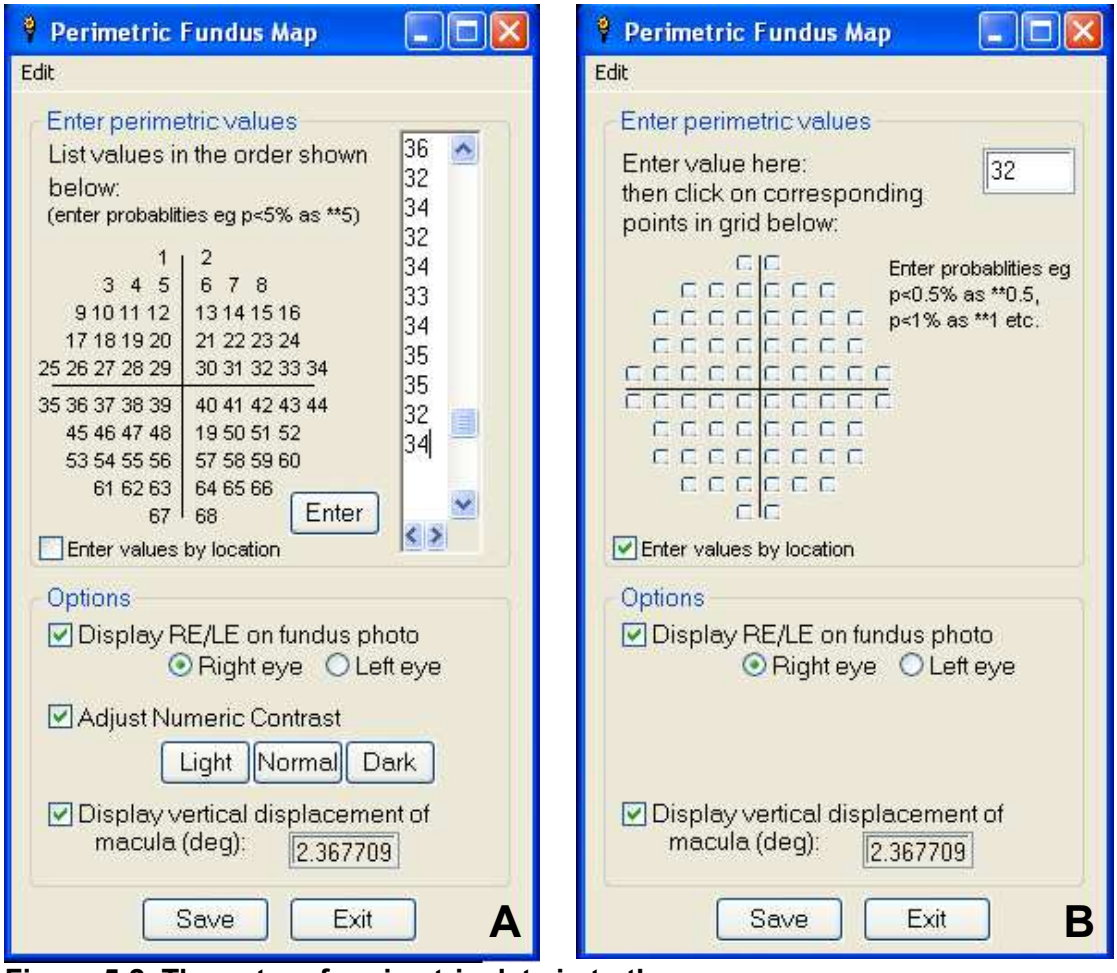

Figure 5-2. The entry of perimetric data in to the program:
(A) Numerals pasted from a spreadsheet or manually typed, or (B) the typed value can be entered to numerous positions by clicking the corresponding button arranged in the stimulus grid.

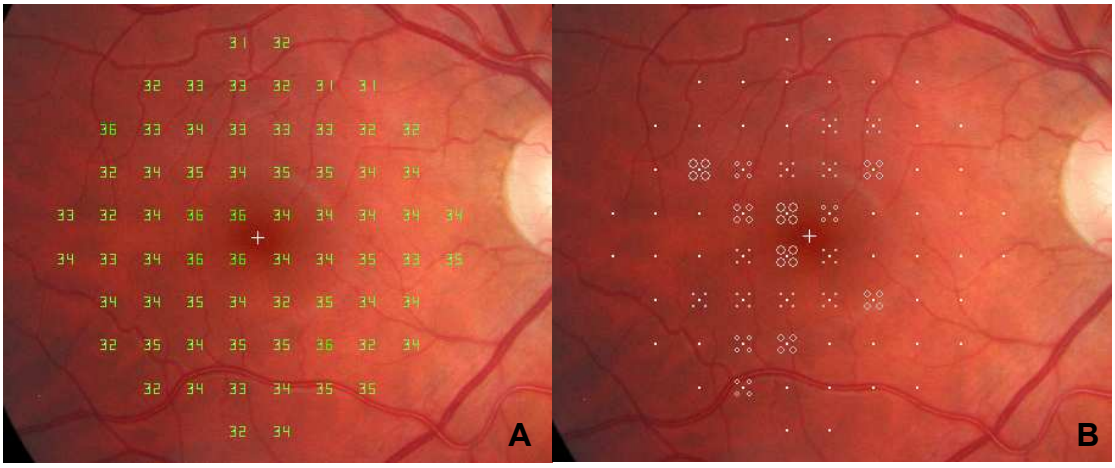

Figure 5-3. Perimetric fundus maps displaying (A) threshold sensitivities and (B) defects

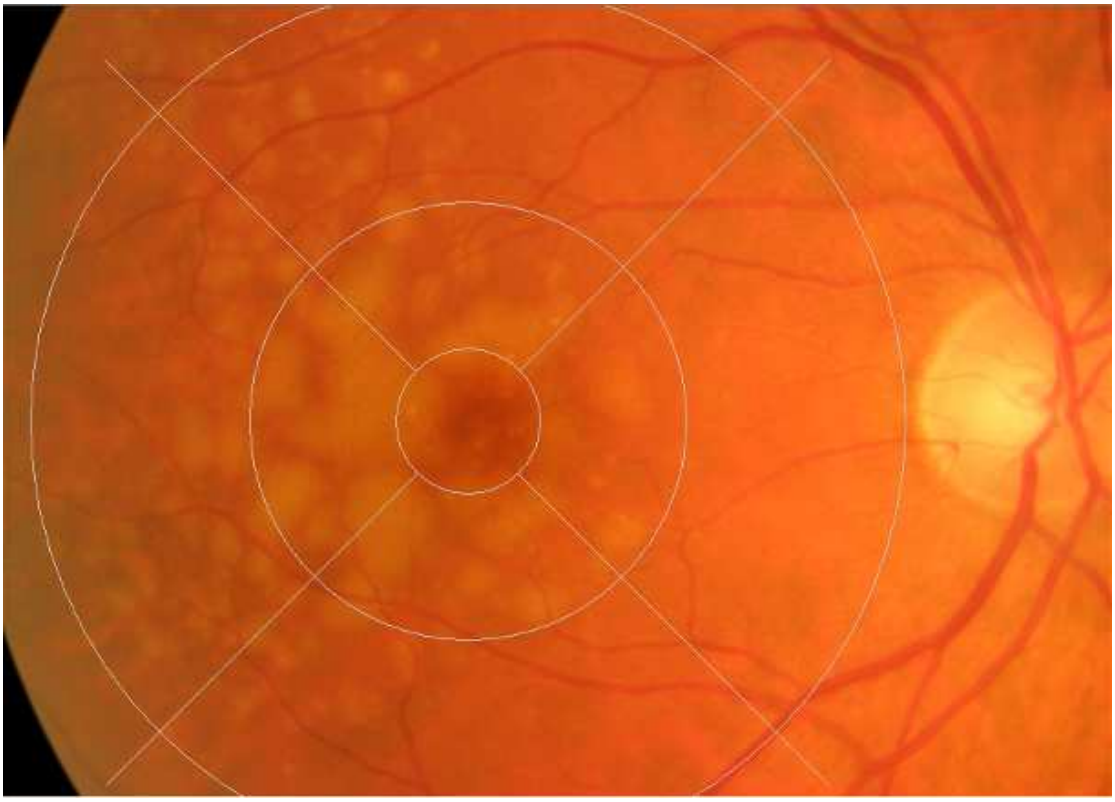

Figure 5-4. Grading grid mapped upon fundus image

5.3 PROGRAM 2: Fundus Grading Grid

In order to map the circular grading grid onto the fundus image, the program runs as follows:

1. The first dialogue box allows the user to open a bitmap fundus image.

2. The user is instructed to mark superior and inferior disc margins and macula with mouse clicks, which gives the vertical disc diameter in pixels and the pixel to µm conversion factor is calculated.

3. The circular grading grid is generated onto the fundus image (Figure 5-4).

4. The following window allows marking on the image with mouse clicks for counting features, and a measuring tool. The user may mark the diameter of a circular feature on the image and a circle will be drawn around the feature (Figure 5-5). The diameter and area of the marked circle in µm are returned to the textboxes in the window, as well as the nearest standard circle size as defined by the International Grading System (Bird et al. 1995). Another feature allows the diameter to be added to a list and the total areas of the features in the list are expressed as a percentage of the central, middle or outer circle. The list may be copied and pasted out of the program.

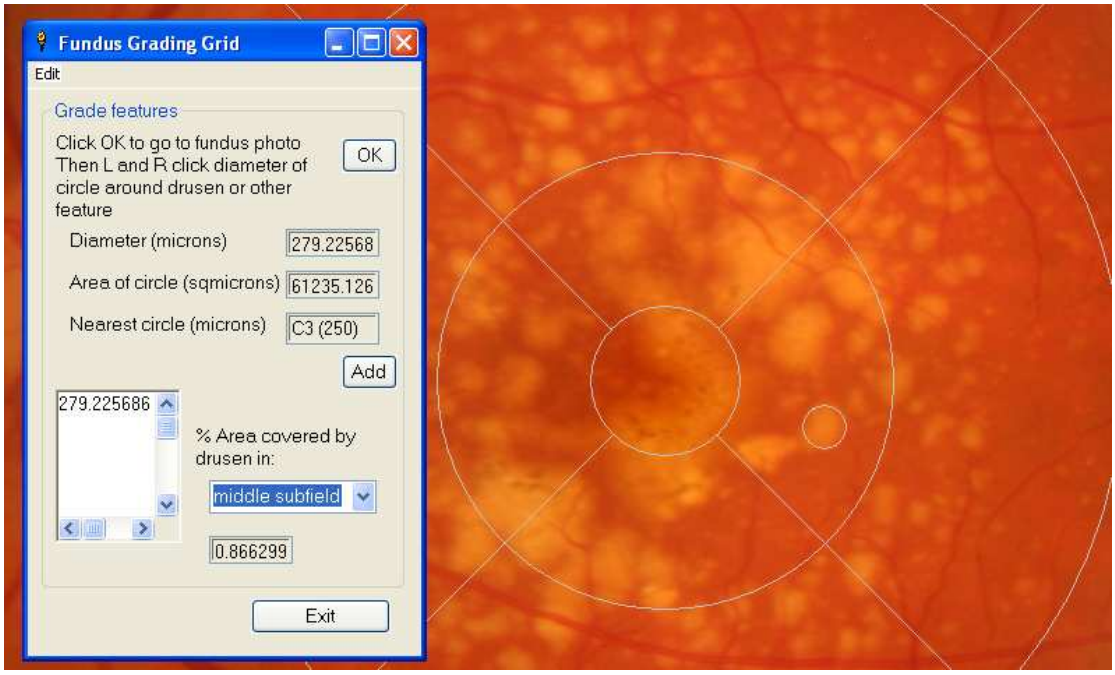

Figure 5-5. Fundus Grading Grid. Marking drusen gives diameter and area measures

5.4 Evaluation

An evaluation of the repeatability of positional measures of the programs was performed. The programs described rely on the accurate marking of the fundus landmarks by the user. In images where disc margins are blurred and the macula is ill-defined, identification of retinal landmarks is more difficult. It was therefore necessary to quantify the user error associated with the accurate positioning of the firstly the perimetric map and secondly the grading grid onto the fundus image in Programs 1 and 2, respectively.

Positional error was defined as the repeatability of two measures of a point on each grid. Possible between measure differences in the user-defined papillomacular distance or optic disc diameter indicates that the repeatability will vary with retinal eccentricity. For Program 1, two points were chosen, at stimulus locations 40 and 44 (of a right eye) which constitute a central and a peripheral location. For Program 2, the inferior right intersection of the central circle of the grid was chosen (Figure 5-6). Additional features were written into each program, such that the vertical disc diameter in pixels and the pixel coordinates of the chosen points were displayed. The variable was then calculated as the distance of the chosen point from a reference point (0,0).

Based on the estimate of the SD (8.5 pixels) from within-subject variability from repeated measures in Program 1, on one image with particularly blurry disc margins and poorly defined macula, the number of images required to detect repeatability between measures to within 3 pixels with 95% power is 31. 31 images were opened twice in each program and the image repeatability parameters were recorded. The repeatability between the two measures for each program was calculated as the coefficient of repeatability (COR = 1.96 x SD of the differences between measure 1 and 2). The COR represents the 95% limits of agreement between the two measures, or the limit within which 95% of the differences lie and gives an indication of variability.

Pixel distances were converted into μm using the standard disc diameter assumption of 1500μm.

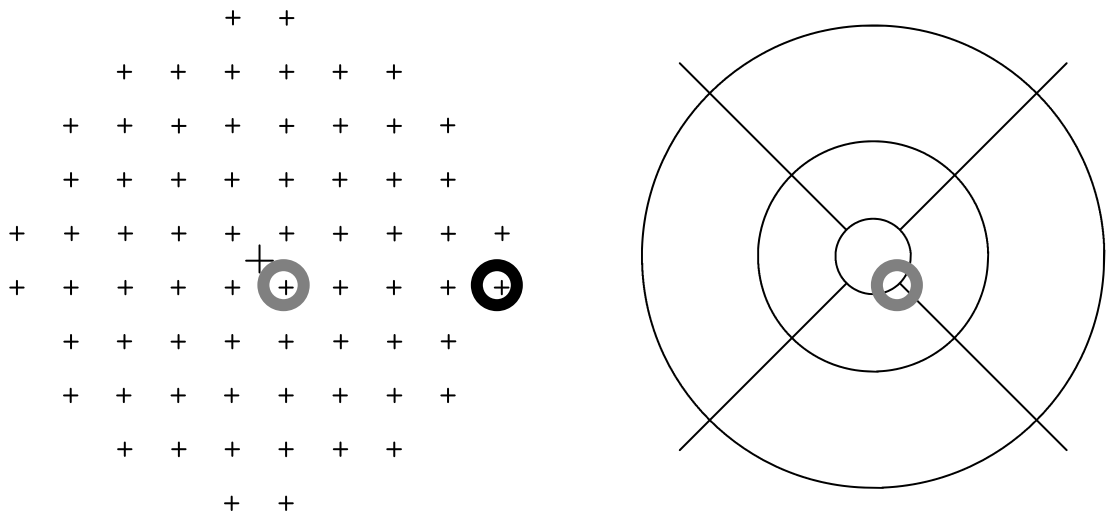

Figure 5-6. Spatial position of repeatability parameters indicated by circles.
Grey circles indicate central stimulus location 40 on visual field and intersection on central circle of grading grid. Black circle shows peripheral stimulus location 44 on visual field.

A summary of differences between first and second measures of grid positions is presented in Table 5-1. The peripheral stimulus location had a slightly greater mean difference and COR value than the central stimulus location. The repeatability difference between the central and peripheral stimulus locations were not considered to be clinically significant.

	Program 1		Program 2
	Central point	Peripheral point	
Mean	0.31	12.66	0.37
SD	39.62	42.52	33.28
COR	77.66	83.36	65.24

Table 5-1. The difference in distance between first and second measures of grid positions, in μm

5.5 Application of Program 2 to the Grading of Images

The difference between two graders in making clinical judgements whilst using Program 2 was assessed. Grading was performed using the bitmap image in

conjunction with the Fundus Grading Grid program with reference made to the stereoscopic pair stored in the original JPEG format, where necessary. The graders, an optometrist (JA) and consultant ophthalmologist (JMG) performed all grading independently. The graders were masked to the identity of the patients and images were graded in a random order to reduce observer bias.

49 images from patients with AMD were viewed on a 20.1" screen. A prismatic stereoviewer was used to facilitate differentiation of large drusen from areas of hypopigmentation and to aid viewing of any raised lesions, such as a pigment epithelial detachment. Visualisation factors such as the distance and angle of viewing, monitor resolution and magnification were kept constant. Images were graded according to the International Classification and Grading System (Bird et al. 1995). Stage of disease was determined according to the stages of severity defined by an epidemiologic study, based on progression rates of features over a 6.5-year period (van Leeuwen et al. 2003b). Stage of disease was then redefined based on an alternative staging system the CARMS system (Seddon et al. 2006). Modified from the AREDS staging system and originally designed to be used by graders with minimal training, the CARMS stages could be easily identified from the features already graded.

The inter-observer agreement was determined using the weighted kappa statistic (κ) for each feature graded and is shown in Table 5-2. The κ statistic can be used with categorical data and can range from -1 indicating exact disagreement to +1, representing exact agreement (Landis & Koch 1977). The following interpretation of κ values was proposed as 0.41 to 0.60 indicating moderate agreement, 0.61 to 0.80 substantial agreement, and 0.81 to 0.99 almost perfect agreement (Landis & Koch 1977). The agreement between graders ranged from 0.42 to 1. All characteristics showed substantial agreement except for area covered by drusen, main location of hyper/hypopigmentation and main location of neovascular AMD, which showed

moderate agreement. Agreement between graders of identification of stage was excellent.

The difference between two staging systems is shown in Figure 5-7. The line of best fit has a gradient of 0.73. Were the two stages to agree exactly, this value would be 1 (illustrated by dotted line).

		Weighted κ	Standard error
Drusen	Type	0.91	0.03
	Number	0.90	0.05
	Size	0.90	0.04
	Main location	0.80	0.07
	Area covered	0.56	0.10
Pigmentary Changes	Hyperpigmentation	0.76	0.08
	Hypopigmentation	0.94	0.05
	Main location	0.42	0.16
Geographic Atrophy	Presence	1	0
	Location	0.73	0.16
	Area covered	0.82	0.18
Neovascular AMD	Presence	1	0
	Typifying features	0.84	0.17
	Location	0.57	0.35
	Area covered	1	0
Stage of AMD		0.90	0.05

Table 5-2. Inter-observer agreement for grading characteristics of AMD

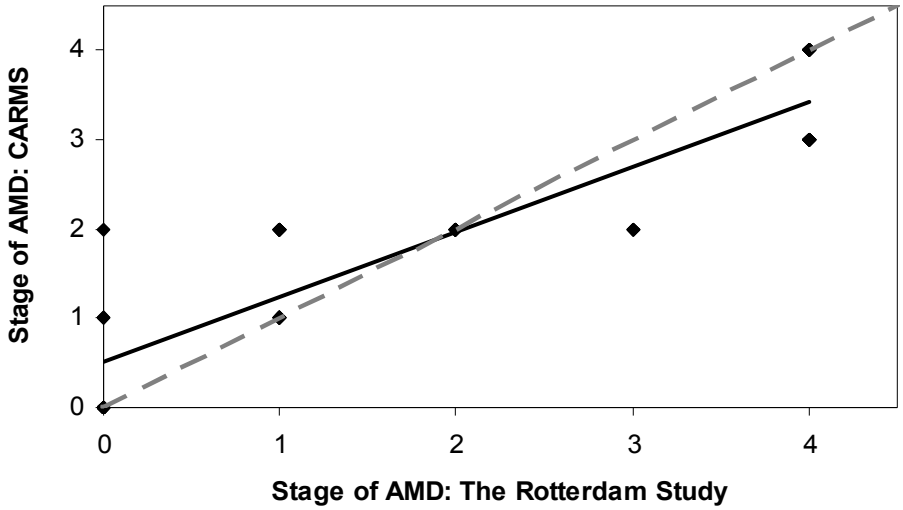

Figure 5-7. Comparison of two systems for staging of severity of AMD
Two staging systems for AMD were used to grade the same fundus images. A converted scale for the CARMS staging system (Seddon et al. 2006) is plotted against the Rotterdam Study staging system (van Leeuwen et al. 2003b). The solid line shows the line of best fit which has a gradient of 0.73. The dotted line shows the line of exact agreement which has a gradient of 1.

5.6 Discussion

Two separate applications of the programming were to map visual field data and the standard AMD grading grid onto the fundus image. The programs were evaluated for accuracy of the spatial mapping in terms of retinal distances. Once the grading program was developed and evaluated, it was then applied in order to assess the inter-observer agreement in grading of AMD. The evaluation results present evidence of accurate mapping to within approximately 80μm for Program 1: Perimetric Fundus Map and approximately 65μm for Program 2: Fundus Grading Grid. Interpretation of Program 1 in relating drusen or other features with coinciding visual field defects at individual stimulus locations is therefore limited to drusen larger than 80μm, since it is not possible to make the same interpretations with smaller features. Overall inter-observer agreement of the grading of AMD features when using the program was good.

It is not surprising that the repeatability of Program 2 yielded greater accuracy than Program 1, since less user defined measures are made in Program 2. The accuracy of the Perimetric Fundus Map program to detect whether visual field defects lie over

retinal signs should be limited to features larger than 80μm, therefore hard drusen or other small features in isolation cannot be confidently associated with defects on the output map. Factors influencing the grid positioning were the degree of definition of the optic disc margins and the macula, which affected the ease for the user of mouse click placement. A more magnified image, in cases where very small drusen were present in the central subfield, was less likely to give positional errors, than a less magnified image. This was due to better visibility of the retinal landmarks despite a greater number of pixels contained within the same area.

In photography, compression algorithms reduce the size of image. TIFF (tagged image file format) and bitmap files use lossless compression, in which the algorithms search for redundancy of information in the image to recode more efficiently. Lossless compression permits the original image data to be retrieved, whereas lossy image files do not. JPEG (Joint Photographic Experts Group) files are lossy files and were designed to reduce the file size without causing a significant visible difference to the image. It is possible to vary the compression ratio to suit the image quality versus file size requirements. The camera used in this evaluation was a 6.3 megapixel camera with a pixel resolution of 3072 x 2048 and is a camera recommended by the National Screening Committee guidelines for diabetic retinopathy (UK National Screening Committee, 2009). The monitor resolution used for all grading was a 20.1" display with a pixel resolution of 1600 x 1200 in accordance with the standards for grading diabetic retinopathy (UK National Screening Committee, 2009), which fulfils the image resolution requirement of at least 20 pixels per degree. A limitation of the camera was that the best possible image quality output was a high quality JPEG, as opposed to a lossless file such as a TIFF. However, since the maximum quality JPEG image reduces the file size by 90.2% compared with a TIFF image, it was considered that the visible difference in image quality was negligible. The only image file format which could be programmed and manipulated in Liberty BASIC software was the bitmap.

This necessitated conversion from the original JPEGs to bitmaps. The bitmap conversion of these files therefore, represents a lossless compression of the original JPEG files, where there was no observable degradation to small features such as hard drusen. Notably, the automated drusen segmentation program (Smith et al. 2005a,b) converts all imported images to bitmaps before performing segmentation, which validates the programming methods in the present evaluation.

The standard assumption of retinal distance used in AMD grading is in itself a major source of error relevant to the grid positioning in the programs. The COR values in the above results recalculated using 1850μm as the disc diameter gave values of 100μm and 78μm for Programs 1 and 2, respectively. Further caution regarding the interpretation of the COR values is necessary based on the parametric nature of their calculation, in this case being applied to non-Gaussian data. Unfortunately no non-parametric equivalent exists and transformation of the variables rendered the COR values clinically meaningless. The International classification system quotes diameters of hard drusen as <125μm and soft intermediate drusen as >63μm and <125μm (Bird et al. 1995), therefore the ranges of repeatability still fall within the same range of drusen type.

The MP1 microperimeter allows for superimposition of the retinal differential light thresholds onto the fundus image. This is achieved by a calculation of the true size of the retinal image, involving the camera and ocular factors. Based on the Gullstrand schematic eye, a camera factor of 0.438 is used. The ocular magnification is calculated according to the ametropia of the eye. This is measured by correcting for any size difference in the diameter of the superior temporal vein as it leaves the optic disc. It is assumed that this vessel diameter is constant for all eyes. This technique of superimposition appears to rely on a greater number of assumptions than the methods described in this evaluation.

The worst agreement between graders for features of AMD related to location of pigmentary and neovascular changes and the percentage area covered by the drusen. The greatest error in grading thus involved spatial aspects rather than the identification of the features. This highlights the importance of the initial accurate positioning of the grading grid. Spatial inter-observer error could also be reduced by agreement on precise counting or measuring of drusen at the subfield margins prior to grading. Less variability surrounded the assignation of images to stage of severity of AMD, since this relied primarily on feature identification. Comparison of two staging systems determined from the same images showed close agreement of severity of disease. Both staging systems distinguished five stages of AMD (Tables 1-2 and 1-3), the main differences between the systems involved the observation of pigmentary changes and drusen together. The CARMS system (Seddon et al. 2006) classified the presence of pigmentary changes and drusen at an earlier stage, whereas this was considered to carry higher risk based on incidence data from the Rotterdam Study (van Leeuwen et al. 2003b). Furthermore the CARMS system included approximate counts of drusen number, however the system after van Leeuwen et al. (2003b) did not. Parallel findings in a previous study were reported, where little difference was observed between grading of images using the systems proposed by the Rotterdam Study and AREDS (Tikellis et al. 2006). Although definitions of features differ between staging systems, this evidence suggests the determination of functional progression of disease may yield similar results between systems.

Program 1: Perimetric Fundus Map was written to relate visual function to structural changes at the macula (see Chapter 8). The clinical application may be to aid the detection and monitoring of central retinal diseases, where visual field defects can be easily mapped to fundus photographs or other images such as infra-red SLO images. Retinal photography and perimetry are routinely carried out in Optometric practice, therefore the program could be a useful tool integrated into everyday patient care.

Program 2: Fundus Grading Grid represents a rapid and convenient method of grading AMD for research purposes, which avoids the traditional method of plastic overlays. These programs provide useful tools for the analysis of digital fundus images.

6. Drusen Detection in Retro-Mode Imaging by a Scanning Laser Ophthalmoscope

Purpose: The F-10 (Nidek, Japan) is a new scanning laser ophthalmoscope that is capable of a novel fundus imaging technique, retro-mode. The conventional imaging of drusen in age-related macular degeneration (AMD) is by fundus photography. The aims of the study were to assess drusen quantification using retro-mode imaging.

Methods: Stereoscopic fundus photographs and retro-mode images were captured in 31 eyes of 20 patients with varying stages of AMD. Two experienced masked graders independently graded images for the number and size of drusen, using custom software.

Results: Drusen observed by fundus photography were significantly fewer in number ($p < 0.001$) than subretinal deposits seen in retro-mode, using the F-10. The predominant deposit diameter was on average 5μm smaller in retro-mode imaging than in fundus photography ($p = 0.004$). Agreement between graders was substantial for number of drusen (weighted $\kappa = 0.69$) and moderate for size of drusen (weighted $\kappa = 0.42$).

Conclusion: The results demonstrate significantly more subretinal deposits detected in retro-mode imaging than in conventional fundus photography, thus this technique is capable of providing additional subtle spatial information extra to that which is available in photography. The large subretinal deposits in retro-mode imaging were consistent with the appearance of drusen on OCT imaging. Retro-mode imaging provides a rapid non-invasive technique, useful in monitoring subtle changes and progression of AMD.

6.1 Introduction

Drusen are early fundus changes characteristic of AMD and early detection is likely to be increasingly important in view of future possible interventions. Conventional fundus photography is widely used in imaging and detecting drusen and although non-mydriatic cameras exist, pupillary dilation is often necessary in elderly patients with small pupils and lenticular opacities.

The use of scanning laser ophthalmoscopy in fundus imaging is well documented and has a wide variety of clinical applications. Briefly, a scanning laser ophthalmoscope (SLO) images the retina, whereby the optics of the eye serve as the objective lens. A narrow laser beam is scanned through the pupil onto the retina in a raster pattern, and is focused by the optics of the eye to illuminate a spot on to the retina. Reflected light returns through the optics of the eye to a detector, which serially produces a two-dimensional image of the retina. Reflected light is predominantly used in confocal imaging and the fundus reflectance is greater at near infrared wavelengths than shorter wavelengths (Elsner et al. 1996). Confocal imaging employs an aperture before the detector, which is in a plane conjugate to the retina, reducing the amount of light reaching the detector (Elsner & Multer 2008; Webb et al. 1987). This design allows better control of the light returning from the retina and generates high contrast images. Scattered light and reflections from planes which are not in focus are blocked by the aperture, so that only light from the illuminated focal plane is detected (Wormington 2003).

The F-10 is a confocal SLO (Figure 6-1), which non-invasively scans the fundus with a Class 1 laser. Different modes of imaging include reflectance modes for various wavelengths (490nm, 532nm, 660nm and 790nm), fluorescein angiography, indocyanine green angiography and a novel technique, retro-mode. It captures images with a field of view of 40° or 60°, an optical resolution of 16-20μm and image size of up to 1024 x 720 pixels.

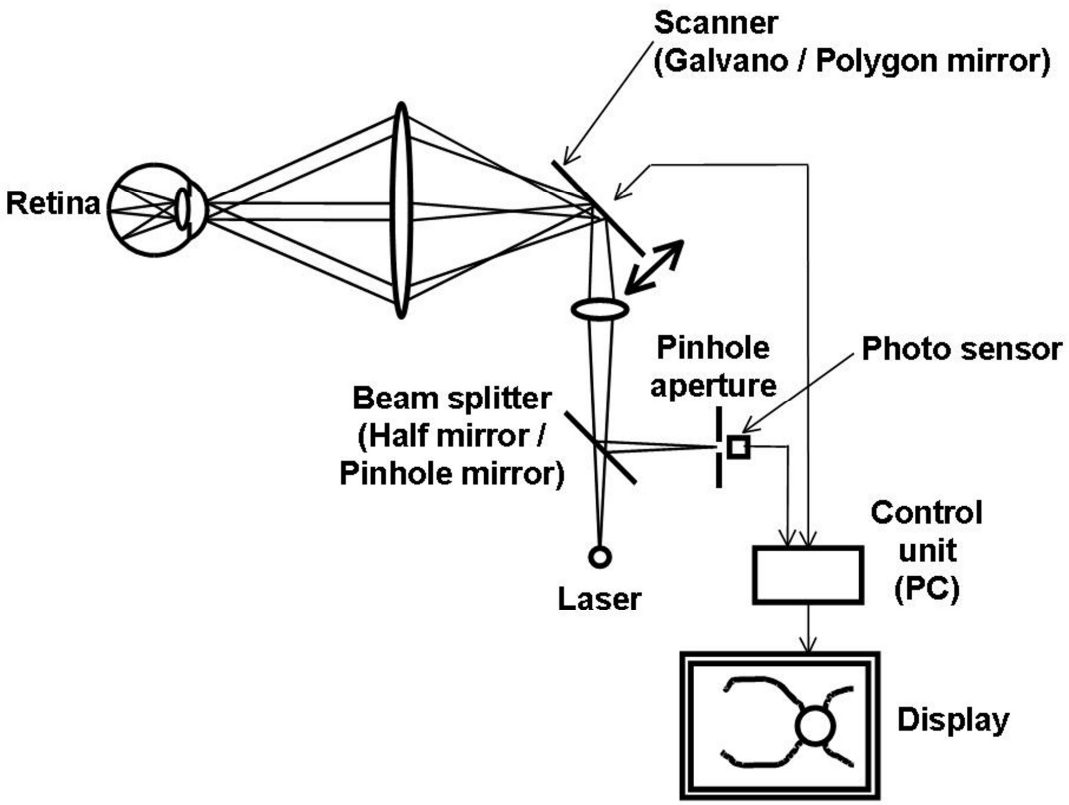

Figure 6-1. Optical diagram of a confocal scanning laser ophthalmoscope

Retro-mode imaging uses an infrared laser (wavelength 790nm) and employs an aperture with a modified central stop, which is deviated laterally from the confocal light path, and may be positioned to the left or right side of the fundus (Figure 6-2). The scattered light passing through the deviated aperture gives a shadow to features such as subretinal deposits thus enhancing the contrast and delineation of the features (Figure 6-3). Retro-mode images from a recent case study of two patients with cystoid macular oedema secondary to polypoidal choroidal vasculopathy, revealed cystoid spaces detected by OCT imaging, but not visible on fundus photography (Yamamoto et al. 2008).

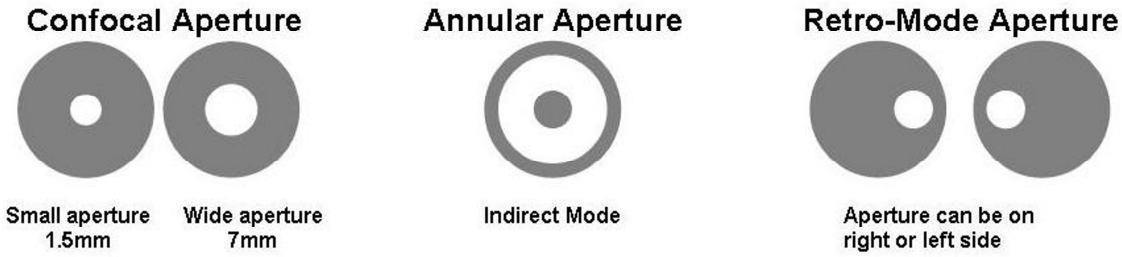

Figure 6-2. SLO apertures
The confocal aperture width can be varied from 1.5mm to 7mm. The smallest aperture is pinhole-like, and produces a high contrast image, whereas the wider aperture collects light from a larger area, but produces a lower contrast image. Scattered light is collected by the annular aperture, and reflected light is blocked by the central stop. The aperture in retro-mode incorporates the central stop in indirect mode, but also blocks light from either the left or right side, which creates the shadow to one side of the abnormal feature, such as drusen.

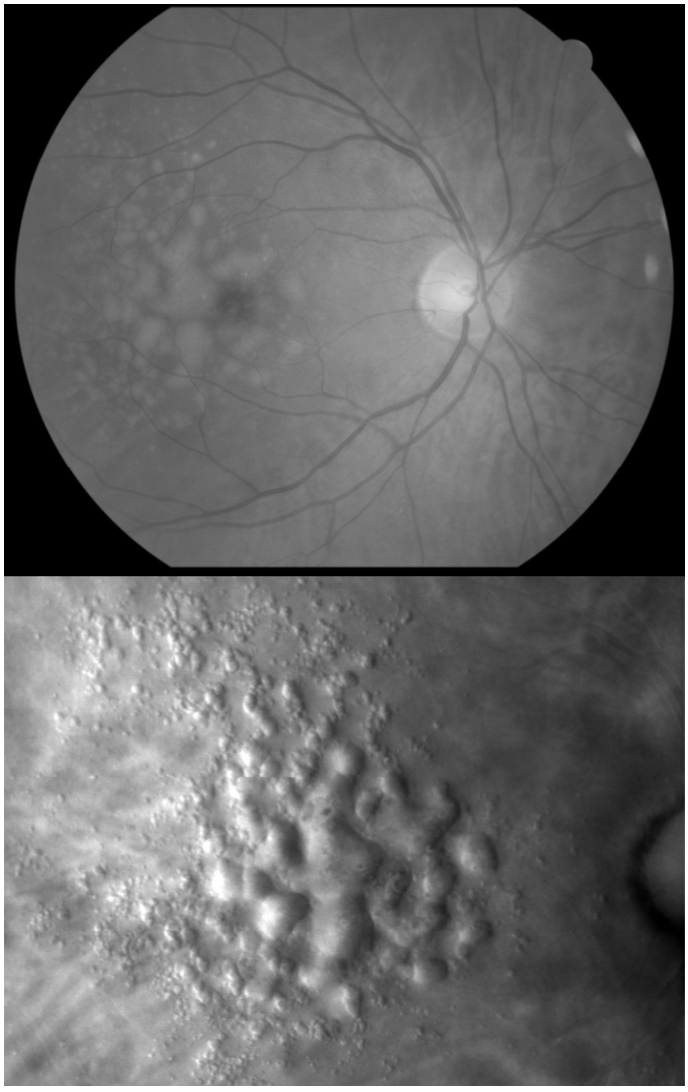

Figure 6-3. Fundus photograph and F-10 retro-mode image
Differing appearance of drusen from the same patient captured by colour fundus photography (top) and retro-mode image (bottom).

The use of infrared imaging is advantageous in elderly patients with lens opacities, since light is minimally scattered in the presence of media opacities (Elsner et al. 1996). The deeper penetration of infrared light compared to visible wavelengths allows for easier observation of subretinal structures such as drusen and choroidal neovascularisation (Hartnett & Elsner 1996).

Retro-mode imaging has a similarity to indirect imaging of a SLO, since scattered light is collected in both. Both imaging methods employ an aperture with a central stop, where indirect mode uses a large annular aperture and retro-mode only uses part of the annular aperture (Figure 6-2). Directly reflected light from the fundus is blocked by the central stop and only the scattered light passes through the aperture (Webb et al. 1987). In this way, more laterally scattered light is sampled than in the direct mode (Elsner et al. 1996). Only retinal structures which scatter incident light laterally are detected, thus this technique highlights features such as drusen which act as an efficient source of light scatter (Wormington 2003). Indirect mode has demonstrated enhanced imaging of macular drusen in a small number of patients (Hartnett & Elsner 1996; Manivannan et al. 1994), an area of elevation in choroidal neovascularisation (Hartnett & Elsner 1996), easy detection of detachment of the neuroretina in central serous retinopathy (Remky et al. 1998), and the emphasised appearance of borders in cystoid macular oedema (Remky et al. 1999). Retro-mode only allows laterally scattered light from one direction, depending on the position of the aperture (Figure 6-4).

The aims of this study were to compare images captured using the F-10 scanning laser ophthalmoscope in retro-mode with standard fundus photography to quantify macular drusen. The nature of the retro-mode images was demonstrated previously in a small pilot study (Gibson et al. 2009).

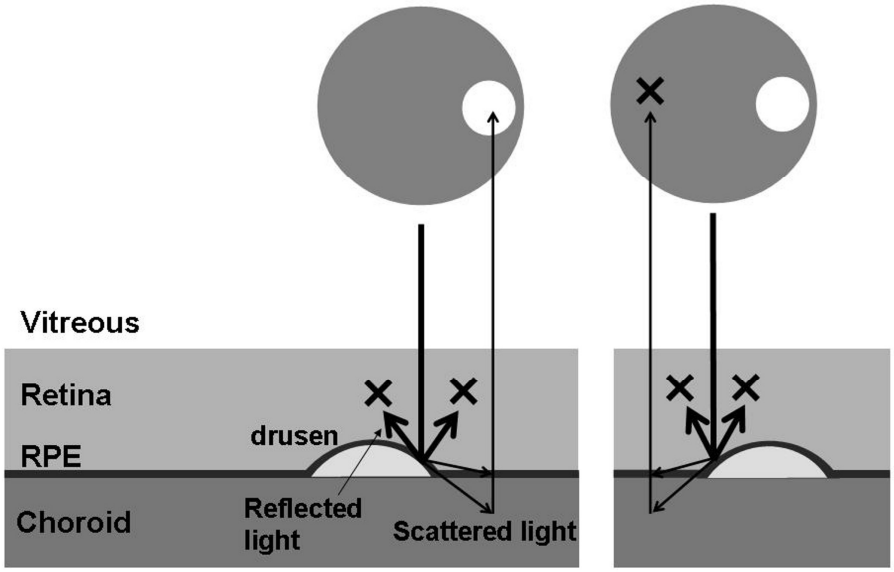

Figure 6-4. Retro-mode imaging
Directly reflected light and scattered light from one side of the drusen are blocked. The right side of the drusen appears lighter in the image, when the aperture is in this position.

6.2 Methods

6.2.1 Sample

Patients over the age of 45 years were recruited at various stages of AMD. Exclusions were made where there was any history of other ocular disease or diabetes. Eyes with ocular trauma or eyes which had been treated for AMD were excluded.

Ethical approval was obtained from the Aston University, Human Sciences Ethical Committee. Informed consent was obtained from each patient including detailed explanations of all procedures before participation. 31 eyes of 20 patients were eligible for the study and ranged in age from 48 to 79 years (mean 67, SD 6.7), 16 patients were female and 4 were male.

A subset of the patient group, 13 eyes of 8 patients, attended 6 months (mean 185.8 days, SD 37.4) later for further images, using the F-10 and RS-3000 OCT (Nidek, Japan).

6.2.2 Imaging

In order to optimise image quality, all imaging was performed on patients with dilated pupils, with tropicamide 0.5% (*Minims*, Bausch & Lomb). Fundus photography was carried out with a non-mydriatic camera (Canon EOS 10D camera, 6.3 megapixels) to acquire stereoscopic pairs of digital images. 30° field images centred at the macula were stored as high quality JPEG files (large/fine, ~2.4MB, 3072 x 2048). 20° (horizontal dimension, or 40° field of view) images were captured in retro-mode using the F-10, and stored as high quality JPEG files (1280 x 960 or 800 x 600 pixels).

Images were acquired using the RS-3000 OCT. This is a spectral domain OCT and SLO infrared imaging system, whose axial and transverse resolution is 7μm and 20μm, respectively. The fundus was imaged with the "macular map" scan, in which the appropriate field was selected.

The images were manipulated using commercially available software (Adobe Photoshop 8.0) such that the retinal positions of the OCT scans as shown by the infrared images were matched to the retro-mode images using the flicker on and off and transparency features.

6.2.3 Grading

Fundus photography images were graded in a random order for the retinal features according to the International Classification and Grading System (Bird et al. 1995). Stage of disease was determined according to the stages of severity defined by an epidemiologic study, based on progression rates of features over a 6.5-year period (van Leeuwen et al. 2003b). Grading and stage determination was carried out by two independent, masked graders (JMG & JA).

Further grading of the fundus photographs was then performed using custom software (Program 2, Chapter 5) for number of drusen and predominant drusen diameter within the central 3000μm circle, by two masked graders (HK & PG), experienced in grading AMD and diabetic retinopathy. The software allows for mapping of the circular grading

grid onto the fundus image, manual marking of drusen and a measurement tool. The subretinal deposits visible on the retro-mode images were assessed in the same way.

6.2.4 Data Analysis

Normality was achieved by transforming the variables number of drusen (square root transformation) and size of drusen (logarithmic transformation), by the Kolmogorov-Smirnov test, $p = 0.555$ and $p = 0.663$, respectively. Between stages of AMD, the variance of the transformed data was homogeneous for number of drusen (Levene's statistic = 0.663, $p = 0.619$) but not for size of drusen (Levene's statistic = 4.437, $p = 0.002$). Paired t tests were performed to assess the differences between imaging methods. Drusen size and drusen number data was converted to ordinal data according to the definitions specified in the International Classification and Grading System (Bird et al. 1995) in order to calculate a weighted κ statistic to measure agreement between graders. Bland-Altman plots were constructed for comparisons between imaging methods and graders (Bland & Altman 1986). A one-way ANOVA was performed to examine the effect of stage of AMD on the normalised dependent variables.

6.3 Results

Classification of stage of disease resulted in nine eyes at stage 0, 10 eyes at stage 1, 4 eyes at stage 2, 2 eyes at stage 3 and 6 eyes at stage 4 of disease. Drusen were present in all eyes, 25 eyes had drusen and pigmentary changes only, 4 eyes exhibited geographic atrophy and 2 eyes had signs of choroidal neovascularisation.

6.3.1 Effect of Stage

A significant (One-way ANOVA: $F = 5.913$, $p < 0.001$) variation of number of drusen (square root) was noted when comparing by stage of severity of AMD. Post-hoc analysis (Tukey HSD) revealed significant differences between the following pairs of stages only; stage 0 and stage 1 ($p = 0.006$), stage 0 and stage 2 ($p = 0.001$), stage 0 and stage 4 ($p = 0.004$). A significant variation of size of drusen (log base 10) was

found when comparing by stage of severity of AMD (one-way ANOVA: $F = 11.211$, $p < 0.001$). Post-hoc analysis (Games/Howell) revealed significant differences between the following pairs of stages only; stage 0 and stage 1 ($p < 0.001$), stage 0 and stage 2 ($p = 0.009$), stage 0 and stage 3 ($p = 0.030$), stage 0 and stage 4 ($p = 0.001$).

	Mean	SD	Range	Coefficient of Variation
Number of drusen – Fundus Photography	33.55	39.1	0 – 230	1.17
Number of subretinal deposits – Retro-Mode	81.63	72.8	0 – 318	0.89
Size of drusen - Fundus Photography	101.43	69.7	0 – 325.65	0.69
Size of subretinal deposits – Retro-Mode	96.52	75.2	0 – 475.26	0.78

Table 6-1. Number and size (μm) of drusen for colour fundus photography and retro-mode imaging

Paired t test transformed data (sqrt no. drusen, log size drusen)	t	df	p
Difference between fundus photography & retro-mode: Number of drusen	-9.314	61	**<0.001***
Difference between fundus photography & retro-mode: Size of drusen	3.009	53	**0.004***

* indicates significance

Table 6-2. Summary of differences between imaging methods for number and size of drusen and subretinal deposits

6.3.2 Difference between Fundus Photography and Retro-Mode Imaging

Table 6-1 shows the mean number and predominant drusen diameter graded for colour fundus photography and retro-mode imaging. There were significant differences between imaging methods for number ($p < 0.001$) and size of drusen ($p = 0.004$; Table 6-2). A consistently greater number of deposits were detected by the retro-mode images and the mean difference was 48 deposits (Figure 6-5A). Drusen were graded very slightly larger in fundus photography, by a mean difference of 5μm (Figure 6-5B). Greater levels of agreement were seen when fewer drusen were present, whereas there was no clear relationship between the magnitude of drusen diameter and

agreement between imaging modes (Figure 6-5A,B). These relationships should be interpreted with some degree of caution due to this parametric analyses being applied to non-Gaussian data. There is no non-parametric equivalent of a Bland-Altman plot and when applied to the transformed variables, rendered the analyses clinically meaningless.

6.3.3 Inter-Grader Differences

Although there was a significant difference between graders for number ($p < 0.001$) and size ($p < 0.001$) of drusen, the agreement between graders when applying the categories used in the International Classification and Grading System was substantial for number of drusen (weighted κ value 0.69) and moderate for size of drusen (weighted κ value 0.42; Table 6-3). Grader 2 (PG) tended to grade fewer and larger drusen than grader 1 (HK). For drusen number, the difference was greater when there were more than 100 drusen (Figure 6-5C), and there was no clear bias in the difference between graders for size of drusen (Figure 6-5D).

6.3.4 OCT and Retro-Mode comparison

Some drusen were identified as present on both fundus photography and retro-mode images manifested on OCT scans as displacement of the RPE. When analysing larger retro-mode deposits not present on fundus photography, the same appearance was noted on the OCT scans (Figure 6-6). Comparison between the second and first set of retro-mode images revealed appreciable change in four of 13 eyes where two of the images showed enlargement of deposits and two images showed confluence of deposits (Figure 6-7).

Figure 6-5. Bland-Altman plots (overleaf)
The black line indicates the mean difference and the grey lines represent the 95% limits of agreement. A: The difference in drusen number counted on fundus photography and retro-mode images. B: The difference in drusen size (μm) between imaging types. C: The difference between drusen number counted by grader 1 and grader 2. D: The difference between drusen size (μm) measured by grader 1 and grader 2.

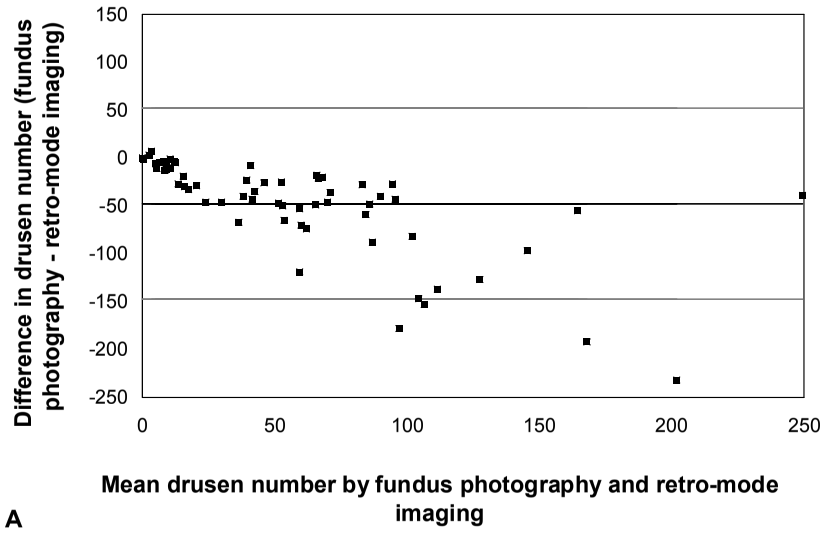

A

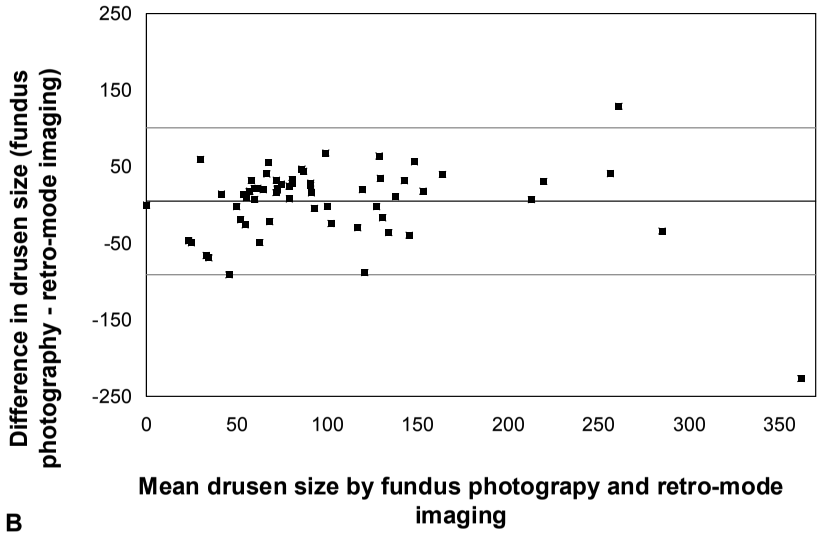

B

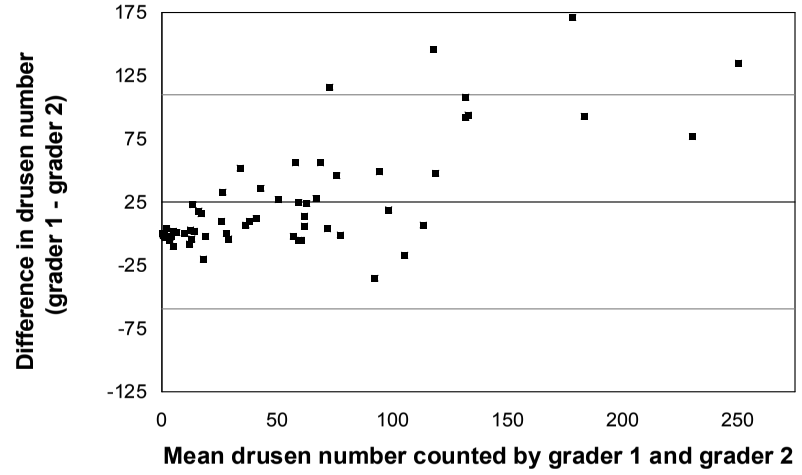

C

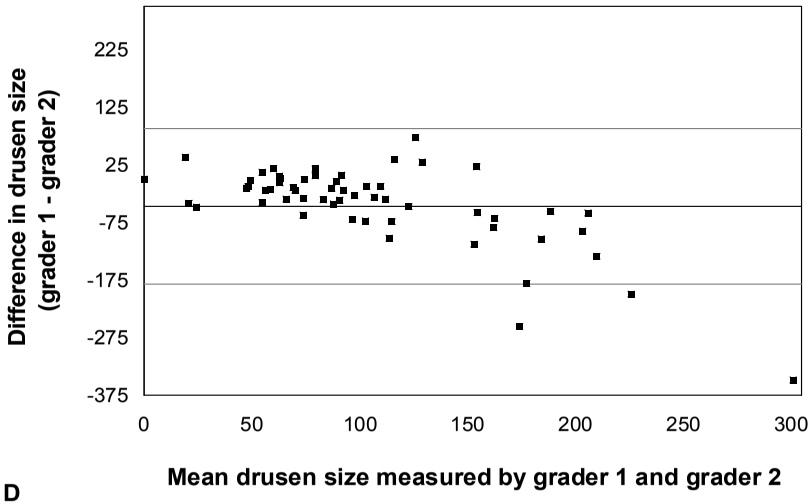

D

Figure 6-5. Bland-Altman plots

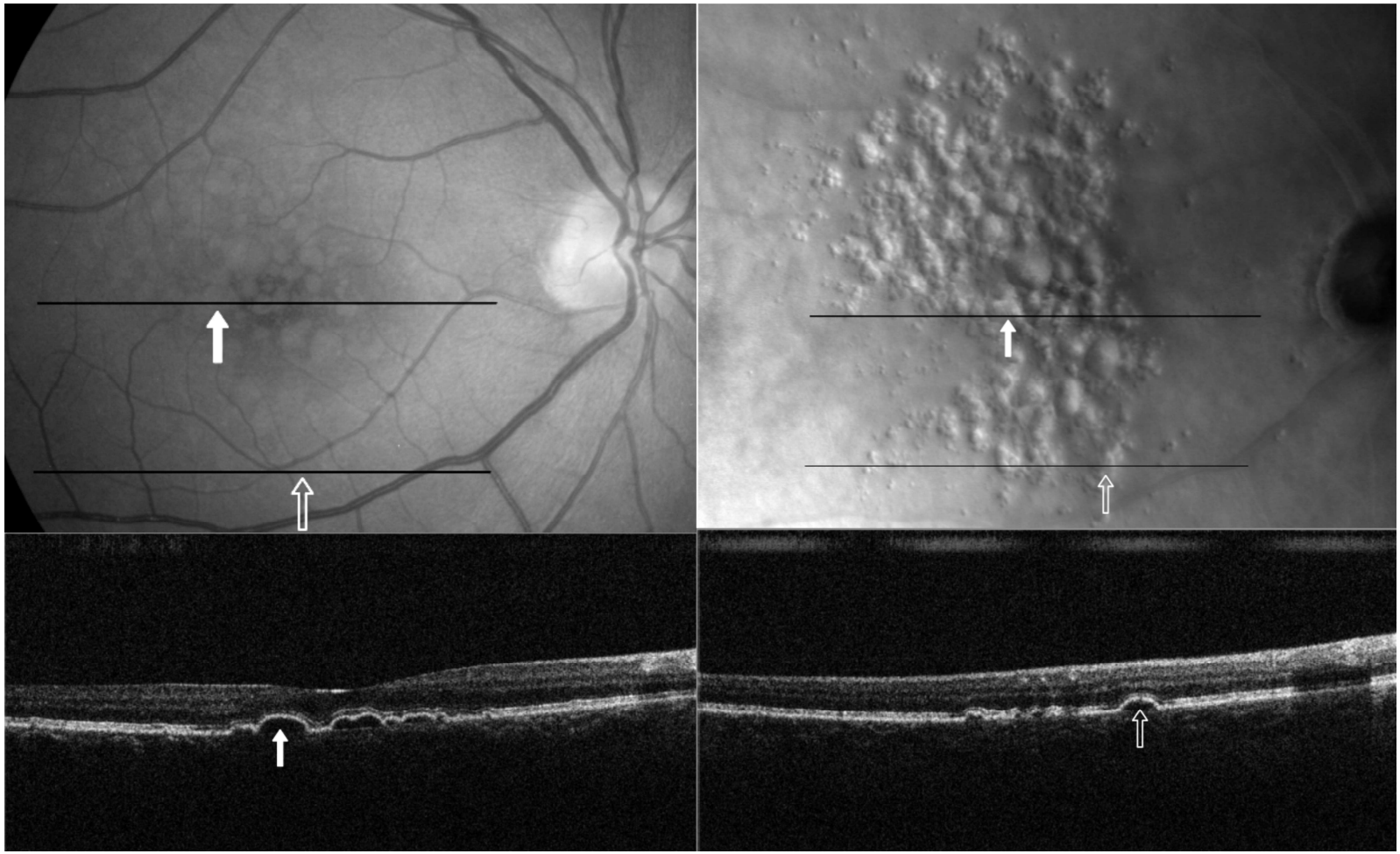

Figure 6-6. Fundus photograph, retro-mode image and OCT images.

Solid arrow indicates drusen visible in all three imaging modes. Outline arrow indicates retro-mode deposit not visible on fundus photograph, but visible on OCT scan, whose displacement of the RPE is consistent with the appearance of drusen

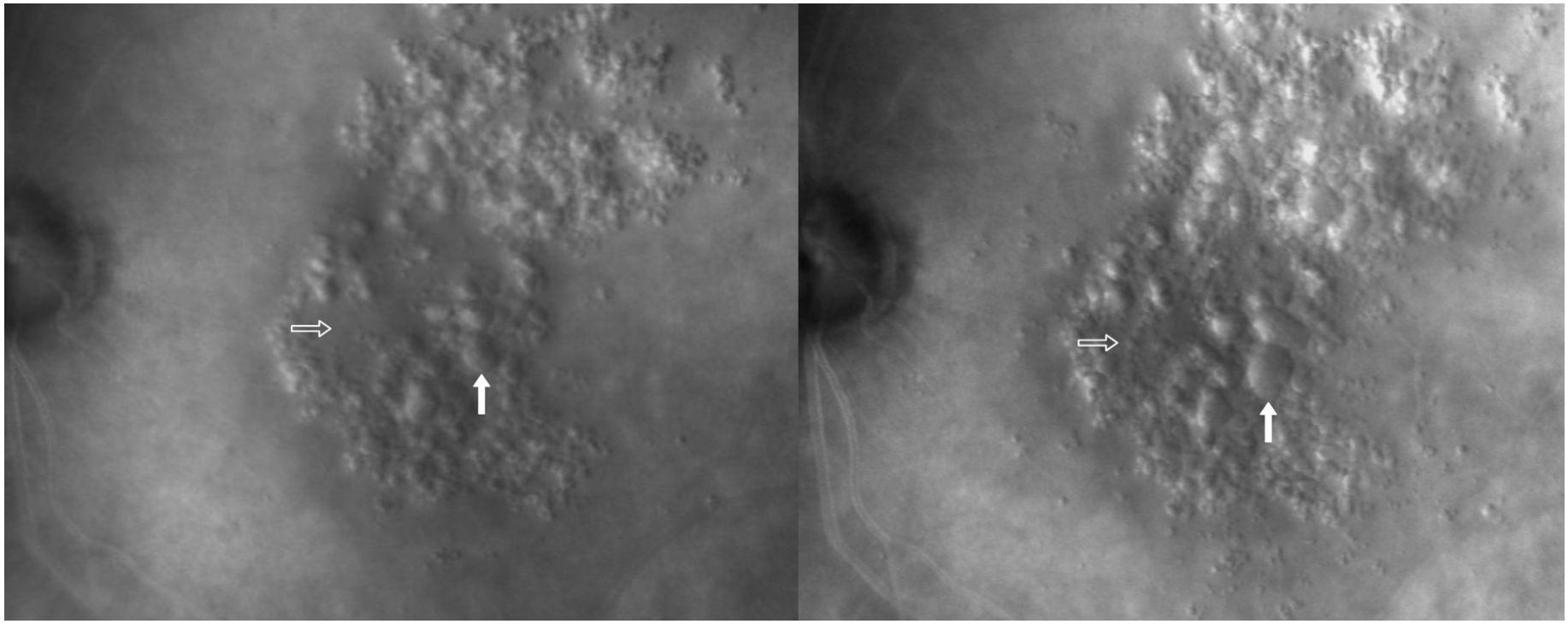

Figure 6-7. Change in retro-mode image over time
The image on the right was captured 6 months after the left. Solid arrows indicate a deposit which enlarged. Outline arrows indicate formation of new deposits in the image on the right.

Agreement between graders	Weighted K	Standard Error
Number of drusen	0.69	0.09
Size of drusen	0.42	0.08

Table 6-3. Weighted kappa values of agreement between graders

6.4 Discussion

In this study, the comparison between drusen quantification on retro-mode images and digital fundus photographs was investigated. The images taken using the F-10 in retro-mode show a pseudo-three-dimensional appearance to drusen, which is consistent with the enhanced imaging of drusen using infrared SLO in indirect mode (Hartnett & Elsner 1996; Manivannan et al. 1994).

Large subretinal deposits visible in the retro-mode images appear to be consistent with the appearance of retinal drusen on OCT imaging, however the smaller subretinal deposits less than approximately 40μm in diameter, which were present in large numbers were not apparent on OCT imaging. The retro-mode deposits appeared in significantly greater numbers than the drusen in the same area in fundus photography. This is in agreement with observation of a single patient case study of macular drusen (Manivannan et al. 1994), and a study of ten patients with exudative AMD in which drusen were manually counted using acetate overlays (Hartnett & Elsner 1996). Conversely, no significant difference between drusen area in colour fundus slides and indirect SLO slides was noted when manually marking drusen onto an acetate sheet over slides of 5 eyes of 6 patients (Kirkpatrick et al. 1995).

Drusen are deposits of extracellular material which lie between the RPE and Bruch's membrane. Histologically, drusen smaller than 25-30μm, the diameter of two RPE cells, are not clinically detectable (Sarks et al. 1999). Various types of pre-clinical drusen, less than 25μm in diameter, have been identified histologically, which occur in the formation of clinically detectable drusen. In eyes which have small numbers of drusen, these may be the entrapment of coated membrane bodies between the RPE

and Bruch's membrane. In eyes with many hard drusen, pre-clinical drusen are small focal plaques of thickened hyalinised Bruch's membrane or microdrusen, 1-2μm in diameter, composed of dense amorphous material (Sarks et al. 1999). Microdrusen occur discretely or in rows and were noted to be a frequent occurrence in eyes with many drusen and may have a role in soft drusen formation (Sarks et al. 1999). It has been suggested that the subretinal deposits seen in indirect SLO mode, which do not correspond to drusen in images derived by colour fundus photography are either identical to drusen or material under the RPE or within Bruch's membrane (Hartnett & Elsner 1996). Since the resolution of the F-10 is 16-20μm, drusen smaller than 25μm were not graded in this study. For all image pairs, of retro-mode and colour fundus images, subretinal deposit number was greater than drusen number, with the exception of two image pairs graded by grader 1(HK), where there was a difference of less than 7. In all images where subretinal deposits in retro-mode were more numerous, the subretinal deposits which did not corresponded to drusen in the colour fundus photographs did not have a different appearance to the deposits which did correspond to drusen.

The most commonly used grading scales for AMD (AREDS 2001b; Bird et al. 1995; Klein et al. 1991) use the circle C_0 which has a diameter of 63μm, as the smallest increment for grading drusen size. Comparison between grading of drusen size for the imaging methods shows good agreement since 87% of diameter differences in grading was less than 63μm and the 95% limits of agreement was 95.9μm (Figure 6-5). Inter-grader agreement was clinically acceptable, 74% of diameter differences in grading between graders were less than 63μm, despite only moderate level of agreement calculated between graders for predominant drusen size (weighted κ value 0.42). Graders showed substantial agreement for number of drusen (weighted κ value 0.69).

The shadow effect to drusen imaged in retro-mode was observed to create light or dark drusen edges. This differed between images captured by the apertures in opposite

positions, where a high contrast edge was seen on a particular drusen edge, a low contrast border would be seen at the same edge when imaged with the opposite aperture. In this way, the retro-mode imaging provides directional information and would be expected to better enhance subtle features such as low lying drusen than infrared SLO indirect imaging. Furthermore, since drusen tend to be circular and uniformly elevated, the directional effect does not influence the detection capability, but may provide useful spatial information about the nature of deposits which are not uniformly shaped.

Supplementary observations regarding the nature of the subretinal deposits were the variations in edge sharpness, which combined with the variations in edge contrast, may affect automated drusen segmentation of retro-mode images. A previous study attempted computerised automated quantification of drusen area, of indirect SLO images, but this technique was found to have a low sensitivity of 35% (Kirkpatrick et al. 1995). Automated drusen detection was confounded in the study by Kirkpatrick et al. (1995), since it was deemed inappropriate to apply a simple thresholding image processing technique to both light and dark edges, and the edge-detection method lacked specificity due to the large variability of the sharpness of the drusen edges (Kirkpatrick et al. 1995).

For images where there were many small subretinal deposits at the image edge, it was noted that the image quality in retro-mode was not uniform across the entire image, even after careful focusing of the instrument. The subretinal deposits appeared to fade or blur at the periphery of the retro-mode images, which was outside of the grading area used in this study. This was further investigated by the capture of images at different fundus areas, using different points of fixation. It was noted that the corresponding drusen which appeared faded in the periphery of one image, were clearly imaged when central in another image. Increased subretinal deposits in the area temporal to the optic disc were also observed in two patients. The peripheral

image degradation could be explained by the retinal curvature and increased distance from the light source causing the brightness profile of the image to be reduced. Peripheral image degradation to subretinal deposits in the 20° images in this study occurred on average in the peripheral 3° outside an approximately horizontal elliptical area of good image quality. Therefore the peripheral features of a retro-mode image, in this area, should be ignored since useful clinical information can only be obtained from the central 17° of a 20° image. It is recommended that further or multiple images be captured where the features of interest lie central to the image.

The results demonstrate that significantly more subretinal deposits, consistent with the OCT appearance of drusen, are detected in retro-mode imaging than in standard fundus photography. Comparison of retro-mode images over time revealed the enlargement and confluence of the deposits in a small number of patients (Figure 6-7). Alteration to the appearance of drusen has not previously been observed over such a short period. A larger scale longitudinal follow-up of patients is required to confirm whether these subretinal deposits are sub-clinical drusen which will eventually manifest as clinically visible drusen or other features of disease.

Retro-mode imaging provides a rapid non-invasive technique which is useful in the monitoring of subtle changes and progression of AMD. Early detection of retinal drusen in asymptomatic younger patients will become increasingly important in the future so that persons at risk of AMD can be identified and future preventative treatments can be targeted effectively.

7. Quantification of Visual Field Progression in Age-Related Macular Degeneration

Purpose: To investigate the visual field progression in the central ten degree field in age-related macular degeneration (AMD).

Methods: Central 10° standard and short-wavelength automated perimetry (SWAP) visual fields were acquired using a Humphrey Field Analyser. 44 eyes of 27 patients (mean age 68.8 years, SD 7.8, range 46-84 years) with AMD and 41 eyes of 22 normal subjects (mean age 67.2 years, SD 7.5, range 49-78 years) were examined. Stereoscopic fundus photographs were graded (Bird et al. 1995) by two independent observers and the stage of disease determined (van Leeuwen et al. 2003b).

Results: Visual field parameters worsened significantly with stage of disease. Data exhibited a non-Gaussian distribution. The standard perimetry median mean deviation (MD) and pattern standard deviation (PSD) was 0.39dB (IQR 1.45) and 1.20dB (IQR 0.16) for patients at stage 0; and -8.62dB (IQR 6.12) and 8.14dB (IQR 4.43) for patients at stage 4. The SWAP median MD and PSD was -3.52dB (IQR 5.00) and 2.14dB (IQR 0.38) for patients at stage 0; and -17.73dB (IQR 6.23) and 5.96dB (IQR 3.49) for patients at stage 4. MD and PSD varied significantly with stage of disease in standard perimetry (both: $p < 0.001$) and SWAP (both: $p < 0.001$), however post hoc analysis revealed overlap of functional values between stages. SWAP defects were consistently greater in depth and area than defects in standard perimetry. Global indices of focal loss, PSD and local spatial variability (LSV) were the most sensitive to detecting differences between normal subjects and early stage AMD patients, in standard perimetry and SWAP, respectively. Threshold variability was considerably increased in late stage AMD eyes. On average, defects were confined to the central 5°. The most vulnerable region of the 10° field to sensitivity loss with increasing stage of AMD was the central 1°, in which the sensitivity decline was -4.8dB per stage in standard perimetry and -4.9dB per stage in SWAP. Based on the pattern deviation defect maps, a severity index of AMD visual field loss was derived.

Conclusions: Sensitivity was significantly reduced at late stage AMD compared to early stage AMD, with a greater effect demonstrated in SWAP than in standard perimetry, although the trend was not strong across all stages of disease. The central field became less uniform and yielded greater threshold variability as stage increased. In SWAP, defects occurred at similar locations to those found with standard perimetry but were deeper and wider. Central visual field loss in SWAP is a sensitive marker of functional progression in AMD.

7.1 Introduction

The functional loss of central vision due to AMD is well documented by a variety of measures such as visual acuity and contrast sensitivity (Abadi & Pantazidou 1996; Bellman et al. 2003; Feigl et al. 2005; Hogg et al. 2003; Klein et al. 1995; Kleiner et al. 1988; Stangos et al. 1995; Sunness et al. 1997, 1999, 2008; see review in Chapter 1.4.1.1). A number of studies have investigated perimetric loss in AMD (Atchison et al. 1990; Cheng & Vingrys 1993; Feigl et al. 2005; Frennesson et al. 1995; Midena et al. 1994, 1997; Remky et al. 2001b; Remky & Elsner 2005; Tolentino et al. 1994; see Chapter 1.4.2). Contradictory results exist such that some studies have reported reduced perimetric thresholds in AMD whilst others have not. Comparison of findings between past studies are complicated by the methods used to grade the retinal signs of AMD and the limited statistical examination of visual field loss which confounds the clinical interpretation of these findings. No attempt has yet been made to quantify the rate of visual loss across stage of severity of AMD, using perimetry. Knowledge of the rate of functional loss is fundamental to the comprehension of the natural progression of disease in terms of visual function and the development of macular lesions. This information may facilitate clinical decisions regarding treatment. The earlier identification of patients where treatment is necessary may help to improve visual prognosis, thereby diminishing the social and financial burden of partial sight and blind registration.

Previous research in other ocular diseases has shown that the use of short-wavelength automated perimetry (SWAP) may be of value in the investigation of AMD (see Chapter 1.4.2.2). Detection of glaucomatous visual field progression using SWAP was noted three to four years earlier than standard perimetry (Johnson et al. 1993a,b). However, the use of SWAP failed to become clinically ubiquitous since SWAP has greater variability in the 30° field (Wild et al. 1998). Nevertheless, in the 10° field the profile of the hill of vision is flatter and therefore allows for more accurate statistical interpretation and greater capability in the detection of focal loss (Cubbidge et al. 2002), which is of

paramount importance in AMD. It is known that AMD patients have a reduced short-wavelength sensitive pathway sensitivity (Applegate et al. 1987; Eisner et al. 1987b; Haegerstrom-Portnoy et al. 1989). Investigation of the 10-2 visual field in SWAP has revealed significantly diminished mean sensitivity (MS) in eyes with soft drusen compared to eyes without drusen (Remky et al. 2001b).

The aims of the study were to quantify the rate of central visual loss in AMD patients at various stages of disease in standard perimetry and SWAP using a cross-sectional design. Secondary aims were to evaluate the position of visual field loss in AMD and the appropriateness of statistical measures which describe the visual field, in the detection of progression.

7.2 Methods

7.2.1 Sample

Based on the SF and the standard deviation for MS in SWAP using the FASTPAC threshold estimating algorithm (1.89dB and 5.20dB, respectively; Wild et al. 1998), a sample of 20 patients would give a 90% confidence level and a sample of 29 patients would give 95% confidence of detecting change. Recalculation of these values using the SF and maximum standard deviation for MS in the normal 10° SWAP field (2.84dB and 4.28dB, respectively; Conway 2003), a sample of 7 or 9 would give 90% or 95% confidence. SWAP was used to calculate the sample size because it exhibits greater variability than standard perimetry.

Patients were recruited from Birmingham and Midland Eye Centre and the Aston University Eye Clinic and normal subjects were recruited from the general public. The sample consisted of 27 patients (mean age 68.8 years, SD 7.8, range 46-84 years, 8 males, 19 females) at various stages of AMD and 22 normal control subjects (mean age 67.2 years, SD 7.5, range 49-78 years, 13 males, 9 females). The normal control subjects were age-matched to the AMD patients as closely as possible. All patients had experience of at least one visual field screening examination, as part of routine

Optometric care, but all patients were naïve to SWAP and to the 10-2 visual field examination. At least one eye of participating subjects conformed to the inclusion criteria of distance refractive error of less than ±5.00D sphere and ±2.00D cylinder in each eye, clear ocular media as defined by Lens Opacity Classification System LOCS III (Chylack et al. 1993) graded at a slit lamp, no greater than NC3, NO3, C1, P1, no pseudophakia, intraocular pressures less than 21mmHg measured by non-contact tonometry (Pulsair), normal optic nerve head appearance, no family history of glaucoma, no history of ocular disease other than untreated AMD, no ocular trauma, no neurological history or systemic disease, no systemic medication known to influence the visual field and no congenital colour vision defect. Corrected visual acuity was at least 0.1 logMAR in each eye, in the normal group. Informed consent was obtained from each subject and the study had approval from the Aston University Human Sciences Ethical Committee and the NHS West Midlands Research Ethics Committee.

7.2.2 AMD Grading

Fundus photography was performed on patients with pupils dilated with 0.5% tropicamide (*Minims*, Bausch & Lomb), in order to optimise image quality. Pupils were dilated in normal subjects only where small pupils limited image quality. A non-mydriatic camera (Canon EOS 10D camera, 6.3 megapixels) was used to acquire 30° field digital images centred at the macula. Stereoscopic pairs of images were captured whereby the first image was taken near the left edge of the pupil and following a lateral shift of the camera base, the second image was taken near the right pupil edge. Images were stored as high quality JPEG files (large/fine, ~2.4MB, 3072 x 2048) and graded in a random order for the retinal features according to the International Classification and Grading System (Bird et al. 1995). For the purposes of this thesis, the subjects who had gradable features using this classification were defined as belonging to the AMD patient group. Images were viewed on a 20.1" 4:3 monitor (1200 x 1600 pixel resolution), using a prismatic stereoviewer. Stage of disease was

determined according to the stages of severity defined by an epidemiologic study, based on progression rates of features over a 6.5 year period (van Leeuwen et al. 2003b). Grading and stage determination was carried out by two independent, masked graders (JMG & JHA), using custom software (Program 2, Chapter 5).

7.2.3 Perimetry

Subjects where only one eye was within the study criteria, underwent all visual field testing on both eyes, however perimetric data from the excluded eye was discarded. Each subject underwent standard and SWAP visual field examinations with the Humphrey Field Analyser 750 on two occasions. Program 10-2 was used which is a 10° field, with a stimulus separation of 2°. For standard perimetry, the stimulus size was Goldmann size III (0.43°) and background illumination was 31.5 apostilbs. The projected stimuli may be varied in intensity over a range of more than 51 decibels (0 to 10,000 apostilbs) and were presented with a duration of 200ms. Background and stimulus conditions for SWAP are described in Chapter 1.2. SITA Standard and FASTPAC algorithms were employed for the standard and SWAP fields, respectively, in order to mimic clinical practice as closely as possible. Visits were separated by 11 days, and the results from the first visit were discarded to account for the learning effect.

The right eye was always examined first with the exception of subjects in the patient group where there was a large difference in visual acuity between the two eyes, in which case the better eye was examined first. Standard perimetry examinations were performed before SWAP examinations. Fatigue effects are known to be greater in SWAP than in standard perimetry (Cubbidge 1997). As a result a greater recovery period would have been necessary had the SWAP fields been performed first. One researcher (JHA) conducted all testing and issued identical instructions to each patient. The non-examined eye was occluded with an opaque patch and the refractive

correction appropriate to the bowl distance was placed before the test eye with full aperture trial lenses.

Before each examination, patients underwent three minutes of adaptation to the bowl luminance and its chromatic properties. If fixation losses were greater than the recommended 33%, subjects returned for repetition of those fields and if fixation was still judged as inadequate, the data was discarded. Fixation losses were less than 33% in 159 field examinations, in which 143 fields had fixation losses less than 20%. The remaining 10 fields had losses less than 41% errors but were included as they were judged as having good fixation based on the gaze tracker which continually assesses fixation in real time, video monitor observation and other parameters of fixation monitoring. False negative and false positive responses were less than 33%. Rest periods were enforced, lasting one minute at four minute intervals during examination, five minutes between eyes, and then ten minutes between standard perimetry and SWAP examinations.

7.2.4 Analysis

Visual field results from 44 eyes of 26 patients and 41 eyes of 22 normal subjects, were included in the analysis. There were 12 eyes graded at stage 0, 11 eyes graded at stage 1, 6 eyes at stage 2, 3 eyes at stage 3 and 12 eyes at stage 4. Progression of the visual field change with stage of AMD was calculated in terms of the visual field indices mean deviation (MD), pattern standard deviation (PSD) and the number of defects on pattern deviation and total deviation analyses. The MD and PSD in standard perimetry were the weighted indices obtained from the HFA printout. The unweighted SWAP indices were calculated from a normal database previously collected (Conway 2003). Additionally for SWAP, the short-term fluctuation (SF) and corrected pattern standard deviation (CPSD) indices were calculated. Spatial filtering was applied to the visual fields and the less common index of local spatial variability (LSV) was calculated, using the median filter (Crabb et al. 1995; see Chapter 1.2.4).

The change in LSV with stage of disease was investigated. Variation between groups was displayed as the percentage coefficient of variation, for each of the 68 stimulus locations for both standard perimetry and SWAP. Maps of frequency of defects were constructed from the pattern deviation (PD) and total deviation (TD) analyses, which enabled the eccentricities of defects to be examined.

Sectorisation of the 10° field into concentric regions, based on the frequency of PD defects, was employed in the analysis in order to evaluate visual field indices in relation to eccentricity. The unweighted MD and slope of change of MD with stage were calculated for each sector. Regression analyses were performed in each sector, which offers the advantage of incorporating spatial information whilst avoiding the variability associated with a pointwise regression analysis (Katz et al. 1997; Smith et al. 1996).

A severity index was derived in order to quantify the nature of visual field loss on a continuous scale. The sector analysis of defect frequency was used to weight sectors of the 10° field according to spatial location. A scoring system of defect depths was employed. The product of the spatial location weight and the defect depth score was obtained and summed for each stimulus location. Normalisation of this result according to the ceiling defect severity score produced the AMD severity index, which ranged between 0 and 1, where 0 indicates no field loss and 1 indicates a maximum probability defect at all stimulus locations.

7.3 Results

7.3.1 Statistical Normality Evaluation

In the patient group visual field parameters did not exhibit a normal distribution (Kolmogorov-Smirnov test), except for the SWAP SF ($p = 0.148$). The control group had normal distributions for the MD and PSD for both standard perimetry ($p = 0.200$ and $p = 0.200$, respectively) and SWAP ($p = 0.200$ and $p = 0.200$), the SWAP SF ($p = 0.200$) and the number of PD ($p = 0.052$) defects in standard perimetry. Therefore for comparative purposes, non-parametric tests were employed throughout the analyses.

		Standard Perimetry					SWAP						
		MS	MD	PSD	LSV	AMD Severity Index	MS	MD	PSD	SF	CPSD	LSV	AMD Severity Index
Normals	Mean	32.43	0.37	1.19	1.13	0.03	24.01	-2.03	2.27	2.24	0.67	1.79	0.05
	SD	1.16	1.04	0.21	0.72	0.04	3.29	3.02	0.43	0.68	0.77	0.38	0.04
	Median	32.44	0.38	1.18	0.96	0.02	24.39	-1.63	2.19	2.22	0.32	1.74	0.04
	IQR	1.54	1.55	0.26	0.20	0.03	4.26	3.88	0.69	0.91	1.20	0.33	0.05
Stage 0	Mean	32.43	0.40	1.19	1.26	0.03	22.66	-3.36	2.18	2.64	0.39	1.97	0.05
	SD	1.02	1.08	0.20	0.96	0.02	2.58	2.52	0.31	1.01	0.49	0.29	0.03
	Median	32.40	0.39	1.20	1.01	0.04	22.32	-3.52	2.14	2.42	0.00	1.99	0.05
	IQR	1.02	1.45	0.16	0.23	0.03	5.24	5.00	0.38	1.77	0.84	0.42	0.05
Stage 1	Mean	32.34	0.13	1.28	1.05	0.05	22.08	-3.86	2.58	2.37	2.52	1.84	0.11
	SD	1.22	1.24	0.20	0.18	0.05	4.25	3.73	0.80	0.52	3.14	0.47	0.10
	Median	32.18	-0.26	1.19	0.97	0.03	22.60	-3.58	2.40	2.22	1.71	1.74	0.05
	IQR	0.59	1.55	0.23	0.20	0.03	6.64	5.24	0.89	0.75	2.22	0.62	0.10
Stage 2	Mean	32.37	0.57	1.51	1.14	0.10	21.13	-4.46	3.14	2.95	1.09	2.21	0.20
	SD	0.38	0.48	0.36	0.19	0.08	3.64	3.11	0.35	0.26	1.76	0.46	0.06
	Median	32.45	0.55	1.46	1.13	0.10	21.47	-4.24	3.09	2.96	0.00	2.07	0.21
	IQR	0.38	0.31	0.63	0.32	0.14	4.51	4.13	0.22	0.39	1.83	0.45	0.07
Stage 3	Mean	26.24	-5.74	4.11	3.25	0.38	13.09	-12.86	7.01	2.92	2.93	2.64	0.50
	SD	5.31	5.23	5.59	2.21	0.31	8.63	8.66	3.99	1.47	3.66	0.73	0.36
	Median	27.29	-4.94	1.14	3.33	0.47	11.69	-14.49	8.53	2.60	1.76	2.44	0.61
	IQR	5.24	5.19	4.97	2.21	0.30	8.55	8.55	3.76	1.44	3.52	0.71	0.35
Stage 4	Mean	21.04	-10.72	8.14	4.09	0.53	9.22	-16.15	6.12	2.34	4.63	2.96	0.50
	SD	8.26	8.27	3.43	1.78	0.17	6.16	5.76	1.97	1.34	2.37	0.51	0.16
	Median	23.02	-8.62	8.14	4.17	0.52	7.82	-17.73	5.96	1.90	4.09	2.92	0.57
	IQR	5.73	6.12	4.43	2.75	0.27	6.87	6.23	3.49	1.24	3.17	0.71	0.24

Table 7-1. Summary table of global indices as a function of stage of severity of AMD

A summary of global indices as a function of stage is shown in Table 7-1. The use of boxplot representations of the data in this chapter is discussed in more detail in Appendix 3.

7.3.2 Change in Visual Field Parameters with Stage: MD

The distribution of MD values for normal subjects and for patients at each stage of severity of AMD is shown in Figure 7-1, for standard perimetry and SWAP. The standard perimetry median MD and PSD was 0.39dB (IQR 1.45) and 1.20dB (IQR 0.16) for patients at stage 0; and -8.62dB (IQR 6.12) and 8.14dB (IQR 4.43) for patients at stage 4. The SWAP median MD and PSD was -3.52dB (IQR 5.00) and 2.14dB (IQR 0.38) for patients at stage 0; and -17.73dB (IQR 6.23) and 5.96dB (IQR 3.49) for patients at stage 4. A significant decline in MD with increasing severity of stage was evident for both standard perimetry (Kruskal-Wallis test: Chi-square = 25.993, $p < 0.001$) and SWAP (Kruskal-Wallis test: Chi-square = 20.156, $p < 0.001$). Post hoc analysis (Mann-Whitney U test) did not reveal significant differences between normal subjects and AMD patients until disease stage 3 for standard perimetry and SWAP ($p = 0.006$, $p = 0.021$, respectively). For standard perimetry, the MD at stages 3 and 4 was significantly statistically different (Mann-Whitney U test) from stage 0 ($p = 0.009$, $p < 0.001$, respectively), stage 1 ($p = 0.024$, $p < 0.001$) and stage 2 ($p = 0.020$, $p = 0.001$). In SWAP, the MD at stage 4 was significantly different from stage 0 ($p < 0.001$), stage 1 ($p < 0.001$) and 2 ($p = 0.003$). All other post hoc comparisons were not significant.

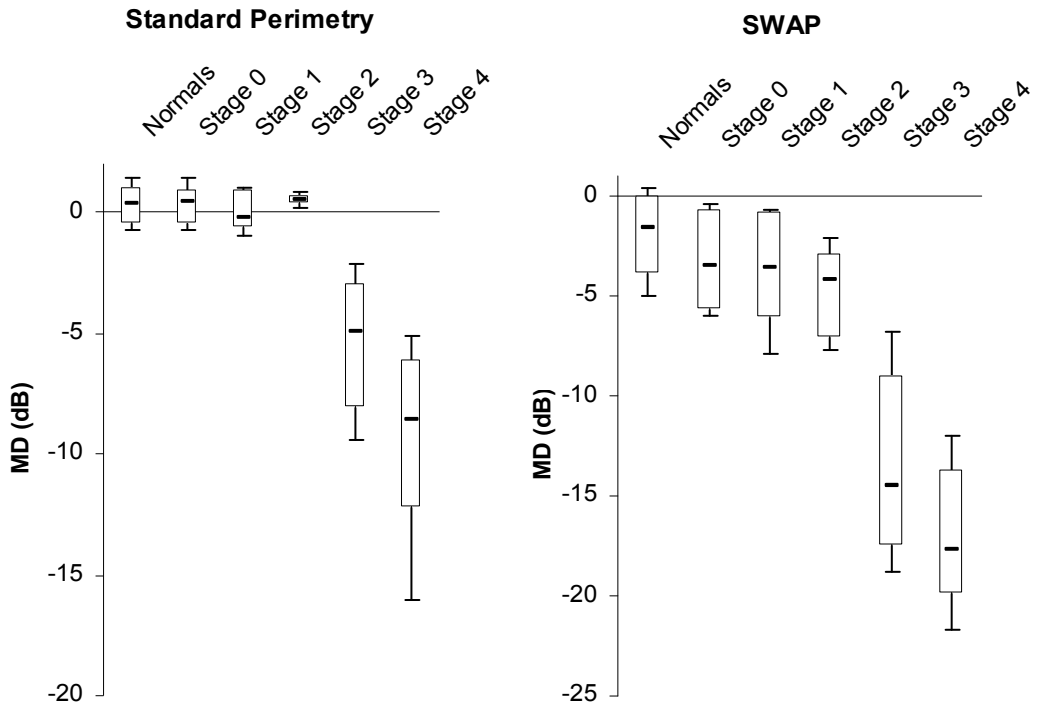

Figure 7-1. Boxplots representing the change in MD (dB) as a function of stage of severity of disease, for standard perimetry and SWAP
Boxplot limits represent the 15th, 25th, 50th, 75th and 85th percentiles.

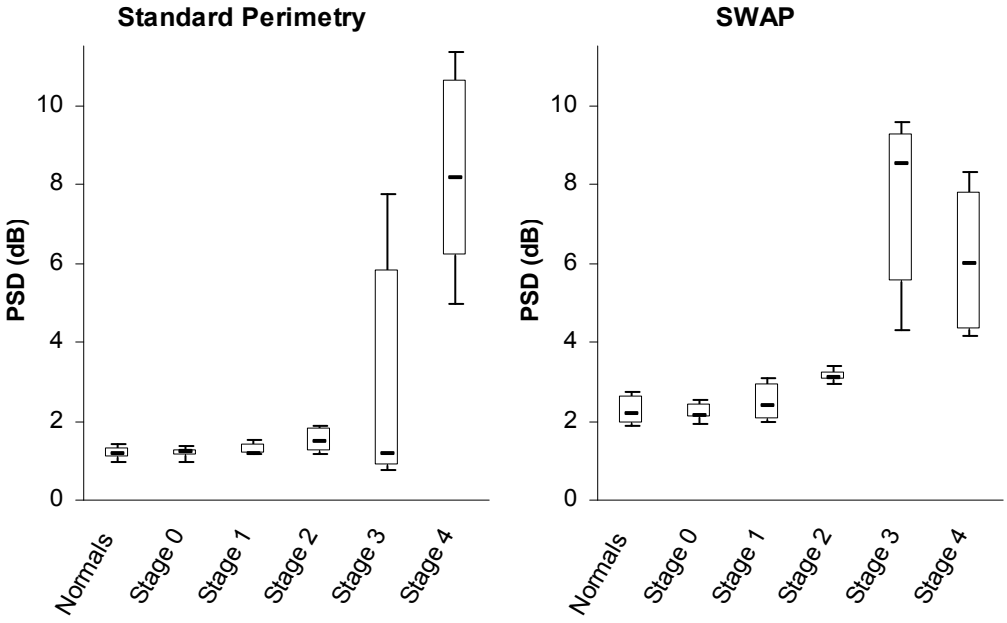

Figure 7-2. Boxplots representing change in PSD (dB) as a function of stage of AMD, for standard perimetry and SWAP
Boxplot limits represent the 15th, 25th, 50th, 75th and 85th percentiles.

Standard Perimetry

PSD	0	1	2	3	4	Stage
	0.975	0.267	0.048	0.834	<0.001	Normal
		0.388	0.101	0.828	<0.001	0
			0.145	0.533	<0.001	1
				0.606	0.001	2
					0.139	3

SWAP

PSD	0	1	2	3	4	Stage
	0.702	0.330	0.001	0.019	<0.001	Normal
		0.424	0.001	0.030	<0.001	0
			0.035	0.052	<0.001	1
				0.439	0.001	2
					0.484	3

Table 7-2. Post hoc analysis (Mann-Whitney U test) for differences in PSD values between stages.
Significant differences are shaded in grey.

7.3.3 Change in Visual Field Parameters with Stage: PSD and Other Indices

The distribution of PSD values for normal subjects and for patients at each stage of severity of AMD is shown in Figure 7-2, for standard perimetry and SWAP. Patients at stage 3 and 4 showed a greater spread of values of PSD than early stage patients and normal controls. The variation in PSD with change in severity of stage was statistically significant for both standard perimetry (Kruskal-Wallis test: Chi-square = 25.146, $p < 0.001$) and SWAP (Kruskal-Wallis test: Chi-square = 28.426, $p < 0.001$). Post hoc analysis (Mann-Whitney U test; Table 7-2) revealed significant differences between normal subjects and AMD patients at stage 2 ($p = 0.048$) and stage 4 ($p < 0.001$) for standard perimetry; and between normal subjects and AMD patients at stages 2, 3 and 4 for SWAP ($p = 0.001$, $p = 0.019$, $p < 0.001$, respectively). A greater number of post hoc differences were noted between stages in SWAP, than in standard perimetry (shaded areas in Table 7-2).

For global indices unique to SWAP in this study, SF did not vary significantly with stage of disease ($p = 0.355$) and in the patient groups, was not significantly different from the normal subjects. CPSD did vary significantly with stage of disease ($p = 0.003$).

7.3.4 Change in Visual Field Parameters with Stage: Local Spatial Variability (LSV)

The distribution of LSV values for normal subjects and for patients at each stage of severity of AMD is shown in Figure 7-3, for standard perimetry and SWAP. There was a smaller range of values for SWAP than for standard perimetry, across stages of severity of disease. Local Spatial Variability (LSV) which did not exhibit a Gaussian distribution varied significantly with stage of disease for standard perimetry (Kruskal-Wallis test: Chi-square = 24.644, $p < 0.001$) and SWAP (Chi-square = 21.538, $p < 0.001$). Post hoc analysis (Mann-Whitney U test; Table 7-3) did not reveal significant differences between normal subjects and AMD patients until stage 3 ($p = 0.045$) in standard perimetry, however in SWAP stage 0 patients exhibited a significantly higher LSV than normal subjects ($p = 0.046$). For both standard perimetry and SWAP, the LSV at stage 4 was significantly statistically different (Mann-Whitney U test) from stage 0 (both: $p < 0.001$), stage 1 (both: $p < 0.001$) and stage 2 ($p = 0.001$, $p = 0.016$, respectively). All other post hoc comparisons were not significant. Significant correlations were noted between LSV and PSD for standard perimetry (Spearman correlation coefficient: rho = 0.586, $p < 0.001$) and SWAP (Spearman correlation coefficient: rho = 0.754, $p < 0.001$).

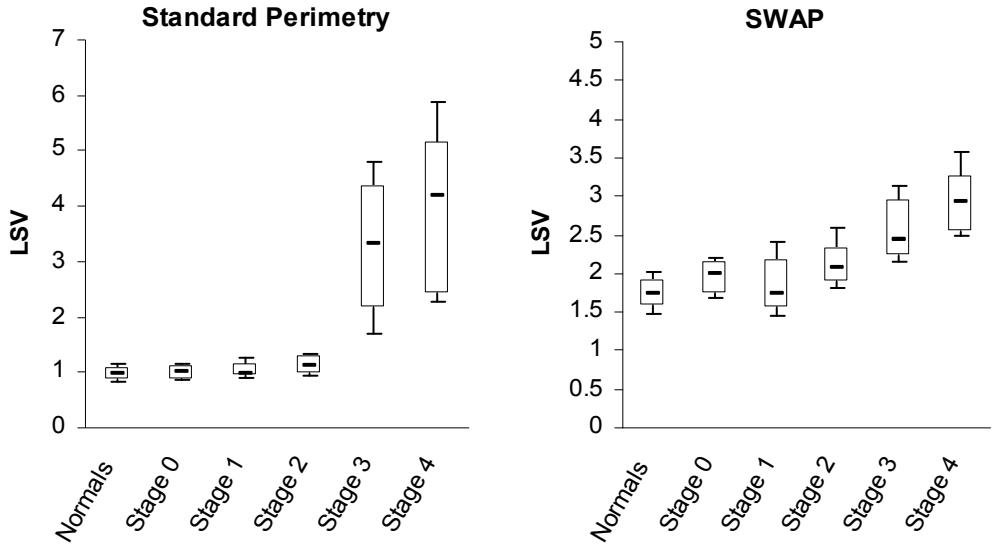

Figure 7-3. Local Spatial Variability (LSV) as a function of stage of AMD, for standard perimetry and SWAP.
Boxplot limits represent the 15th, 25th, 50th, 75th and 85th percentiles.

Standard Perimetry

LSV	0	1	2	3	4	Stage
	0.463	0.364	0.077	0.045	<0.001	Normal
		0.853	0.223	0.112	<0.001	0
			0.450	0.073	<0.001	1
				0.197	0.001	2
					0.470	3

SWAP

LSV	0	1	2	3	4	Stage
	0.046	0.670	0.009	0.015	<0.001	Normal
		0.389	0.399	0.083	<0.001	0
			0.132	0.073	<0.001	1
				0.302	0.016	2
					0.392	3

Table 7-3. Post hoc analysis (Mann-Whitney U test) for differences in LSV values between stages.
Significant differences are shaded in grey.

7.3.5 Change in Visual Field Parameters with Stage: Number of Defects

Stimulus locations were recorded as a defect if they occurred with a significance of less than 5% of the perimetric normal database. The distribution of the number of defects on total deviation (TD) and pattern deviation (PD) for normal subjects and for patients at each stage of severity of AMD is shown in Figure 7-4, for standard perimetry and SWAP. The number of TD and PD defects increased significantly with stage of disease for standard perimetry (Kruskal-Wallis test: Chi-square = 28.403, $p < 0.001$; Chi-square = 25.627, $p < 0.001$) and SWAP (Kruskal-Wallis test: Chi-square = 19.225, $p = 0.001$; Chi-square = 25.145, $p < 0.001$). Post hoc analysis (Mann-Whitney U test; Table 7-4) of TD defects exhibited significant differences from the normal controls at stage 1 in SWAP and stage 3 in standard perimetry. Similarly, the PD defects revealed significant differences between normal subjects and patients at stage 2 and worse for SWAP, whereas standard perimetry did not manifest significant differences from the normal controls until stage 4. TD values were more variable than PD values (Figure 7-4).

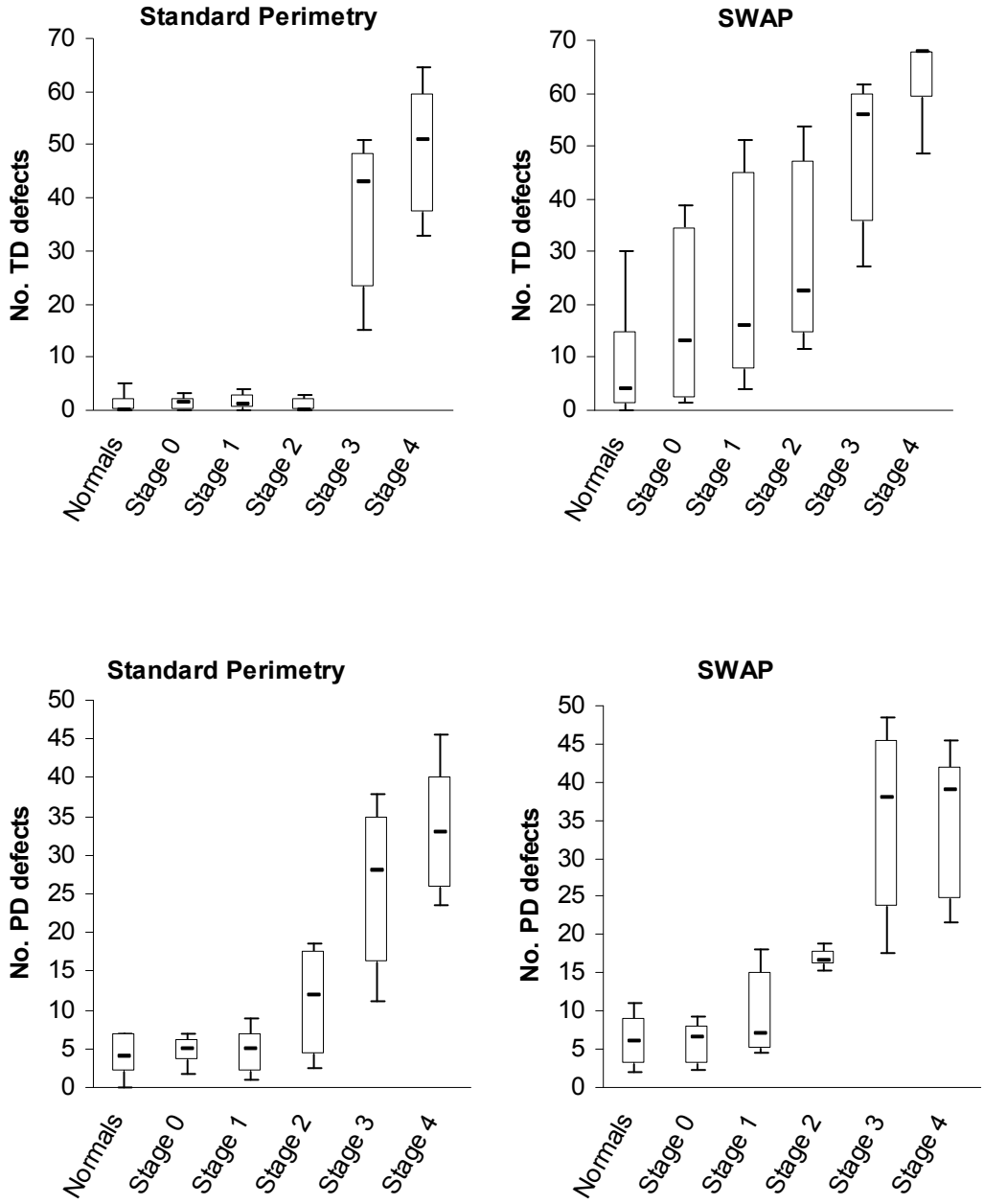

Figure 7-4. Boxplots representing change in number of PD and TD defects as a function of stage of AMD, for standard perimetry and SWAP
Boxplot limits represent the 15th, 25th, 50th, 75th and 85th percentiles.

Standard Perimetry

No. TD defects	0	1	2	3	4	Stage
	0.655	0.262	0.648	0.008	<0.001	Normal
		0.613	0.428	0.022	<0.001	0
			0.248	0.033	<0.001	1
				0.028	0.001	2
					0.392	3

No. PD defects	0	1	2	3	4	Stage
	0.600	0.380	0.063	0.052	<0.001	Normal
		0.664	0.132	0.146	<0.001	0
			0.287	0.136	<0.001	1
				0.197	0.001	2
					0.755	3

SWAP

No. TD defects	0	1	2	3	4	Stage
	0.227	0.044	0.037	0.028	<0.001	Normal
		0.423	0.373	0.070	<0.001	0
			0.650	0.186	0.002	1
				0.302	0.005	2
					0.134	3

No. PD defects	0	1	2	3	4	Stage
	0.806	0.075	<0.001	0.015	<0.001	Normal
		0.387	0.009	0.030	<0.001	0
			0.049	0.072	<0.001	1
				0.439	0.007	2
					0.815	3

Table 7-4. Post hoc analysis (Mann-Whitney U test) for differences in number of PD and TD defects between stages, for standard perimetry and SWAP.
Significant differences are shaded in grey.

7.3.6 Coefficient of Variation

The group mean pointwise threshold sensitivities and one standard deviation for standard perimetry and SWAP are shown in Figure 7-5 and Figure 7-6. All maps are displayed as a right eye. As expected, the AMD patient group yielded lower sensitivities and considerably greater standard deviations than the normal group for both types of perimetry. For both perimetry types, lower sensitivities occurred at the centre of the visual field in the patient group. In the normal group, the opposite was true, where lower sensitivities relative to the field occurred in the periphery. It is not

possible to make direct comparisons of sensitivity values between standard perimetry and SWAP, due to the difference between the decibel scales which are referenced to the maximum stimulus luminance of the perimeter. The dynamic range in standard perimetry is 0 to 10,000 apostilbs (5 log units) whereas in swap it is 0 to 65 apostilbs (1.5 log units). Therefore variability may be compared using the coefficient of variation statistic, which is calculated as the standard deviation divided by the mean and expressed as a percentage at each stimulus location. The coefficient of variation represents a normalised measure of dispersion such that distributions which differ in the magnitude of their measurement scales may be compared.

SWAP consistently revealed greater coefficients of variation across the entire visual field when compared to standard perimetry and the AMD patient group had higher values than the normal group (Figure 7-7 and Figure 7-8). In fact, the coefficient of variation values did not differ from the normal values in the early stages of AMD, however eyes at stage 3 and 4 exhibited large coefficients of variation (Table 7-5).

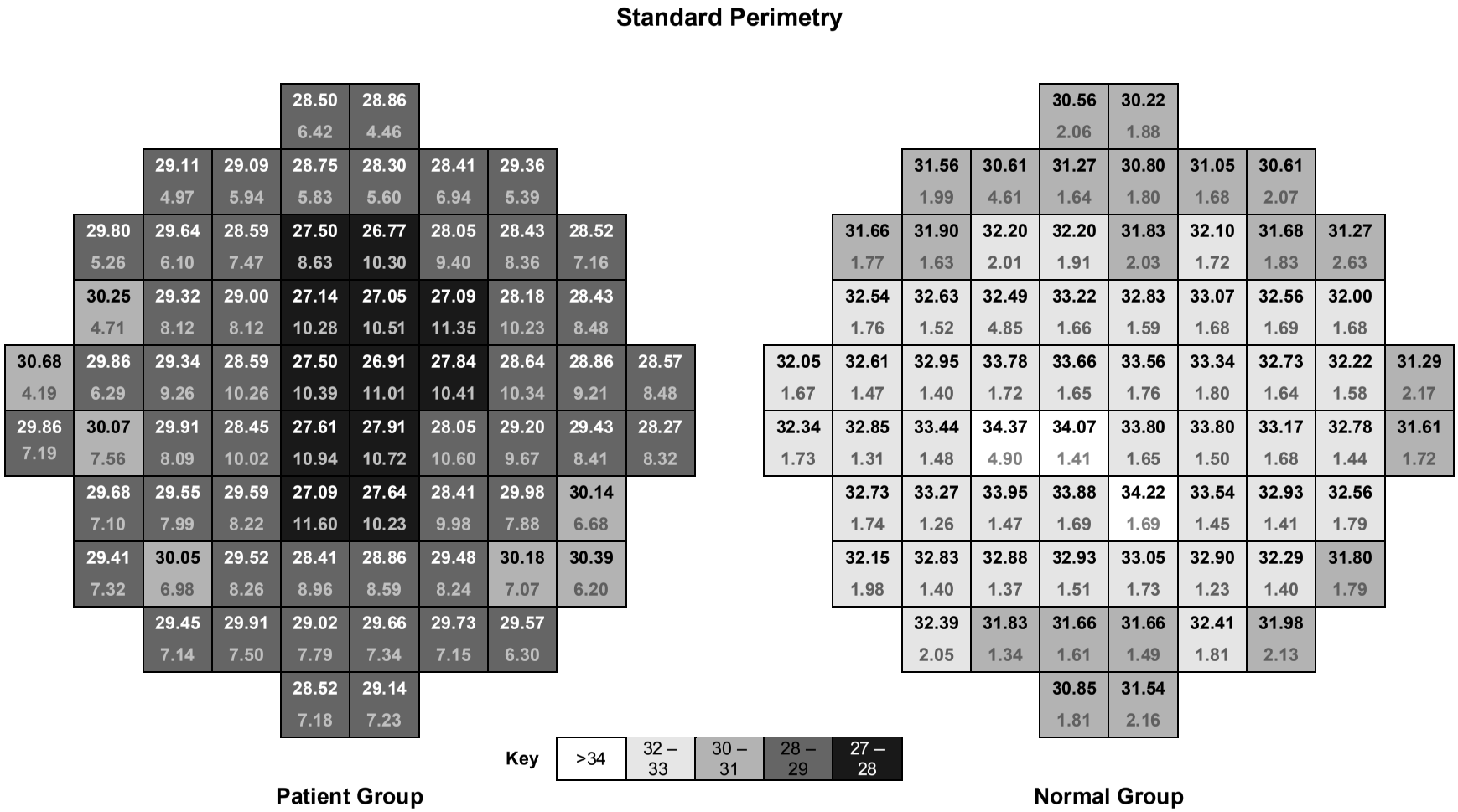

Figure 7-5. Maps of mean MS thresholds ± one standard deviation for standard perimetry

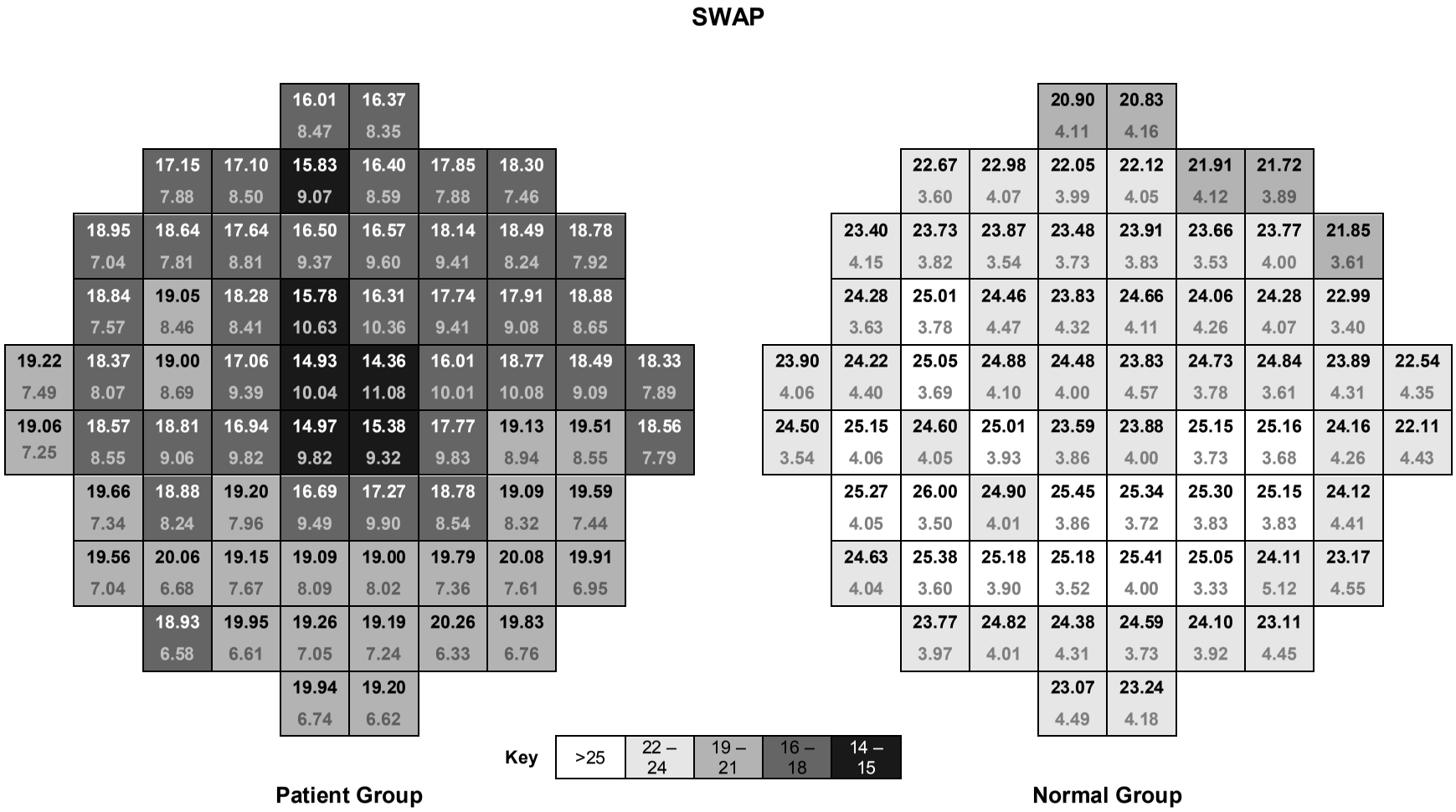

Figure 7-6. Maps of mean MS thresholds ± one standard deviation for SWAP

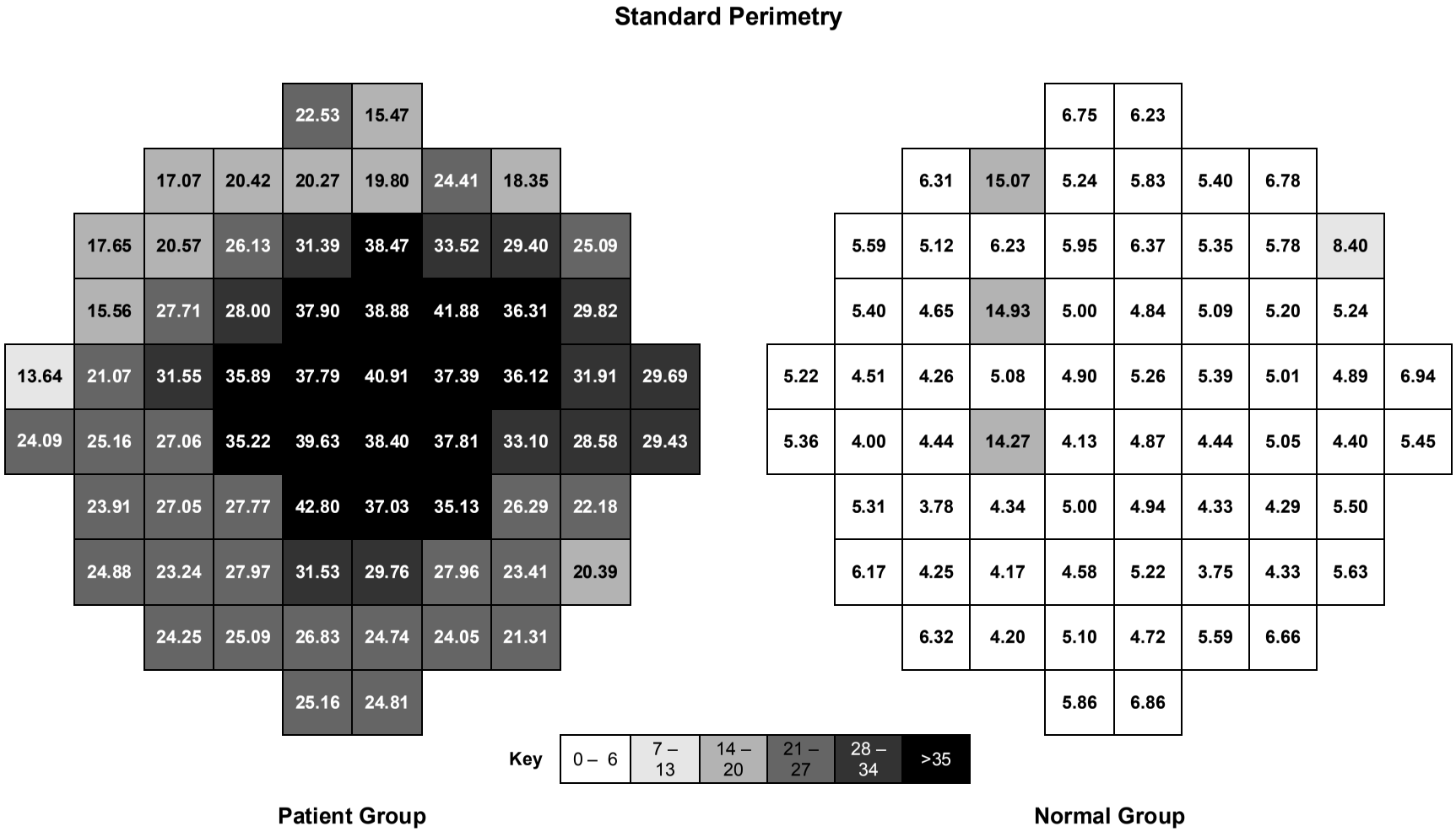

Figure 7-7. Coefficient of variation (%) map for standard perimetry

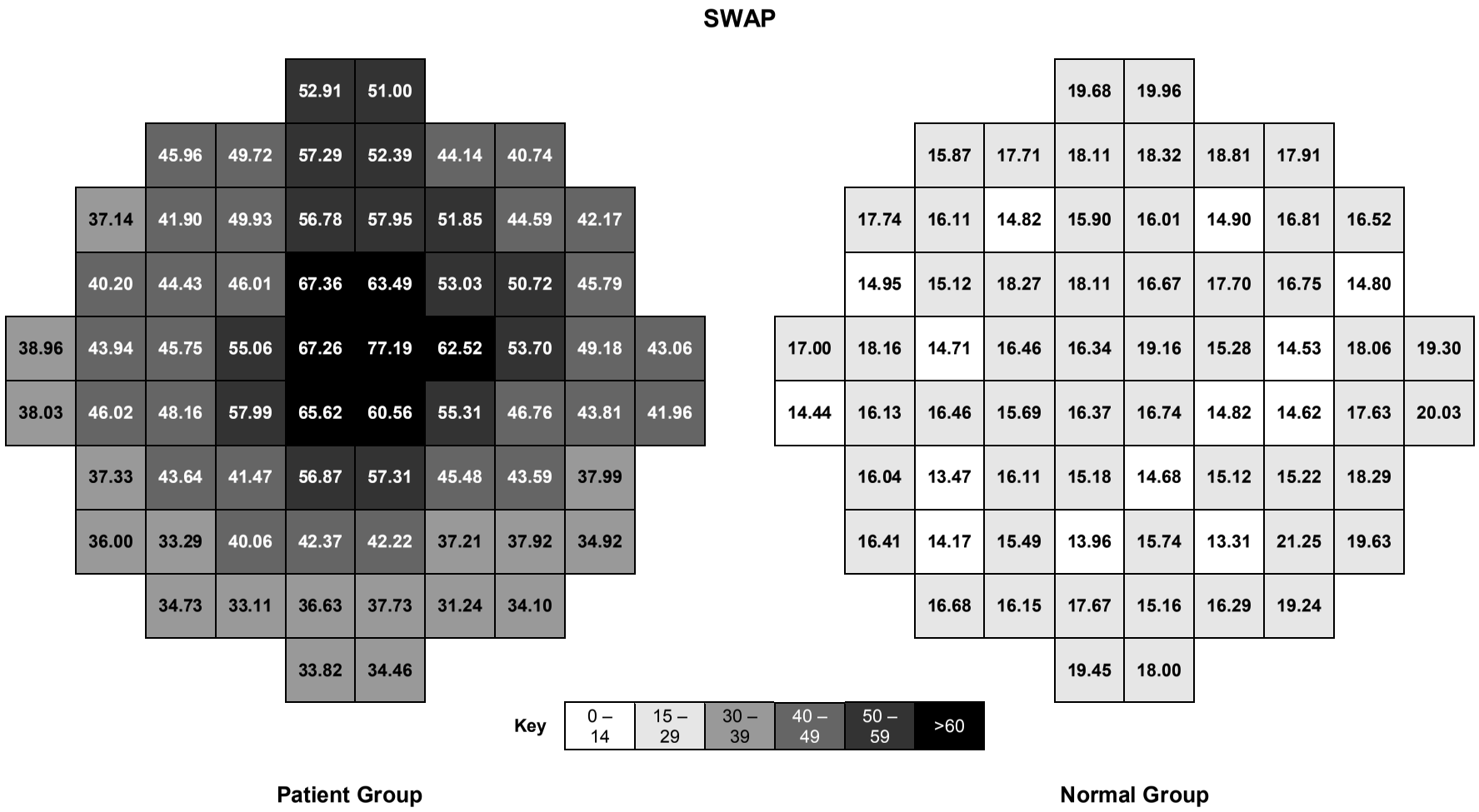

Figure 7-8. Coefficient of variation (%) map for SWAP

Stage	Standard	SWAP
Normal	5.67	16.65
0	4.55	14.34
1	5.47	22.23
2	4.57	21.42
3	27.08	105.69
4	56.52	115.47

Table 7-5. Group mean coefficient of variation (%) for patients at each stage of disease

7.3.7 Frequency of Defect

The frequency of defect maps representing the percentage of eyes at each stimulus location which have significant defects on TD and PD analysis for standard perimetry and SWAP as a function of stage of disease is shown in Figure 7-9 and Figure 7-10. The corresponding maps for normal subjects are shown in Figure 7-11. Defects were significant if thresholds occurred in less than 5% of the normal population. All maps are displayed as a right eye, where the left eye data was inflected to the right eye for analysis. Defects worsened with stage and SWAP defects tended to occur more frequently than defects in standard perimetry. An enlargement of a central scotoma was noted with progressing stage of disease. The appearance of the maps in the patient group at stage 0 did not significantly differ from the maps in the normal group. The increase in frequency of defects with worsening severity of disease appeared to occur at an earlier stage in SWAP than in standard perimetry.

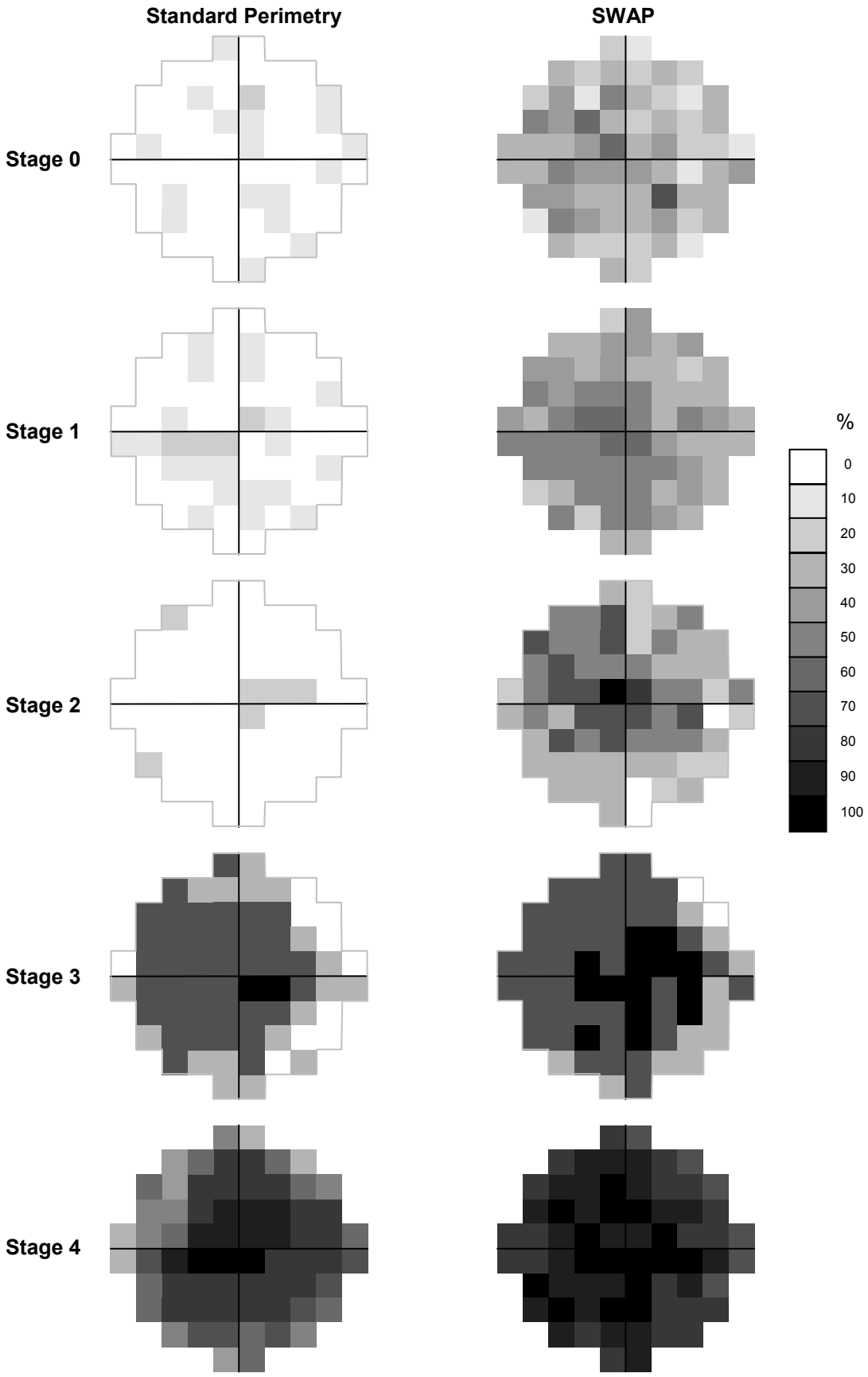

Figure 7-9. Frequency of defect maps, % of eyes at each stimulus location which have significant defects on TD analysis for standard perimetry and SWAP as a function of stage of disease

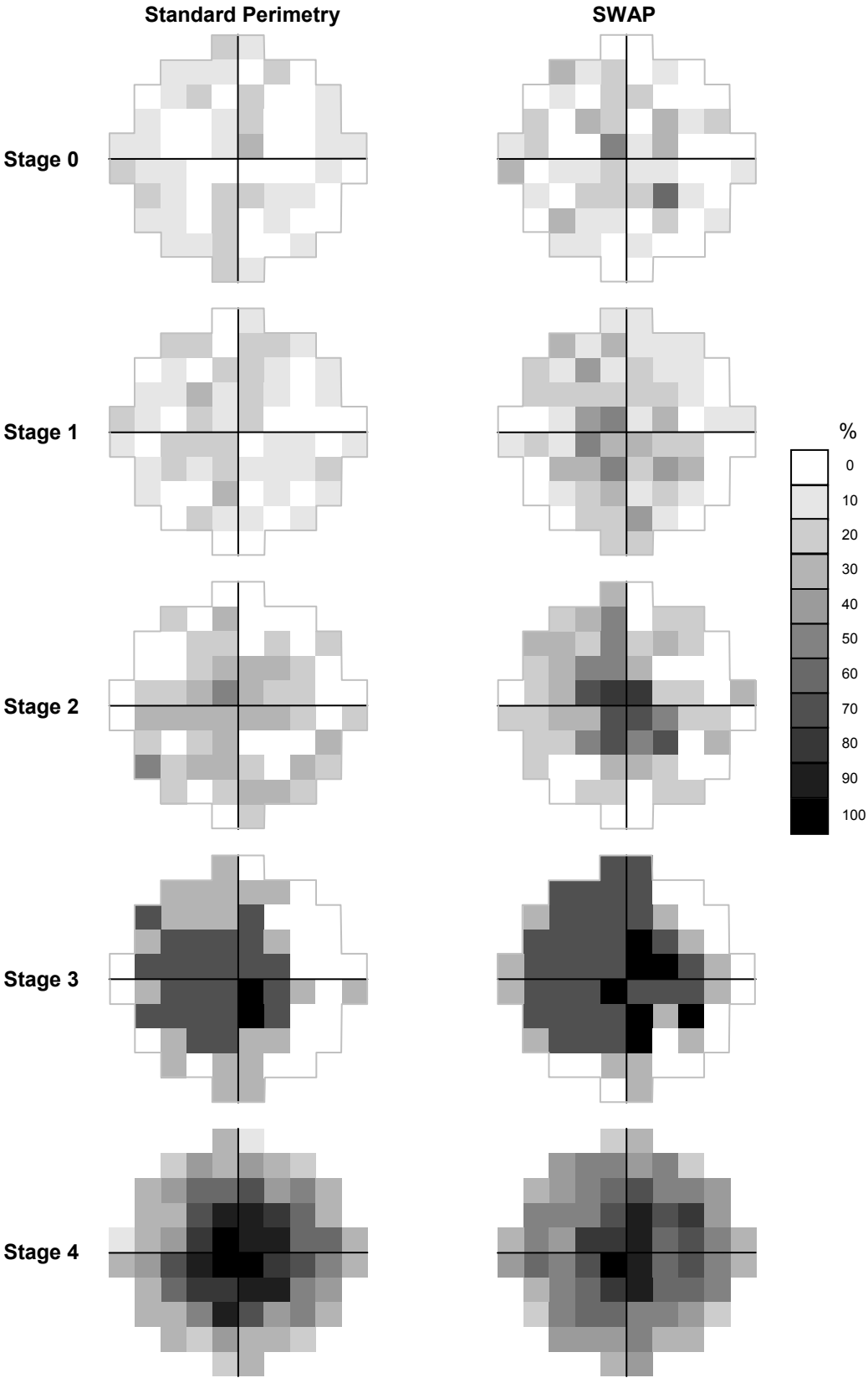

Figure 7-10. Frequency of defect maps, % of eyes at each stimulus location which have significant defects on PD analysis for standard perimetry and SWAP as a function of stage of disease

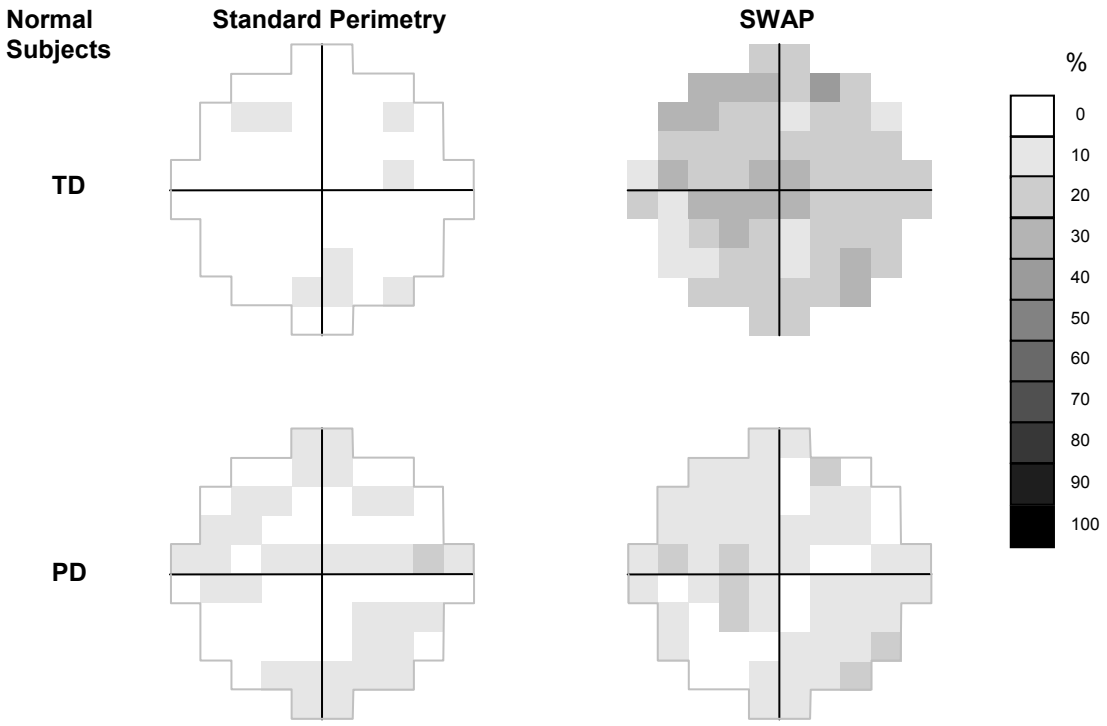

Figure 7-11. Frequency of defect maps, in normal subjects. % of eyes at each stimulus location which have significant defects on probability analyses for standard perimetry and SWAP

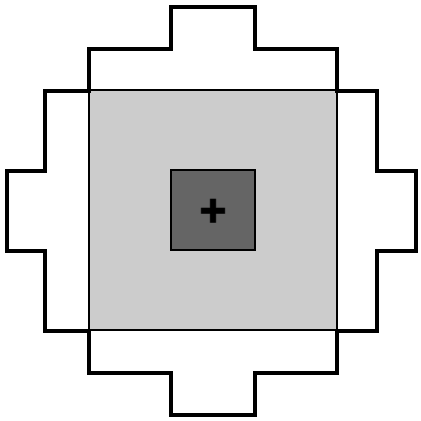

Figure 7-12. Sectorisation of the 10° field based on the frequency of PD defects. The centre and middle sectors are represented by dark and light grey shading, and the periphery is not shaded.

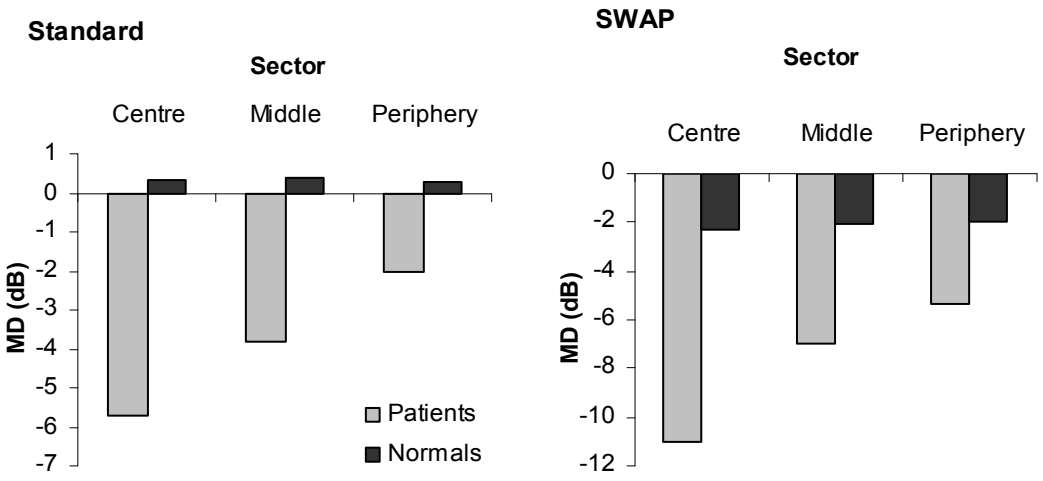

Figure 7-13. The group mean MD in each sector for standard perimetry and SWAP

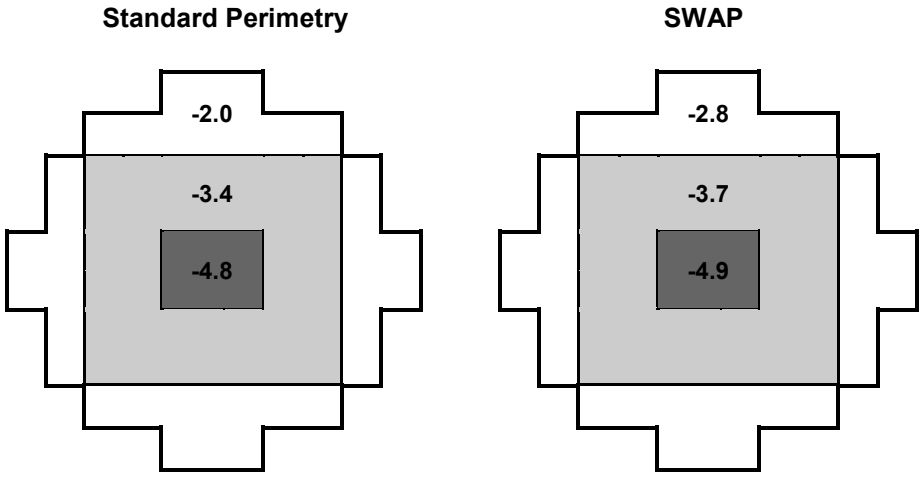

Figure 7-14. The slope of univariate linear regression of MD as a function of severity of AMD, in dB per stage, in each sector

7.3.8 Sector Analysis

The 10° field was divided into three sectors based on the frequency of PD defects, representing the centre, middle and periphery of the field (Figure 7-12). The PD frequency maps were used in preference to the TD maps as they are less affected by possible lens yellowing in SWAP. The unweighted MD values in each sector for standard perimetry and SWAP were calculated. In the patient group, it was found that the central sector contained the most severe MD values and the peripheral sector

contained the least severe values, for standard perimetry and SWAP (Figure 7-13). For the normal control group, the MD values remained stable across all sectors. The slope of change in MD with stage of AMD, for each sector with stage of AMD showed the most rapid sensitivity loss to occur in the central sector and the least rapid loss occurred in the periphery for both types of perimetry (Figure 7-14).

7.3.9 AMD Severity Index of Field Defect Score

The sector analysis was used to weight the sectors of the 10° field and is applicable for both standard perimetry and SWAP. Weights of 3, 2 and 1 were assigned to the centre, middle and periphery, respectively. The weight was multiplied by the assigned depth defect score according to the Pattern Deviation probability analysis of the field (where 0 = not significant, 1 = $p < 5\%$, 2 = $p < 2\%$, 3 = $p < 1\%$, 4 = $p < 0.5\%$). The sum of this for each stimulus location was divided by the maximum possible score to give the AMD severity index which ranged between 0 and 1, where 0 indicates no field loss and 1 indicates significant defects across the entire field.

Severity scores were not normally distributed and varied significantly with stage of disease for standard perimetry (Chi-square = 27.067, $p < 0.001$) and SWAP (Chi-square = 29.735, $p < 0.001$). Post hoc analysis (Mann-Whitney U test) revealed significant differences between normal subjects and AMD patients at stage 2 and worse in standard perimetry, whereas in SWAP stage 1 and worse patients exhibited a significantly higher scores than normal subjects.

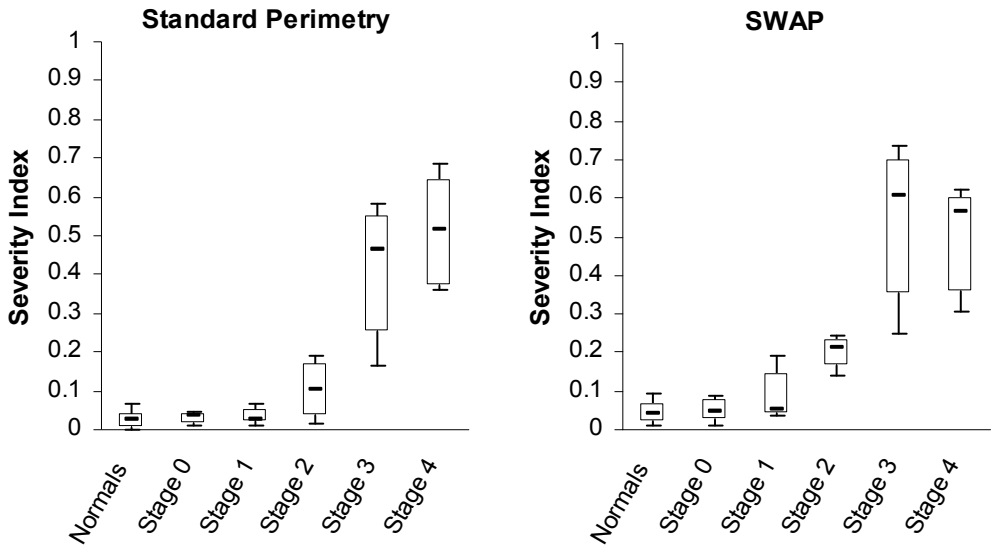

Figure 7-15. Boxplots representing the change in Severity Index as a function of stage of severity of disease, for standard perimetry and SWAP
Boxplot limits represent the 15th, 25th, 50th, 75th and 85th percentiles.

Standard Perimetry

Severity Index	0	1	2	3	4	Stage
	0.431	0.230	0.048	0.021	<0.001	Normal
		0.712	0.122	0.070	<0.001	0
			0.226	0.073	<0.001	1
				0.197	0.001	2
					0.564	3

SWAP

Severity Index	0	1	2	3	4	Stage
	0.924	0.031	<0.001	0.008	<0.001	Normal
		0.175	0.001	0.014	<0.001	0
			0.044	0.051	<0.001	1
				0.364	0.001	2
					0.697	3

Table 7-6. Post hoc analysis (Mann-Whitney U test) for differences in AMD Severity Index values between stages, for standard perimetry and SWAP.
Significant differences are shaded in grey.

7.4 Discussion

The findings presented indicate sensitivity loss in the central 10° standard and SWAP visual field with increased severity of AMD in a cross-sectional population. The reduced MS and greater standard deviation around the MS in the AMD patient group compared to the normal group is consistent with previous research (Cheng & Vingrys 1993; Midena et al. 1994, 1997; Remky et al. 2001b; Remky & Elsner 2005). MS values and coefficients of variation in the normal group are similar to those found previously for standard perimetry and SWAP in the 10° field and further agreement exists where sensitivity in the superior field is greater than in the inferior field (Conway 2003; Sample et al. 1997). It has been suggested that lower thresholds in the superior field were attributed to blinking, since stimuli positioned superiorly have a greater chance of being missed (Katz & Sommer 1986). The relationship between ganglion cell density and perimetric thresholds is equivocal. It was proposed that the asymmetry in SWAP thresholds can be explained by an asymmetry in ganglion cell density, predicted by measuring short-wavelength sensitive resolution acuity, using sinusoidal gratings (Demirel & Robinson 2003). In contrast, grating resolution thresholds bear a stronger relationship to ganglion cell density than perimetric thresholds (Beirne et al. 2005).

The visual field in the AMD patient groups was examined for departure from the empirical normal visual field, with attention to delineation of the early AMD visual field from the normal field. SWAP had greater capability in the detection of early stage AMD compared to standard perimetry, since more significant differences between early stage AMD patients and normal subjects were found for SWAP than for standard visual field parameters. Past studies in diabetic patients have reported the advantage of SWAP over standard perimetry in evaluating change in the 10° field (Agardh et al. 2006; Bengtsson et al. 2005; Hudson et al. 1998; Remky et al. 2000). Of the SWAP visual field indices measured in the present study, the LSV and the AMD severity index were the most sensitive to the detection of differences between normal and early stage

AMD subjects. The LSV index has the additional advantage that it is not influenced by the effects of pre-receptoral absorption. The MD was the least sensitive parameter and did not detect a significant difference between the normal and patient groups until stage 3. The implications of these findings on the pattern of SWAP visual field loss in AMD are firstly a focal component to visual field loss at early stages, and a subsequent diffuse loss affecting the field at the later disease stages 3 and 4. This pattern of loss is further illustrated by changes in the PSD and MD between stages 3 and 4, although not significant, there was a slight decline in the PSD, whilst the MD continued to increase (Figure 7-1 and Figure 7-2). In standard perimetry, the visual field parameters with the greatest sensitivity to detection of early stage AMD from normal were the PSD and the severity index, which did not detect a significant difference from normal, in the patient group, until stage 2. The pattern of standard visual field loss demonstrated minimal change in the early stages of AMD, followed by large changes at stages 3 and 4.

Unlike PSD, the LSV is not a commonly used index of focal loss, however it is statistically less manipulated, and hence offers the advantage over PSD of greater accuracy in reflecting the raw threshold measures. SWAP is limited by pre-receptoral absorption, whereby the stimulus may be absorbed by macular pigment and lenticular changes (see Chapter 1.2.1). The amount of lenticular absorption was limited in this study by the exclusion criteria, however it is possible that a significant amount of absorption remained thus influencing the measures of diffuse loss, the MD and TD. If this was the case, the measures of focal loss, the PSD and the PD, whose calculation involves the MD and TD respectively, could be affected by absorption. LSV was significantly correlated with PSD and therefore may represent a more accurate index of focal loss than PSD in SWAP. Any significant attenuation of SWAP thresholds by the presence of macular pigment was not evident from inspection of the defect maps in the

normal control group (Figure 7-11). The presence of any defects in the normal group was uniform across the entire field rather than confined to the central stimulus locations.

A central scotoma within an eccentricity of 5°, was demonstrated in late stage AMD, in the present study. Past studies have described varying patterns of visual field loss in AMD. Supportive of the present results, significantly lower short-wavelength sensitivity in the centre of the 10° field compared to the periphery was measured with a SLO, in patients with drusen and pigmentary changes (Remky & Elsner 2005). However, another study involving SLO perimetry noted both central and parafoveal scotomata, when presenting monochromatic stimuli to eyes with subfoveal CNV (Fujii et al. 2003). Some studies have indicated paracentral scotoma and preservation of central vision in AMD patients using achromatic perimetry (Hart et al. 1983; Swann & Lovie-Kitchin 1991). Others have noted no difference in sensitivity between the central 5° and periphery of the 10° SWAP field (Remky et al. 2001b). The general lack of agreement between studies appears to originate in differences in methodology. Differences in instrumentation, sample sizes, classifications of the features of AMD and definitions of visual field loss could account for the varied results.

In the present study, the most vulnerable region of the 10° field to sensitivity loss with increasing stage of AMD was the central 1°, in which the sensitivity decline was -4.8dB per stage in standard perimetry and -4.9dB per stage in SWAP. Analysis of the frequency in which defects occurred at each stimulus location led to the assumption of a symmetrical defect, upon which the severity index was based. The severity index may offer a useful method for monitoring progression of the visual field in AMD, as visual field loss is classified on a continuous scale. From the sample used in this study, visual fields with a severity index above 0.1 would be considered abnormal, however this value and the scale would need to be developed further by quantification of the field loss in a larger population study.

The staging system for AMD, used in this study, describes the severity of the disease according to epidemiological progression rates of morphological features of AMD (van Leeuwen et al. 2003b). Short-wavelength-sensitive resolution acuity was previously measured in patients assigned to the same staging system and it was found that the functional loss did not correlate well with the stages of severity of disease, due to significant overlap of short-wavelength-sensitive acuity between stages (Beirne et al. 2006). In the present study, despite none of the visual field parameters significantly discerning between all stages, some parameters did significantly differentiate between the majority of stages. A greater number of significant differences between stages were found for SWAP than for standard perimetry. In fact, for SWAP, the index of focal loss, PSD, showed the least functional overlap between stages, whilst the MD, indicating diffuse loss, showed relatively more overlap between stages. This finding suggests SWAP as a more sensitive method of detecting focal loss in the early stages of AMD, in patients with minimal lenticular opacities. Indeed, Bengtsson et al. (2005) observed that detection of focal loss by the number of defects on pattern deviation maps in SWAP, had a stronger relationship with diabetic retinopathy than standard perimetry. The statistical analysis involving the stages of severity of disease is limited by the ordinal nature of the staging system. Chapter 8 describes the interaction between visual field parameters and drusen area, which is measured on a continuous scale and is independent of the grading system.

All visual field parameters showed significant variation with increasing stage of disease, with the exception of the SWAP SF, whose value of 2-3dB is consistent with previous estimates (Conway 2003). Further agreement in existing research was indicated by the finding of no significant difference in the SF between patients with drusen and normal subjects, in the standard 10° visual field (Midena et al. 1994). This implies a measurement error in the patient group which was not significantly different normal, and supports the reliability of the data in the determination of progression. However,

the ten points of double threshold determination, which produce the SF index, are positioned in the mid-periphery and periphery of the 10° field (Figure 1-2). Pointwise analysis of these stimulus locations showed them to be less vulnerable to sensitivity loss than the central field. Further investigation into the positioning of the points of double determination in the calculation of SF in the 10° field is required. There was an inconsistency in the PSD results, where the difference from the normal controls was significant for stage 2 eyes but not for stage 3 eyes in the standard field (Table 7-2). This may be erroneous and explained by the small number of eyes in the stage 3 group (n = 3) failing to achieve statistical significance.

Larger coefficients of variation were found in SWAP visual fields than in standard perimetry, which is supported by earlier studies (Conway 2003; Wild et al. 1998). The patient group as a whole displayed very large coefficient of variation values (Figure 7-7 and Figure 7-8), however this was skewed by the large values at stages 3 and 4 (Table 7-5). It is to be expected that the variability is extreme in cases where sensitivities fluctuate between areas of absolute and relative scotomata within the same field, for some stage 4 eyes. Coefficients of variation in eyes at stage 0 to 2 were similar to the normal group in both perimetry types. The centre of the 10° field in the patient group displayed larger coefficients of variation than the periphery. The central areas corresponded to the areas of defect, as indicated by reduced MS values. Between-subject variability was therefore larger in areas of defect. In the normal group, the coefficient of variation was relatively uniform across the entire field, although the largest values tended to occur at the periphery of the field. This finding is concordant with previous evidence of between-subject variability in the visual field (Conway 2003; Cubbidge et al. 2002; Kwon et al. 1998; Wild et al. 1998) and the magnitude of the coefficients of variation in the normal group were similar to those obtained in previously (Conway 2003; Cubbidge et al. 2002).

The results present evidence of a relationship between the SWAP visual field and stage of AMD, whereby sensitivity declined with advancing stage of AMD. The relationship was weaker in standard perimetry. SWAP had greater capability in the detection of early stage AMD as well as in the delineation of focal loss between stages, compared to standard perimetry. The importance of early detection of functional change due to AMD leads to sooner identification of progression of disease, and possible earlier intervention or lifestyle changes. Early loss in AMD was focal in nature and the central field became less uniform and more variable as stage increased. SWAP defects occurred at similar locations but were deeper and wider than corresponding defects in standard perimetry. Overall the defects were confined to the central 5°. Although not all patients are capable of examination using SWAP, it remains a valuable tool in evaluation of the vision loss in the disease.

The cross-sectional design of the study limits the correlations which may be examined between structure and function. A longitudinal study is warranted, in order to follow the visual field progression of the same group of patients over several years to obtain the exact rate of functional change due to AMD. The severity index proposed in this study may be a useful index for this quantification, as well as correlation with other functional measures or risk factors of AMD.

8. Investigation of Structure to Function Relationships in AMD

Purpose: To relate structural change to functional change in age-related macular degeneration (AMD) in a cross-sectional population using fundus imaging and the visual field status.

Methods: Ten degree standard visual fields, SWAP visual fields and colour fundus photographs were acquired in 44 eyes of 27 patients with various stages of AMD. Retro-mode scanning laser ophthalmoscopic images were also captured in a subset of 29 eyes of 19 of the patients. A further subset of 9 patients performed visual fields at two further visits at three monthly intervals. Drusen area was correlated with visual field data. The position of visual field defects was compared to the position of drusen and deposits found with fundus photography and retro-mode imaging. The longitudinal change of the visual field over 6 months was compared to fundus photographs over the same period.

Results: The effect of AMD stage on drusen area within the 6000μm subfield was significant (One-way ANOVA: $F = 17.231$, $p < 0.001$), post hoc analysis revealed differences only between drusen areas at stage 0 and other stages. The standard mean deviation (MD) declined by 3.00dB for each log % drusen area and the SWAP MD declined by 3.92dB for each log % drusen area. The visual field parameters of focal loss displayed the strongest correlations with drusen area. The number of pattern deviation (PD) defects increased by 9.30 and 9.68 defects per log % drusen area for standard perimetry and SWAP, respectively. Medium strength significant linear relationships were found for all standard and SWAP visual field parameters with drusen area, except for the SWAP SF. 72.6% of standard PD defects and 65.2% of SWAP PD defects coincided with retinal signs of AMD on colour fundus images. 67.5% of standard PD defects and 69.7% of SWAP PD defects coincided with deposits on retro-mode images. Visual field indices did not change over the 6 month evaluation period. Perimetry exhibited a stronger relationship with drusen area than other measures of visual function.

Conclusions: The structure to function relationship between visual field parameters and drusen area was linear. A high coincidence proportion of visual field defects and retinal manifestations were observed. There was no structural change to the colour fundus images nor was there a functional change in the visual fields over 6 months. Therefore, a longer period is required to examine the longitudinal variability of the visual field in patients with AMD.

8.1 Introduction

Visual field loss in AMD has not previously been related to structural changes on the retina, in terms of the development of macular lesions. Categorisation of structural changes on the fundus in AMD, by standardised grading and staging systems and the relation to visual field change was examined in Chapter 7. The precise quantification of retinal change has been studied with increasingly sophisticated methods of fundus image analysis, such as the computerised automated measurement of drusen area from digital fundus photographs.

In image processing, segmentation is the isolation of features of interest, such as drusen, from the image. Thresholding is the process whereby features of interest are separated from their background using their pixel intensity. An example of a thresholding algorithm is the separation of object pixels which have a certain range of intensity values from background pixels which have intensity values outside of this range, which is usually calculated from intensity distributions within a local region of interest (Shin & Berger 1999).

Early methods of drusen segmentation of digitised colour slides involved adaptive thresholding, in which threshold selection was altered depending on the local properties in the image (Kirkpatrick et al. 1995; Peli & Lahav 1986). Following thresholding, non-drusen areas which had been erroneously selected, had to be manually deleted before measurements were made from binary conversions of the images (Peli & Lahav 1986). Kirkpatrick et al. (1995) pre-processed images to correct for variation in illumination and utilised a combination of both local and global thresholding. Pre-processing was developed by Shin et al. (1999) in their software to quantify drusen area. Green channel images underwent pre-processing to reduce noise, before drusen segmentation was carried out. Pixel intensities of local subfields of the region of interest were analysed and it was specified that if drusen were present, the skewness of the intensities was greater than -0.5. The user was then able to adjust

the sensitivity of the pixels identified as drusen, erase erroneously segmented drusen or add pixels. Close agreement was found between the drusen segmentation software and manual grading by an expert observer. The flaw in this method occurred when a large drusen dominated a local region, such that the distribution would not be skewed, and this would have to be manually corrected after segmentation.

Segmentation techniques were developed with the aim of becoming fully automated with the histogram-based adaptive local thresholding (HALT) operator, which extracted useful information from an image without being affected by the presence of other structures (Rapantzikos et al. 2003). Similar to the method employed by Shin et al. (1999), local histogram distributions of the green channel image were analysed. In addition, contrast was enhanced taking into account global and local variations using equalisation of the histograms. Equalisation (or EQ) is the process of using digital algorithms to alter or flatten the frequency response characteristics of a system. This was done in order to accurately segment the drusen which appear to be hidden in their surrounding background. This method however did not account for the inherent background variability of the retina.

In a normal fundus, the macular reflectance increases from the centre to the periphery, partly due to luteal pigment at the fovea (Bone et al. 1992; Snodderly et al. 1984). The normal fundus background reflectance was found to have a geometric pattern of concentric elliptical patterns in which the reflectance increased radially from the macular centre. Based on these patterns, a method which levelled the background of images containing drusen was developed, which was independent of the reflectivity of the overlying drusen (Smith et al. 2003). The intensity of user-defined regions of the green channel image was raised so that the background became more uniform and drusen were brightened, before user selection of threshold for drusen segmentation, thereby providing a semi-automated digital technique for global drusen quantification.

This method was found to have good correlation with standard fundus grading (Smith et al. 2003) and good inter-institutional reproducibility (Sivagnanaval et al. 2005).

Continuation by the same group replaced the interactive process with a mathematical model, the “dots” method, which automatically reconstructed and levelled the macular background (Smith et al. 2005a). In the “dots” method, a partial correction for luteal pigment was made to the green channel image, containing drusen. Then a user selection of squares representing normal macular background was used to produce a geometric model of the background. The model was displayed as an elliptical contour map of grey scale intensity levels and subtracted from the luteal corrected fundus image, which levelled the background and brightened drusen. After global segmentation, drusen area was expressed as a percentage of the grading grid subfield. This method yielded good inter-observer reproducibility (Smith et al. 2005a).

A fully automated drusen segmentation program was subsequently described by Smith et al. (2005b). An automatic histogram-based thresholding technique was applied to the corrected green channel image and combined with the model for the macular background generating a completely automated measurement of drusen area. Sensitivity and specificity of the segmentation was high when compared to manually applied expert grading by stereo-viewing and drusen tracing using a graphics tablet (Smith et al. 2005b).

The aims of this study were to relate visual field changes to the automated quantification of drusen area. Secondary aims were to examine the longitudinal variation of the functional and structural measures over a six month period in a pilot study.

8.2 Methods

8.2.1 Visual Fields and Images

Visual fields and retinal images were collected in a previous study (see Chapter 7). Briefly, the central 10° field was measured using Program 10-2 on the Humphrey Field

Analyser 750 using standard perimetry and SWAP, in a group of patients with AMD who had undergone a training set of visual fields one week earlier. Fundus photography and retro-mode images using the Nidek F-10 were acquired in the same group of patients. Pupils were dilated with one drop of tropicamide 0.5% for all images captured. The colour fundus photographs were captured at the same visit as the visual fields or one week earlier, the retro-mode images were taken 5-6 months later.

Digital colour fundus photographs and perimetric data from 44 eyes of 27 patients with AMD were initially investigated. Six eyes were excluded on the basis of treatment for AMD, 3 eyes were excluded due to the presence of other pathology and one eye was excluded due to pseudophakia. Retro-mode images were obtained in a subset of 29 eyes of 19 patients. Recall of all patients for retro-mode imaging was not possible due to limited instrument availability and eyes were excluded for the same reasons outlined above.

A subset of 9 patients volunteered to attend a further part of the study. Longitudinal visual field testing was performed at 3 months and 6 months. Data from patients who did not complete all four visits was discarded, such that the visual field and image data from 13 eyes of 9 patients was analysed for longitudinal change.

8.2.2 Other Functional Measures

Distance visual acuity was determined using a Bailey-Lovie Test Chart. Contrast sensitivity was measured using a Pelli-Robson Chart. Colour vision testing was performed using the Farnsworth-Munsell 100 Hue colour vision test and the total error score was noted. Reading speed was assessed with the MNRead test, in which the fastest reading speed at the critical print size was recorded in words per minute.

8.2.3 Drusen Segmentation

A version of the drusen segmentation program, RIALAB, which runs in MATLAB (version 7.8.0.347, Mathworks, Natick, Massachusetts, USA) was acquired. The

software was developed in the Heffner Biomedical Imaging Lab by Noah Lee, in collaboration with R. Theodore Smith at Columbia University, New York City, USA.

Digital colour fundus images were imported to RIALAB as high quality JPEG files, which was the maximum allowable quality of the camera. The positions of the macula and temporal optic disc margin were manually marked using a mouse. The images were then resized to 324 x 324 pixels which the program scaled as 6000μm, and centred at the fovea. The images were converted to bitmaps at this point and background levelling in the green channel took place. Drusen segmentation performed best when the user selected a region of interest, using a "paint" feature, which allowed exclusion of areas of peripapillary atrophy or other bright non-drusen areas. The automated image analysis identified the outlines of drusen and segmentation output was drusen area in pixels and as a percentage of the three subfields. It was not possible to use this program on the retro-mode images since the segmentation algorithm was not suitable for the edges of the lesions in the retro-mode images.

The custom written program Perimetric Fundus Map (see Chapter 5) was used to analyse the retinal position of perimetric stimulus locations for the colour fundus photographs. Some retro-mode images had more indistinct disc margins and maculae compared to their colour fundus image counterparts. Due to the critical nature of the exact positioning of the perimetric stimulus points onto the fundus images and in order to gain the greatest positioning accuracy possible, the retro-mode images were not manipulated with the Perimetric Fundus Map program. Instead, the retro-mode images were matched to the colour perimetric fundus map using commercially available software (Photoshop 8.0; Adobe Systems Inc, San Jose, Calif) such that the retinal landmarks were precisely aligned using the flicker on/off and transparency features. In this way, the perimetric points were visible on the retro-mode images and it was possible to count the coincidence of deposits on the retro-mode images with perimetric defects.

8.3 Analysis

The output of the segmentation program was drusen area within the three standard grading subfields centred at the macula, of diameter 1000, 3000 and 6000μm. The effect of stage on drusen area was examined. Correlations between visual field parameters and drusen area were calculated, as well as correlations between other functional measures and drusen area.

Perimetric colour fundus images were produced and the stimulus locations which coincided with retinal features of AMD were entered onto a spreadsheet. This was then compared to the spreadsheet of SWAP and standard visual field defects as defined by pattern and total deviation probability analyses, in order to find the number of defects coinciding with areas of damaged retina. The number of associated defects to retinal manifestations of disease was expressed as a percentage of total number of defects and also as a percentage of the total number of stimulus locations coinciding with retinal features of AMD.

Longitudinal stability of visual field indices was analysed using the Friedman test. Drusen area on colour fundus photographs was compared for change over time.

8.4 Results

8.4.1 Statistical Normality Evaluation

The drusen area values did not exhibit a normal distribution (Kolmogorov-Smirnov test). Logarithmic (base 10) transformation of drusen area within 6000μm achieved normality ($p = 0.200$) and the variance was homogeneous across stages of AMD (Levene's statistic = 1.263, $p = 0.312$). Thus, parametric analyses were applied to the data.

8.4.2 Effect of Stage on Drusen Area

The bar chart in Figure 8-1 shows the change in drusen area with stage of AMD, for drusen area within all three subfields of the standard grading grid. A similar function is evident for the drusen area within all three subfields, whereby the % area of drusen steadily increases until stage 3 and declines for eyes at stage 4. A statistically

significant (Table 8-1; One-way ANOVA: $F = 17.231$, $p < 0.001$) variation of drusen area (transformed log10) arose when comparing different stages of AMD. Post hoc analysis (Tukey HSD) revealed that the drusen areas of stages 1, 2, 3 and 4 were larger than at stage 0 ($p = 0.001$, $p = 0.001$, $p < 0.001$, $p < 0.001$, respectively), however drusen areas at pairs of stages between stages 1 to 4 were not significantly different from each other.

It was not possible to achieve a normal distribution by transformation of the drusen areas within the other subfields. Nevertheless, drusen area showed a significant variation with stage of AMD using the Kruskal-Wallis test, for drusen within the 3000µm (Chi-Square = 18.722, $p < 0.001$) and 1000µm (Chi-Square = 16.003, $p = 0.001$). Drusen area data from all three subfields therefore yielded corresponding results. Further analysis concentrated on drusen area within the 6000µm subfield since it accounted for the total grading area and encompassed the entire 10° visual field. Furthermore, the normally distributed variable made it possible to use parametric statistics thus yielding maximum power.

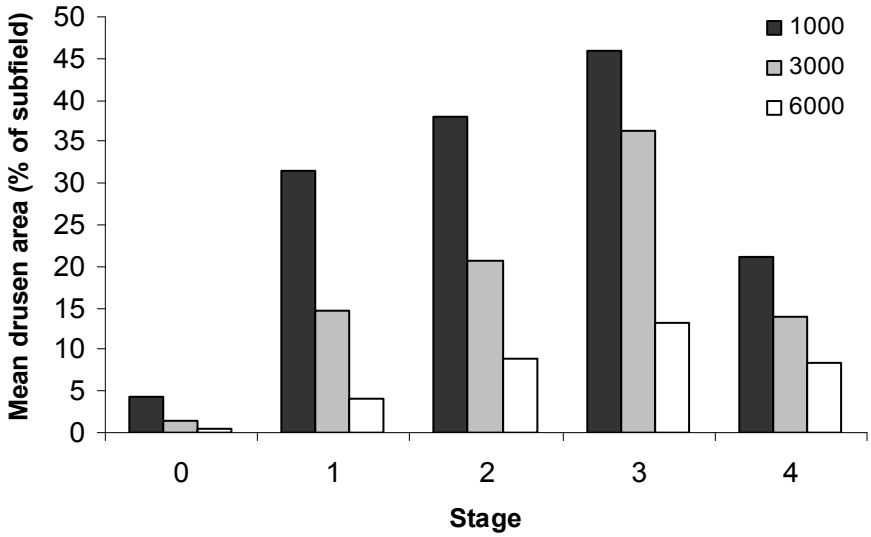

Figure 8-1. Mean drusen area (% area of subfields 6000, 3000 and 1000µm in diameter) as a function of stage of AMD

	Sum of Squares	df	Mean Square	F	p
Between Groups	14.906	4	3.726	17.231	<0.001
Within Groups	8.002	37	0.216		
Total	22.908	41			

Table 8-1. One-way ANOVA table of the effect of stage of AMD on drusen area within the central 6000µm

8.4.3 Correlations between Visual Field Parameters and Drusen Area

The correlation between each defect defining visual field parameter and drusen area, for each perimetry type is shown in Table 8-2. All correlations were found to be linear. The standard MD declined by 3.00dB for each % log drusen area and the SWAP MD declined by 3.92dB for each percentage log drusen area (Figure 8-2). The coefficient of determination, r^2, in this case indicates the proportion of variance in the visual field parameters attributable to drusen area and portrays the strength of the relationship. The correlations accounted for between 10 and 29% of the variance in the visual field parameters, except for the SWAP SF, which yielded a very weak negative correlation with drusen area and the relationship was not significantly linear.

		r	r^2	slope	F	p
Standard perimetry	MD	-0.439	0.193	-3.00	9.568	**0.004***
	PSD	0.429	0.184	2.18	9.047	**0.005***
SWAP	MD	-0.416	0.173	-3.92	8.353	**0.006***
	PSD	0.413	0.171	1.27	8.249	**0.006***
	SF	-0.091	0.008	-0.12	0.333	0.567
	CPSD	0.315	0.099	1.16	4.413	**0.042***
Standard perimetry	No. PD defects	0.492	0.242	9.30	12.759	**0.001***
	No. TD defects	0.468	0.219	14.09	11.243	**0.002***
	LSV	0.458	0.210	1.10	10.595	**0.002***
	Severity Score	0.497	0.247	0.16	13.142	**0.001***
SWAP	No. PD defects	0.496	0.246	9.68	13.025	**0.001***
	No. TD defects	0.355	0.126	11.50	5.785	**0.021***
	LSV	0.510	0.260	0.44	14.086	**0.001***
	Severity Score	0.537	0.288	0.17	16.208	**<0.001***

* significant linear relationship

Table 8-2. Correlation coefficients (r), coefficients of determination (r^2), slope and significance (p) of linear relationship between visual field parameters and log drusen area within 6000µm subfield

8.4.4 Correlations between Other Functional Measures and Drusen Area

In order to reflect clinical practice, visual acuity and contrast sensitivity were measured monocularly, whilst reading speed and colour vision were tested binocularly. Reading speed and colour vision measures were correlated with drusen area in the eye with the best functional results. The correlations of visual acuity and contrast sensitivity with drusen area were significantly linear, whereas reading speed and colour vision error score were not (Table 8-3). Coefficients of determination were overall weaker than those between visual field parameters and drusen area. Detailed results of the functional measures are given in Appendix 1.

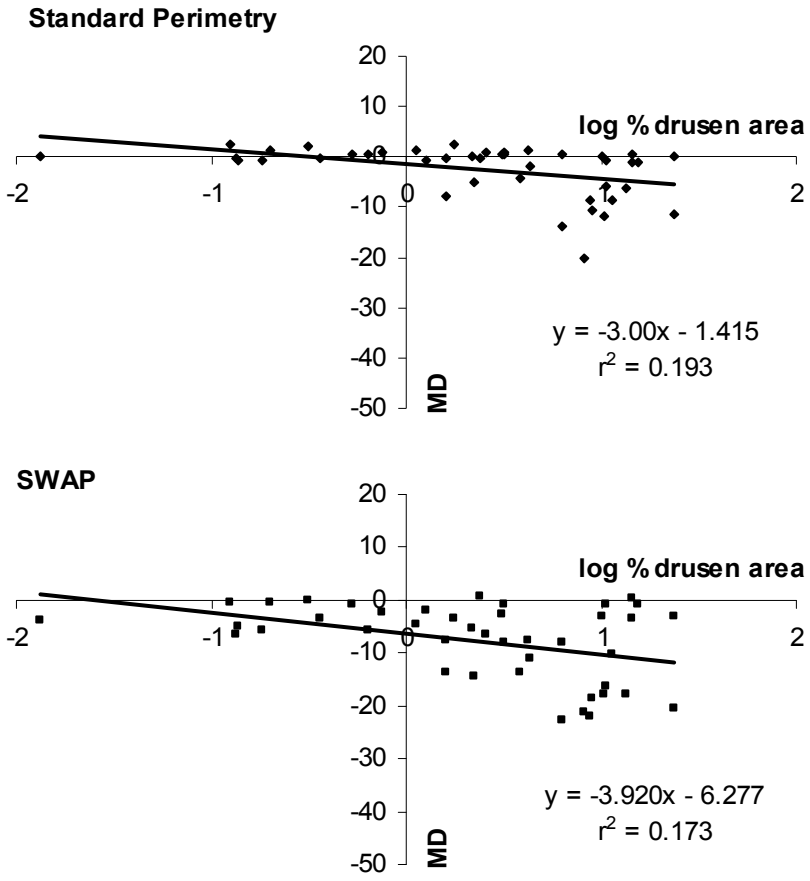

Figure 8-2. Graphs illustrating MD as a function of log % drusen area within 6000µm subfield, for standard perimetry and SWAP

	r	r^2	slope	F	p
LogMAR	0.386	0.149	0.166	6.821	**0.013***
CS	-0.362	0.131	-0.130	5.865	**0.020***
Reading Speed	-0.211	0.045	-14.257	1.030	0.321
100 Hue TES	0.386	0.149	47.080	4.031	0.057

* significant linear relationship

Table 8-3. Correlation coefficients (r), coefficients of determination (r^2), slope and significance (p) of linear relationships of visual acuity (LogMAR), contrast sensitivity (CS, log units), reading speed (words per minute) and colour vision total error score (TES) with log drusen area within 6000µm

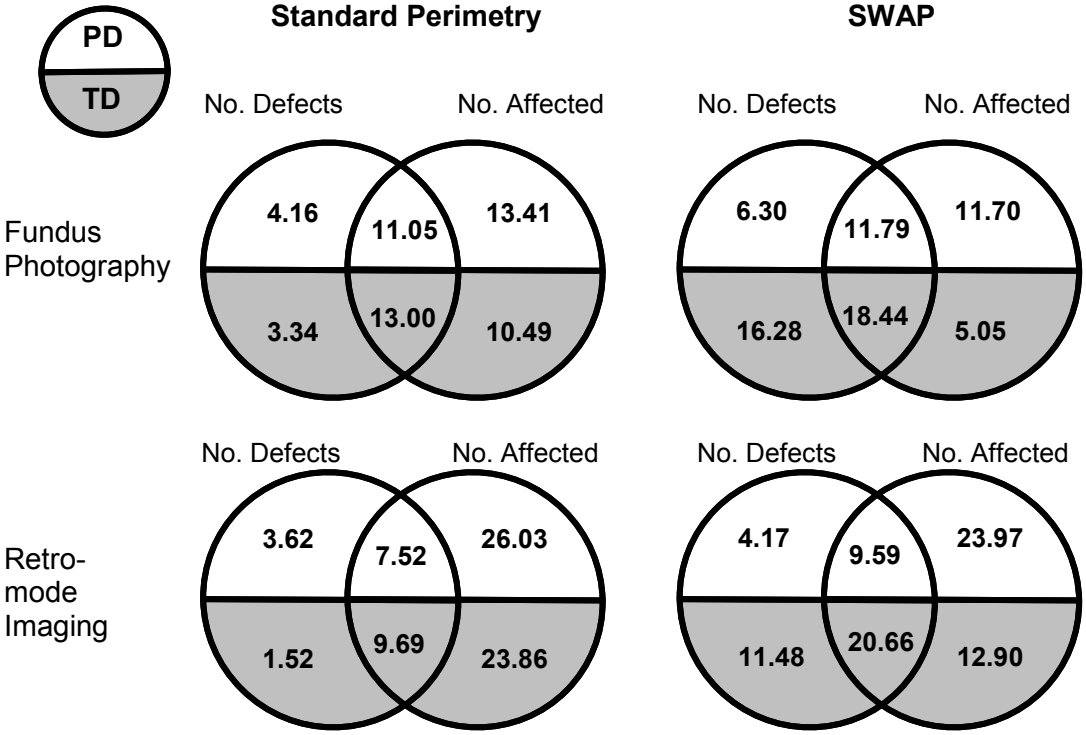

Figure 8-3. Venn diagrams depicting the group mean number of stimulus locations where visual field defects coincide with drusen or other features of AMD, for both imaging types

No. defects = total number of visual field defects. No. Affected = total number of stimulus locations which have the same position with features of AMD. The intersection represents the visual field defects which have the same position as features of AMD. Pattern deviation defects (unshaded top) and total deviation defects (shaded bottom) are represented for standard perimetry and SWAP.

	Colour fundus photos				F10 retro-mode images			
	Standard Perimetry		SWAP		Standard Perimetry		SWAP	
	PD	TD	PD	TD	PD	TD	PD	TD
% of total defects	72.6	79.6	65.2	53.1	67.5	86.4	69.7	64.3
% of total points overlying AMD features	45.2	55.3	50.2	78.5	22.4	28.9	28.6	61.6

Table 8-4. Number of total deviation (TD) and pattern deviation (PD) defects associated with retinal manifestations of AMD expressed as a percentage of total number of defects, and total number of stimulus locations associated with AMD features

8.4.5 Association of Visual Field Defects with Retinal Manifestations of AMD

The number of visual field defects overlying retinal features of AMD is shown in Figure 8-3 and Table 8-4, in relation to the total number of defects and in relation to the total number of stimulus locations in the visual field overlying retinal features of AMD. Overall, a proportionally greater number of total defects coincided with areas of damaged retina than the amount of points overlying damaged retina coincided with visual field defects. One exception to this was observed for the SWAP total deviation defects on colour fundus photography, where the reverse was true.

8.4.6 Longitudinal Stability of Visual Field Indices

For 13 eyes of the 9 patients followed over 6 months, each visual field index was tested for stability over time using the Friedman test. The results are shown in Table 8-5, where no significant variation over time was found for each index, therefore the visual fields showed no significant change over time.

	Standard Perimetry			SWAP				
	MS	MD	PSD	MS	MD	PSD	SF	CPSD
Chi-Square	0.154	0.615	0.462	0.510	0.154	2.923	0.154	0.000
p	0.926	0.735	0.794	0.775	0.926	0.232	0.926	1.000

Table 8-5. Friedman test for effect of time on visual field indices

8.4.7 Longitudinal Colour Fundus Image Analysis

In the same group of patients, drusen segmentation was performed on the first set of fundus photographs and on the final set of fundus photographs, approximately 6 months later. The Wilcoxon signed rank test demonstrated no significant difference in drusen area within the central 6000μm over a period of 6 months in 13 eyes ($Z = -0.734$, $p = 0.463$).

8.5 Discussion

A linear structure to function relationship exists between the automated quantification of drusen area from digital colour fundus photographs and standard and SWAP visual field parameters. The parameters which yielded strongest correlations to drusen area were the local spatial variability in SWAP, and the AMD severity index and number of pattern deviation defects for both standard perimetry and SWAP. These measures pertain to focal loss in the visual field, which corresponds to the findings in Chapter 7, where the global indices of focal loss were found to be the most sensitive to progression of loss in AMD. Overall the correlations between drusen area and the indices of focal loss, were stronger for SWAP than for standard perimetry. The AMD severity index accounts for pattern deviation defect severity and area, and in this way proves to be a sensitive measure to structural change.

The results of this study show that of the functional measures, perimetry was the strongest indicator of structural change. The correlations between drusen area and other standard clinical measures of visual function yielded weaker linear relationships, for several reasons. Visual acuity, contrast sensitivity, reading speed and colour vision are principally foveal measures of visual function, whereas perimetry makes measures over a larger retinal area, which more closely matches the area of drusen segmentation. Less control over fixation was available for these functional measures compared to perimetry, therefore it is possible that patients with a greater severity of disease were using eccentric fixation, which introduces further variability around the measures. More

complex processes are involved in the other functional measures compared to perimetry, although visual acuity and contrast sensitivity did decline significantly with drusen area. Visual acuity is the highest spatial frequency that can be detected at 100% contrast, whereas the contrast sensitivity measure used in this study is designed to detect the minimum contrast at which a letter can be identified. The measure of visual acuity has been described as a three stage hierarchical sequence leading to letter recognition, involving the processes detection of contrast, resolution of elements and letter identification (Thibos & Bradley 1993). Identification of a letter is influenced by cognitive factors such as attention and memory, as well as experience and number of letters in the test alphabet (Thibos & Bradley 1993). As a complex task which includes a variety of processes, reading depends on letter and word resolution, stable retinal images (Bouma et al. 1974), saccadic accuracy (O'Regan 1980), lexical assessing (Just 1980) and cognitive processes required for comprehension and memory storage (Taft 1979; Thorndyke 1977). Colour vision error scores were very variable between individuals, despite being within normal limits in all but three patients, who demonstrated tritan defects. A past study involving structural and functional comparisons in patients with diabetes is in agreement with the present study, whereby visual field loss was a better correlate than visual acuity of the severity of diabetic retinopathy (Bengtsson et al. 2005)

No structural to functional correlations have previously been reported in studies using automated measures of drusen area in AMD. The closest comparisons which can be made with existing literature are with studies which have compared manual drusen measures to perimetry. It is not surprising therefore, that past research conflicts with some results in the present study, due to differing methodologies and the lack of consistency in manual grading. Indeed, considerable variability in manual drusen grading has been noted between even expert graders (Smith et al. 2005b). Tolentino et al. (1994) reported no correlation between an estimation of drusen area with number

of defects in a custom 6° by 4° macular perimetric grid. Lower mean sensitivities in standard perimetry were found with larger drusen size (Midena et al. 1994), which is supportive of the results in this study. However the same group found no change in sensitivity with drusen number (Midena et al. 1994, 1997) and another group using SLO microperimetry discerned no relationship between sensitivity loss and size of drusen (Takamine et al. 1998). In SLO perimetry, reduced sensitivity was demonstrated over large drusen compared to smaller drusen (Midena et al. 2007) and compared to non-drusen areas in some eyes (Takamine et al. 1998). This evidence further supports the correlation between drusen area and visual field loss. In general, a larger proportion of visual field defects were associated with retinal manifestations than retinal manifestations associated with defects. This suggests that not all retinal manifestations of AMD produce abnormal function that is detectable by visual field parameters, which is further enforced by the finding that retinal sensitivity over small drusen was not reduced (Midena et al. 2007).

The design of the study was to model functional change, by examining the visual fields of patients with varying stages of severity of AMD. As a product of the cross-sectional comparisons between patients, it was not possible to derive a precise time scale of functional decline, since the length of duration of disease was mostly anecdotal and accuracy could not be confirmed. An attempt was made to pilot a corresponding longitudinal design of the study, such that change over time could be investigated in a small number of patients with a view to a larger future study. In these patients, there was no structural change to their colour fundus images nor was there a functional change in the visual fields over six months. Thus, a longer period is required to examine the longitudinal progression of the visual field due to AMD. Indeed, slow progression rates of drusen and pigmentary changes have been described in epidemiological studies (van Leeuwen et al. 2003b; Klein et al. 2002). Longitudinal stability of the fields lends itself to the calculation of long-term fluctuation, which was

previously calculated in stable fields using a two-factor analysis of variance (ANOVA) with replications (Hutchings et al. 2000), however this method was not appropriate for this study, due to the non-Gaussian nature of the data and the small number of cases in the longitudinal group. An appropriate examination of visual field progression over time in AMD would be regression analysis of the PSD, LSV and AMD severity index, as these indices describe focal loss.

Automated drusen segmentation analysis represents a useful tool in the structural measure of progression in AMD. A significant overall effect of stage of disease on drusen area was demonstrated, however the trend was not strong across all the stages. The greatest change in drusen area occurred between the early stages, since stages 0-3 represent fundi which feature pigmentary changes and progressively larger drusen. At stage 4, fundi have atrophic or neovascular changes, which results in fewer drusen, therefore no change in drusen area was evident. It is possible that more eyes at each stage may have achieved a greater number of between stage significant differences in drusen area. Drusen area provides a useful structural measure for the purpose of comparison to functional data, since linear correlations may be made, which are not possible with the ordinal data of stage of AMD. Automated segmentation of drusen area could improve the accuracy of grading the early features of AMD and facilitate the development of the staging systems.

The advantage of automated segmentation over manual methods is that of convenience, consistency and repeatability. Indeed, two experts making drawings from the same macula using stereo images and a graphics tablet were found to vary comparably to automated segmentation of non-stereo images (Smith et al. 2005b). An important limitation of the program was described relating to the segmentation of highly reflective lesions, such as retinal pigment epithelial hypopigmentation, geographic atrophy, exudates, and scars as well as photographic dust spots, which may be mistaken for drusen; however the interactive selection feature to avoid these areas is a

simple solution to this problem (Smith et al. 2005b), and was employed in this study. The assumptions of retinal distance incorporated into the program assume the distance between the fovea and the temporal optic disc margin as 3000μm, or approximately two disc diameters, based on the longstanding clinical assumption of the optic disc diameter, as employed in standard AMD grading systems. Although the same disc diameter assumption was used in creating the programs in Chapter 5, the retinal distance assumptions differed. In terms of the visual field it was more appropriate to include the visual angle between the macula and the centre of the optic disc, 15° (Rabbetts 1998), as it was necessary to allow for the empirically determined measure between the macula and the optic disc centre. The conversion of this retinal distance to μm using the standard assumptions based on trigonometrical ray tracing in a schematic eye (Drasdo & Fowler 1974) then differed to that used in the automated drusen segmentation program. Therefore, percentage values were employed throughout so that the exact retinal distance value became arbitrary. The main source of error in using the program was the process of marking the macula and optic disc by the user, which was performed in a small window, and affected the resized area of the image which ultimately determined the drusen area output.

Chapter 5 showed the accuracy of the custom program Perimetric Fundus Map to be within approximately 80μm and these limits were observed in this study. In the analysis of visual field locations associated with retinal manifestations of AMD, points were not counted if they only had small drusen in isolation lying within the area of the stimulus location. The size of a small hard drusen is 63μm and subtends approximately 0.23° according to standard assumption of retinal distance (Drasdo & Fowler 1974). This was smaller than the stimulus diameters used in standard perimetry and SWAP, which were 0.43° and 1.74° respectively. Consequently a larger area around each point was measured for the SWAP perimetric fundus map analysis.

A high percentage of defects were associated with retinal manifestations on fundus photography. A larger number of SWAP PD and TD defects were associated with retinal features in both imaging types than standard perimetry defects. Conversely, when expressed as a percentage of the total number of defects, fewer SWAP defects were associated with colour retinal features of AMD than in standard perimetry. However this is because SWAP defects were more numerous than standard defects, and were present with no structural associations. This could indicate that SWAP may be predictive of future structural change, but a larger scale longitudinal study would be required to evaluate this finding.

As a percentage of the stimulus locations that were associated with retinal signs, the number of defects was relatively small for retro-mode images. This could be explained by the greater number of deposits on retro-mode images, which had no functional associations. It would appear that fundus photography gives a stronger indication of functional loss. Nevertheless, the comparison between colour fundus photography and retro-mode imaging should be approached with caution since the time difference between the images captured differed by 5-6 months. As a result, the quantification of retinal associations in retro-mode images with visual field defects (Figure 8-3 and Table 8-4) are more subject to variability than the corresponding values for colour fundus photography and can only provide an estimate of the structure to function relationship. The results of the study in Chapter 6 indicated an observable change in retro-mode images over a six month period in four of 13 eyes (3 of 8 patients), which reinforces the use of retro-mode imaging in the detection of subtle change in AMD. Although the retro-mode images were captured 5-6 months later than the initial visual field and colour fundus images, the lack of longitudinal change in the visual field over such a period allows the comparison between these images and the earlier functional data. Further investigation using accurate drusen segmentation of retro-mode images would

be necessary to fully compare the structure to function relationships with retro-mode images.

In order to reduce the morbidity of AMD, it is necessary to scrutinise the natural history and response to treatment of both structural changes at the macula and early changes to functional vision. Retro-mode imaging could represent a tool for monitoring fundus changes which may precede visual loss. The linear nature of the structure to function relationship between visual field parameters and drusen area in fundus photography, and the high coincidence proportion of visual field defects and retinal manifestations; offers insight into the natural history of AMD, which may be further developed with a larger scale longitudinal study.

9. Summary of Results and Conclusions and Future Work

9.1 Summary of Results and Conclusions

9.1.1 Investigation of Longitudinal Chromatic Aberration on SWAP Using Spherical Defocus

SWAP was more robust to negative defocus than positive defocus. Spherical defocus up to +2.00D caused a small but significant decline in threshold sensitivity, however negative defocus up to -2.00D had no significant effect on sensitivity. The lack of influence of negative defocus infers that when correcting for the bowl distance of the perimeter, slight undercorrection is not significant. However overcorrection may cause an artefactual decrease in sensitivity and should be avoided in patients with presbyopia or insufficient accommodative facility for the working distance of the perimeter.

The profile of threshold sensitivity with eccentricity peaked at 7.2° and declined towards the periphery with the physiological shape of the hill of vision. In the sample, which consisted of young subjects, the slight depression in sensitivity towards the fovea may be accounted for by the presence of macular pigment.

9.1.2 The Learning Effect in the Central Standard and Short-Wavelength Visual Fields

A learning effect was demonstrated between two visits for standard perimetry and SWAP, which was not significantly different between the AMD patient group and the normal control group. The global index MD increased by 0.4-0.6dB in standard perimetry and 0.7-0.9dB in SWAP, at the second visit. The magnitude of the learning effect was not significantly different between the patient group and the normal group, and was not influenced by stage of AMD. The deterioration in the threshold sensitivity between eyes during visits could be attributed to the fatigue effect. MD was the index most sensitive to the influence of learning which is of importance when examining AMD patients, where change in focal loss and variability is of more interest, rather than diffuse changes. Thus, the suitability and reliability of 10° visual field assessment of functional change in AMD is reinforced.

9.1.3 Programming in Ophthalmic Imaging Analyses

Two programs were written to map spatial information onto digital fundus images, with the purpose of reducing the error of performing such tasks manually. Program 1: Perimetric Fundus Map relates visual function to structural changes at the macula by mapping visual field data onto the fundus image. Program 2: Fundus Grading Grid allows the standard AMD grading grid to be mapped to the fundus image and incorporates a measurement tool without the necessity for the traditional method of plastic overlays. The repeatability associated with the mapping processes was approximately 80μm and 65μm for Programs 1 and 2, respectively. This is clinically acceptable for relating large drusen to functional change and for grading the features of AMD. Program 2 was implemented to grade the features of AMD and the inter-observer agreement was moderate to perfect between two graders. These programs provide useful tools for the analysis of digital fundus photographs.

9.1.4 Drusen Detection in Retro-Mode Imaging by a Scanning Laser Ophthalmoscope

Subretinal deposits manifested in greater numbers on retro-mode images compared to standard digital fundus images. The large subretinal deposits on retro-mode images in patients with AMD appeared to be consistent with the appearance of drusen detected on OCT. Deposits were significantly smaller in retro-mode images than in fundus photography, but the magnitude of the difference was marginal. Moderate to substantial agreement between graders was found. Comparison of retro-mode images over a period of six months revealed observable change to the deposits in a small number of images. Retro-mode imaging provides a rapid non-invasive technique, useful in monitoring subtle changes and progression of AMD.

9.1.5 Quantification of Visual Field Progression in AMD

The decline in visual field sensitivity with advancing stage of AMD indicated a stronger relationship in SWAP than in standard perimetry. SWAP had greater capability in the detection of early stage AMD as well as in the delineation of focal loss between stages

and represents a useful tool in the detection of early functional change in AMD in patients with minimal lenticular opacities. Early loss in AMD was focal in nature and the central field became less uniform and more variable as stage increased. Defects were on average confined to the central 5°. SWAP defects were deeper and wider than corresponding standard perimetry defects. The most vulnerable region of the 10° field to sensitivity loss with increasing stage of AMD was the central 1°, in which the sensitivity decline was -4.8dB per stage in standard perimetry and -4.9dB per stage in SWAP. Global indices of focal loss, pattern standard deviation (PSD) and local spatial variability (LSV) were the most sensitive to detecting differences in the profile of the hill of vision between normal subjects and early stage AMD patients, in standard perimetry and SWAP, respectively. LSV can be considered as a less statistically manipulated global index and consequently may represent a more accurate index of focal loss than PSD in SWAP. Threshold variability was considerably increased in late stage AMD eyes. A severity index was derived to define visual field defects attributed to AMD on a continuous scale.

9.1.6 Investigation of Structure to Function Relationships in AMD

The automated measurement of drusen area in digital fundus photographs was correlated with visual field parameters. A linear relationship between visual field parameters and drusen area was found. In standard perimetry, the MD declined by 3.00dB for each log percentage drusen area and the SWAP MD declined by 3.92dB for each log percentage drusen area, however it was the visual field parameters that indicate focal loss which displayed the strongest correlations with drusen area. The number of pattern deviation defects increased by 9.30 and 9.68 defects per log percentage drusen area for standard perimetry and SWAP, respectively. Stronger relationships were evident for SWAP indices of focal loss than for standard perimetry. There was a high coincidence proportion of visual field defects with retinal manifestations. In a subset of patients followed over 6 months, no structural change to

the colour fundus images was apparent nor was there a functional change in the visual fields. It would be necessary to monitor patients over a longer period in order to examine the longitudinal variability of the visual field in patients with AMD. Perimetry exhibited a stronger relationship with drusen area than other measures of visual function.

9.2 Future Work

9.2.1 Investigation of Longitudinal Chromatic Aberration on SWAP Using Spherical Defocus

The influence of cylindrical defocus on perimetric thresholds is currently unknown. The prismatic effect of incorrect positioning of the correcting lens has not been investigated.

9.2.2 The Learning Effect in the Central Standard and Short-Wavelength Visual Fields

Evaluation of the learning effect in the 10° field over five visits, each separated by one week has yet to be carried out to determine any residual learning effects following the first two visits and confirm that their magnitude is smaller than the initial effects. The short-term fluctuation (SF) in the 10-2 pattern on the HFA has received little attention, in terms of the spatial location of the ten points of double determination. In Chapter 7, the SF was found to be relatively insensitive to progression of disease. It remains unknown as to whether alternative stimulus locations, situated in areas of greater vulnerability to loss, would be more sensitive to fluctuation and more influenced by later stages of AMD. The corrected pattern standard deviation, whose calculation accounts for the SF, would also be affected. Knowledge of the magnitude of the fatigue effect in the 10° field in AMD patients who are experienced in both standard perimetry and SWAP would be of use in examining progressive changes.

9.2.3 Programming in Ophthalmic Imaging Analyses

Within-observer agreement of the spatial accuracy of the programs would give additional information to assess the quality of the programs. Future work to improve the programs described in Chapter 5 may include being rewritten in alternative

programming language such as Java, in which JPEG files or other file formats may be manipulated. More complex features such as interactive zooming of the image may then be incorporated. Program 1 has the potential to store the normal database for SWAP, such that perimetric indices and defects may be automatically calculated. The potential online availability of the software would allow direct clinical application and referral support with digital image analysis, which presents an advantage with the increasing use of telemedicine.

9.2.4 Drusen Detection in Retro-Mode Imaging by a Scanning Laser Ophthalmoscope

Retro-mode imaging provides further opportunity to use digital image analysis for the objective measurements and quantitative grading of features, whilst offering supplementary information to standard imaging techniques. The results in this thesis suggest retro-mode imaging is advantageous in the monitoring of subtle structural changes which may precede visual loss. A larger scale longitudinal follow-up study of AMD patients and normal subjects would be required to confirm whether the subretinal deposits in retro-mode images are sub-clinical drusen which will eventually manifest as clinically visible drusen or other features of disease. Histological examination of the subretinal deposits is also indicated.

9.2.5 Quantification of Visual Field Progression in AMD

Due to the time limitations of this PhD, a cross-sectional study design was chosen to quantify functional changes at different stages of AMD with a limited degree of longitudinal monitoring. Unfortunately, such a methodology gives no information regarding the variation in the course of progression between patients. An optimal model for quantifying functional change would collect longitudinal data from AMD patients, which requires a large sample to be followed over several years. This would delineate stable and progressing functional and structural changes. The data already collected in this PhD would facilitate the design of a longitudinal study in the assessment of limits for significant change and increment of time between visits.

Examination of the indices of focal loss, such as the less commonly used LSV, is of greater importance when defining visual field progression in AMD. The AMD severity index measures visual field loss on a continuous scale. This index may offer a single figure from which it would be possible to derive limits to stage the functional loss in AMD, and may be of value when defining treatment thresholds and clinical outcomes. The long-term fluctuation (LF) is of value in the detection of progression and is currently unknown for AMD. It would be necessary to develop methods for the calculation of both homogeneous and heterogeneous components of LF, from visual fields generated using SITA algorithms.

The correlation between numerous risk factors and visual field loss would gain insight into the risk of functional loss. Such an investigation would require a large, unbiased sample as well as a control. Risk factors such as light exposure (Darzins et al. 1997), abnormal skin sensitivity to sunlight (Mitchell et al. 1998) and diet (Seddon et al. 2003b, AREDS 2001a) require complex techniques of quantification and would require detailed information from a lengthy questionnaire or interview. Other risk factors such as the effect of a fellow eye with neovascular disease would necessitate careful recruitment.

9.2.6 Investigation of Structure-Function Relationships in AMD

A longitudinal study would benefit from grading which involved the automated segmentation of drusen. The potential segmentation of other features of AMD would provide better objective measures and further improve grading systems, by reducing the variability error associated with manual methods. This may then be applied to a re-evaluation of the staging systems, and subsequently their relationship to functional changes. The segmentation of deposits on retro-mode images is confounded by the lack of edge definition and lack of uniformity in the pixel value of the deposits. Further work would involve attention to the segmentation algorithms and pre-processing of images, for this purpose.

References

Abadi R.V. & Pantazidou M. (1996). Low contrast letter acuity in age-related maculopathy. *Ophthalmic and Physiological Optics* 16:455-459.

Adams A.J., Schefrin B. & Huie K. (1987). New Clinical Color Threshold Test for Eye Disease. *American Journal of Optometry and Physiological Optics* 64:29-37.

Afrashi F., Erakgun T., Kose S., Ardic K. & Mentes J. (2003). Blue-on-yellow perimetry versus achromatic perimetry in type diabetes patients without retinopathy. *Diabetes Research and Clinical Practice* 61:7-11.

Agardh E., Stjernquist H., Heijl A. & Bengtsson B. (2006). Visual acuity and perimetry as measures of visual function in diabetic macular oedema. *Diabetologia* 49:200-206.

Ahlers C., Michels S., Beckendorf A., Birngruber R. & Schmidt-Erfurth U. (2006). Three-dimensional imaging of pigment epithelial detachment in age-related macular degeneration using optical coherence tomography, retinal thickness analysis and topographic angiography. *Graefes Archive for Clinical and Experimental Ophthalmology* 244:1233-1239.

Alster Y., Bressler N.M., Bressler S.B., Brimacombe J.A., Crompton R.M., Duh Y.J., Gabel V.P., Heier J.S., Ip M.S., Loewenstein A., Packo K.H., Stur M., & Toaff T. (2005). Preferential hyperacuity perimeter (PreView PHP) for detecting choroidal neovascularization study. *Ophthalmology* 112:1758-1765.

Ambati J., Ambati B.K., Yoo S.H., Ianchulev S., & Adamis A.P. (2003). Age-related macular degeneration: Etiology, pathogenesis, and therapeutic strategies. *Survey of Ophthalmology* 48:257-293.

Anderson A.J. & Vingrys A.J. (2000). Interactions between flicker thresholds and luminance pedestals. *Vision Research* 40:2579-2588.

Anderson A.J., Johnson C.A., Fingeret M., Keltner J.L., Spry P.G.D., Wall M. & Werner J.S. (2005). Characteristics of the normative database for the Humphrey Matrix perimeter. *Investigative Ophthalmology & Visual Science* 46:1540-1548.

Anderson D.R. & Patella M.V. (1992) *Automated static perimetry.* Ed: Anderson D.R. & Patella M.V. Mosby-Year Book Inc., St. Louis.

Anderson R.S., McDowell R.D. & Ennis F.A. (2001). Effect of localized defocus on detection thresholds for different sized targets in the fovea and periphery. *Acta Ophthalmologica Scandinavica* 79:60-63.

Anderson R.S., Zlatkova M.B. & Beirne R.O. (2002). The contrast sensitivity function for detection and resolution of blue-on-yellow gratings in foveal and peripheral vision. *Ophthalmic and Physiological Optics* 22:420-426.

Applegate R.A., Adams A.J., Cavender J.C. & Zisman F. (1987). Early Color-Vision Changes in Age-Related Maculopathy. *Applied Optics* 26:1458-1462.

Arden G.B. & Wolf J.E. (2004). Colour vision testing as an aid to diagnosis and management of age related maculopathy. *British Journal of Ophthalmology* 88:1180-1185.

AREDS (2001a). A randomized, placebo-controlled, clinical trial of high-dose supplementation with vitamins C and E, beta carotene, and zinc for age-related macular degeneration and vision loss - AREDS Report No. 8. *Archives of Ophthalmology* 119:1417-1436.

AREDS (2001b). The age-related eye disease study system for classifying age-related macular degeneration from stereoscopic color fundus photographs: The Age-Related Eye Disease Study Report Number 6. *American Journal of Ophthalmology*, 132:668-681.

Arnalich-Montiel F., Casas-Llera P., Munoz-Negrete F.J. & Rebolleda G. (2009). Performance of glaucoma progression analysis software in a glaucoma population. *Graefes Archive for Clinical and Experimental Ophthalmology* 247:391-397.

Arnold J.J., Sarks S.H., Killingsworth M.C. & Sarks J.P. (1995). Reticular pseudodrusen: a risk factor in age-related maculopathy. *Retina-the Journal of Retinal and Vitreous Diseases* 15:183-191.

Artes P.H., Iwase A., Ohno Y., Kitazawa Y. & Chauban B.C. (2002). Properties of perimetric threshold estimates from full threshold, SITA standard, and SITA fast strategies. *Investigative Ophthalmology & Visual Science* 43:2654-2659.

Artes P.H., Nicolela M.T., LeBlanc R.P. & Chauhan B.C. (2005). Visual field progression in glaucoma: total versus pattern deviation analyses. *Investigative Ophthalmology & Visual Science* 46:4600-4606.

Åsman P. & Heijl A. (1992). Glaucoma Hemifield Test. *Archives of Ophthalmology* 110:812-819.

Åsman P. & Olsson J. (1995). Physiology of Cumulative Defect Curves Consequences in Glaucoma Perimetry. *Acta Ophthalmologica Scandinavica* 73:197-201.

Åsman P., Wild J.M. & Heijl A. (2004). Appearance of the pattern deviation map as a function of change in area of localized field loss. *Investigative Ophthalmology & Visual Science* 45:3099-3106.

Atchison D.A. (1987). Effect of Defocus on Visual-Field Measurement. *Ophthalmic and Physiological Optics* 7:259-265.

Atchison D.A., Loviekitchin J.E. & Swann P.G. (1990). Investigation of Central Visual-Fields in Patients with Age-Related Macular Changes. *Optometry and Vision Science* 67:179-183.

Atchison D.A. & Smith G. (2005). Chromatic dispersions of the ocular media of human eyes. *Journal of the Optical Society of America A-Optics Image Science and Vision* 22:29-37.

Augood C.A., Vingerling J.R., De Jong P.T.V.M., Chakravarthy U., Seland J., Soubrane G., Tomazzoli L., Topouzis F., Bentham G., Rahu M., Vioque J., Young I.S. & Fletcher

A.E. (2006). Prevalence of age-related maculopathy in older Europeans - The European Eye Study (EUREYE). *Archives of Ophthalmology* 124:529-535.

Autzen T. & Work K. (1990). The Effect of Learning and Age on Short-Term Fluctuation and Mean Sensitivity of Automated Static Perimetry. *Acta Ophthalmologica* 68:327-330.

Avery R.L., Pieramici D.J., Rabena M.D., Castellarin A.A., Nasir M.A. & Giust M.J. (2006). Intravitreal bevacizumab (Avastin) for neovascular age-related macular degeneration. *Ophthalmology* 113:363-372.

Barkana Y., Gerber Y., Mora R., Liebmann J.M. & Ritch R. (2006). Effect of eye testing order on automated perimetry results using the Swedish interactive threshold algorithm standard 24-2. *Archives of Ophthalmology* 124:781-784.

Bayer A.U. & Erb C. (2002). Short wavelength automated perimetry, frequency doubling technology perimetry, and pattern electroretinography for prediction of progressive glaucomatous standard visual field defects. *Ophthalmology* 109:1009-1017.

Beatty S., Boulton M., Henson D., Koh H.H. & Murray I.J. (1999). Macular pigment and age related macular degeneration. *British Journal of Ophthalmology* 83:867-877.

Beatty S., Koh H., Phil M., Henson D. & Boulton M. (2000) The role of oxidative stress in the pathogenesis of age-related macular degeneration. *Survey of Ophthalmology* 45:115-134.

Beatty S., Murray I.J., Henson D.B., Carden D., Koh H.H. & Boulton M.E. (2001). Macular pigment and risk for age-related macular degeneration in subjects from a Northern European population. *Investigative Ophthalmology & Visual Science* 42:439-446.

Bebie H., Fankhauser F. & Spahr J. (1976). Static Perimetry - Accuracy and Fluctuations. *Acta Ophthalmologica* 54:339-348.

Beirne R.O., Zlatkova M.B. & Anderson R.S. (2005). Changes in human short-wavelength-sensitive and achromatic resolution acuity with retinal eccentricity and meridian. *Visual Neuroscience* 22:79-86.

Beirne R.O., Hogg R.E., Stevenson M.R., Zlatkova M.B., Chakravarthy U. & Anderson R.S. (2006). Severity staging by early features of age-related maculopathy exhibits weak relationships with functional deficits on SWS grating acuity. *Investigative Ophthalmology & Visual Science* 47:4624-4631.

Bellmann C., Unnebrink K., Rubin G.S., Miller D. & Holz F.G. (2003). Visual acuity and contrast sensitivity in patients with neovascular age-related macular degeneration - Results from the Radiation Therapy for Age-Related Macular Degeneration (RAD-) Study. *Graefes Archive for Clinical and Experimental Ophthalmology* 241:968-974.

Benedetto M.D. & Cyrlin M.N. (1985). The effect of blur upon static perimetric thresholds. *Doc Ophthalmol Proc Ser 42*. Proceedings of the Sixth International Visual Field Symposium. Eds: A.Heijl & E.L.Greve Dordrecht. Dr W.Junk.pp 563-567.

Bengtsson B. & Krakau C.E.T. (1977). Some Essential Optical Features of Zeiss Fundus Camera. *Acta Ophthalmologica* 55:123-131.

Bengtsson B. & Krakau C. (1992) Correction of optic disc measurements on fundus photographs. *Graefes Archive for Clinical and Experimental Ophthalmology* 230:24-28.

Bengtsson B., Lindgren A., Heijl A., Lindgren G., Åsman P. & Patella M. (1997a). Perimetric probability maps to separate change caused by glaucoma from that caused by cataract. *Acta Ophthalmologica Scandinavica* 75:184-188.

Bengtsson B., Olsson J., Heijl A. & Rootzen H. (1997b). A new generation of algorithms for computerized threshold perimetry, SITA. *Acta Ophthalmologica Scandinavica* 75:368-375.

Bengtsson B. & Heijl A. (1998a). SITA Fast, a new rapid perimetric threshold test. Description of methods and evaluation in patients with manifest and suspect glaucoma. *Acta Ophthalmologica Scandinavica* 76:431-437.

Bengtsson B. & Heijl A. (1998b). Evaluation of a new perimetric threshold strategy, SITA, in patients with manifest and suspect glaucoma. *Acta Ophthalmologica Scandinavica* 76:268-272.

Bengtsson B., Heijl A. & Olsson J. (1998). Evaluation of a new threshold visual field strategy, SITA, in normal subjects. Swedish Interactive Thresholding Algorithm. *Acta Ophthalmologica Scandinavica* 76:165-169.

Bengtsson B. & Heijl A. (1999a). Inter-subject variability and normal limits of the SITA standard, SITA fast, and the Humphrey full threshold computerized perimetry strategies, SITA STATPAC. *Acta Ophthalmologica Scandinavica* 77:125-129.

Bengtsson B. & Heijl A. (1999b). Comparing significance and magnitude of glaucomatous visual field defects using the SITA and Full Threshold strategies. *Acta Ophthalmologica Scandinavica* 77:143-146.

Bengtsson B. & Heijl A. (2003). Normal intersubject threshold variability and normal limits of the SITA SWAP and full threshold SWAP perimetric programs. *Investigative Ophthalmology & Visual Science* 44:5029-5034.

Bengtsson B., Heijl A. & Agardh E. (2005). Visual fields correlate better than visual acuity to severity of diabetic retinopathy. *Diabetologia* 48:2494-2500.

Bengtsson B. & Heijl A. (2006). Diagnostic sensitivity of fast blue-yellow and standard automated perimetry in early glaucoma - A comparison between different test programs. *Ophthalmology* 113:1092-1097.

Bengtsson B. & Heijl A. (2008). A visual field index for calculation of glaucoma rate of progression. *American Journal of Ophthalmology* 145:343-353.

Bengtsson B., Hellgren K.J. & Agardh E. (2008). Test-retest variability for standard automated perimetry and short-wavelength automated perimetry in diabetic patients. *Acta Ophthalmologica* 86:170-176.

Bennett A., Rudnicka A. & Edgar D. (1994). Improvements on Littman's method of determining the size of retinal features by fundus photography. *Graefe's Archive for Clinical and Experimental Ophthalmology* 232:361–367

Bindewald A., Bird A.C., Dandekar S.S., Dolar-Szczasny J., Dreyhaupt J., Fitzke F.W., Einbock W., Holz F.G., Jorzik J.J., Keilhauer C., Lois N., Mlynski J., Pauleikhoff D., Staurenghi G. & Wolf S. (2005a). Classification of fundus autofluorescence patterns in early age-related macular disease. *Investigative Ophthalmology & Visual Science* 46:3309-3314.

Bindewald A., Schmitz-Valckenberg S., Jorzik J.J., Dolar-Szczasny J., Sieber H., Keilhauer C., Weinberger A.W.A., Dithmar S., Pauleikhoff D., Mansmann U., Wolf S., Holz F.G. & FAM S.G. (2005b). Classification of abnormal fundus autofluorescence patterns in the junctional zone of geographic atrophy in patients with age related macular degeneration. *British Journal of Ophthalmology* 89:874-878.

Bird A.E.C., Bressler N.M., Bressler S.B., Chisholm I.H., Coscas G., Davis M.D., Dejong P.T.V.M., Klaver C.C.W., Klein B.E.K., Klein R., Mitchell P., Sarks J.P., Sarks S.H., Sourbane G., Taylor H.R. & Vingerling J.R. (1995). An International Classification and Grading System for Age-Related Maculopathy and Age-Related Macular Degeneration. *Survey of Ophthalmology* 39:367-374.

Bjornsson O.M., Syrdalen P., Bird A.C., Peto T. & Kinge B. (2006). The prevalence of age-related maculopathy (ARM) in an urban Norwegian population: the Oslo Macular Study. *Acta Ophthalmologica Scandinavica* 84:636-641.

Bland J.M. & Altman D.G. (1986). Statistical methods for assessing agreement between two methods of clinical measurement. *Lancet* 1:307-310.

Blumenthal E. Z., Sample P.A., Zangwill L., Lee A.C., Kono Y. & Weinreb R.N. (2000). Comparison of long-term variability for standard and short-wavelength automated perimetry in stable glaucoma patients. *American Journal of Ophthalmology* 129:309-313.

Bone R.A., Landrum J.T. & Tarsis S.L. (1985). Preliminary Identification of the Human Macular Pigment. *Vision Research* 25:1531-1535.

Bone R.A., Landrum J.T. (2004). Heterochromatic flicker photometry. *Archives of Biochemistry and Biophysics* 430:137-142.

Bouma H. & deVoogd A.H. (1974). On the control of eye saccades in reading. *Vision Research* 14:273-283.

Brenton R.S. & Argus W.A. (1987). Fluctuations on the Humphrey and Octopus Perimeters. *Investigative Ophthalmology & Visual Science* 28:767-771.

Bressler S.B., Maguire M.G., Bressler N.M. & Fine S.L. (1990). Relationship of Drusen and Abnormalities of the Retinal-Pigment Epithelium to the Prognosis of Neovascular Macular Degeneration. *Archives of Ophthalmology* 108:1442-1447.

Brown B., Adams A.J., Coletta N.J. & Haegerstromportnoy G. (1986). Dark-Adaptation in Age-Related Maculopathy. *Ophthalmic and Physiological Optics* 6:81-84.

Bullimore M.A., Bailey I.L. (1995). Reading and Eye-Movements in Age-Related Maculopathy. *Optometry and Vision Science* 72:125-138.

Cackett P., Tay W.T., Aung T., Wang J.J., Shankar A., Saw S.M., Mitchell P. & Wong T.Y. (2008). Education, socio-economic status and age-related macular degeneration in asians: the Singapore Malay Eye Study. *British Journal of Ophthalmology* 92:1312-1315.

Capris P., Autuori S., Capris E. & Papadia M. (2008). Evaluation of threshold estimation and learning effect of two perimetric strategies, SITA Fast and CLIP, in damaged visual fields. *European Journal of Ophthalmology* 18:182-190.

Cauchy A.L. (1895) Mémoire sur la dispersion de la lumière, Nouveaux Exercices de Mathématiques. *Oeuvres Complètes d'Augustin Cauchy*, 2nd Series, Vol. 10. Paris. Gauthier-Villars et Fils. (cited by Atchison & Smith, 2005, see above).

Cello K.E., Nelson-Quigg J.M. & Johnson C.A. (2000). Frequency doubling technology perimetry for detection of glaucomatous visual field loss. *American Journal of Ophthalmology* 129:314-322.

Chauhan B.C., Drance S.M. & Douglas G.R. (1990). The Use of Visual-Field Indexes in Detecting Changes in the Visual-Field in Glaucoma. *Investigative Ophthalmology & Visual Science* 31:512-520.

Chauhan B.C., Leblanc R.P., Drance S.M., Wijsman K. & Cruz A.M. (1991). Effect of the Number of Threshold Determinations on Short-Term Fluctuation in Automated Perimetry. *Ophthalmology* 98:1420-1424.

Chauhan B.C., LeBlanc R.P., Shaw A.M., Chan A.B. & McCormick T.A. (1997). Repeatable diffuse visual field loss in open-angle glaucoma. *Ophthalmology* 104:532-538.

Chen C.Z., Wu L.Z., Wu D.Z., Huang S.Z., Wen F., Luo G.W. & Long S.X. (2004). The local cone and rod system function in early age-related macular degeneration. *Documenta Ophthalmologica* 109:1-8.

Chen F.K., Patel P.J., Xing W., Bunce C., Egan C., Tufail A.T., Coffey P.J., Rubin G.S. & Da Cruz L. (2009). Test-Retest Variability of Microperimetry Using the Nidek MP1 in Patients with Macular Disease. *Investigative Ophthalmology & Visual Science* 50:3464-3472.

Cheng A.S. & Vingrys A.J. (1993). Visual Losses in Early Age-Related Maculopathy. *Optometry and Vision Science* 70:89-96.

Christen W.G., Glynn R.J., Manson J.E., Ajani U.A. & Buring J. E. (1996). A prospective study of cigarette smoking and risk of age-related macular degeneration in men. *Journal of the American Medical Association* 276:1147-1151.

Chylack L.T., Leske M.C., Mccarthy D., Khu P., Kashiwagi T. & Sperduto R. (1989). Lens Opacities Classification System-Ii (Locs-Ii). *Archives of Ophthalmology* 107:991-997.

Chylack L.T., Wolfe J.K., Singer D.M., Leske M.C., Bullimore M.A., Bailey I.L., Friend J., Mccarthy D. & Wu S.Y. (1993). The Lens Opacities Classification System-Iii. *Archives of Ophthalmology* 111:831-836.

Collins M.J. (1986) Pre-age-related maculopathy and the desaturated D-15 colour vision test. *Clinical and Experimental Optometry* 69:223-7.

Conway M. (2003) Investigation into visual defects attributed to Vigabatrin. Ph.D Thesis

Crabb D.P., Edgar D.F., Fitzke F.W., Mcnaught A.I. & Wynn H.P. (1995). New Approach to Estimating Variability in Visual-Field Data Using An Image-Processing Technique. *British Journal of Ophthalmology* 79:213-217.

Crabb D.P., Fitzke F.W., Mcnaught A.I., Edgar D.F. & Hitchings R.A. (1997). Improving the prediction of visual field progression in glaucoma using spatial processing. *Ophthalmology* 104:517-524.

Crossland M.D., Culham L.E. & Rubin G.S. (2004). Fixation stability and reading speed in patients with newly developed macular disease. *Ophthalmic and Physiological Optics* 24:327-333.

Crossland M.D. & Rubin G.S. (2006). Eye movements and reading in macular disease: Further support for the shrinking perceptual span hypothesis. *Vision Research* 46:590-597.

Cubbidge R.P. (1997) Examination Variability in Short-Wavelength Automated Perimetry. Ph.D Thesis.

Cubbidge R.P., Hosking S.L. & Embleton S. (2002). Statistical modelling of the central 10-degree visual field in short-wavelength automated perimetry. *Graefes Archive for Clinical and Experimental Ophthalmology* 240:650-657.

Cubbidge R.P. & Wild J.M. (2001). The influences of stimulus wavelength and eccentricity on short-wavelength pathway isolation in automated perimetry. *Ophthalmic and Physiological Optics*, 21:1-8.

Curcio C.A., Sloan K.R., Kalina R.E. & Hendrickson A.E. (1990). Human Photoreceptor Topography. *Journal of Comparative Neurology* 292:497-523.

Curcio C. A., Allen K. A., Sloan K. R., Lerea C. L., Hurley J. B., Klock I. B. & Milam A. H. (1991). Distribution and Morphology of Human Cone Photoreceptors Stained with Anti-Blue Opsin. *Journal of Comparative Neurology* 312:610-624.

Curcio C.A., Millican C.L., Allen K.A. & Kalina R.E. (1993). Aging of the Human Photoreceptor Mosaic - Evidence for Selective Vulnerability of Rods in Central Retina. *Investigative Ophthalmology & Visual Science* 34:3278-3296.

Curcio C.A., Medeiros N.E. & Millican C.L. (1996). Photoreceptor loss in age-related macular degeneration. *Investigative Ophthalmology & Visual Science* 37:1236-1249.

Dacey D. M. & Lee B. B. (1994). The Blue-on Opponent Pathway in Primate Retina Originates from A Distinct Bistratified Ganglion-Cell Type. *Nature* 367:731-735.

Darzins P., Mitchell P. & Heller R.F. (1997). Sun exposure and age-related macular degeneration. An Australian case-control study. *Ophthalmology* 104:770-776.

Das A. & McGuire P.G. (2003). Retinal and choroidal angiogenesis: pathophysiology and strategies for inhibition. *Progress in Retinal and Eye Research* 22:721-748.

de la Rosa M.G., Gonzalez-Hernandez M., Abraldes M. & zuara-Blanco A. (2002). Quantification of interpoint topographic correlations of threshold values in glaucomatous visual fields. *Journal of Glaucoma* 11:30-34.

de la Rosa M.G. (2008). Method to increase the sensitivity of perimetric trend progression analysis. *British Journal of Ophthalmology* 92:1564-1565.

de Waard P.W.T., Ijspeert J.K., Vandenberg T.J.T.P. & Dejong P.T.V.M. (1992). Intraocular Light-Scattering in Age-Related Cataracts. *Investigative Ophthalmology & Visual Science* 33:618-625.

Demirel S. & Johnson C.A. (2000). Isolation of short-wavelength sensitive mechanisms in normal and glaucomatous visual field regions. *Journal of Glaucoma* 9:63-73.

Demirel S. & Johnson C.A. (2001). Incidence and prevalence of short wavelength automated perimetry deficits in ocular hypertensive patients. *American Journal of Ophthalmology* 131:709-715.

Demirel S. & Robinson R. (2003). Upper vs. lower field asymmetry in SAP and SWAP thresholds: comparison to psychophysical estimates of ganglion cell density. *Investigative Ophthalmology and Visual Science* 44: E-abstract 69

Diaz-Aleman V.T., Anton A., de la Rosa M.G., Johnson Z.K., McLeod S. & zuara-Blanco A. (2009). Detection of visual-field deterioration by Glaucoma Progression Analysis and Threshold Noiseless Trend programs. *British Journal of Ophthalmology* 93:322-328.

Drasdo N. & Fowler C.W. (1974). Non-linear projection of the retinal image in a wide-angle schematic eye. *British Journal of Ophthalmology* 58:709-14.

Eisner A., Fleming S.A., Klein M.L. & Mauldin W.M. (1987a). Sensitivities in Older Eyes with Good Acuity - Cross-Sectional Norms. *Investigative Ophthalmology & Visual Science* 28:1824-1831.

Eisner A., Fleming S.A., Klein M.L. & Mauldin W.M. (1987b). Sensitivities in Older Eyes with Good Acuity - Eyes Whose Fellow Eye Has Exudative AMD. *Investigative Ophthalmology & Visual Science* 28:1832-1837.

Eisner A., Stoumbos V.D., Klein M.L. & Fleming S.A. (1991). Relations Between Fundus Appearance and Function - Eyes Whose Fellow Eye Has Exudative Age-Related Macular Degeneration. *Investigative Ophthalmology & Visual Science* 32:8-20.

Eisner A., Klein M.L., Zilis J.D. & Watkins M.D. (1992). Visual function and the subsequent development of exudative age-related macular degeneration. *Investigative Ophthalmology & Visual Science* 33:3091-3102.

Elliott D.B., Patel B. & Whitaker D. (2001). Development of a reading speed test for potential-vision measurements. *Investigative Ophthalmology & Visual Science* 42:1945-1949.

Elsner A.E., Burns S.A., Weiter J.J. & Delori F.C. (1996). Infrared imaging of subretinal structures in the human ocular fundus. *Vision Research* 36:191-205.

Elsner A.E. & Muller M.S. (2008). Laser applications and system considerations in ocular imaging. *Laser & Photonics Reviews* 2:350-376.

Ergun E., Maar N., Radner W., Barbazetto I., Schmidt-Erfurth U. & Stur M. (2003). Scotoma size and reading speed in patients with subfoveal occult choroidal neovascularization in age-related macular degeneration. *Ophthalmology* 110:65-69.

Erlich R., Harris A., Kheradiya N.S., Winston D.M., Ciulla T.A. & Wirostko B. (2008) Age-related macular degeneration and the aging eye. *Clinical Interventions in Aging* 3:473-482.

Evans J.R. (2001). Risk factors for age-related macular degeneration. *Progress in Retinal and Eye Research* 20:227-253.

Evans J.R., Fletcher A.E. & Wormald R.P.L. (2004). Age-related macular degeneration causing visual impairment in people 75 years or older in Britain - An add-on study to the Medical Research Council Trial of Assessment and Management of Older People in the Community. *Ophthalmology* 111:513-517.

Evans J.R., Fletcher A.E. & Wormald R.P.L. (2005). 28,000 Cases of age related macular degeneration causing visual loss in people aged 75 years and above in the United Kingdom may be attributable to smoking. *British Journal of Ophthalmology* 89:550-553.

Fankhauser F. & Enoch J.M. (1962). The effects of blur upon perimetric thresholds. *Archives of Ophthalmology* 68:240-251.

Feigl B., Brown B., Lovie-Kitchin J. & Swann P. (2005). Monitoring retinal function in early age-related maculopathy: visual performance after 1 year. *Eye* 19:1169-1177.

Felius J., Dejong L.A.M.S., Vandenberg T.J.T.P. & Greve E.L. (1995). Functional-Characteristics of Blue-On-Yellow Perimetric Thresholds in Glaucoma. *Investigative Ophthalmology & Visual Science* 36:1665-1674.

Fine S.L., Berger J.W. & Maguire M.G. (1999) *Age-related macular degeneration*. Eds: S.L. Fine, J.W. Berger & M.G. Maguire. St. Louis. Mosby.

Fink W. & Sadun A.A. (2004). Three-dimensional computer-automated threshold Amsler grid test. *Journal of Biomedical Optics* 9:149-153.

Fitzke F.W., Crabb D.P., Mcnaught A.I., Edgar D.F. & Hitchings R.A. (1995). Image-Processing of Computerized Visual-Field Data. *British Journal of Ophthalmology* 79:207-212.

Fitzke F.W., Hitchings R.A., Poinoosawmy D., McNaught A.I. & Crabb D.P. (1996). Analysis of visual field progression in glaucoma. *British Journal of Ophthalmology* 80:40-48.

Flammer J., Drance S.M. & Schulzer M. (1983). The estimation and testing of the components of long-term fluctuation of the differential light threshold. *Doc Ophthalmol Proc Ser 35.* Proceedings of the Fifth International Visual Field Symposium. Eds: E. L. Greve & A. Heijl. Dr W Junk. The Hague. pp. 383-389.

Flammer J., Drance S.M., Fankhauser F. & Augustiny L. (1984a). Differential Light Threshold in Automated Static Perimetry- Factors Influencing Short-Term Fluctuation. *Archives of Ophthalmology* 102:876-879.

Flammer J., Drance S.M. & Schulzer M. (1984b). Covariates of the Long-Term Fluctuation of the Differential Light Threshold. *Archives of Ophthalmology* 102:880-882.

Flammer J., Drance S.M. & Zulauf M. (1984c). Differential Light Threshold - Short-Term and Long-Term Fluctuation in Patients with Glaucoma, Normal Controls, and Patients with Suspected Glaucoma. *Archives of Ophthalmology* 102:704-706.

Flanagan J.G., Moss I.D., Wild J.M., Hudson C., Prokopich L., Whitaker D. & Oneill E.C. (1993a). Evaluation of Fastpac - A New Strategy for Threshold Estimation with the Humphrey Field Analyzer. *Graefes Archive for Clinical and Experimental Ophthalmology* 231:465-469.

Flanagan J.G., Wild J.M. & Trope G.E. (1993b). Evaluation of Fastpac, A New Strategy for Threshold Estimation with the Humphrey Field Analyzer, in A Glaucomatous Population. *Ophthalmology* 100:949-954.

Fletcher A.E., Bentham G.C., Agnew M., Young I.S., Augood C., Chakravarthy U., de Jong P.T.V.M., Rahu M., Seland J., Soubrane G., Tomazzoli L., Topouzis F., Vingerling J.R. & Vioque J. (2008). Sunlight exposure, antioxidants, and age-related macular degeneration. *Archives of Ophthalmology* 126:1396-1403.

Freeman E.E., Munoz B., Bressler S.B. & West S.K. (2005). Hormone replacement therapy, reproductive factors, and age-related macular degeneration: The Salisbury eye evaluation project. *Ophthalmic Epidemiology* 12:37-45.

Freeman W.R., El-Bradey M. & Plummer D.J. (2004). Scanning laser entoptic perimetry for the detection of age-related macular degeneration. *Archives of Ophthalmology* 122:1647-1651.

Frennesson C., Nilsson U.L. & Nilsson S.E.G. (1995). Color Contrast Sensitivity in Patients with Soft Drusen, An Early-Stage of ARM. *Documenta Ophthalmologica* 90:377-386.

Friedman E. (2000). The role of the atherosclerotic process in the pathogenesis of age-related macular degeneration. *American Journal of Ophthalmology* 130:658-663.

Friedman D.S., O'Colmain B., Tomany S.C., McCarty C., De Jong P.T.V.M., Nemesure B., Mitchell P., Kempen J., Congdon N. & Eye Dis Prevalence Res Grp (2004). Prevalence of age-related macular degeneration in the United States. *Archives of Ophthalmology* 122:564-572.

Fuhr P.S., Hershner T.A. & Daum K.M. (1990). Ganzfeld Blankout Occurs in Bowl Perimetry and Is Eliminated by Translucent Occlusion. *Archives of Ophthalmology* 108:983-988.

Fujii G.Y., De Juan E., Humayun M.S., Sunness J.S., Chang T.S. & Rossi J.V. (2003). Characteristics of visual loss by scanning laser ophthalmoscope microperimetry in eyes with subfoveal choroidal neovascularization secondary to age-related macular degeneration. *American Journal of Ophthalmology* 136:1067-1078.

Fujimoto N. & Adachiusami E. (1993). Fatigue Effect Within 10-Degrees Visual-Field in Automated Perimetry. *Annals of Ophthalmology* 25:142-144.

Funkhouser A. & Fankhauser F. (1991). The Effects of Weighting the Mean Defect Visual-Field Index According to Threshold Variability in the Central and Midperipheral Visual-Field. *Graefes Archive for Clinical and Experimental Ophthalmology* 229:228-231.

Gaasterland D.E., Ederer F., Sullivan E.K., Caprioli J. & Cyrlin M.N. (1994). Advanced Glaucoma Intervention Study .2. Visual-Field Test Scoring and Reliability. *Ophthalmology* 101:1445-1455.

Gao H. & Hollyfield J.G. (1992). Aging of the human retina. Differential loss of neurons and retinal pigment epithelial cells. *Investigative Ophthalmology & Visual Science* 33:1-17.

Gardiner S.K. & Crabb D.P. (2002). Examination of different pointwise linear regression methods for determining visual field progression. *Investigative Ophthalmology & Visual Science* 43:1400-1407.

Gardiner S.K., Crabb D.P., Fitzke F.W. & Hitchings R.A. (2004). Reducing noise in suspected glaucomatous visual fields by using a new spatial filter. *Vision Research* 44:839-848.

Gardiner S.K., Demirel S. & Johnson C.A. (2008). Is There Evidence for Continued Learning Over Multiple Years in Perimetry? *Optometry and Vision Science* 85:1043-1048.

Garway-Heath D.F., Rudnicka A., Lowe T., Foster P., Fitzke F. and Hitchings R. (1998). Measurement of optic disc size: equivalence of methods to correct for ocular magnification. *British Journal of Ophthalmology* 82:643-649.

Gass J.D.M. (1973). Drusen and Disciform Macular Detachment and Degeneration. *Archives of Ophthalmology* 90:206-217.

Gerth C., Hauser D., Delahunt P.B., Morse L.S. & Werner J.S. (2003). Assessment of multifocal electroretinogram abnormalities and their relation to morphologic characteristics in patients with large drusen. *Archives of Ophthalmology* 121:1404-1414.

Gibson J.M., Acton J.H., Berrow E., Galsworthy P., King H, Quant L. & Whitehouse K. (2009). Retinal Drusen Detection Using the Nidek F-10 SLO in Retro-Mode. *Investigative Ophthalmology & Visual Science* 50:E-Abstract 5262

Gilmore E.D., Hudson C., Nrusimhadevara R.K. & Harvey P.T. (2005). Frequency of seeing characteristics of the short wavelength sensitive visual pathway in clinically normal subjects and diabetic patients with focal sensitivity loss. *British Journal of Ophthalmology* 89:1462-1467.

Goldstein M., Loewenstein A., Barak A., Baruch E., Feitt N., Yair-Pur G., Pollack A., Bukelman A., Eisner Z., Gabby A., Katz H., Gelbart Z., Shleikman E., Springer A., Schachat A.P., Bressler N.M., Belt J., Bressler S.B., Cain D., Cooney M.J., Doll W., Emmert D., Herring M., Falk R., McDonald J., Tian Y., Alster Y., Even-Chen Z., Leshno M., Rafaeli O., Malach R. & Toaff T. (2005). Results of a multicenter clinical trial to evaluate the preferential hyperacuity perimeter for detection of age-related macular degeneration. *Retina-the Journal of Retinal and Vitreous Diseases* 25:296-303.

Gordon M.O. & Kass M.A. (1999). The ocular hypertension treatment study - Design and baseline description of the participants. *Archives of Ophthalmology* 117:573-583.

Green D.G. (1968). The contrast sensitivity of the colour mechanisms of the human eye. *Journal of Physiology* 196:415-429.

Haddad S., Chen C.A., Santangelo S.L. & Seddon J.M. (2006). The genetics of age-related macular degeneration: A review of progress to date. *Survey of Ophthalmology* 51:316-363.

Haegerstrom-Portnoy G. & Brown B. (1989). Two-Color Increment Thresholds in Early Age-Related Maculopathy. *Clinical Vision Sciences* 4:165-172.

Haimovici R., Owens S.L., Fitzke F.W. & Bird A.C. (2002). Dark adaptation in age-related macular degeneration: relationship to the fellow eye. *Graefes Archive for Clinical and Experimental Ophthalmology* 240:90-95.

Hamada S., Jain S., Sivagnanavel V., Patel N.& Chong N.V. (2006). Drusen classification in bilateral drusen and fellow eye of exudative age-related macular degeneration. *Eye* 20:199-202.

Hammond B.R. & Fuld K. (1992). Interocular Differences in Macular Pigment Density. *Investigative Ophthalmology & Visual Science* 33:350-355.

Hammond B.R., CurranCelentano J., Judd S., Fuld K., Krinsky N.I., Wooten B.R. & Snodderly D.M. (1996a). Sex differences in macular pigment optical density: Relation to plasma carotenoid concentrations and dietary patterns. *Vision Research* 36:2001-2012.

Hammond B.R., Fuld K. & Snodderly D.M. (1996b). Iris color and macular pigment optical density. *Experimental Eye Research* 62:293-297.

Hammond B.R., Wooten B.R. & Snodderly D.M. (1996c). Cigarette smoking and retinal carotenoids: Implications for age-related macular degeneration. *Vision Research* 36:3003-3009.

Hammond B.R., Wooten B.R. & Snodderly D.M. (1997). Individual variations in the spatial profile of human macular pigment. *Journal of the Optical Society of America A-Optics Image Science and Vision* 14:1187-1196.

Hammond B.R., Wooten B.R. & Snodderly D.M. (1998). Preservation of visual sensitivity of older subjects: Association with macular pigment density. *Investigative Ophthalmology & Visual Science* 39:397-406.

Hart W.M., Burde R.M. (1983). 3-Dimensional Topography of the Central Visual-Field - Sparing of Foveal Sensitivity in Macular Disease. *Ophthalmology* 90:1028-1038.

Hart W.M., Silverman S.E., Trick G.L., Nesher R. & Gordon M.O. (1990). Glaucomatous Visual-Field Damage - Luminance and Color-Contrast Sensitivities. *Investigative Ophthalmology & Visual Science* 31:359-367.

Hartnett M.E., Weiter J.J., Garsd A. & Jalkh A.E. (1992). Classification of Retinal-Pigment Epithelial Detachments Associated with Drusen. *Graefes Archive for Clinical and Experimental Ophthalmology* 230:11-19.

Hartnett M.E. & Elsner A.E. (1996). Characteristics of exudative age-related macular degeneration determined in vivo with confocal and indirect infrared imaging. *Ophthalmology* 103:58-71

Hazel C.A., Petre K.L., Armstrong R.A., Benson M.T. & Frost N.A. (2000). Visual function and subjective quality of life compared in subjects with acquired macular disease. *Investigative Ophthalmology & Visual Science* 41:1309-1315.

Heijl A. (1977). Time Changes of Contrast Thresholds During Automatic Perimetry. *Acta Ophthalmologica* 55:696-708.

Heijl A. & Drance S.M. (1983). Changes in Differential Threshold in Patients with Glaucoma During Prolonged Perimetry. *British Journal of Ophthalmology* 67:512-516.

Heijl A., Lindgren G. & Olsson J. (1987a). Normal Variability of Static Perimetric Threshold Values Across the Central Visual-Field. *Archives of Ophthalmology* 105:1544-1549.

Heijl A., Lindgren G. & Olsson J. (1987b) A package for the statistical analysis of visual fields. *Doc Ophthalmol Proc Ser 49*. Proceedings of the Seventh International Visual field Symposium. Eds: E.L. Greve & A. Heijl. Dordrecht. Dr W. Junk. pp. 153-168.

Heijl A., Lindgren G. & Olsson J. (1989). The Effect of Perimetric Experience in Normal Subjects. *Archives of Ophthalmology* 107:81-86.

Heijl A., Lindgren G., Olsson J. & Åsman P. (1992). On Weighted Visual-Field Indexes. *Graefes Archive for Clinical and Experimental Ophthalmology* 230:397-398.

Heijl A. & Bengtsson B. (1996). The effect of perimetric experience in patients with glaucoma. *Archives of Ophthalmology* 114:19-22.

Heijl A., Leske M.C., Bengtsson B., Hyman L., Bengtsson B. & Hussein M. (2002). Reduction of intraocular pressure and glaucoma progression - Results from the early manifest glaucoma trial. *Archives of Ophthalmology* 120:1268-1279.

Heijl A., Leske M.C., Bengtsson B. & Hussein M. (2003). Measuring visual field progression in the early manifest glaucoma trial. *Acta Ophthalmologica Scandinavica* 81:286-293.

Henson D.B. & Emuh T. (2009) Measuring Patient Vigilance During Perimetry; The Pupillary Fatigue Index. *Investigative Ophthalmology & Visual Science* 50:E-abstract 6195.

Herse P.R. (1992). Factors Influencing Normal Perimetric Thresholds Obtained Using the Humphrey Field Analyzer. *Investigative Ophthalmology & Visual Science* 33:611-617.

Hogg R., Curry E., Muldrew A., Winder J., Stevenson M., McClure M. & Chakravarthy U. (2003). Identification of lesion components that influence visual function in age related macular degeneration. *British Journal of Ophthalmology* 87:609-614.

Hogg R.E., Stevenson M.R., Chakravarthy U., Beirne R.O. & Anderson R.S. (2007). Early Features of AMD. *Ophthalmology* 114:1028.

Holz F.G., Pauleikhoff D., Klein R. & Bird A.C. (2004). Pathogenesis of lesions in late age-related macular disease. *American Journal of Ophthalmology* 137:504-510.

Hopkins G.A. & Lyle W.M. (1977). Potential Systemic Side-Effects of 6 Common Ophthalmic Drugs. *Journal of the American Optometric Association* 48:1241-1245.

Horn F.K., Brenning A., Junemann A.G. & Lausen B. (2007). Glaucoma detection with frequency doubling perimetry and short-wave length perimetry. *Journal of Glaucoma* 16:363-371.

Hoskins H.D., Magee S.D., Drake M.V. & Kidd M.N. (1988). Confidence intervals for change in automated visual fields. *British Journal of Ophthalmology* 72:591-597.

Howarth P.A. & Bradley A. (1986). The Longitudinal Chromatic Aberration of the Human-Eye and Its Correction. *Vision Research* 26:361-366.

Huang D., Swanson E.A., Lin C.P., Schuman J.S., Stinson W.G., Chang W., Hee M.R., Flotte T., Gregory K., Puliafito C.A. & Fujimoto J.G. (1991). Optical Coherence Tomography. *Science* 254:1178-1181.

Hudson C., Wild J.M. & Archerhall J. (1993). Maximizing the Dynamic-Range of the Humphrey Field Analyzer for Blue-On-Yellow Perimetry. *Ophthalmic and Physiological Optics* 13:405-408.

Hudson C., Wild J.M. & Oneill E.C. (1994). Fatigue Effects During A Single Session of Automated Static Threshold Perimetry. *Investigative Ophthalmology & Visual Science* 35:268-280.

Hudson C., Flanagan J.G., Turner G.S., Chen H.C., Young L.B. & McLeod D. (1998). Short-wavelength sensitive visual field loss in patients with clinically significant diabetic macular oedema. *Diabetologia* 41:918-928.

Hutchings N., Wild J.M., Hussey M.K., Flanagan J.G. & Trope G.E. (2000). The long-term fluctuation of the visual field in stable glaucoma. *Investigative Ophthalmology & Visual Science* 41:3429-3436.

Hutchings N., Hosking S.L., Wild J.M. & Flanagan J.G. (2001). Long-term fluctuation in short-wavelength automated perimetry in glaucoma suspects and glaucoma patients. *Investigative Ophthalmology & Visual Science* 42:2332-2337.

Hyman L., Schachat A.P., He Q.M., Leske M.C. & Age-Related Macular Degenerat Risk Fact (2000). Hypertension, cardiovascular disease, and age-related macular degeneration. *Archives of Ophthalmology* 118:351-358.

Jackson G.R., Owsley C. & McGwin G. (1999). Aging and dark adaptation. *Vision Research* 39:3975-3982.

Jackson G.R., Owsley C. & Curcio C.A. (2002). Photoreceptor degeneration and dysfunction in aging and age-related maculopathy. *Ageing Research Reviews* 1:381-396.

Jackson G.R., Curcio C.A., Sloan K.R. & Owsley C. (2005) Photoreceptor degeneration in aging and age-related maculopathy. *Macular Degeneration.* Eds P.L. Penfold & J.M. Provis. Berlin, Heidelberg & New York. Springer Verlag. pp. 45-62.

Jackson G.R., Felix T. & Owsley C. (2006). The Scotopic Sensitivity Tester-1 and the detection of early age-related macular degeneration. *Ophthalmic and Physiological Optics* 26:431-437.

Jaffe G.J., Alvarado J.A. & Juster R.P. (1986). Age-related changes of the normal visual field. *Archives of Ophthalmology* 104:1021-1025.

Jenni A., Rammer J., Funkhouser A. & Fankhauser F. (1983) Special Octopus Software for clinical investigations. *Doc Ophthalmol Proc Ser 35.* Proceedings of the Fifth International Visual Field Symposium. Eds: E. L. Greve & A. Heijl. Dr W Junk. The Hague. pp. 351-359.

Johnson C.A., Adams A.J., Twelker J.D. & Quigg J.M. (1988a). Age-Related-Changes in the Central Visual-Field for Short-Wavelength-Sensitive Pathways. *Journal of the Optical Society of America A-Optics Image Science and Vision* 5:2131-2139.

Johnson C.A., Adams C.W. & Lewis R.A. (1988b). Fatigue Effects in Automated Perimetry. *Applied Optics* 27:1030-1037.

Johnson C.A., Adams A.J. & Lewis R.A. (1989). Evidence for A Neural Basis of Age-Related Visual-Field Loss in Normal Observers. *Investigative Ophthalmology & Visual Science* 30:2056-2064.

Johnson C. (1993a). Blue-on-yellow perimetry: a five year overview. *Perimetry Update 1992/3.* Proceedings of the Tenth International Perimetric Society Meeting. Ed: R. Mills. Amsterdam. Kugler Publications. pp.459-465.

Johnson C.A., Adams A.J., Casson E.J. & Brandt J.D. (1993b). Blue-On-Yellow Perimetry Can Predict the Development of Glaucomatous Visual Loss. *Archives of Ophthalmology* 111:645-650.

Johnson C.A., Adams A.J., Casson E.J. & Brandt J.D. (1993c). Progression of Early Glaucomatous Visual-Field Loss As Detected by Blue-On-Yellow and Standard White-On-White Automated Perimetry. *Archives of Ophthalmology* 111:651-656.

Johnson C.A. & Nelson-Quigg J.M. (1993). A prospective three-year study of response properties of normal subjects and patients during automated perimetry. *Ophthalmology* 100:269-274.

Jonas J.B., Gusek G.C., Guggenmoosholzmann I. & Naumann G.O.H. (1988). Variability of the Real Dimensions of Normal Human Optic Disks. *Graefes Archive for Clinical and Experimental Ophthalmology* 226:332-336.

Jurklies B., Weismann M., Husing J., Sutter E.E. & Bornfeld N. (2002). Monitoring retinal function in neovascular maculopathy using multifocal electroretinography - early

and long-term correlation with clinical findings. *Graefes Archive for Clinical and Experimental Ophthalmology* 240:244-264.

Just M.A., Carpenter P.A. (1980). A Theory of Reading - from Eye Fixations to Comprehension. *Psychological Review* 87:329-354.

Kabanarou S.A.& Rubin G.S. (2006). Reading with central scotomas: Is there a binocular gain? *Optometry and Vision Science* 83:789-796.

Kaiser H.J., Flammer J., Bucher P.J.M., Denatale R., Stumpfig D. & Hendrickson P. (1994). High-Resolution Perimetry of the Central Visual-Field. *Ophthalmologica* 208:10-14.

Karbassi M., Khu P.M., Singer D.M. & Chylack L.T. (1993). Evaluation of Lens Opacities Classification-System-Iii Applied at the Slitlamp. *Optometry and Vision Science* 70:923-928.

Katz J. & Sommer A. (1987). A longitudinal study of age adjusted variability of automated visual field. *Archives of Ophthalmology* 105:1083-1086.

Katz J. & Sommer A. (1988). Reliability indexes of automated perimetric tests. *Archives of Ophthalmology* 106:1252-1254.

Katz J. (2000). A comparison of the pattern- and total deviation-based Glaucoma Change Probability programs. *Investigative Ophthalmology & Visual Science* 41:1012-1016.

Katz J., Gilbert D., Quigley H.A. & Sommer A. (1997) Estimating progression of visual field loss in glaucoma. *Ophthalmology* 104:1017-1025.

Kelly D.H. (1973). Lateral inhibition in human colour mechanisms. *Journal of Physiology* 228:55-72.

Keltner J.L. & Johnson C.A. (1995). Short-Wavelength Automated Perimetry in Neuroophthalmological Disorders. *Archives of Ophthalmology* 113:475-481.

Khan J.C., Shahid H., Thurlby D.A., Bradley M., Clayton D.G., Moore A.T., Bird A. C. & Yates J.R.W. (2006). Age related macular degeneration and sun exposure, iris colour, and skin sensitivity to sunlight. *British Journal of Ophthalmology* 90:29-32.

Kirkpatrick J.N.P., Spencer T., Manivannan A., Sharp P.F. & Forrester J.V. (1995). Quantitative image-analysis of macular drusen from fundus photographs and scanning laser ophthalmoscope images. *Eye* 9:48-55

Klaver C.C.W., Assink J.J.M., van Leeuwen, R., Wolfs R.C.W., Vingerling J.R., Stijnen T., Hofman A. & De Jong P.T.V.M. (2001). Incidence and progression rates of age-related maculopathy: The Rotterdam study. *Investigative Ophthalmology & Visual Science* 42:2237-2241.

Klein M.L., Mauldin W.M. & Stoumbos V.D. (1994). Heredity and Age-Related Macular Degeneration - Observations in Monozygotic Twins. *Archives of Ophthalmology* 112:932-937.

Klein R., Davis M.D., Magli Y.L., Segal P., Klein B.E.K. & Hubbard L. (1991). The Wisconsin Age-Related Maculopathy Grading System. *Ophthalmology* 98:1128-1134.

Klein R., Wang Q., Klein B.E.K., Moss S.E. & Meuer S.M. (1995). The Relationship of Age-Related Maculopathy, Cataract, and Glaucoma to Visual-Acuity. *Investigative Ophthalmology & Visual Science* 36:182-191.

Klein R., Klein B.E., Tomany S.C., Meuer S.M. & Huang G. (2002). Ten-year incidence and progression of age-related maculopathy: the Beaver Dam Eye Study. *Ophthalmology* 109:1767-1779.

Klein R., Klein B.E.K., Marino E.K., Kuller L.H., Furberg C., Burke G.L. & Hubbard L.D. (2003). Early age-related maculopathy in the cardiovascular health study. *Ophthalmology* 110:25-33.

Klein R., Meuer S.M., Moss S.E., Klein B.E.K., Neider M.W. & Reinke J. (2004a). Detection of age-related macular degeneration using a nonmydriatic digital camera and a standard film fundus camera. *Archives of Ophthalmology* 122:1642-1646.

Klein R., Peto T., Bird A. & Vannewkirk M.R. (2004b). The epidemiology of age-related macular degeneration. *American Journal of Ophthalmology* 137:486-495.

Klein R., Klein B.E.K., Knudtson M.D., Meuer S.M., Swift M. & Gangnon R.E. (2007). Fifteen-year cumulative incidence of age-related macular degeneration. *Ophthalmology* 114:253-262.

Klein R., Meuer S.M., Knudtson M.D., Iyengar S.K. & Klein B.E.K. (2008a). The epidemiology of retinal reticular drusen. *American Journal of Ophthalmology* 145:317-326.

Klein R., Meuer S.M., Knudtson M.D. & Klein B.E.K. (2008b). The Epidemiology of Progression of Pure Geographic Atrophy: The Beaver Dam Eye Study. *American Journal of Ophthalmology* 146:692-699.

Kleiner R.C., Enger C., Alexander M.F. & Fine S.L. (1988). Contrast Sensitivity in Age-Related Macular Degeneration. *Archives of Ophthalmology* 106:55-57.

Kono Y., Sample P.A., Emdadi A. & Weinreb R.N. (2000). Comparative study between pointwise and ranked threshold distribution analyses of change in serial fields for short-wavelength automated perimetry. *Journal of Glaucoma* 9:419-427.

Kulze J.C., Stewart W.C. & Sutherland S.E. (1990). Factors Associated with A Learning Effect in Glaucoma Patients Using Automated Perimetry. *Acta Ophthalmologica* 68:681-686.

Kwon Y.H., Park H.J., Jap A., Ugurlu S. & Caprioli J. (1998). Test-retest variability of blue-on-yellow perimetry is greater than white-on-white perimetry in normal subjects. *American Journal of Ophthalmology* 126:29-36.

Landers J., Sharma A., Goldberg, I. & Graham, S. (2003a). A comparison of perimetric results with the Medmont and Humphrey perimeters. *British Journal of Ophthalmology* 87:690-694.

Landers J.A., Goldberg I. & Graham S.L. (2003b). Detection of early visual field loss in glaucoma using frequency-doubling perimetry and short-wavelength automated perimetry. *Archives of Ophthalmology* 121:1705-1710.

Landers J., Sharma A., Goldberg, I. & Graham S. (2006). Topography of the frequency doubling perimetry visual field compared with that of short wavelength and achromatic automated perimetry visual fields. *British Journal of Ophthalmology* 90:70-74.

Landis J.R. & Koch G.G. (1977). Measurement of Observer Agreement for Categorical Data. *Biometrics* 33:159-174.

Leeprechanon N., Giaconi J.A., Manassakorn A., Hoffman D. & Caprioli J. (2007). Frequency doubling perimetry and short-wavelength automated perimetry to detect early glaucoma. *Ophthalmology* 114:931-937.

Legge G.E., Rubin G.S., Pelli D.G. & Schleske M.M. (1985). Psychophysics of Reading .2. Low Vision. *Vision Research* 25:253-265.

Legge G.E., Mullen K.T., Woo G.C. & Campbell F.W. (1987). Tolerance to Visual Defocus. *Journal of the Optical Society of America A-Optics Image Science and Vision* 4:851-863.

Legge G.E., Ross J.A., Isenberg L.M. & Lamay J.M. (1992). Psychophysics of Reading - Clinical Predictors of Low-Vision Reading Speed. *Investigative Ophthalmology & Visual Science* 33:677-687.

Lewis R.A., Johnson C.A. & Adams A.J. (1993). Automated Perimetry and Short-Wavelength Sensitivity in Patients with Asymmetric Intraocular Pressures. *Graefes Archive for Clinical and Experimental Ophthalmology* 231:274-278.

Li J., Tso M.O.M. & Lam T.T. (2001). Reduced amplitude and delayed latency in foveal response of multifocal electroretinogram in early age related macular degeneration. *British Journal of Ophthalmology* 85:287-290.

Loewenstein A., Malach R., Goldstein M., Leibovitch I., Barak A., Baruch E., Alster Y., Rafaeli O., Avni I. & Yassur Y. (2003). Replacing the Amsler grid - A new method for monitoring patients with age-related macular degeneration. *Ophthalmology* 110:966-970.

Maguire C. (1971). Ametropia in the visual field. *Transactions of the Ophthalmological Societies of the UK* 91:663-678.

Manassakorn A., Nouri-Mahdavi K., Kouecheki B., Law S.K. & Caprioli J. (2006). Pointwise linear regression analysis for detection of visual field progression with absolute versus corrected threshold sensitivities. *Investigative Ophthalmology & Visual Science* 47:2896-2903.

Manivannan A., Kirkpatrick J.N.P., Sharp P.F. & Forrester J.V. (1994).Clinical investigation of an infrared digital scanning laser ophthalmoscope. *British Journal of Ophthalmolgy* 78:84-90

Mansour A.M., Walsh J.B. & Henkind P. (1990). Optic disc size in central retinal vein occlusion. *Ophthalmology* 97:165-166.

Marchini G., Pisano F. & Bertagnin F. (1991). Perimetric learning effect in glaucoma patients. *Glaucoma* 13:102-106.

Mayer M.J., Ward B., Klein R., Talcott J.B., Dougherty R.F. & Glucs A. (1994). Flicker Sensitivity and Fundus Appearance in Pre-Exudative Age-Related Maculopathy. *Investigative Ophthalmology & Visual Science* 35:1138-1149.

McClure M.E., Hart P.M., Jackson A.J., Stevenson M.R., Chakravarthy U. (2000). Macular degeneration: do conventional measurements of impaired visual function equate with visual disability? *British Journal of Ophthalmology* 84:244-250.

McNaught A.I., Crabb D.P., Fitzke F.W., Hitchings R.A. (1996). Visual field progression: comparison of Humphrey Statpac2 and pointwise linear regression analysis. *Graefes Archive for Clinical and Experimental Ophthalmology* 234:411-418.

McMahon T.T., Hansen M. & Viana M. (1991). Fixation Characteristics in Macular Disease - Relationship Between Saccadic Frequency, Sequencing, and Reading Rate. *Investigative Ophthalmology & Visual Science* 32:567-574.

Medeiros N.E. & Curcio C.A. (2001). Preservation of ganglion cell layer neurons in age-related macular degeneration. *Investigative Ophthalmology & Visual Science* 42:795-803.

Midena E., Segato T., Blarzino M.C. & Angeli C.D. (1994). Macular Drusen and the Sensitivity of the Central Visual-Field. *Documenta Ophthalmologica* 88:179-185.

Midena E., Angeli C.D., Blarzino M.C., Valenti M. & Segato T. (1997). Macular function impairment in eyes with early age-related macular degeneration. *Investigative Ophthalmology & Visual Science* 38:469-477.

Midena E., Cavarzeran F. & Microperimetry Study Group (2006). Normal Age–Related Values for Fundus–Related Perimetry (Microperimetry) with MP1 Microperimeter. *Investigative Ophthalmology & Visual* Science 47:E-Abstract 5349.

Midena E., Vujosevic S., Convento E., Manfre A., Cavarzeran F. & Pilotto E. (2007). Microperimetry and fundus autofluorescence in patients with early age-related macular degeneration. *British Journal of Ophthalmology* 91:1499-1503.

Mikelberg F.S., Schulzer M., Drance S.M. & Lau W. (1986). The Rate of Progression of Scotomas in Glaucoma. *American Journal of Ophthalmology* 101:1-6.

Mills R.P., Barnebey H.S., Migliazzo C.V. & Li Y. (1994). Does Saving Time Using Fastpac Or Suprathreshold Testing Reduce Quality of Visual-Fields. *Ophthalmology* 101:1596-1603.

Milton R.C., Clemons T.E., Kurinij N., Sperduto R.D. & Age Related Eye Dis Study Res Grp (2005). Risk factors for the incidence of advanced age-related macular degeneration in the age-elated eye disease study (AREDS) - AREDS report no.19. *Ophthalmology* 112:533-539.

Mitchell P., Smith W. & Wang J. J. (1998). Iris color, skin sun sensitivity, and age-related maculopathy. The Blue Mountains Eye Study. *Ophthalmology* 105:1359-1363.

Mitchell P., Wang J.J., Foran S. & Smith W. (2002). Five-year incidence of age-related maculopathy lesions: The Blue Mountains Eye Study. *Ophthalmology* 109:1092-1097.

Morgan R.K., Feuer W.J. & Anderson D.R. (1991). Statpac-2 Glaucoma Change Probability. *Archives of Ophthalmology* 109:1690-1692.

Moss I.D., Wild J.M.& Whitaker D.J. (1995). The influence of age-related cataract on blue-on-yellow perimetry. *Investigative Ophthalmology & Visual Science* 36:764-773.

Navarro R., Gonzalez L. & Hernandez-Matamoros J.L. (2006). On the prediction of optical aberrations by personalized eye models. *Optometry and Vision Science* 83:371-381.

Neelam K., O'Gorman N., Nolan J., O'Donovan O., Wong H.B., Eong K.G.A. & Beatty S. (2005). Measurement of macular pigment: Raman spectroscopy versus heterochromatic flicker photometry. *Investigative Ophthalmology & Visual Science* 46:1023-1032.

Neelam K., Muldrew A., Hogg R., Stack J., Chakravartry U. & Beatty S. (2009a). Grading of Age-Related Maculopathy Slit-Lamp Biomicroscopy Versus An Accredited Grading Center. *Retina-the Journal of Retinal and Vitreous Diseases* 29:192-198.

Neelam K., Nolan J., Chakravarthy U. & Beatty S. (2009b). Psychophysical Function in Age-related Maculopathy. *Survey of Ophthalmology* 54:167-210.

Nicolas C.M., Robman L.D., Tikellis G., Dimitrov P.N., Dowrick A., Guymer R.H. & McCarty C.A. (2003). Iris colour, ethnic origin and progression of age-related macular degeneration. *Clinical and Experimental Ophthalmology* 31:465-469.

Nolan J.M., Stack J., Donovan O.O., Loane E. & Beatty S. (2007). Risk factors for age-related maculopathy are associated with a relative lack of macular pigment. *Experimental Eye Research* 84:61-74.

Nouri-Mahdavi K., Hoffman D., Ralli M. & Caprioli J. (2007). Comparison of methods to predict visual field progression in glaucoma. *Arch.Ophthalmol.* 125:1176-1181.

O'Brien C., Poinooswamy D., Wu J. & Hitchins R. (1994). Evaluation of the Humphrey FASTPAC threshold program in glaucoma. *British Journal of Ophthalmology* 78:516-519.

Ogle KN (1960). Blurring of the retinal image and contrast thresholds in the fovea.. *Journal of the Optical Society of America* 50 307-315.

Olsson J., Åsman P. & Heijl A. (1997). A perimetric learner's index. *Acta Ophthalmologica Scandinavica* 75:665-668.

O'Regan J.K. (1980). The control of saccade size and fixation duration in reading: The limits of linguistic control. *Perception & Psychophysics* 28:112-117.

Owsley C., Jackson G.R., Cideciyan A.V., Huang Y.J., Fine S.L., Ho A.C., Maguire M.G., Lolley V. & Jacobson S.G. (2000). Psychophysical evidence for rod vulnerability in age-related macular degeneration. *Investigative Ophthalmology & Visual Science* 41:267-273.

Owsley C., Jackson G.R., White M., Feist R. & Edwards D. (2001). Delays in rod-mediated dark adaptation in early age-related maculopathy. *Ophthalmology* 108:1196-1202.

Panda-Jonas S., Jonas J.B. & Jakobczyk-Zmija M. (1995). Retinal photoreceptor density decreases with age. *Ophthalmology* 102:1853-1859.

Patton N., Aslam T.M., MacGillivray T., Deary I.J., Dhillon B., Eikelboom R.H., Yogesan K. & Constable I.J. (2006) Retinal image analysis: Concepts, applications and potential. *Progress in Retinal and Eye Research* 25:99-127

Pease P.L., Adams A.J. & Nuccio E. (1987). Optical-Density of Human Macular Pigment. *Vision Research* 27:705-710.

Peli E. & Lahav M. (1986). Drusen measurement from fundus photographs using computer image analysis. *Ophthalmology* 93:575-580.

Pease P.L., Adams A.J. & Nuccio E.(1987).Optical-Density of Human Macular Pigment. *Vision Research* 27:705-710.

Phipps J.A., Dang T.M., Vingrys A.J. & Guymer R.H. (2004). Flicker perimetry losses in age-related macular degeneration. *Investigative Ophthalmology & Visual Science* 45:3355-3360.

Pieroni C.G., Witkin A.J., Ko T.H., Fujimoto J.G., Chan A., Schuman J.S., Ishikawa H., Reichel E. & Duker J.S. (2006). Ultrahigh resolution optical coherence tomography in non-exudative age related macular degeneration. *British Journal of Ophthalmology* 90:191-197.

Polo V., Larrosa J.M., Pinilla I., Perez S., Gonzalvo F. & Honrubia F.M. (2002). Predictive value of short-wavelength automated perimetry - A 3-year follow-up study. *Ophthalmology* 109:761-765.

Rabbetts RB. (1998) The eye's optical system. *Bennet & Rabbetts' Clinical Visual Optics.* Ed: R.B.Rabbetts. Oxford. Butterworth-Heinemann 3rd edition. pp.7-18.

Rabin J. & Adams A.J. (1990). Visual-Acuity and Contrast Sensitivity of the S-Cone Pathway - Preliminary Measures with Letter Charts. *Optometry and Vision Science* 67:799-802.

Rabineau P.A., Gloor B. & Tobler H.J. (1985). Fluctuations in threshold and effect of fatigue in automated static perimetry. *Doc Ophthalmol Proc Ser 42.* Proceedings of the Sixth International Visual Field Symposium. Eds: A. Heijl & E. L. Greve. Dordrecht. Dr W Junk. pp. 25-33.

Rapantzikos K., Zervakis M. & Balas K. (2003). Detection and segmentation of drusen deposits on human retina: Potential in the diagnosis of age-related macular degeneration. *Medical Image Analysis* 7:95-108.

Reitner A., Tittl M., Ergun E. & BaradaranDilmaghani R. (1996). The efficient use of perimetry for neuro-ophthalmic diagnosis. *British Journal of Ophthalmology* 80:903-905.

Remky A., Arend O. & Toonen F. (1998). Infrared imaging of central serous chorioretinopathy: A follow-up study. *Acta Ophthalmologica Scandinavica* 76:339-342

Remky A., Beausencourt E., Hartnett M.E., Trempe C.L., Arend O. & Elsner A.E. (1999). Infrared imaging of cystoid macular edema. *Graefes Archive for Clinical and Experimental Ophthalmology* 237:897-901

Remky A., Arend O. & Hendricks S. (2000). Short-wavelength automated perimetry and capillary density in early diabetic maculopathy. *Investigative Ophthalmology & Visual Science* 41:274-281.

Remky A., Elsner A.E., Morandi A.J., Beausencourt E. & Trempe C.L. (2001a) Blue-on-yellow perimetry with a scanning laser ophthalmoscope: small alterations in the central macula with aging. *Journal of the Optical Society of America – A* 18:1425-1436.

Remky A., Lichtenberg K., Elsner A.E. & Arend O. (2001b). Short wavelength automated perimetry in age related maculopathy. *British Journal of Ophthalmology* 85:1432-1436.

Remky A., Weber A., Hendricks S., Lichtenberg K. & Arend O. (2003). Short-wavelength automated perimetry in patients with diabetes mellitus without macular edema. *Graefes Archive for Clinical and Experimental Ophthalmology* 241:468-471.

Remky A. & Elsner A.E. (2005). Blue on yellow perimetry with scanning laser ophthalmoscopy in patients with age related macular disease. *British Journal of Ophthalmology* 89:464-469.

Rohrschneider K., Springer C., Bultmann S. & Volcker H.E. (2005). Microperimetry - Comparison between the Micro Perimeter 1 and scanning laser ophthalmoscope - Fundus perimetry. *American Journal of Ophthalmology* 139:125-134.

Rohrschneider K., Bultmann S. & Springer C. (2008). Use of fundus perimetry (microperimetry) to quantify macular sensitivity. *Progress in Retinal and Eye Research* 27:536-548.

Rossetti L., Fogagnolo P., Miglior S., Centofanti M., Vetrugno M. & Orzalesi N. (2006). Learning effect of short-wave length automated perimetry in patients with ocular hypertension. *Journal of Glaucoma* 15:399-404.

Rucker F.J. & Kruger P.B. (2001). Isolated short-wavelength sensitive cones can mediate a reflex accommodation response. *Vision Research* 41:911-922.

Rucker F.J. & Kruger P.B. (2004). The role of short-wavelength sensitive cones and chromatic aberration in the response to stationary and step accommodation stimuli. *Vision Research* 44:197-208.

Rutishauser C., Flammer J. & Haas A. (1989). The Distribution of Normal Values in Automated Perimetry. *Graefes Archive for Clinical and Experimental Ophthalmology* 227:513-517.

Rynders M., Lidkea B., Chisholm W. & Thibos L.N. (1995). Statistical Distribution of Foveal Transverse Chromatic Aberration, Pupil Centration, and Angle-Psi in A Population of Young-Adult Eyes. *Journal of the Optical Society of America A-Optics Image Science and Vision* 12:2348-2357.

Saine P.J. & Tyler M.E. (1997) *Ophthalmic photography, a textbook of fundus photography, angiography and electronic imaging.* Boston & Oxford. Butterworth-Heinemann

Sample P.A., Esterson F.D., Weinreb R.N. & Boynton R.M. (1988). The aging lens: in vivo assessment of light absorption in 84 human eyes. *Investigative Ophthalmology & Visual Science* 29:1306-1311.

Sample P.A., Esterson F.D. & Weinreb R.N. (1989). A practical method for obtaining an index of lens density with an automated perimeter. *Investigative Ophthalmology & Visual Science* 30:786-787.

Sample P.A. & Weinreb R.N. (1990). Color Perimetry for Assessment of Primary Open-Angle Glaucoma. *Investigative Ophthalmology & Visual Science* 31:1869-1875.

Sample P.A. & Weinreb R.N. (1992). Progressive Color Visual-Field Loss in Glaucoma. *Investigative Ophthalmology & Visual Science* 33:2068-2071.

Sample P.A., Taylor J.D.N., Martinez G.A., Lusky M. & Weinreb R.N. (1993). Short-Wavelength Color Visual-Fields in Glaucoma Suspects at Risk. *American Journal of Ophthalmology* 115:225-233.

Sample P.A., Martinez G.A. & Weinreb R.N. (1994). Short-Wavelength Automated Perimetry Without Lens Density Testing. *American Journal of Ophthalmology* 118:632-641.

Sample P.A., Johnson C.A., HaegerstromPortnoy G. & Adams A.J. (1996). Optimum parameters for short-wavelength automated perimetry. *Journal of Glaucoma* 5:375-383.

Sample P.A., Irak I., Martinez G.A. & Yamagishi N. (1997). Asymmetries in the normal short-wavelength visual field: Implications for short-wavelength automated perimetry. *American Journal of Ophthalmology* 124:46-52.

Sanabria O., Feuer W.J. & Anderson D.R. (1991). Pseudo-Loss of Fixation in Automated Perimetry. *Ophthalmology* 98:76-78.

Sandberg M.A., Weiner A., Miller S. & Gaudio A.R. (1998). High-risk characteristics of fellow eyes of patients with unilateral neovascular age-related macular degeneration. *Ophthalmology* 105:441-447.

Sarks S.H., Arnold J.J., Killingsworth M.C. & Sarks J.P. (1999). Early drusen formation in the normal and aging eye and their relation to age related maculopathy: a clinicopathological study. *British Journal of Ophthalmology* 83:358-368.

Schimiti R.B., Avelino R.R., Kara-Jose N. & Costa V.P. (2002). Full-threshold versus Swedish interactive threshold algorithm (SITA) in normal individuals undergoing automated perimetry for the first time. *Ophthalmology* 109:2084-2092.

Schnapf J.L., Kraft T.W. & Baylor D.A. (1987). Spectral Sensitivity of Human Cone Photoreceptors. *Nature* 325:439-441.

Schneider U., Inhoffen W., Gelisken F. & Kreissig I. (1996). Assessment of visual function in choroidal neovascularization with scanning laser microperimetry and

simultaneous indocyanine green angiography. *Graefes Archive for Clinical and Experimental Ophthalmology* 234:612-617.

Scholl H.P.N., Peto T., Dandekar S., Bunce C., Xing W., Jenkins S. & Bird A.C. (2003). Inter- and intra-observer variability in grading lesions of age-related maculopathy and macular degeneration. *Graefes Archive for Clinical and Experimental Ophthalmology* 241:39-47.

Scholl H.P.N., Bellmann C., Dandekar S.S., Bird A.C. & Fitzke F.W. (2004). Photopic and scotopic fine matrix mapping of retinal areas of increased fundus autofluorescence in patients with age-related maculopathy. *Investigative Ophthalmology & Visual Science* 45:574-583.

Schwartz S.H. (2004) *Visual Perception: A Clinical Orientation.* Eds: S.H.Schwartz. 3rd edn. McGraw-Hill. pp.23-59.

Searle A.E. T., Wild J.M., Shaw D.E. & Oneill E.C. (1991). Time-Related Variation in Normal Automated Static Perimetry. *Ophthalmology* 98:701-707.

Seddon J.M., Ajani U.A., Sperduto R.D., Hiller R., Blair N., Burton T.C., Farber M.D., Gragoudas E.S., Haller J., Miller D.T. & et a. (1994). Dietary carotenoids, vitamins A, C, and E and advanced age-related macular degeneration. Eye Disease Case-Control Study Group. *Jounal of the American Medical Association* 272:1413-1420.

Seddon J.M., Willett W.C., Speizer F.E. & Hankinson S.E. (1996). A prospective study of cigarette smoking and age-related macular degeneration in women. *Journal of the American Medical Association* 276:1141-1146.

Seddon J.M., Cote J., Davis N. & Rosner B. (2003a). Progression of age-related macular degeneration - Association with body mass index, waist circumference, and waist-hip ratio. *Archives of Ophthalmology* 121:1728-1737.

Seddon J.M., Cote J. & Rosner B. (2003b). Progression of age-related macular degeneration - Association with dietary fat, transunsaturated fat, nuts, and fish intake. *Archives of Ophthalmology* 121:785-792.

Seddon J.M., Sharma S. & Adelman R.A. (2006). Evaluation of the Clinical Age-Related Maculopathy Staging System. *Ophthalmology* 113:260-266.

Seidemann A. & Schaeffel F. (2002). Effects of longitudinal chromatic aberration on accommodation and emmetropization. *Vision Research* 42:2409-2417.

Seiple W., Szlyk J.P., McMahon T., Pulido J. & Fishman G.A. (2005). Eye-movement training for reading in patients with age-related macular degeneration. *Investigative Ophthalmology & Visual Science* 46:2886-2896.

Shah V.A., Chalam K.V. (2009). Values for Macular Perimetry Using the MP-1 Microperimeter in Normal Subjects. *Ophthalmic Research* 41:9-13.

Sheu S.J., Chen Y.Y., Chou L.C., Wu T.T. & Cheng K.K. (2002). Frequency doubling technology perimetry in age-related macular degeneration. *Journal of the Chinese Medical Association* 65:435-440

Shin D. & Berger J. (1999). Digital fundus imaging and analysis. *Age-Related Macular Degeneration.* Eds:, S.L. Fine, J. Berger & M. Maguire. St Louis. Mosby Inc. pp. 207-218.

Shirato S., Inoue R., Fukushima K. & Suzuki Y. (1999). Clinical evaluation of SITA: a new family of perimetric testing strategies. *Graefes Archive for Clinical and Experimental Ophthalmology* 237:29-34.

Sloan L.L. (1961). Area and luminance of test object as variables in examination of the visual field by projection perimetry. *Vision Research* 1:121-124.

Sivagnanavel V., Smith R.T., Lau G.B., Chan J., Donaldson C. & Chong N.V. (2005). An interinstitutional comparative study and validation of computer aided drusen quantification. *British Journal of Ophthalmology* 89:554-557

Smith R.T., Nagasaki T., Sparrow J.R., Barbazetto I., Klaver C.C.W. & Chan J.K. (2003). A method of drusen measurement based on the geometry of fundus reflectance. *Biomedical Engineering Online* 2:10.

Smith R.T., Chan J.K., Nagasaki T., Sparrow J.R. & Barbazetto I. (2005a). A method of drusen measurement based on reconstruction of fundus background reflectance. *British Journal of Ophthalmology* 89:87-91.

Smith R.T., Chan J.K., Nagasaki T., Ahmad U.F., Barbazetto I., Sparrow J., Figueroa M. & Merriam J. (2005b). Automated detection of macular drusen using geometric background leveling and threshold selection. *Archives of Ophthalmology* 123:200-206.

Smith R.T., Chan J.K., Busuoic M., Sivagnanavel V., Bird A.C. & Chong N.V. (2006). Autofluorescence characteristics of early, atrophic, and high-risk fellow eyes in age-related macular degeneration. *Investigative Ophthalmology & Visual Science* 47:5495-5504.

Smith S.D., Katz J. & Quigley H.A. (1996). Analysis of progressive change in automated visual fields in glaucoma. *Investigative Ophthalmology & Visual Science* 37:1419-1428.

Snodderly D.M., Auran J.D. & Delori F.C. (1984). The macular pigment. II. Spatial distribution in primate retinas. *Investigative Ophthalmology & Visual Science* 25:674-685.

Springer C., Bultmann S., Volcker H.E. & Rohrschneider K. (2005). Fundus perimetry with the micro perimeter 1 in normal individuals - Comparison with conventional threshold perimetry. *Ophthalmology* 112:848-854.

Steinmetz R.L., Haimovici R., Jubb C., Fitzke F.W. & Bird A.C. (1993). Symptomatic Abnormalities of Dark-Adaptation in Patients with Age-Related Bruchs Membrane Change. *British Journal of Ophthalmology* 77:549-554.

Stangos N., Voutas S., Topouzis F. & Karampatakis V. (1995). Contrast Sensitivity Evaluation in Eyes Predisposed to Age-Related Macular Degeneration and Presenting Normal Visual-Acuity. *Ophthalmologica* 209:194-198.

Strouthidis N.G., Vinciotti V., Tucker A.J., Gardiner S.K., Crabb D.P. & Garway-Heath D.F. (2006). Structure and function in glaucoma: The relationship between a functional

visual field map and an anatomic retinal map. *Investigative Ophthalmology & Visual Science* 47:5356-5362.

Strouthidis N.G., Scott A., Viswanathan A.C., Crabb D.P. & Garway-Heath D.F. (2007). Monitoring glaucomatous visual field progression: The effect of a novel spatial filter. *Investigative Ophthalmology & Visual Science* 48:251-257.

Sunness J.S., Massof R.W., Bressler N.M. & Bressler S.B. (1989). S-Cone Pathway Sensitivity in Eyes with High-Risk and Low-Risk Drusen Characteristics. *Applied Optics* 28:1158-1164.

Sunness J.S., Rubin G.S., Applegate C.A., Bressler N.M., Marsh M.J., Hawkins B.S. & Haselwood D. (1997). Visual function abnormalities and prognosis in eyes with age-related geographic atrophy of the macula and good visual acuity. *Ophthalmology* 104:1677-1691.

Sunness J.S. (1999). The natural history of geographic atrophy, the advanced atrophic form of age-related macular degeneration. *Molecular Vision* 5:25

Sunness J.S., Gonzalez-Baron J., Applegate C.A., Bressler N.M., Tian Y., Hawkins B., Barron Y. & Bergman A. (1999). Enlargement of atrophy and visual acuity loss in the geographic atrophy form of age-related macular degeneration. *Ophthalmology* 106:1768-1779.

Sunness J.S., Rubin G.S., Broman A., Applegate C.A., Bressler N.M. & Hawkins B.S. (2008). Low luminance visual dysfunction as a predictor of subsequent visual acuity loss from geographic atrophy in age-related macular degeneration. *Ophthalmology* 115:1480-1488.

Swanson W.H. (1989). Short Wavelength Sensitive Cone Acuity - Individual-Differences and Clinical Use. *Applied Optics* 28:1151-1157.

Swann P.G. & Lovie-Kitchin J.E. (1991). Age-Related Maculopathy .2. the Nature of the Central Visual-Field Loss. *Ophthalmic and Physiological Optics* 11:59-70.

Swanson W.H. (1989). Short Wavelength Sensitive Cone Acuity - Individual-Differences and Clinical Use. *Applied Optics* 28:1151-1157.

Taft M. (1979). Recognition of affixed words and the word frequency effect. *Memory & Cognition* 7:263-272.

Takahashi G., Aoki Y. & Kitahara K. (1999). Short term fluctuation of blue-on-yellow perimetry in normal eyes. *Nippon Ganka Gakkai Zasshi* 103:108-111.

Takamine Y., Shiraki K., Moriwaki M., Yasunari T. & Miki T. (1998). Retinal sensitivity measurement ever drusen using scanning laser ophthalmoscope microperimetry. *Graefes Archive for Clinical and Experimental Ophthalmology* 236:285-290.

Teesalu P., Airaksinen P.J., Tuulonen A., Nieminen H. & Alanko H. (1997). Fluorometry of the crystalline lens for correcting blue-on-yellow perimetry results. *Investigative Ophthalmology & Visual Science* 38:697-703.

Thibos L. & Bradley A. (1993) New methodologies for discriminating neural and optical losses of vision. *Optometry and Vision Science* 70:279-287

Thibos L.N., Ye M., Zhang X.X. & Bradley A. (1992). The Chromatic Eye - A New Reduced-Eye Model of Ocular Chromatic Aberration in Humans. *Applied Optics* 31:3594-3600.

Thornton J., Edwards R., Mitchell P., Harrison R.A., Buchan I. & Kelly S.P. (2005). Smoking and age-related macular degeneration: a review of association. *Eye* 19:935-944.

Thorndyke P.W. (1977). Cognitive structures in comprehension and memory of narrative discourse. *Cognitive Psychology* 9:77-110.

Tikellis G., Robman L.D., Harper A., Mcneil J.J., Taylor H.R. & McCarty C.A. (2000). Methods for detecting age-related maculopathy: a comparison between photographic and clinical assessment. *Clinical and Experimental Ophthalmology* 28:367-372.

Tikellis G., Robman L.D., Dimitrov P., Nicolas C., McCarty C.A. & Guymer R.H. (2006). Characteristics of progression of early Age-related macular degeneration: the Cardiovascular Health and Age-related maculopathy Study. *Eye* 21:169-176.

Timberlake G.T., Mainster M.A., Peli E., Augliere R.A., Essock E.A. & Arend L.E. (1986). Reading with A Macular Scotoma .1. Retinal Location of Scotoma and Fixation Area. *Investigative Ophthalmology & Visual Science* 27:1137-1147.

Tolentino M.J., Miller S., Gaudio A.R. & Sandberg M.A. (1994). Visual-Field Deficits in Early Age-Related Macular Degeneration. *Vision Research* 34:409-413.

Turpin A., McKendrick A.M., Johnson C.A. & Vingrys A.J. (2003). Properties of perimetric threshold estimates from Full Threshold, ZEST, and SITA-like strategies, as determined by computer simulation. *Investigative Ophthalmology & Visual Science* 44:4787-4795.

UK National Screening Committee. Essential Elements in Developing a Diabetic Retinopathy Screening Programme. Workbook 4 (release 4.3 June 2009). http://www.retinalscreening.nhs.uk/

van Leeuwen R., Chakravarthy U., Vingerling J.R., Brussee C., Hooghart A.J., Mulder P.G. & de Jong P.T. (2003a). Grading of age-related maculopathy for epidemiological studies: is digital imaging as good as 35-mm film?. *Ophthalmology* 110:1540-1544.

van Leeuwen R., Klaver C.C., Vingerling J.R., Hofman A. & de Jong P.T. (2003b). The risk and natural course of age-related maculopathy: follow-up at 6 1/2 years in the Rotterdam study. *Archives of Ophthalmology* 121:519-526.

Viswanathan A.C., Fitzke F.W. & Hitchings R. A. (1997). Early detection of visual field progression in glaucoma: a comparison of PROGRESSOR and STATPAC 2. *British Journal of Ophthalmology* 81:1037-1042.

Viswanathan A.C., Crabb D.P., McNaught A.I., Westcott M.C., Kamal D., Garway-Heath D.F., Fitzke F.W. & Hitchings R.A. (2003). Interobserver agreement on visual field progression in glaucoma: a comparison of methods. *British Journal of Ophthalmology* 87:726-730.

von Rückmann A., Fitzke F.W. & Bird A.C. (1997). Fundus autofluorescence in age-related macular disease imaged with a laser scanning ophthalmoscope. *Investigative Ophthalmology & Visual Science* 38:478-486.

Wang J.J., Jakobsen K.B., Smith W. & Mitchell P. (2004). Refractive status and the 5-year incidence of age-related maculopathy: the Blue Mountains Eye Study. *Clinical and Experimental Ophthalmology* 32:255-258.

Webb R.H., Hughes G.W. & Delori F.C. (1987) Confocal scanning laser ophthalmoscope. *Applied Optics* 26:492-499.

Weber J. & Krieglstein G.K. (1989). Graphical Analysis of Topographical Trends (Gatt) in Automated Perimetry. *International Ophthalmology* 13:351-356.

Weinreb R.N. & Perlman J.P. (1986). The Effect of Refractive Correction on Automated Perimetric Thresholds. *American Journal of Ophthalmology* 101:706-709.

Werner E.B. & Drance S.M. (1977). Early visual field disturbances in glaucoma. *Archives of Ophthalmology* 106:619-623.

Werner E.B., Petrig B., Krupin T. & Bishop K.I. (1989). Variability of Automated Visual-Fields in Clinically Stable Glaucoma Patients. *Investigative Ophthalmology & Visual Science* 30:1083-1089.

Werner E.B., Krupin T., Adelson A. & Feitl M.E. (1990). Effect of patient experience on the results of automated perimetry in glaucoma suspect patients. *Ophthalmology* 97:44-48.

Werner J.S. & Steele V.G. (1988). Sensitivity of Human Foveal Color Mechanisms Throughout the Life-Span. *Journal of the Optical Society of America A-Optics Image Science and Vision* 5:2122-2130.

White A.J.R., Sun H., Swanson W.H. & Lee B.B. (2002). An examination of physiological mechanisms underlying the frequency-doubling illusion. *Investigative Ophthalmology & Visual Science* 43:3590-3599.

White J.M. & Bedell H.E. (1990). The Oculomotor Reference in Humans with Bilateral Macular Disease. *Investigative Ophthalmology & Visual Science* 31:1149-1161.

Whittaker S.G., Cummings R.W. & Swieson L.R. (1991). Saccade Control Without A Fovea. *Vision Research* 31:2209-2218.

Wild J.M., Denglerharles M., Searle A.E.T., Oneill E.C. & Crews S.J. (1989). The Influence of the Learning Effect on Automated Perimetry in Patients with Suspected Glaucoma. *Acta Ophthalmologica* 67:537-545.

Wild J.M., Searle A.E.T., Denglerharles M. & Oneill E.C. (1991). Long-Term Follow-Up of Base-Line Learning and Fatigue Effects in the Automated Perimetry of Glaucoma and Ocular Hypertensive Patients. *Acta Ophthalmologica* 69:210-216.

Wild J.M. & Hudson C. (1995). The Attenuation of Blue-On-Yellow Perimetry by the Macular Pigment. *Ophthalmology* 102:911-917.

Wild J.M., Moss I.D., Whitaker D. & O'Neill E.C. (1995). The statistical interpretation of blue-on-yellow visual field loss. *Investigative Ophthalmology & Visual Science* 36:1398-1410.

Wild J.M. & Moss I.D. (1996). Baseline alterations in blue-on-yellow normal perimetric sensitivity. *Graefes Archive for Clinical and Experimental Ophthalmology* 234:141-149.

Wild J.M., Cubbidge R.P., Pacey I.E. & Robinson R. (1998). Statistical aspects of the normal visual field in short-wavelength automated perimetry. *Investigative Ophthalmology & Visual Science* 39:54-63.

Wild J.M., Pacey I.E., Hancock S.A. & Cunliffe I.A. (1999). Between-algorithm, between-individual differences in normal perimetric sensitivity: Full threshold, FASTPAC, and SITA. *Investigative Ophthalmology & Visual Science* 40:1152-1161.

Wild J.M. (2001). Short wavelength automated perimetry. *Acta Ophthalmologica Scandinavica* 79:546-559.

Wild J.M., Kim L.S., Pacey I.E. & Cunliffe I.A. (2006). Evidence for a Learning Effect in Short-Wavelength Automated Perimetry. *Ophthalmology* 113:206-215.

Wilkins M.R., Fitzke F.W. & Khaw P.T. (2006). Pointwise linear progression criteria and the detection of visual field change in a glaucoma trial. *Eye* 20:98-106.

Williams D.R., Collier R.J. & Thompson B.J. (1983). Spatial Resolution of the Short-Wavelength Mechanism. In *Colour Vision: Physiology and Psychophysics.* Eds: J.D. Mollon & L..T. Sharpe. Academic Press. London. pp. 487-503.

Williams D.R., Sekiguchi N., Haake W., Brainard D. & Packer O. (1991) The cost of trichromacy for spatial vision. In *From Pigments to Perception*. Eds: A. Valberg & B.B. Lee. Plenum Press. New York, London. pp.11-22.

Wolf S. (2006). Macular pigment measurements: which method should we use? *Graefes Archive for Clinical and Experimental Ophthalmology* 244:1562-1564.

Wolf-Schnurrbusch U.E.K., Enzmann V., Brinkmann C.K. & Wolf S. (2008). Morphologic changes in patients with geographic atrophy assessed with a novel spectral OCT-SLO combination. *Investigative Ophthalmology & Visual Science* 49:3095-3099.

Wolf-Schnurrbusch U.E.K., Ceklic L., Brinkmann C.K., Iliev M.E., Frey M., Rothenbuehler S.P., Enzmann V. & Wolf S. (2009). Macular Thickness Measurements in Healthy Eyes Using Six Different Optical Coherence Tomography Instruments. *Investigative Ophthalmology & Visual Science* 50:3432-3437.

Wood J.M., Wild J.M., Hussey M.K. & Crews S.J. (1987). Serial Examination of the Normal Visual-Field Using Octopus Automated Projection Perimetry Evidence for A Learning Effect. *Acta Ophthalmologica* 65:326-333.

Wormington C.M. (2003). Ophthalmic diagnostic use of lasers. In *Ophthalmic Lasers.* Ed: C.M. Wormington. Philadelphia. Butterworth-Heinemann. pp 85-182.

Wu J., Seregard S., Spangberg B., Oskarsson M. & Chen E. (1999). Blue light induced apoptosis in rat retina. *Eye* 13:577-583.

Wyszecki G. & Stiles W.S. (1982). Color Science: concepts and methods, quantitative data and formulae. 2nd edn. New York. Wiley.

Xu L., Li Y.B., Wang S., Wang Y., Wang Y.X. & Jonas J.B. (2007). Characteristics of highly myopic eyes - The Beijing Eye Study. *Ophthalmology* 114:121-126.

Yamamoto M., Tsujikawa A., Mizukami S., Miyoshi N. & Yoshimura N. (2008). Cystoid macular edema in polypoidal choroidal vasculopathy viewed by a scanning laser ophthalmoscope. *International Ophthalmology* Published Online First: 15 October 2008. doi:10.1007/s10792-008-9274-7

Yannuzzi L.A., Sorenson J.A., Sobel R.S., Daly J.R., Derosa J.T., Seddon J.M., Gragoudas E.S., Puliafito C.A., Gelles E., Gonet R., Burton T.C., Culver J., Metzger K., Kalbfleisch N., Zarling D., Farber M.D., Blair N., Stelmack T., Axelrod A., Waitr S.E., Cross A., Rolnick C., Flom T., Haller J., Pusin S., Cassel G., Applegate C.A., Seigel D., Sperduto R.D., Hiller R., Mowery R., Chew E., Tamboli A., Miller D.T., Sowell A.L., Gunter E.W., Dunn M., Seddon J.M., Shamban K., Gelles E., Lento D., Alexander J.A., Phillips D.A. (1992). Risk factors for neovascular age-related macular degeneration. The Eye Disease Case-Control Study Group. *Archives of Ophthalmology* 110:1701-1708.

Yeh T., Smith V.C. & Pokorny J. (1989). The Effect of Background Luminance on Cone Sensitivity Functions. *Investigative Ophthalmology & Visual Science* 30:2077-2086.

Yenice O. & Temel A. (2005). Evaluation of two Humphrey perimetry programs: full threshold and SITA standard testing strategy for learning effect. *European Journal of Ophthalmology* 15:209-212.

Zarbin M.A. (2004). Current concepts in the pathogenesis of age-related macular degeneration. *Archives of Ophthalmology* 122:598-614.

Zhang X.X., Bradley A. & Thibos L.N. (1993). Experimental-Determination of the Chromatic Difference of Magnification of the Human Eye and the Location of the Anterior Nodal Point. *Journal of the Optical Society of America A-Optics Image Science and Vision* 10:213-220.

Zhong Y., Chen L., Cheng Y. & Huang P. (2008). Influence of learning effect on blue-on-yellow perimetry. *European Journal of Ophthalmology* 18:392-399.

Appendix 1. Sample characteristics

The known risk factors of AMD and standard clinical functional measures in AMD were reviewed in Chapter 1. Information about the risk factors of AMD was collected within the patient and normal groups who took part in the studies described in Chapters 4, 7 and 8, in order to observe the within group frequency distributions of these risk factors (26 patients, 8 males and 18 females, mean age 68.8 years, SD 7.8, range 46-84 years, at various stages of AMD; and 22 normal subjects, 13 males and 9 females, mean age 67.2 years, SD 7.5, range 49-78 years). A summary of the standard clinical measures is shown in Table A1-1. A medical history was taken and a self-administered non-qualitative questionnaire was used to obtain routine demographic and epidemiological information from each study subject Table A1-2.

	Test
Visual acuity	Bailey-Lovie logMAR Chart (monocular)
Contrast sensitivity	Pelli-Robson Chart (monocular)
Colour vision	100 Hue Score (binocular)
Reading Speed	MNRead (binocular)
Body Mass Index	Height and weight
Waist to hip ratio	Tape measure

Table A1-1. Standard clinical measures

Personal Data	Age
	Gender
	Iris Colour
	Family History of AMD
Lifestyle	Smoking
	Alcohol Intake
General Health	Hypertension
	Cholesterol
	No. of Births and HRT use
Socio-demographic	Years of Education
	Occupation
	Postcode: Deprivation Index
	Ethnicity

Table A1-2. Data collected by questionnaire and taking a medical history.

Frequency data was obtained for the measures in Tables A1-1 and A1-2, for analysis of differences between the subject groups. Where normal distributions were present (Kolmogorov-Smirnov), parametric statistics were employed to test for statistical differences between groups. Questionnaires were returned with 100% compliance and complete data was collected for all subjects, with the exception of reading speed for which there were 2 and 4 missing cases in the patient and normal subject groups, respectively, due to recording equipment failure. Figures 1-7 show the frequency distributions of risk factors within the patient and normal groups. Table 3 shows the number and average values of various risk factors in the patient and normal groups.

The results presented here cannot be used to draw conclusions about the risk factors of AMD since the distributions displayed here are biased. The sample was not selected randomly from the population and is far smaller than required for an epidemiological study. It is not possible within a local scale to control for all risk factors in such a study, therefore there were factors in which differences existed between the normal and patient groups. Nevertheless, it is of use to define the distributions of common risk factors within the patient and control groups, since the strongest of risk factors may be more prevalent in the patient group compared to the normal group, even in a small sample.

A greater proportion of females to males were present in the patient group (Table A1-3), whereas the opposite was true in the normal group, which would appear to support the overall evidence from several population based studies that females have a slight increased risk of AMD (Evans 2001). The percentage of the number of births amongst females in the patient group was double that of the normal group, however the number of births, which was the reported risk factor (Freeman et al. 2005) was similar to the normal group. The majority of subjects had had their blood pressure measured within the past year, and a very small minority within the last 5 years. There were more subjects with hypertension in the patient group, a risk factor which has been considered inconsistent (Evans 2001).

Smoking, which is a major risk factor (Christen et al. 1996; Evans et al. 2005; Seddon et al. 1996), was not found to be greater in the patient group in this study, rather, the opposite was noted, where more control subjects smoked than patients (Table A1-3). Age was successfully controlled for between the subject groups. Many other risk factors had similar distributions between the patient and normal groups, such as family history of AMD, alcohol intake, years of education ethnicity and obesity. Normal subjects with a family history of AMD were especially motivated to take part in the

study. Therefore it is likely that their proportion was greater than is representative of the population.

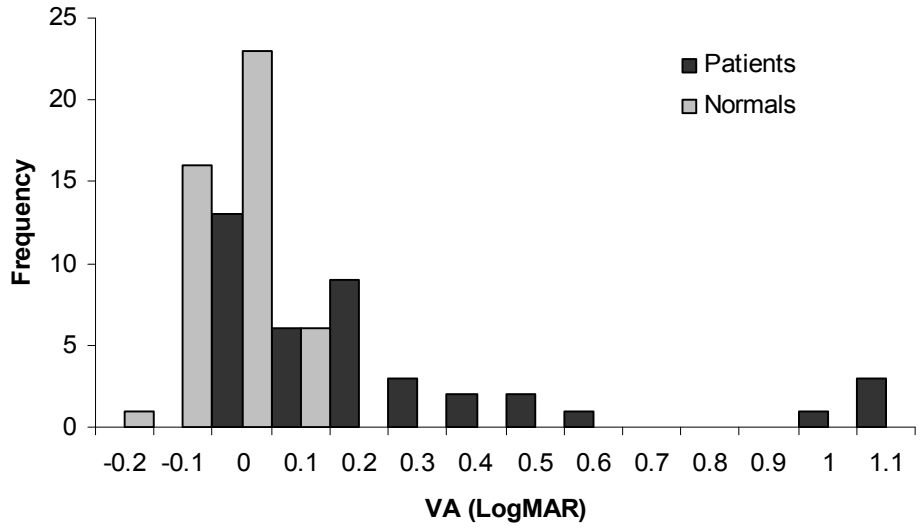

Figure A1-1. Frequency histogram showing the distribution of visual acuity (VA) in the patient and normal groups

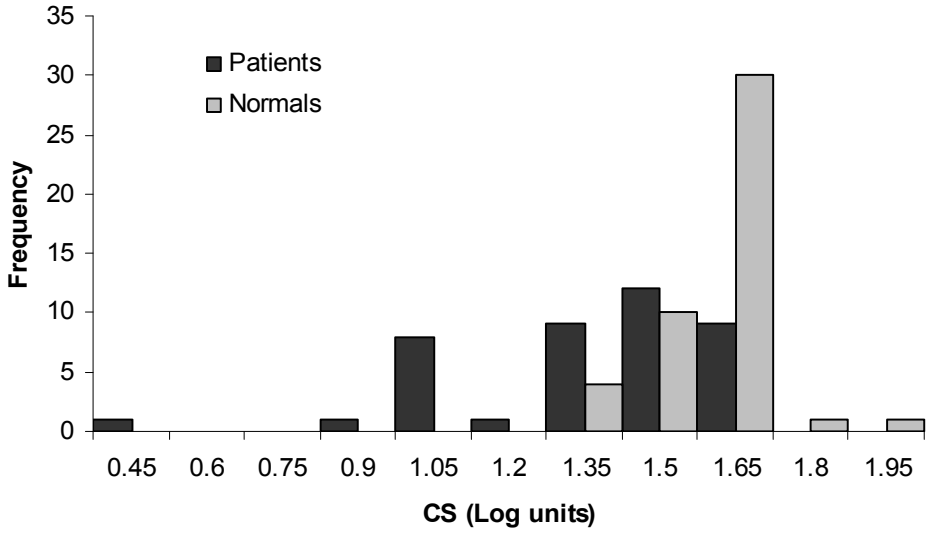

Figure A1-2. Frequency histogram showing the distribution of contrast sensitivity (CS) in the patient and normal groups

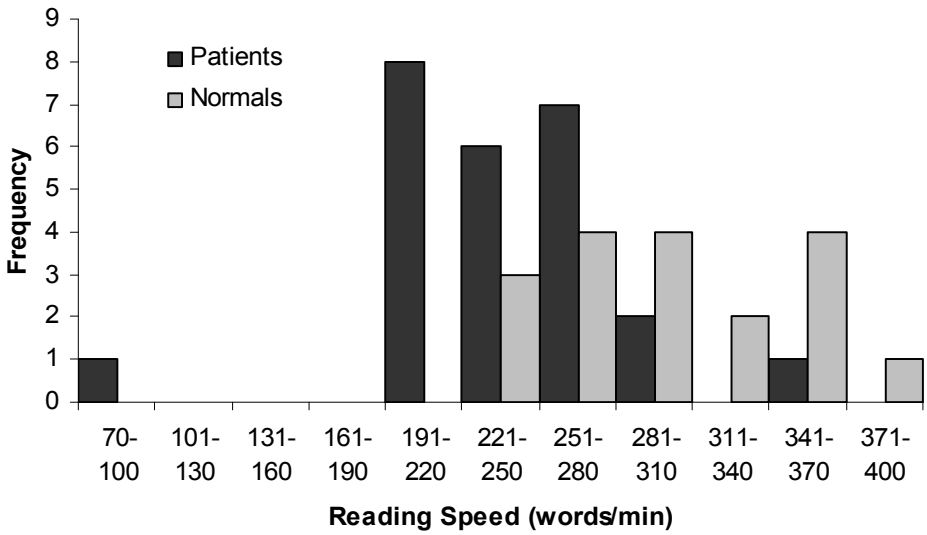

Figure A1-3. Frequency histogram showing the distribution of reading speed in the patient and normal groups

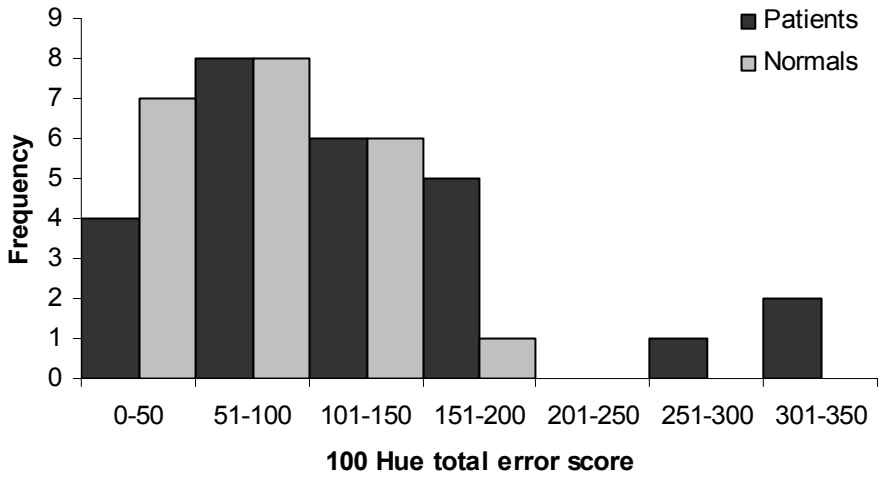

Figure A1-4. Frequency histogram showing the distribution of 100 Hue total error scores in patient and normal groups

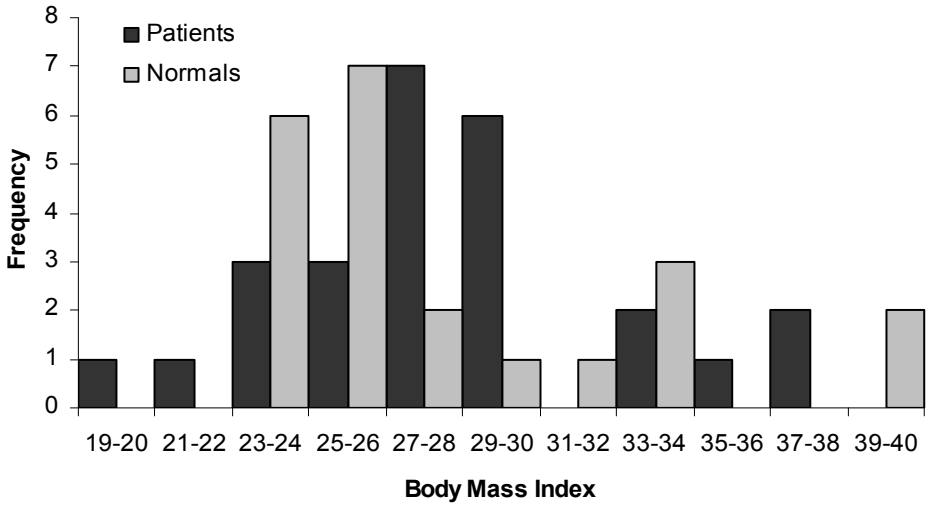

Figure A1-5. Frequency histogram showing the distribution of body mass index (kg/m^2) in the patient and normal groups

Standard clinical measures of visual function indicated worsened values in the patient group as expected. The positively skewed distributions of visual acuity (VA) values showed good VAs in the normal group which were significantly better (Mann-Whitney U test: $Z = -5.445$, $p < 0.001$) than the spread of VAs in the patient group (Figure A1-1). A similar pattern was observed in the results for contrast sensitivity (CS), where the normal group achieved significantly higher values (Mann-Whitney U test: $Z = -4.373$, $p < 0.001$) than the spread of values in the patient group (Figure A1-2). The reading speed of the normal group was greater than that of the patient group (Figure A1-3; unpaired t test: $t = -4.298$, $p < 0.001$). Total error score of the Farnsworth-Munsell 100 Hue test was within normal limits for all subjects except three who had atrophic or neovascular disease. Consequently the normal group achieved a significantly lower error score than the patient group (Figure A1-4; unpaired t test: $t = 2.372$, $p = 0.022$).

Although the normal group tended to exhibit greater measures of obesity than the patient group (Figure A1-5 and Figure A1-6), the differences did not achieve significance for body mass index (BMI) (unpaired t test: $t = 0.593$, $p = 0.555$) and waist to hip ratio (Mann-Whitney U test: $Z = -1.930$, $p = 0.054$). Age had a significantly Gaussian distribution (Kolmogorov-Smirnov: $p=0.200$), in which the patient and normal group did not differ significantly (Figure A1-7; unpaired t test: $t = 0.860$, $p = 0.394$). Most subjects had blue eyes (Figure A1-8).

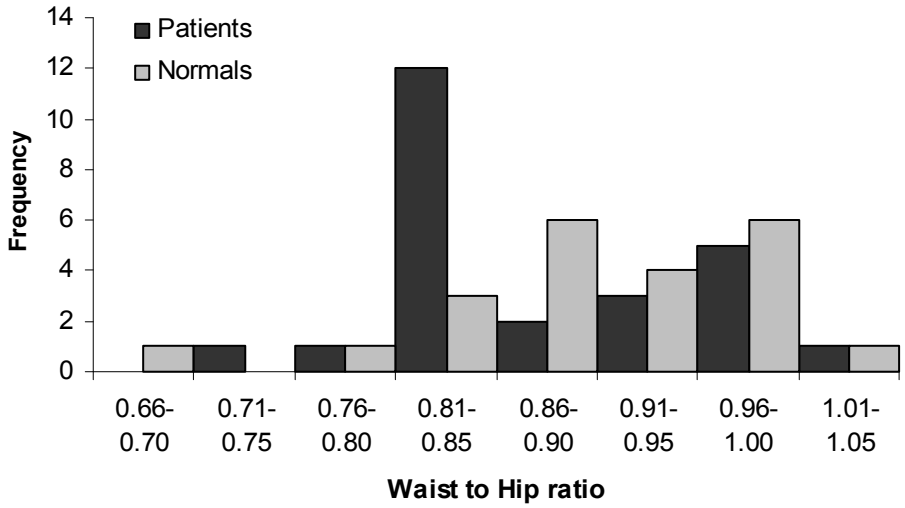

Figure A1-6. Frequency histogram showing the distribution of waist to hip ratio (waist/hip) in the patient and normal groups

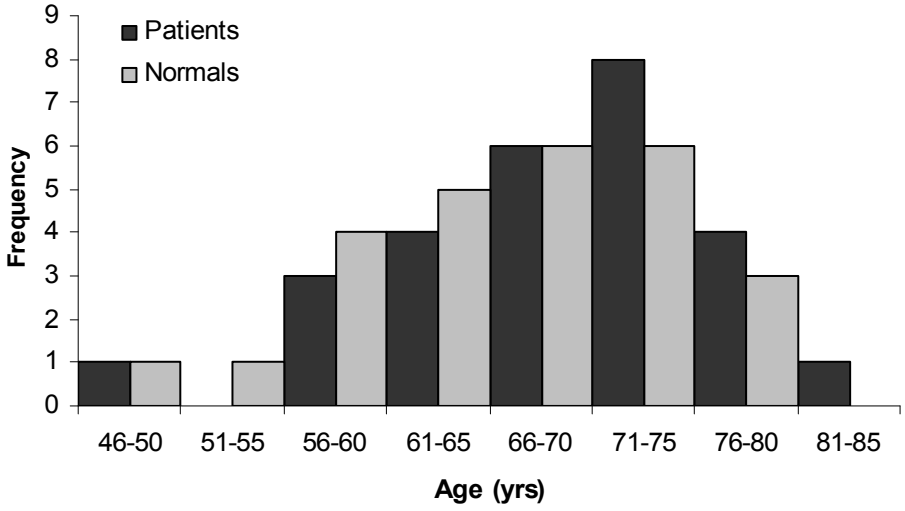

Figure A1-7. Frequency histogram showing the distribution of age (years) in the patient and normal groups

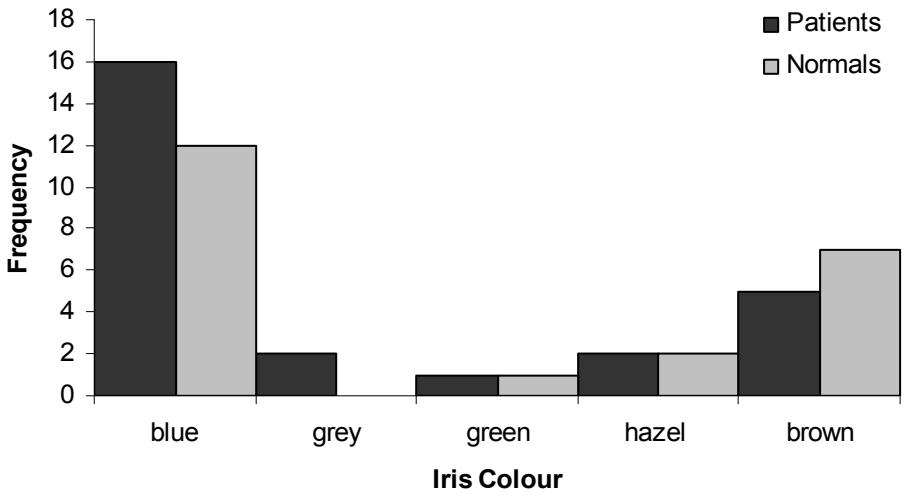

Figure A1-8. Frequency histogram showing the distribution of iris colour in the patient and normal groups

		AMD Patients (total 26)	**Normal Subjects** (total 22)
Gender	Males	8 (30.8%)	13 (59.1%)
	Females	18 (69.2%)	9 (40.9%)
Family history of AMD		8 (30.8%)	6 (27.3%)
Smoking	Never	15 (57.7%)	9 (40.9%)
	Current	0	1 (4.5%)
	Past	11 (42.3%)	12 (54.5%)
	Average pack years	20.9 (SD 15.5)	19.3 (SD 24.2)
Alcohol intake	Drinkers	19 (73.1%)	22 (100%)
	Average units per week	5.7 (SD 7.2)	6.4 (SD 4.8)
Medication or elevated level	Hypertension	15 (57.7%)	6 (27.3%)
	Cholesterol	8 (30.8%)	7 (31.8%)
Females only	Females who had given birth	16 (88.9%)	4 (44.4%)
	Average no. births	2.7 (SD 1.1)	2.8 (SD 1.0)
	HRT use	1 (5.6%)	1 (11.1%)
Socio-demographic	Years of education	11.6 (SD 3.1)	13.0 (SD 5.0)
	Deprivation index	20709.4 (SD 9113.9)	18074.9 (SD 8688.2)
	Ethnicity - White	26 (100%)	22 (100%)

Table A1-3. Risk factors of AMD in the patient and normal groups

Similar proportions between groups were present for family history of AMD, subjects taking medication for cholesterol and ethnicity (Table A1-3). There were more females, number of women who had pregnancies and subjects taking blood pressure medication in the patient group.

There were less alcohol drinkers in the patient group. A greater number of subjects in the patient group had never smoked, although of the smokers the amount of smoking in terms of pack years was similar between groups. A pack year represents twenty manufactured cigarettes, or 20g tobacco, smoked per day for a period of one year and is calculated by the following equation:

Pack-years = (no. of cigarettes smoked per day/20) x no. of years been smoking

Of the current and past smokers, this was calculated for both groups of subjects and similar measures were evident between the groups.

The deprivation index is a measure which may be determined by postcode and the patient group overall came from less deprived areas. All 32,482 neighbourhoods in England are ranked on a range of topics, including income, employment, health, education and crime, to give a 'Total Deprivation' ranking. The most deprived neighbourhood in England ranks 1 of 32482 (Indices of Deprivation 2007 http://neighbourhood.statistics.gov.uk/)

The Standard Occupational Classification 2000 (SOC 2000) is a classification system of occupations, based on two concepts, the nature of the work performed and the skill level involved. The ranking is a four digit number, the first digit of which is classified into the following nine groups:

SOC 2000 Major groups (Office for National Statistics website: www.ons.gov.uk)

1. Managers and senior officials
2. Professional occupations
3. Associate professional and technical occupations
4. Administrative and secretarial occupations
5. Skilled trades occupations
6. Personal service occupations
7. Sales and customer service occupations
8. Process, plant and machine operatives
9. Elementary occupation

The SOC 2000 values were not significantly different between the patient and normal groups (unpaired t test: t = -0.284, p = 0.777).

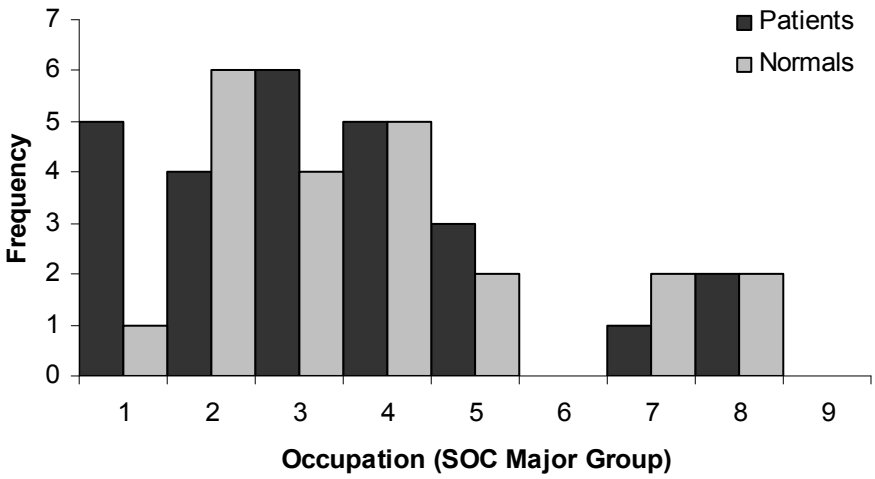

Figure A1-9. Frequency histogram showing the distribution of SOC 2000 major occupation groups in the patient and normal groups

Appendix 2. Program instructions

System requirements

The programs are standalone applications which can run in Windows 95, Windows 98, Windows Me, Windows NT, Windows 2000, or Windows XP and with some permissions, Windows Vista.

Insert the accompanying disc and click on the main torch icon for either Perimetric Fundus Map or Fundus Grading Grid.

Perimetric Fundus Map

To generate the visual field locations on the fundus image:

- In the first window open a bitmap fundus image. An example image is provided on the disc.
- Enter the macula to disc distance in degrees. The standard assumption is 15°. Click Next.
- LEFT click at the superior margin of the optic disc, then RIGHT click at the inferior margin. Click OK. Repeat along the horizontal, using a LEFT and a RIGHT click at the disc margins.
- LEFT DOUBLE click at the macula. Click Next.
- The stimulus locations for the 10-2 Humphrey visual field will be displayed on the fundus image.
- The perimetric data can be entered in two ways, as a list or by location.

To enter perimetric data as a list:

- Make sure the box “Enter values by location” is unticked.
- A list of values may be typed or copied and pasted into the textbox.
- For a numeric display, enter numerals. For a symbolic display of probability values, enter “**1” to indicate p<1%, “**2” to indicate p<2% etc.
- Click Enter. The values will be displayed on the map.

To enter perimetric data by location:

- Make sure the box “Enter values by location” is ticked.

- Enter a value once into the textbox. Do not press enter. Click on the corresponding visual field locations in the schematic grid, to display the numeric or symbol on the map.

Display options:

- Select “Display RE/LE on fundus photo” and select RE or LE, to display RE or LE on the image.
- To adjust the colour contrast of the numeric values on the map, make sure the box “Enter values by location” is unticked and that numeric values have been entered onto the map. Select “Light” or “Dark” according to visibility over the background.
- To display the vertical downward displacement of the macula from the centre of the disc in degrees, select “Display vertical displacement of macula”.

To save the image:

- Click Save. Make sure the file name ends in “.bmp”. The image will save as a bitmap.

To exit the program:

- Click Exit. Answer Yes to “Have you saved your photo?”.

Fundus Grading Grid

To generate the circular grading grid on to the fundus image:

- In the first window open a bitmap fundus image. An example image is provided on the disc.
- LEFT click at the superior disc margin and RIGHT click at the inferior disc margin. Click Next.

  Note: At this stage do not click Next without following the next step.
- LEFT click at the macula. Click the “Draw Grid” button. The grading grid will be displayed on the image. Click Next.

  Note: To access the following window without the circular grading grid in place, do not click the “Draw Grid” button, simply click Next after defining the macula.

To measure features on the image:

- Click OK to begin marking on the image.

- Choose a circular feature. LEFT click and RIGHT click the edges of the feature to draw a circle around it. The diameter, area and nearest circle size (according to the International Grading System) will be displayed.
- Click Add to copy the diameter onto the list in the textbox.
- Repeat the previous two steps for all features of interest.
- Select subfield, to display the % area of the subfield covered by the features listed in the textbox.

Appendix 3. Rationale for choosing boxplot limits

The boxplot is a modified histogram and represents a five number summary of a sample distribution. Heijl et al. (1987b) applied the boxplot to represent change over time of the pointwise differences between the measured field and the normal field. The box limits used were the 15th and 85th percentiles, whilst the tail limits marked the 0 and 100th percentiles.

In Chapters 4 and 7 of this thesis, boxplot representation was used to show change over time and between groups of global indices, number of defects and examination duration. It was therefore necessary to consider the nature of this data in determining the boxplot limits. Of the boxplots represented in Chapters 4 and 7, the majority of distributions were non-Gaussian. Kurtosis values were positive in 60% of the total distributions indicated by the boxplots. Where kurtosis values were negative, the distributions were nearly mesokurtic.

The peak of a leptokurtic distribution indicates a larger proportion of values over a narrower range. Narrowing the limits of the boxplot appeared more appropriate to the data. Furthermore, representation of the interquartile range is a standard measure of dispersion applied to non-Gaussian data. An example of both boxplot representations is given in Figure A3-1, which shows frequency data from MD values in the patient group in Chapter 4.

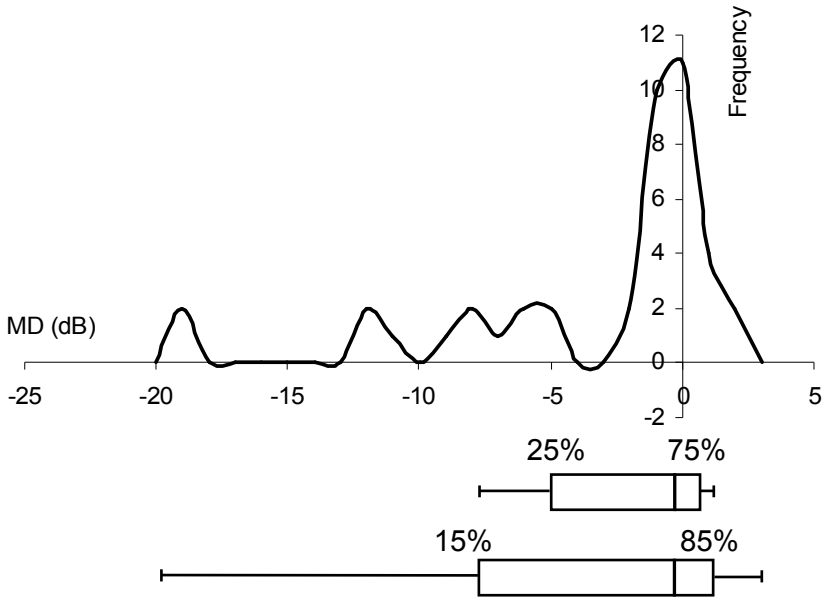

Figure A3-1. Frequency of standard perimetry MD values in the AMD patient group from visit 2 (Chapter 4).
Two versions of a boxplot are shown indicating the box limits. The boxplot above was applied to the data in this thesis, the boxplot below shows the conventional limits.